5-2018

Functional and structural impact of the loss of the leucine-rich repeat protein LRIT1 in the mouse retina.

Catherine Ann Cobb
University of Louisville

FUNCTIONAL AND STRUCTURAL IMPACT OF THE LOSS OF THE LEUCINE-RICH REPEAT
PROTEIN LRIT1 IN THE MOUSE RETINA

By

Catherine Ann Cobb
B.S., Middle Tennessee State University, 2011
M.S., University of Louisville, 2015

A Dissertation
Submitted to the Faculty of the
School of Medicine of the University of Louisville
In Partial Fulfillment of the Requirements

For the Degree of

Doctor of Philosophy
in Biochemistry and Molecular Genetics

Department of Biochemistry and Molecular Genetics
University of Louisville
Louisville, Kentucky

May 2018

FUNCTIONAL AND STRUCTURAL IMPACT OF THE LOSS OF THE LEUCINE-RICH REPEAT
PROTEIN LRIT1 IN THE MOUSE RETINA

By

Catherine Ann Cobb
B.S., Middle Tennessee State University, 2011
M.S., University of Louisville, 2015

A Dissertation Approved on

April 4, 2018

by the following Dissertation Committee:

———————————————————————
Ronald G. Gregg, PhD (Mentor)

———————————————————————
Steven R. Ellis, PhD (Co-Mentor)

———————————————————————
Barbara Clark, PhD

———————————————————————
Carolyn Klinge, PhD

———————————————————————
Cynthia Metz, PhD

———————————————————————
Nazarul Hasan, PhD

DEDICATION

There is one person in whom I found respite from these "constant partial attention" always-on-the-go never-good-enough must-finish I-make-the-most-money lives we lead: my mom. Whether it was physically being there, providing emotional and mental support and guidance, or speaking through her voice in my head and heart, she always showed up for me. For example, when I moved to Louisville for graduate school, it was a difficult adjustment. There was much to absorb about the city, graduate school program, our department, etc. A new job, a new set of peers and professors, a new car, a new apartment. A new life. I wanted to tuck my proverbial tail between my knees and scurry back home for comfort and safety of the familiar. I called her one day during our first week of orientation to confide in her about my feelings. During this call she did not tell me to leave or to stay, scold me, or play the "well, if you left, what would you do" game. Instead she supported me. She sent me the receipt for an already purchased flight out to visit me in Louisville in three weeks from our current conversation and told me to check my e-mail. After I did, she said, "Just promise me you'll stay until I get there to visit. If you don't, I won't have a place to stay." She laughed and continued, "If you still want to leave after that, I'll help you move back." I agreed to remain open-minded and give it my best shot. In three weeks' time, I picked her up from the airport. By then I was adjusted enough and actually excited to show her my new digs on the way to fulfilling my dream of getting a research-based science PhD.

While I was halfway through my PhD, she graciously lost her battle to colon cancer. However, she never left my side. I dedicate my body of work to my mom. Mom, thank you for everything you have given me. I am doing my best to make you proud until we are together again.

I would also like to dedicate this work to God/the universe/infinite energy/that entity which is larger than organisms, all-encompassing, and supreme. The most meaningful, deeply learned life lessons arrive in the form of change, struggle, and suffering. Without guidance from the Spirit, I would be lost in the darkness and unable to find the light.

ACKNOWLEDGEMENTS

ABSTRACT

FUNCTIONAL AND STRUCTURAL IMPACT OF THE LOSS OF THE LEUCINE-RICH REPEAT
PROTEIN LRIT1 IN THE MOUSE RETINA

Catherine Ann Cobb

April 4, 2018

Mutations in genes encoding the leucine-rich repeat (LRR) proteins nyctalopin and LRIT3 lead to complete congenital stationary night blindness because they are critical to depolarizing bipolar cell function in the retina. LRIT3 has two closely related family members, LRIT1 and LRIT2. In silico analyses of publicly available RNA-Seq data showed that *Lrit1* was highly expressed in the retina. Here I describe the expression pattern and impact of loss of LRIT1 on retinal function. To enable these studies, we used CRISPR/Cas9 technology to create an *Lrit1*$^{-/-}$ mouse line. Retinal morphology and morphometry analyses showed no gross changes in retinal structure or retinal layer thickness. Immunohistochemistry (IHC) shows photoreceptor, ON bipolar cell, and horizontal cell proteins localize normally in the absence of LRIT1. These data suggest LRIT1 is unnecessary for normal retinal and synaptic development. IHC also reveals LRIT1 localizes to the OPL with punctate staining similar to proteins expressed in invaginating horizontal cells at rod spherules but does not co-localize with ON or OFF bipolar cell proteins. RNA *in situ* hybridization shows *Lrit1* expression in the ONL and INL, suggesting LRIT1 may also be expressed in photoreceptors. We used electroretinogram analyses to assess retinal function in *Lrit1*$^{-/-}$ mice and demonstrate that the a- and b-waves are decreased in amplitude under both scotopic and photopic conditions. Multi-electrode array recordings of *Lrit1*$^{-/-}$ retinal ganglion cells demonstrated abnormal ganglion cell responses and rhythmic oscillations. Taken together, our data localize LRIT1 to the OPL of the mouse retina where the loss of LRIT1 results in abnormal outer and inner retinal function without altering retinal structure. Thus, LRIT1 is critical for normal retinal signaling.

TABLE OF CONTENTS

PAGE

LIST OF TABLES

LIST OF FIGURES

CHAPTER 1

INTRODUCTION

Vision provides organisms a unique perspective through visual imagery that originates from and depends on tiny packets of discrete light called photons. Our visual system can even detect a single photon (1). We must gather, focus, and channel light from our surroundings onto our retinas via the cornea and lens to capture and transform photonic energy into biologically encoded information our brains can interpret (Fig. 1) (2).

The ability to visually assess and relate to our environment helps us in many ways such as balance control and mobility. Moreover, the integration of vision with other informative inputs such as hearing or taste guide behavior. Imagine you did not possess the ability to see: you would miss reflections in a mirror, the smile the stranger gives you when you walk into a room, or the brake lights on the car that slams to a stop in front of you. Without normal vision, daily activities can become more challenging. The National Federation of the Blind estimates there are 1.3 million legally blind Americans and another 8.7 million Americans who are visually impaired (3). Further, studies suggest a doubling of these numbers in the next 30 years due to aging (3). Several diseases such as macular degeneration, diabetic retinopathy, cataracts, and glaucoma (4) represent some of the major contributors. Achromatopsia, Bardet-Biedl syndrome, congenital stationary night blindness, and retinitis pigmentosa (5) represent some of the rarer contributors to the visually impaired or blind populations. Thus, to help these growing populations of visually impaired or blind people by developing prophylactics and treatments, it is important to fully elucidate and understand the visual circuits through research.
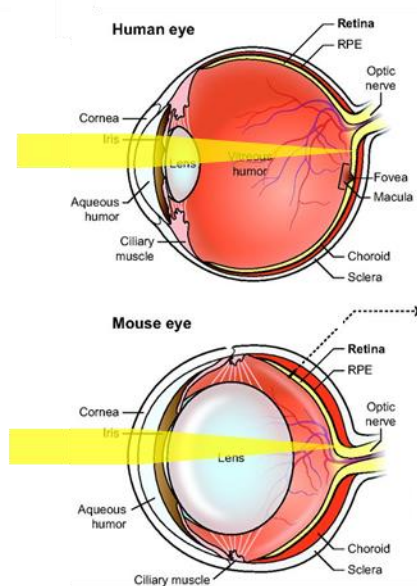
Fig. 1. Cross-sectional schematic of the eye's anatomy. The cornea bends incoming light (yellow) onto the lens that further focuses it onto the retina. (Top) Schematic of the human eye labeled with the central cone-only region known as the fovea, which is surrounded by the macula that is more cone-dense than the peripheral retina. (Bottom) Schematic of the mouse eye which lacks a fovea and macula. Adapted and modified from Shobi Veleri *et al. Dis. Model. Mech.* 2015;8:109-129.

Retinal Layer Organization

The eye gathers, focuses, and converts light into an electrochemical signal sent to the brain for visual processing. But how does the mammalian eye perform these functions? At the eye's posterior is the retina, the tissue responsible for transmitting the information from incident light to the brain. The retina is a seven-layered structure essential for the first steps of vision. Between the posterior-most retinal pigment epithelium and the anterior-most optic nerve fiber layer are seven retinal layers containing (1) the photoreceptor outer segments (OS), (2) the photoreceptor inner segments (IS), (3) the outer nuclear layer (ONL), (4) the outer plexiform layer (OPL), (5) the inner nuclear layer (INL), (6) the inner plexiform layer (IPL), and (7) the ganglion cell layer (GCL) (Fig. 2).
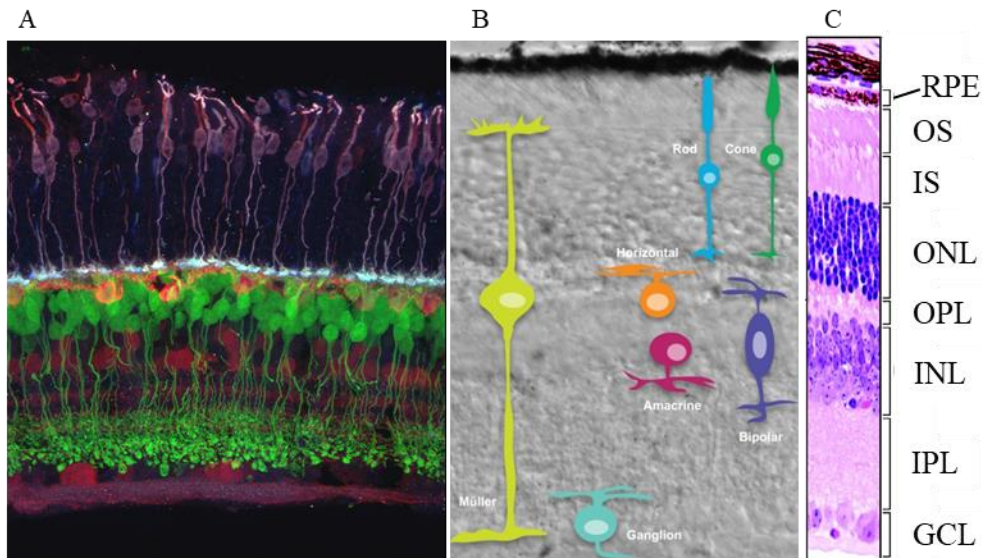
Fig. 2. Retinal cell types and organization. A) Fluorescent microscopy image of a mature mouse retinal section immunolabeled for photoreceptors (purple), horizontal cells (orange), bipolar cells (green), and amacrine and ganglion cells (red). B) Schematic of adult mouse retinal cell types with three cellular layers containing photoreceptors; horizontal, bipolar, and amacrine cells; and ganglion cells that are separated by two synaptic layers, the OPL and IPL, respectively. C) Hematoxylin and eosin-stained section from the mouse retina marking the retinal pigment epithelium (RPE); photoreceptor outer segments (OS), inner segments (IS), and cell bodies (ONL); horizontal, bipolar, and amacrine cell bodies (INL); ganglion cell bodies and displaced amacrine cell bodies (GCL); and synaptic layers (OPL, IPL). Adapted and modified from A) http://wonglab.biostr.washington.edu/research.html, B) Xia Zhang *et al. Bioinform. Biol. Insights.* 2011;5:99–113, and C) Shobi Veleri *et al. Dis. Model. Mech.* 2015;8:109-129.

To add to this complexity, there are cell types specific to each retinal layer. The photoreceptors, or rods and cones, comprise the OS, IS, and ONL. The OS consists of membranous stacks called discs with visual pigment proteins and is the site of phototransduction. The IS contains the mitochondria, ribosomes, and membranes needed for producing and packaging molecules and proteins for later transport to the OS. The photoreceptor nuclei reside in the ONL. The OPL contains synaptic contacts between pre-synaptic photoreceptor axons and both post-synaptic bipolar cell dendrites and horizontal cell dendrites and axons. The INL is composed of bipolar, horizontal, and amacrine cell bodies. The IPL contains the synaptic contacts between bipolar cell axons and ganglion cell dendrites and synaptic contacts between amacrine cells and either bipolar, ganglion, or other amacrine cells. The GCL is the final nuclear layer containing the retinal ganglion cell bodies and displaced amacrine cells. In sum, photoreceptor, bipolar, and ganglion cells are the primary, secondary, and tertiary neurons, respectively, of the vertical pathways in retina whereas horizontal and amacrine cells function in lateral inhibitory pathways to regulate signaling in the outer and

inner retinas, respectively. By post-natal week four, the structure of the mouse retina is built (Fig. 3) (6).

The conserved developmental patterns and final structure of the retinas in all jawed vertebrates (superclass

or subphylum Gnathostomata) suggest a common origin, and points of difference likely result from

necessary adaptations for survival or enhanced fitness (7).
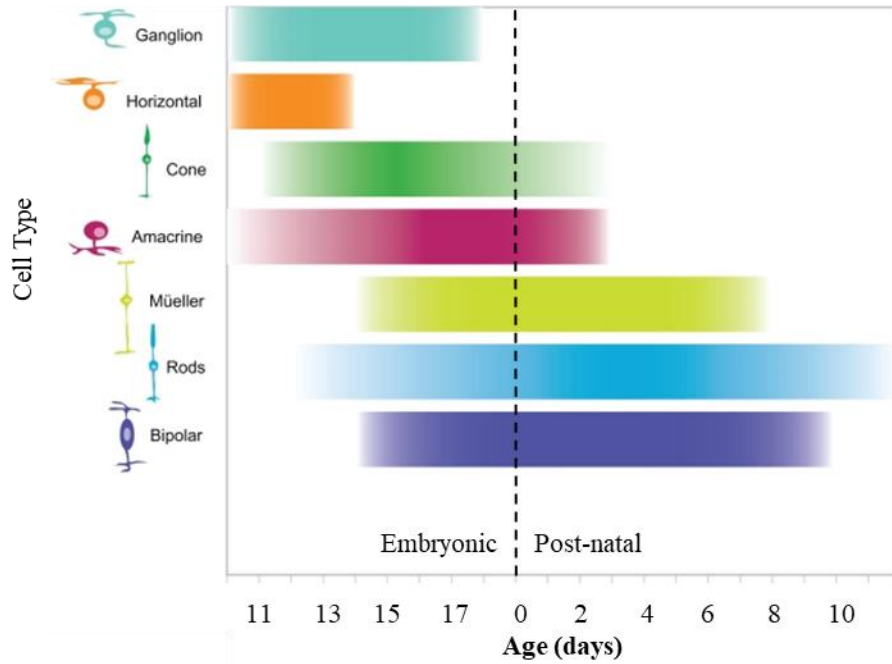
Fig. 3. Timeline for mouse retinal development. Y-axis indicates retinal cell type. X-axis indicates developmental time. Embryonic and postnatal development are to the left and right, respectively, of animal's birth indicated at day 0 (dotted line). Adapted and modified from Xia Zhang *et al. Bioinform. Biol. Insights.* 2011;5:99–113.

Photoreceptors

Hundreds of millions of years ago our early ancestors developed cells skilled in primitive

phototransduction. During the Cambrian explosion when animal body plans underwent major changes such

as the introduction of a skull in animals known as craniates, they also evolved eyes and visual systems (6).

Microvillar and ciliary photoreceptors are the two early types of photoreceptors that are expressed in

separate animal groups (8). Microvillar photoreceptors result from OS plasma membrane microvillar

evaginations. Ciliary photoreceptors develop from OS plasma membrane ciliary invaginations. Humans and

mice express ciliary photoreceptors to receive and transduce light-dependent information. This occurs via initiation of a G-protein-mediated light response culminating in hyperpolarization and graded potentials. Graded potentials differ from action potentials in that they are not restricted to an all-or-none response (Fig. 4). Graded potentials can yield a response based on the degree (or grade) of pre-synaptic input. The changes in photoreceptor membrane potential modulate glutamate release into the synapse that transmits a graded potential to post-synaptic bipolar and horizontal cells (6,7). Several differences between rods and cones arise from their specialized contributions to dim light and daylight vision, respectively.
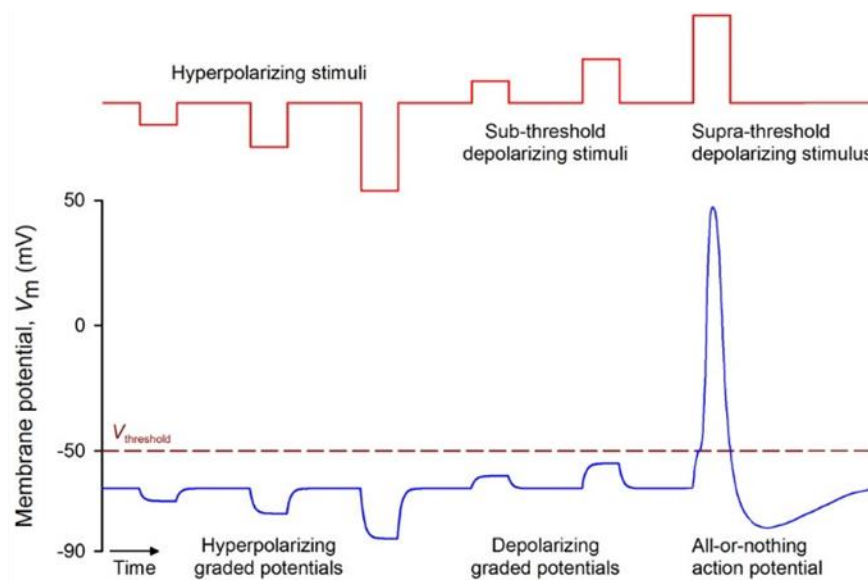
Fig. 4. Stimulus response plot of graded versus action potentials in neurons. Electrical stimulation can result in graded potentials that are proportional in magnitude to the amplitude of the stimulus. Sub- and supra (above)-threshold stimuli cause graded potentials. Because of the all-or-none principle, only supra-threshold stimuli cause action potentials. (Top, red) All square-wave stimuli applied to a neuron generates graded potentials. (Bottom, blue) Neuronal action potentials result only from supra-threshold stimuli. Threshold (dotted line). Adapted and modified from "Neuronal Action Potential." *PhysiologyWeb*. www.physiologyweb.com.

Rods

Rods exhibit an OS structure consisting of individual discs that contain one type of visual pigment called an opsin with a peak sensitivity around 496 nm (Fig. 5). Rods are also more abundant than cones (7). Human retinas are 95% rods and 5% cones. This proportion is more exaggerated in laboratory rodents who

are nocturnal and consequently have a greater proportion of rods to cones in their rod-dominant retinas. This limits the research applications for cone studies in rodents. In contrast, most birds and some diurnal animals display a greater proportion of cones to rods and have what are referred to as cone-dominant retinas (9).
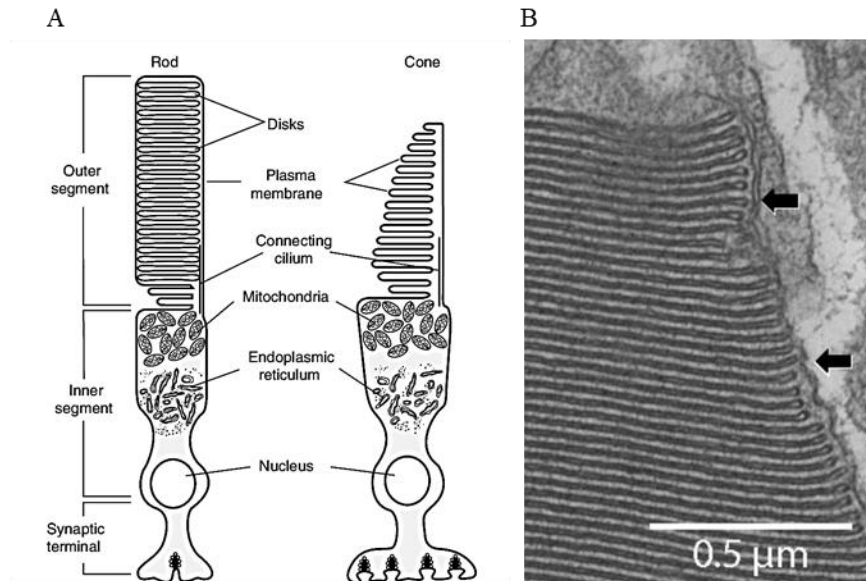
Fig. 5. Photoreceptor rod and cone structure. A) Schematic of vertebrate rod and cone photoreceptor cells with the phototransducing OS joined by the connecting cilium to the organelle-rich IS. B) TEM image of *T. proximus* (garter snake) rod OS structure membranous discs similar to cones but exclusively in rods is completely enclosed by the plasma membrane (arrows). Adapted and modified from A) Rick Cote. *Cyclic Nucleotide Phosphodiesterases in Health and Disease.* CRC Press, 2006. *ResearchGate.* Web. 27 Feb. 2018 Accessed. B) Ryan K. Schott *et al. PNAS.* 2016;3(2):356-361.

Cones

Cones exhibit an OS structure of an interconnected sequence of discs that contain one or more of several opsins (Fig. 5). Cone opsins each have distinct absorption maxima that provide animals with discriminate color vision (1). Cone-dependent color vision in animals forms distinct profiles: humans and related non-human primates are trichromats, most other mammals including mice are dichromats, and birds and fishes are tetrachromats (1,9). In trichromats, cones exist in three types: L, M, and S, which are characterized based on the wavelength to which each type optimally responds. L, M, and S cones respond

to long-, middle-, and short-frequency wavelengths, respectively. In humans, L cones occur twice as often as M cones. L and M cones exist all over the retina but are the only photoreceptors in a small, centralized region of high visual acuity known as the fovea. S cones comprise ~10% of cones and typically exist in the peripheral retina (7). In the dichromatic mouse retina there are only two expressed opsins: S-opsin and L-opsin, sensitive to short and middle-to-long wavelengths, respectively (10). Subtle changes in the opsin proteins among species can cause concurrent changes in opsin sensitivities such that mouse S-opsin has an absorption maximum in the ultraviolet range (10). The pigmented mouse retina displays a non-homogenous cone distribution where the ventral retina has a higher density of S-opsin expressing cones that are rare in the dorsal retina. L-opsin expressing cones exhibit an even distribution. In dichromats like mice, cones can either be genuine or dual. Genuine cones express only one type of opsin whereas dual cones express both. The bulk of the cones in the mouse retina are dual cones co-expressing both opsins. It is important to note that opsin co-expression in dual cones does not hinder color discrimination. All mouse cones can be visualized by staining with peanut agglutinin (PNA) or by co-staining for both genuine cone markers using anti-S or anti-L opsin antibodies (10). Cone opsins exhibit similar photosensitivities to rhodopsin based on their extinction coefficients and quantum yields, which does not account for the difference in rod to cone sensitivity. This difference may instead be due to the faster cone opsin regeneration rate and cone recovery of circulating dark current after photobleaching that matches the function of cone-mediated vision under daylight conditions (1,11,12).

Photoreceptor Synaptic Ribbons

Photoreceptor terminal active zones, or vesicular release zones, contain voltage-dependent calcium channels and sites for vesicular fusion-dependent glutamate exocytosis. Rod terminals are called spherules, and cone terminals are called pedicles. At the photoreceptor glutamate release site, there is an electron-dense structure referred to as a synaptic ribbon (Fig. 6). This is the origin of the term ribbon synapse, which is marked by the well-established photoreceptor ribbon protein RIBEYE (13). The photoreceptor synaptic ribbons are where rod spherules and cone pedicles contact horizontal and ON bipolar cells. When horizontal and ON bipolar cells contact the photoreceptor terminal at one ribbon, they form a triad. In

addition to synaptic ribbon contacts, cone pedicles also make flat contacts to OFF bipolar cells, distinct from the invaginating ribbon synapses.

The synaptic ribbon is critical to highly efficient signal transmission (14). In light increments, the ribbon is charged with vesicles. The rate at which ribbons release vesicles is a function of light intensity such that as light intensity increases, less vesicles are released. At light decrements, photoreceptors depolarize and open calcium channels so that calcium ions can flow into the cell to raise and maintain locally high intracellular calcium levels. This stimulates calcium-dependent vesicular fusion and glutamate exocytosis occurs. This releases the excitatory neurotransmitter glutamate into the synaptic cleft (14).
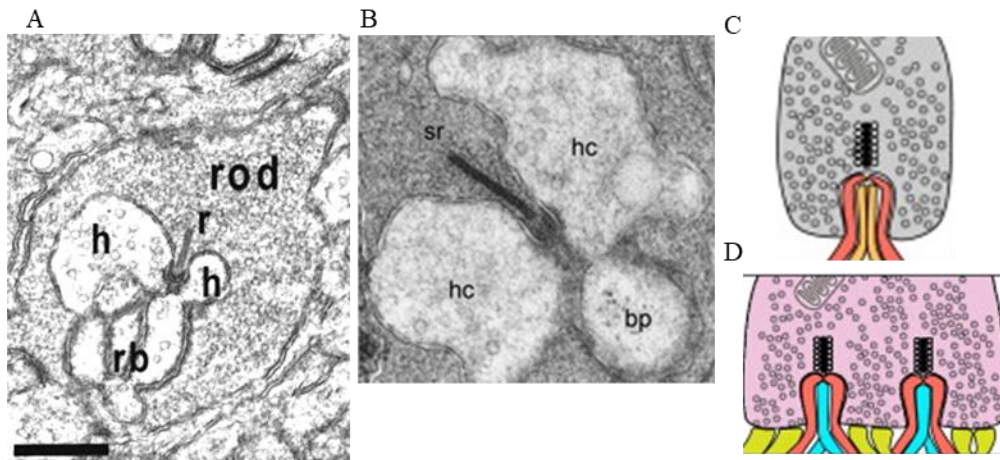
Fig. 6. Photoreceptor rod and cone synaptic structure. A) Electron micrograph of the mouse rod synapse. Synaptic ribbon (r), horizontal cell processes (h), and rod ON bipolar cell dendritic tips (rb); scale bar 500 nm. B) Electron micrograph of the vertebrate invaginating cone synapse showing the synaptic ribbon (sr), horizontal cell processes (hc), and the cone ON bipolar cell dendritic tip (bp). C) Schematic of the mouse rod synapse with ribbon (black), two horizontal cell processes (red) and two rod ON bipolar cell processes (orange). D) Schematic of the mouse cone synapse with ribbon (black), two invaginating horizontal cell processes (red), one-two invaginating cone ON bipolar cell processes (blue), and flat contacting-cone OFF bipolar cell processes (yellow green). Adapted and modified from A) Rick Cote. *Cyclic Nucleotide Phosphodiesterases in Health and Disease.* CRC Press, 2006. *ResearchGate.* Web. 27 Feb. 2018 Accessed. B) Richard H. Kramer *et al. PLoS Biol.* 2015;13:e1002322. C and D) Florence D. D'Orazi *et al. Trends Neurosci.* 2014;37(10):594-603.

Photoreceptor Signaling and Regenerating Signaling Molecules

Rhodopsin is a G-protein coupled receptor whose composition provides its photosensitivity. Rhodopsin's vitamin A-derived chromophore 11-*cis*-retinal absorbs photons in the visible light spectrum. Absorbed photons excite 11-*cis*-retinal's electrons and cause its isomerization into all-*trans*-retinal (1). The *cis* to *trans* isomerization can also occur stochastically or result from a change in thermal energy. These alternate ways to induce *cis* to *trans* isomerization introduce noise into the system (1). Rods demonstrate a low spontaneous thermal isomerization that lowers background noise and provides them with the ability to detect low levels of light. Cone opsins exhibit a much higher rate of spontaneous thermal isomerization compared to rods, therefore making cones less sensitive than rods (11). To regenerate 11-*cis*-retinal in rods, all-*trans*-retinal must be transported to the retinal pigment epithelium where it is reduced, esterified, isomerized, oxidized, and recycled into 11-*cis*-retinal and diffuses back into the photoreceptor OS to conjugate to a new opsin (15).

Incident light enters the retina and traverses to the photoreceptor OS. Membrane-embedded rhodopsin in rod OS and opsins in cone OS absorb photons of light, which causes their activation into metarhodopsin II (rods) and meta-II (cones) (Fig. 7A). Metarhodopsin II activates its G-protein transducin (G_t), which binds to and activates phosphodiesterase 6 (PDE6). Active PDE6 hydrolyzes cyclic GMP (cGMP) into 5'-GMP. The decline of cGMP closes cGMP-gated sodium (CNG) channels, hyperpolarizing the cell. In the dark, CNG channels are open. The cation influx through CNG channels generates what is referred to as the circulating dark current (Fig. 7B). Light increments minimize the dark current and its influx of cations, leading to photoreceptor hyperpolarization. Photoreceptor hyperpolarization is sensed by voltage-gated calcium channels that close, decreasing calcium ion influx at the axon terminal, and thus reducing vesicular glutamate release.

Ca^{2+} and $G_{t\alpha}$-GTP hydrolysis are involved in restoring the high intracellular OS Ca^{2+} levels in the photoreceptor resting state at light decrements. Declining Ca^{2+} levels in photoreceptors during light increments cause OS Ca^{2+} to dissociate from guanylate cyclase-activating protein so that low $[Ca^{2+}]$ activates guanylyl cyclase. Active guanylyl cyclase synthesizes and increases cGMP production (Fig. 7A). This reestablishes cGMP levels, reopens CNG sodium channels, restores the dark current, depolarizes photoreceptors, opens voltage-gated Ca^{2+} channels and Ca^{2+} influx, and increases Ca^{2+}-dependent glutamate

release. Declining calcium levels in photoreceptors also cause the Ca^{2+}-dependent protein recoverin to derepress or activate rhodopsin kinase activity. Rhodopsin kinase phosphorylates metarhodopsin II (16), which causes arrestin binding and inactivation of metarhodopsin II. RGS9 is a GTPase-activating protein that induces $G_{t\alpha}$ GTP hydrolysis. GDP-$G_{t\alpha}$ cannot interact with PDE6, inactivating PDE6.
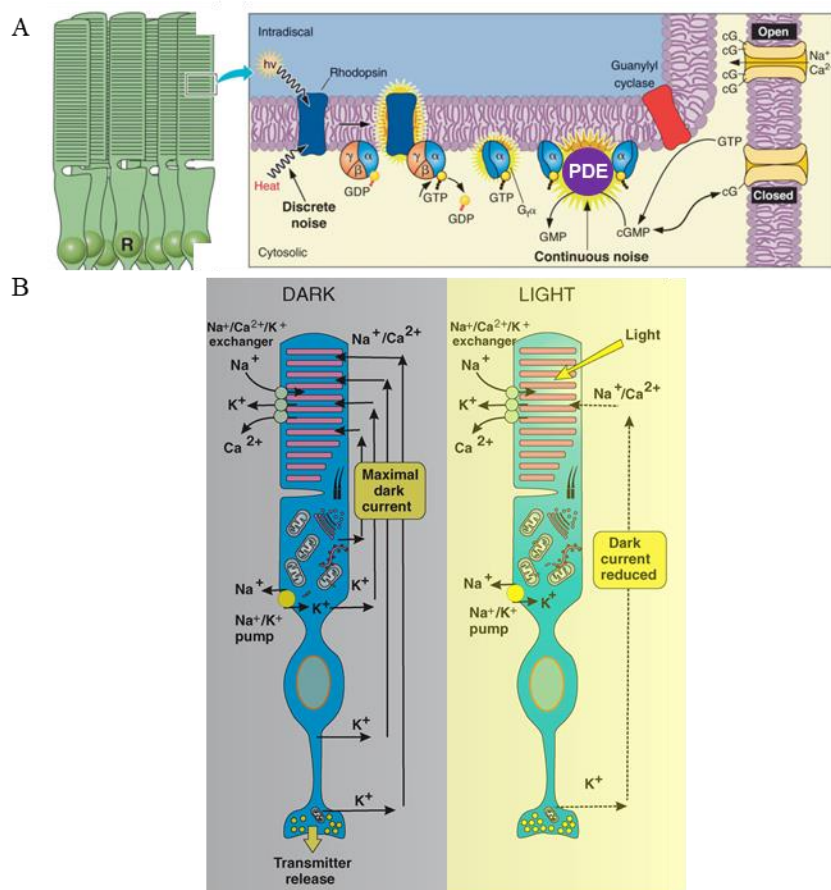
Fig. 7. Rod phototransduction and the circulating dark current. A) In rod OS, rhodopsin's chromophore 11-*cis*-retinal absorbs a photon (hv) and isomerizes to all-*trans*-retinal. This causes a conformational change in rhodopsin, now called metarhodopsin-II, that enables its activation of its associated G-protein transducin (G_t) by triggering exchange of G_t's GDP to GTP. G_t-GTP activates PDE6 and increases cGMP hydrolysis. The decrease in intracellular cGMP results in closure of cGMP-gated Na^+/Ca^{2+} (CNG) channels and hyperpolarization of the cell. This hyperpolarization in rod membrane potential closes voltage-gated calcium channels at the rod terminal (spherule), decreasing calcium-dependent vesicular glutamate release. During recovery cGMP is regenerated via activated guanylyl cyclase opening the CNG channel and re-establishing the dark current. B) (Left, dark) In the dark there is high [cGMP], and the dark current is maximized. OS CNG channels allow Na^+ and Ca^{2+} influx down its concentration gradient. OS also have $Na^+/Ca^{2+}/K^+$ exchangers that pump Na^+ in and Ca^{2+} and K^+ out remove Ca^{2+} from photoreceptors. IS Na^+/K^+ antiporters pump Na^+ out and K^+ in against concentration gradients, which reverses the passive Na^+ influx and K^+ efflux. An additional IS K^+ channel allows K^+ efflux down its concentration gradient. K^+ transport provides charge compensation. Photoreceptors are depolarized and release glutamate. (Right, light) In light increments when [cGMP] falls, OS CNG channels close, which reduces the circulating dark current, hyperpolarizes photoreceptors, and reduces glutamate release. Adapted and modified from A) Johan Pahlberg *et al. BioEssays: news and reviews in molecular, cellular and developmental biology.* 2011;33:438-447 and B) Michael J. Berridge. *Cell Signalling Biology.* 2014; 6csb0001010; doi: 10.1042/csb000101.

Bipolar Cell Signaling

Rods contact a single type of ON bipolar cell. Cones contact 7 types of cone ON bipolar cells and 5 types of cone OFF bipolar cells (Fig. 8). ON/depolarizing bipolar cells (DBCs) express the metabotropic G-protein coupled glutamate receptor mGluR6 to sense changes in glutamate. Metabotropic receptors are indirectly coupled to distinct ion channels through signal transduction typically involving G-protein signaling. OFF/hyperpolarizing bipolar cells (HBCs) express ionotropic glutamate receptors to sense changes in glutamate. Ionotropic receptors are non-selective, ligand-gated transmembrane ion channels. The two ionotropic receptors in OFF bipolar cells are AMPA and kainate receptors, which are activated by α-amino-3-hydroxyl-5-methyl-4-isoxazole-propionate (AMPA) and kainic acid (kainate), respectively. Like photoreceptors, bipolar cells also use a ribbon synapse for glutamate release (13).
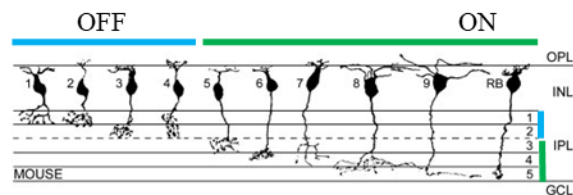
Fig. 8. Schematic diagram of bipolar cells in the mouse retina. Contrast inverted, confocal micrographs of mouse retinal bipolar cell types 1-9 and rod ON bipolar cell from vertical slices following Lucifer yellow/neurobiotin intracellular injection. OFF (types 1-4; blue) and ON (types 5-9, rod bipolar cell; green) bipolar cells differentially extend their axons into the OFF and ON sublamina of the IPL, respectively. OFF type 3 cone bipolar cells include types 3a and 3b. ON type 5 cone bipolar cells include types 5a and 5b. Adapted and modified from Krishna Ghosh *et al. J. Comp. Neurol.* 2004;469:70-82.

In ON bipolar cells, glutamate binds to mGluR6 and closes the cation channel TRPM1, which hyperpolarizes the cell (17). The fact that photoreceptor depolarization, which results in glutamate release, leads to ON bipolar cell hyperpolarization is an example of a sign-inverting synapse. At light increments, photoreceptors hyperpolarize, decreasing synaptic glutamate. This inactivates mGluR6, opens TRPM1, and depolarizes the cell. In direct contrast, glutamate opens OFF bipolar cell ionotropic receptors, and they depolarize. The fact that photoreceptor depolarization leads to OFF bipolar cell depolarization is an example of a sign-conserving synapse. At light increments, the lack of glutamate closes ionotropic

receptors and hyperpolarizes OFF bipolar cells (17). Thus, light decrements hyperpolarize ON bipolar cells and depolarize OFF bipolar cells whereas light increments depolarize ON bipolar cells and hyperpolarize OFF bipolar cells (Fig. 9). Bipolar cells then transmit these excitatory signals to retinal ganglion cells for downstream signal processing.
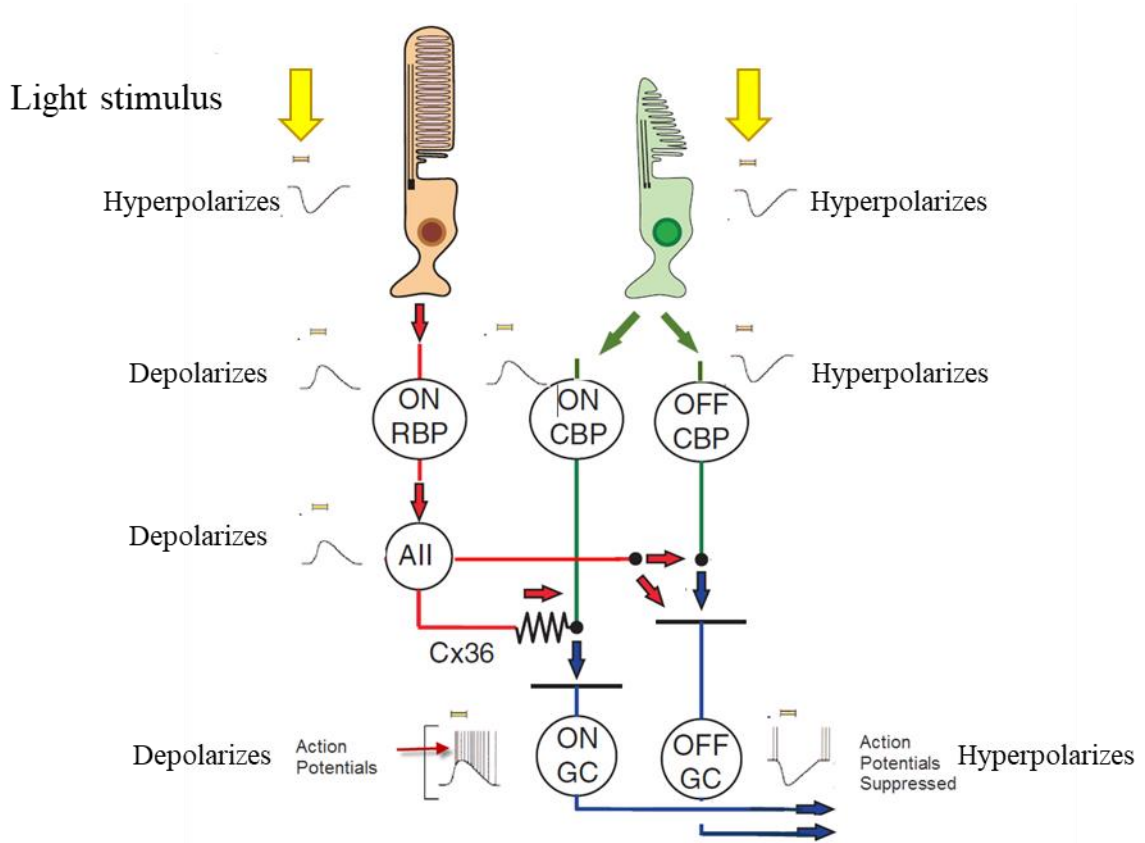
Fig. 9. Schematic of retinal circuitry showing sign-conserving and sign-inverting synapses. Sign-conserving synapses demonstrate the pre-synaptic input generates the equivalent sign of post-synaptic response, *i.e.* hyperpolarization yields hyperpolarization and the converse is true for depolarizing inputs. Sign-inverting synapses demonstrate the pre-synaptic input generates the opposing sign of post-synaptic response, *i.e.* hyperpolarization yields depolarization and the converse is true for depolarizing inputs. Rod (peach) and cone (green) photoreceptors provide sign-inverting input to rod ON (ON RBP) and cone ON (ON CBP) bipolar cells, but cones provide sign-conserving input to cone OFF (OFF CBP) bipolar cells. Rod ON bipolar cells provide sign-conserving input to amacrine AII cells (AII). ON and OFF bipolar cells provide sign-conserving input to ON and OFF retinal ganglion cells (ON GC, OFF GC), respectively. AII cells provide sign-conserving input to ON GCs but provide sign-inverting input to OFF GCs.

In darkness, rods release glutamate that binds to and activates mGluR6. Active mGluR6 regulates the TRPM1 cation channel through a G-protein complex signaling cascade dependent on the intermediary trimeric G-protein complex comprised of $G\alpha_o\beta_3\gamma_{13}$ subunits. This also involves a GAP complex consisting of the 2 regulators of G-protein signaling (RGS) protein complexes, RGS7 and RGS11, and the 2 adaptor protein membrane anchor subunits, the RGS anchor protein R9AP and the orphan receptor GPR179 (Fig. 10). The GAP complex greatly enhances the slow kinetics of $G\alpha_o$'s spontaneous GTP hydrolysis [18]. The RGS7/RGS11 double knockout [19,20], GPR179 knockout [21], and $G\beta 5$ knockout [22] mouse models all exhibit a lack of ON bipolar cell function to light, demonstrating the importance of the GAP complex in mGluR6-mediated signaling. The current model proposes that RGS11 exclusively interacts with R9AP, and R9AP also directly interacts with GPR179 [23]. GPR179 also interacts with $G\beta 5$ and RGS7 [24]. These proteins are responsible for converting GTP to GDP on $G_{\alpha 0}$ [21]. The mechanism of TRPM1 gating is still debated. One model proposes that active mGluR6 activates $G_{\alpha o}$ to bind and close TRPM1. A second model proposes that mGluR6 directly regulates TRPM1's state independent of $G_{\alpha o}$ [25]. It is also possible that TRPM1 gating may require nyctalopin.
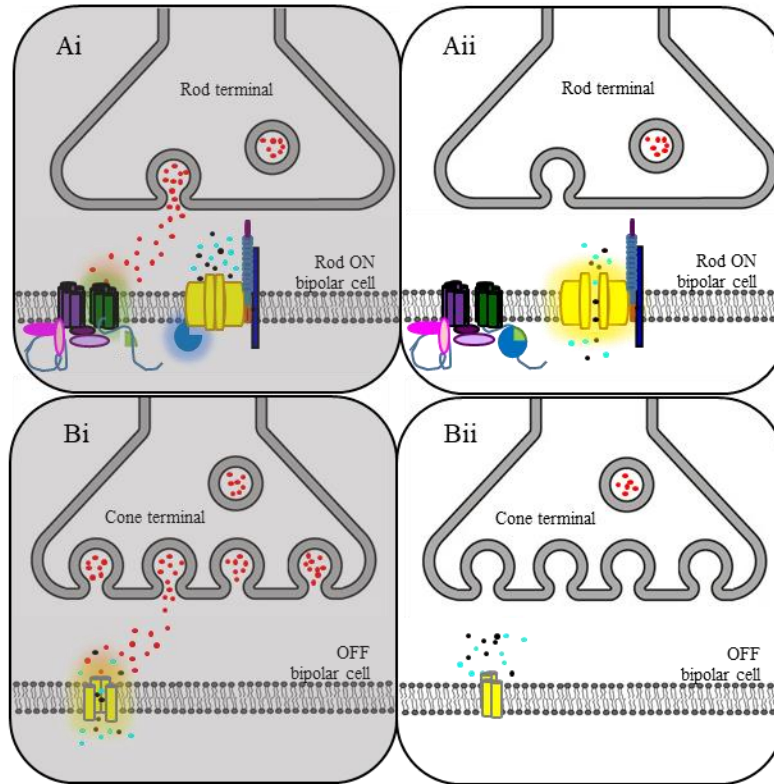
Fig. 10. Schematic diagram of bipolar cell signaling in the mouse retina. A) Rod to rod ON bipolar cell signaling. The same signaling occurs at cone to cone ON bipolar cell synapses. Ai) Light decrements (gray shading) cause photoreceptor depolarization, which opens voltage-gated calcium channels. Calcium influx causes glutamate (red) release sensed by the ON bipolar cell G-protein coupled receptor mGluR6 (green). GDP to GTP exchange activates and dissociates the G-protein $G\alpha_0$ subunit from the $G_{\beta\gamma}$ subunit to bind and close the TRPM1 channel (yellow), inhibiting sodium and calcium cation influx (light blue and black circles) and holding the ON bipolar cell in a hyperpolarized state. Aii) Light increments cause photoreceptor hyperpolarization, which closes calcium channels and inhibits glutamate release. mGluR6 is inactivated, and TRPM1 opens, allowing cation influx causing ON bipolar cell depolarization. B) Cone to cone OFF bipolar cell signaling. Bi) Light decrements cause photoreceptor depolarization resulting in glutamate release. G-protein coupled AMPA and kainate receptors (yellow) bind glutamate, which opens them as ion channels to allow cation influx and OFF bipolar cell depolarization. Bii) Light increments cause photoreceptor hyperpolarization, which inhibits glutamate release. AMPA and kainate receptors are inactivated, and OFF bipolar cells hyperpolarize. GPR179 (purple GPCR), $G\beta 5$ (dark pink oval), RGS7 (light pink oval), R9AP (dark purple oval), RGS11 (light purple oval), $G\alpha_0$ subunit (blue pacman), $G_{\beta\gamma}$ (green quarter circle), Nyctalopin (stacked multicolored cylinder), and LRIT3 (dark blue cylinder).

15

TRPM1 knockout mice exhibited a lack of ON bipolar cell function evidenced by a no b-wave (nob) electroretinogram (ERG) phenotype (26-28), illustrating TRPM1 is indispensable for ON bipolar cell responses. Discovered in *D. melanogaster,* TRPM1 belongs to the transient receptor potential (TRP) family of proteins and was the first member of the TRP melanoma-related subfamily (TRPM) (29). TRPM1 is one of eight TRPM proteins identified in humans and mice. It had also been suggested that TRPV1 might be the cation channel in ON bipolar cells. However, this hypothesis was found to be incorrect in a 2009 study by Shen *et al.* that demonstrates normal b-waves in TRPV1 knockout mice ERGs (27). Because TRPM1 knockout mice exhibited the *nob* ERG phenotype, Li *et al.* screened CSNB patients and identified one recessive TRPM1 mutation (IVS16+2T>C) and four likely disease-causing TRPM1 mutations (c.412delG p.G138fs, c.3105T>A p.Y1035X, c.220C>T p.R74C, and c.3004A>T p.I1002F) (30). Additionally, a recent study identified fourteen missense, splice-site, deletion, or nonsense mutations in TRPM1 for 10 unrelated patients (70+ *TRPM1*: c.31C>T p.Gln11X, c.215A>G p.Tyr72Cys, c.296T>C p.Leu99Pro, c.428-3C>G p.splice defect, c.1197G>A p.Pro399Pro splice defect, c.1418G>C p.Arg473Pro, c.1622T>A p.Met541Lys, c.2322T>A p.Tyr774X, c.2567G>A p.Trp856X, c.2634+1G>A p.splice defect, c.3094G>T p.Glu1032X, c.3491delA p.Gln1164ArgfsX31, c.3834C>T p.Asn1278Asn; 92+ *TRPM1*: c.40C>T p.Arg14Trp) (31). A second study identified 2 deletions (chr15:31355203-31391647del and c.83delA p.Asn28MetfsX62), 3 substitutions (c.220C>T p.Arg74Cys, c.296T>C p.Lys99Pro, c.1091T>G p.Leu364Arg), 2 missense (c.1600G>A p.Gly534Arg and c.1832C>T p.Pro611His), and 2 splice-site (c.3061+1G>A and c.3142G>A) mutations in TRPM1 for 6 patients some of whom exhibited heterozygous compound mutations (32). A third study identified 2 splice-site (IVS2-3C>G and IVS8+3_6delAAGT), 1 nonsense (c.2645C>A p.S882X), and 2 missense (c.1870C>T p.R624C and c.3224T>C p.F1075S) mutations in TRPM1 of 5 patients (33).

Horizontal Cells

When photoreceptors hyperpolarize, horizontal cells also hyperpolarize. Thus, horizontal cell interneurons receive light-evoked glutamatergic input from photoreceptors in a sign-conserving synapse. Hyperpolarized horizontal cells provide photoreceptor feedback and bipolar cell feedforward inhibition. The mechanism underlying this lateral inhibition is currently controversial. Rods contact horizontal cell

axons whereas cones contact horizontal cell dendrites. Horizontal cells receive input from several photoreceptors and other horizontal cells (34). The input field is referred to as a receptive field (Fig. 10A). Horizontal cells have a large receptive field because of connexin57-dependent gap junctions forming electrically coupled horizontal cell networks. The ability to receive this wide field of input and negatively feedback onto photoreceptors in the horizontal cell receptive field surround allows them to directly create the center-surround properties of bipolar cells (Fig. 11A). When photoreceptor hyperpolarization triggers horizontal cell hyperpolarization, the photoreceptor calcium current activation curve undergoes a left shift to a more hyperpolarized potential, increasing glutamate release. Three hypotheses are currently debated concerning the underlying mechanism(s) of photoreceptor feedback: the ephaptic, pH, and GABA hypotheses (Fig.11B-C) (9,35).
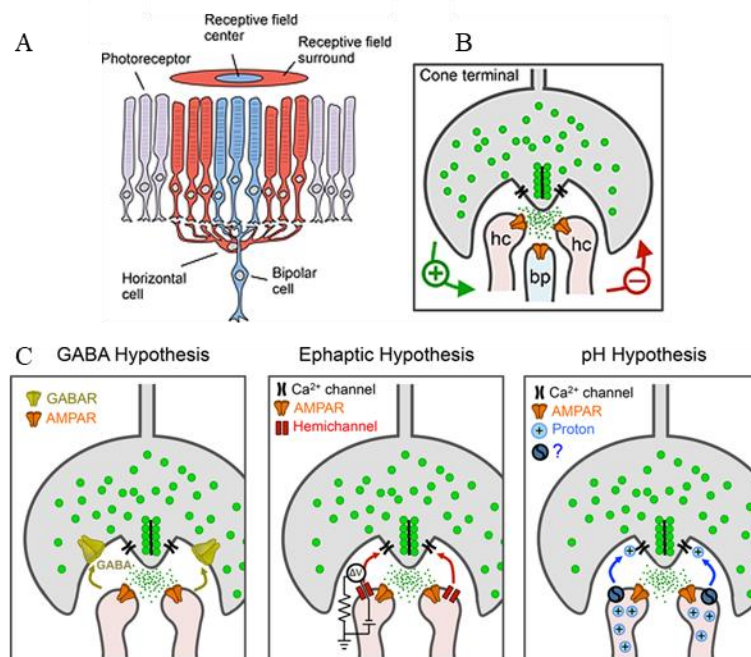
Fig. 11. Schematic diagrams of horizontal cell lateral inhibition in the vertebrate retina. A) Several photoreceptors in the receptive field center (blue spot) and surround (red spot) input information to horizontal cells that feed back onto receptive field center photoreceptors (blue photoreceptors). This generates the antagonistic receptive field surround. B) The cone to horizontal cell sign-conserving synapse modulates feedback inhibition. C) Cones release glutamate (green) to activate horizontal cell AMPA receptors (orange). Horizontal cells feed back onto cones via GABA release, the ephaptic mechanism, or pH changes in the synapse. Adapted and modified from Richard H. Kramer *et al. PLoS Biol.* 2015;13:e1002322.

The ephaptic hypothesis proposes that horizontal cell connexins form large ion hemi channels between cells to create an interconnected network (34). During hyperpolarization when horizontal cells experience a local reduction in membrane potential at their hemichannels, the local synapse becomes slightly more negative than the surrounding extracellular space. Photoreceptor calcium channels sense this local negative potential, which shifts their calcium current activation curve leftward (35). This leftward shift activates voltage-dependent calcium channels, resulting in photoreceptor depolarization. Although the ephaptic mechanism has been shown to shift the calcium activation currents in turtles (36), newts (37), salamanders (38), goldfish (39), zebrafish (40,41), and mice (42), it is unclear if it alone can explain the changes in cone activating calcium currents (43).

The pH hypothesis proposes that horizontal cells modulate the photoreceptor calcium current activation curves by changes in proton concentration. In light decrements, depolarized horizontal cells increase the synaptic proton concentration beyond the extracellular buffering capacity. Protons accumulate in and acidify the synapse, which shifts the calcium current activation curve rightward in cones. In light increments, protons are depleted from and alkalize the synapse (34). Synaptic alkalization, like the ephaptic potential difference, shifts the calcium current activation curve leftward to stimulate photoreceptor depolarization (9,35). The protons have been hypothesized to come from several sources not limited to ATP hydrolysis, proton pumps, proton/bicarbonate permeable channels, and protons released with photoreceptor glutamate (43,44). No study to date has clearly identified the proton source(s) (43).

The GABA hypothesis suggests that photoreceptor hyperpolarization stimulates horizontal cell GABA release into the synaptic space whereby photoreceptors undergo a net depolarization and are inhibited. Data examining this hypothesis demonstrate that GABA-dependent feedback is slow compared to ephaptic and pH-mediated feedback (45,46). The GABA hypothesis has been shown to modulate horizontal cell feedback in newts (37) and salamanders (47) but exhibits no consistent effects in the macaque retina (48). In mice this mechanism is thought to act indirectly through ephaptic or pH-mediated feedback because $GABA_A$ receptors are not found in mouse cones (46). While experimental data support the GABA hypothesis, there are stronger data implicating the ephaptic and pH mechanisms (9,35). It is still possible that the GABA mechanism is a modulator for the ephaptic and pH mechanisms (44,45).

The horizontal to bipolar cell feedforward inhibitory mechanism is much less studied than its feedback inhibition. Hyperpolarized horizontal cells are thought to release GABA sensed by GABA receptors on bipolar cell dendrites. Salamander studies show that GABA receptor antagonists do not prevent horizontal cell surround inhibition (49), but they do in mice (50). This suggests that the GABA hypothesis may be species-specific. Horizontal cell hyperpolarization-induced GABA release is also thought to disrupt the differential bipolar cell chloride gradients that would hyperpolarize ON but depolarize OFF bipolar cells (51). Each bipolar cell type expresses different chloride transporters where ON bipolar cell chloride equilibrium potentials are more depolarized (51).

Amacrine Cells

Amacrine cells are retinal interneurons that provide lateral inhibition within the IPL. More than half of the cells in the mouse retina are amacrine cells (52). Amacrine cells act on bipolar, ganglion, and other amacrine cells. Amacrine cells are the most diverse retinal cell type, and more than 40 types have been identified in the mouse retina (9,53). Amacrine cells modulate their presynaptic glutamatergic bipolar cell input to provide inhibition. Amacrine cells deliver feedback inhibition to bipolar cells and feedforward inhibition to ganglion cells. Amacrine cells can also laterally inhibit other amacrine cells. Amacrine cell feedback is modulated by release of the inhibitory neurotransmitters GABA or glycine. These inhibitory mechanisms together shape the spatiotemporal features of inner retinal neurons. Amacrine cell types are not restricted to connect to only one type of ganglion cell. A study done by Helmstaedter *et al.* reconstructed the mouse IPL, and the resulting connectivity matrix demonstrated that several amacrine cell types connect to many different amacrine and ganglion cell types (54). Some amacrine cells uphold the convention that neurons release one fast and one modulatory neurotransmitter (55). A specific amacrine cell, the starburst amacrine cell, defies the convention because it releases two fast neurotransmitters, inhibitory GABA and excitatory acetylcholine (56).

Retinal Ganglion Cells

Bipolar and amacrine cells are pre-synaptic to retinal ganglion cells, which are the output neurons of the retina. Ganglion cell axons converge at the optic nerve head and transmit their signals to the brain.

There are reports with up to 32 ganglion cell types in mice of which at least 18 can be morphologically distinguished (57,58). It is likely that combinations of expressed molecular markers and structural information will be required to discriminate all ganglion cell types (53).

All bipolar cell glutamatergic input to retinal ganglion cells at the IPL are examples of sign-conserving synapses. When a retinal ganglion cell depolarizes beyond its threshold, it generates an all-or-none action potential known as a spike. ON ganglion cells depolarize in response to ON bipolar cell input. Likewise, OFF ganglion cells depolarize in response to OFF bipolar cell input. ON/OFF ganglion cells depolarize in response to the combination of ON and OFF bipolar cell input. Thus, ganglion cells are divided into ON, OFF, and ON/OFF functional classes. These common functional classes are differentiated by their center surround responses specifically being named for their responses at center stimuli. ON ganglion cells respond to a light increment presented to their centers but are inhibited to a center light decrement (Fig. 12C). This is similar to the way an ON bipolar cell responds to light increments. Thus, ON cells respond to center "light on" stimuli. Similarly, OFF ganglion cells are inhibited when light is presented to their centers but instead exhibit a center response to a light decrement. This is akin to OFF bipolar cell responses. OFF cells respond to center "light off" stimuli. ON/OFF ganglion cells respond to both light increments and decrements presented to their centers.

Retinal ganglion cell responses to stimuli presented to their surrounds are typically the opposite of their center responses (Fig. 12A-B). For example, ON ganglion cells are hyperpolarized/inhibited by light increments presented to their surrounds, but OFF ganglion cells are depolarized/excited by light increments presented to their surrounds. The center surround response organization of ganglion cells functions to emphasize edges.
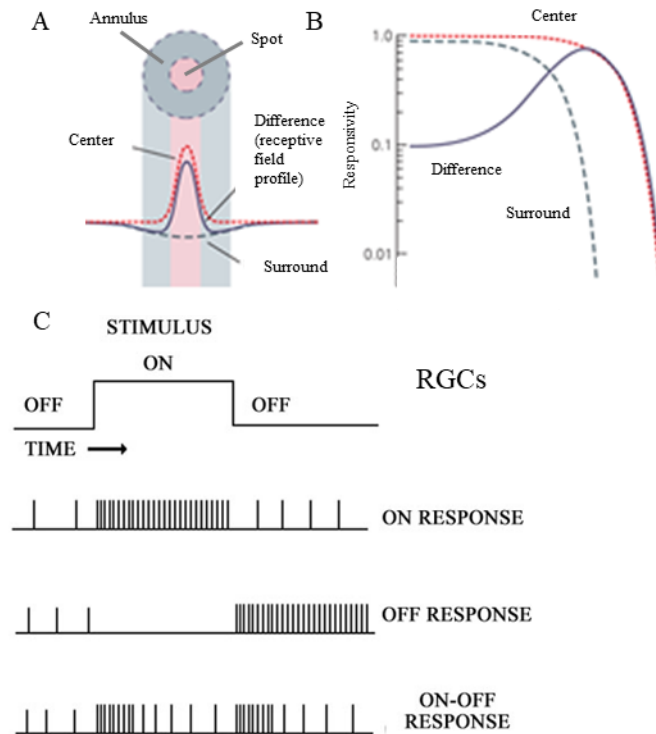
Fig. 12. Schematic diagrams of the ON ganglion cell center surround receptive field. A and B) When a small spot of light (pink) is presented to an ON ganglion cell, the response (red dotted line) generates an action potential. When the outer circular rim of light, or annulus (blue), is presented to an ON ganglion cell, there is no response (blue dotted line). When a larger spot of light is presented to an ON ganglion cell, the response (solid blue line) generates an action potential that is equal to the difference of the agonistic center and antagonistic surround. C) Schematic showing light stimulus onset and offset with corresponding ON, OFF, or ON/OFF responses in retinal ganglion cells (RGCs) indicated by several temporally close vertical spikes. Adapted and modified from A and B) Eric R. Kandel *et al. Principles of Neuroscience,* 5th Ed. McGraw Hill. 2013. C) University of Calgary, "Module 2: The Visual System – Coding." http://www.ucalgary.ca/pip369/mod2/retina/coding.

Within functional classes there are transient and sustained types, which describes the duration of the response. Transient responses exhibit a prominent, sharp peak that decays quickly to baseline. Sustained responses exhibit a sharp peak that declines slightly and plateaus until the stimulus changes.

These functional classes are also differentiated by the IPL sublamina into which their dendrites extend. ON ganglion cells receive input from ON bipolar cells in the ON sublamina of the IPL. OFF ganglion cells receive input from OFF bipolar cells in the OFF sublamina of the IPL. ON/OFF cells are bistratified cells, meaning their dendritic arbors extend into both IPL sublamina. Ganglion cells can further

be classified according to their responses to contrast, frequency, receptive field size, response latency (the time from stimulus to response onset) (59), and motion sensitivity. Each ganglion cell type contributes a specific visual feature in their signal transmission to the brain.

Multiple Vertical Signaling Pathways Arise from Parallel Channels in Interneuron Cell Wiring

Photoreceptor wiring to post-synaptic neurons has been shown to result in the formation of the primary, secondary, and tertiary pathways. The primary visual pathway is the rod to rod ON bipolar cell to amacrine AII cell to cone ON and OFF bipolar cell to ganglion cell pathway where amacrine AII cells provide sign-conserving and -inverting input to cone ON and OFF bipolar cells, respectively. The secondary visual pathway is the rod to cone to cone ON bipolar cell to ganglion cell pathway that functions via connexin36-dependent rod-cone gap junctions that activate cones downstream of light-induced rod activation. An additional tertiary visual pathway is defined as the rod to cone OFF bipolar cell to ganglion cell pathway (60). These parallel pathways create multiple avenues of signaling for the incident photons.

Retinal Support Neurons

Neurons are supported by three types of supporting cells: two macroglial cell populations, Müller glia and astrocytes, and microglia. First identified by Heinrich Müller, Müller glia are the most abundant and span the entire retina with their cell bodies localized to the INL (61). Müller glia maintain the retinal physiological environment by regulating the extracellular milieu and impacting processes such as glutamate uptake and insulation of the electrochemical signals from retinal neurons. Astrocytes cover blood vessels in the INL along with Müller glia where together they form the retinal blood barrier. The majority of astrocytes reside in the nerve fiber layer (61). Astrocytes also help preserve the delicate ion balance of the retina, which is critical to retinal signal transmission. Microglia are support cells that secrete neurotrophic factors and can be activated into neuron-specific macrophages with neurotrophic or neurotoxic functions (62).

Mutations in Critical Retinal Proteins Cause Congenital Stationary Night Blindness

Mutations in genes encoding proteins critical for visual signaling can lead to a disease state. Congenital stationary night blindness (CSNB) refers to a group of clinically and genetically variable, non-progressive (stationary) disorders of the retina (63). The phenotypic effects of the disorder typically but not always include decreased visual acuity, impaired visual adaptation in the dark, refractive error seen as myopia (or rarely, hyperopia), nystagmus, strabismus (misalignment of the eyes), and normal fundus morphology. Diagnosis is assessed by ERG, family history, and genetic screening for all known CSNB-causing mutations. CSNB exhibits near complete penetrance although its frequency is unknown.

CSNB can be subcategorized into two types by the noninvasive standard flash ERG, which measures alterations in the measured a- and b-waves corresponding to photoreceptor hyperpolarization and ON bipolar cell depolarization, respectively (Fig. 13) (64).
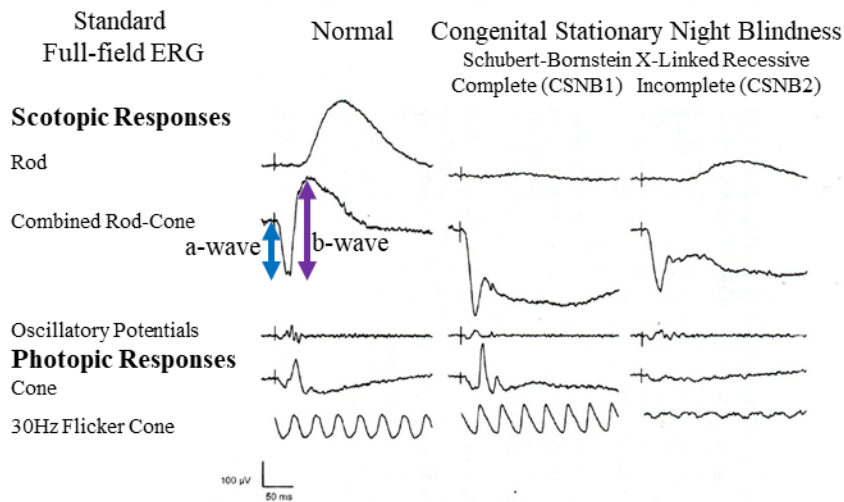
Fig. 13. Representative human electroretinograms for normal and Schubert-Bornstein congenital stationary night blindness for complete/CSNB1 and incomplete/CSNB2. The negative a-wave (blue line) indicates photoreceptor hyperpolarization, which can be rod, cone, or both depending on low or high intensity scotopic or photopic conditions. The positive b-wave (purple line) indicates ON bipolar cell depolarization. The incomplete form exhibits residual rod function. Adapted and modified from Taylor & Francis. *Electrophysiology of Vision*, ISBN: 0-8247-4068-8, Bryan Lam, 2005.

The first of these two CSNB types is Riggs, which is defined by the reduction or absence of the dark adapted a-wave, indicating rod dysfunction. Riggs type CSNB patients also exhibit a comparatively reduced dark-adapted b-wave. Riggs type CSNB is seen with mutations in the guanine nucleotide binding protein, alpha transducin 1 gene encoding GNAT1 (65,66). It is also seen in patients with mutations in *Rho, Pde6b,* and *Slc24A1* (64,67).

A second type is Schubert-Bornstein, which is defined by the absence or reduction of both the dark- and light-adapted b-wave (no b-wave [nob]) and a normal a-wave. The Schubert-Bornstein phenotype indicates abnormal synaptic function and is subgrouped into complete/type I (cCSNB) or incomplete CSNB/type II (iCSNB).

iCSNB is defined by a normal a-wave but partial b-wave in the scotopic ERG and markedly reduced b-waves in the photopic ERG. This is due to the impairment of both rod and cone signaling because of defective pre-synaptic function. iCSNB patients have some degree of scotopic rod function present (64). Because iCSNB affects rod and cone signaling, there is typically a greater loss in visual acuity, causing increased visual restrictions compared to those with cCSNB. iCSNB is known to exhibit an autosomal recessive (*Cabp4, Cacna2d4*) or x-linked recessive (*Cacna1f*) mode of inheritance (68,69).

cCSNB is characterized by the complete absence of the ERG b-wave. This is caused by absence of a functional ON bipolar cell signaling cascade resulting in defective post-synaptic responses. The known modes of inheritance for cCSNB are x-linked (*Nyx)* and autosomal recessive (*Grm6, Trpm1, Gpr179, Lrit3)* (25,30-32,63,70-87).

Leucine-Rich Repeat Proteins Are Critical to Retinal Function

Mutations in three leucine-rich repeat (LRR) proteins, NYX, ELFN1, and LRIT3, are known to cause CSNB. The *nyx* gene encodes the protein nyctalopin, which was the first LRR protein identified for its critical role in the retina (72,88). Pardue *et al.* identified a spontaneously occurring *nob* mouse mutant (89). Gregg *et al.* later showed that the underlying cause of the *nob* ERG resulted from an 85bp deletion in the *Nyx* gene (72) located on the X chromosome (88). Together, these data suggest NYX is required for synaptic transmission from photoreceptors to ON bipolar cells. This was confirmed in a later study where

exogenous addition of glutamate to *nob* ON bipolar cells did not elicit a response whereas *nob* OFF bipolar cells responded normally (63). *In situ* hybridization experiments localized *Nyx* expression to the INL in the human and mouse (71,72). Early efforts to characterize the function of NYX determined that comparison of normal and *nob* mice demonstrated no alteration in rod bipolar cell morphology and no changes in the localization of known pre- and post-synaptic retinal markers mGluR6, $G_{\alpha 0}$, bassoon, PSD95, CACNA1F, trkB, β-dystrophin, and dystroglycan (90). This suggests NYX is not required for normal localization of these proteins. After TRPM1 was identified as the cation channel required for light-evoked ON bipolar cell response in the retina (27,28,91), experimental data from Pearring *et al.* revealed a direct interaction between NYX and TRPM1. Pearring *et al.* also showed the absence of NYX expression in the *nob* mouse results in a loss of TRPM1 expression at ON bipolar cell dendritic tips (73). Bojang *et al.* performed a topological analysis and found that murine NYX does not dimerize when expressed in yeast, its LRR domain is exclusively extracellular, and has one transmembrane domain in contrast to GPI-anchored human NYX (92,93). These findings suggest that NYX's mechanism of anchoring to the membrane is unimportant but implicates its LRR structure may be directly involved in the formation of the ON bipolar cell signaling complex.

A later study revealed the abnormal spontaneous activity and light-evoked responses in *nob* ganglion cells compared to normal ganglion cells and confirmed the normal retinal morphology in the *nob* mouse (63). This suggests the loss of NYX affects synaptic signaling but not synaptic assembly. By creating a transgenic bipolar cell-specific EYFP-nyctalopin mouse model, Gregg *et al.* were able to completely rescue the *nob* phenotype to restore normal outer and inner retinal function while confirming the ON bipolar cell-specific expression pattern of NYX (63).

Pearring *et al.* noted that murine NYX contains only 3 intracellular amino acids and human Nyx is wholly extracellular from which they hypothesized the requirement for an additional transmembrane protein involved in the intracellular scaffolding of the NYX/TRPM1 complex (73). A later whole exome sequencing study in cCSNB patients who did not exhibit known cCSNB mutations identified a novel candidate that may provide a scaffold for the NYX/TRPM1 interaction: leucine-rich repeat, immunoglobulin-like, and transmembrane domain 3, or LRIT3 (79). Follow-up studies localized LRIT3 expression to the OPL in normal mice and showed the *nob* ERG phenotype in *Lrit3^{nob6}* mutant mice. They

showed the loss of LRIT3 and TRPM1 in all *Lrit3^nob6* bipolar cells, suggesting LRIT3 is involved in the localization of TRPM1 like NYX (78). These studies also showed the loss of mGluR6, GPR179, RGS7, RGS11, Gβ5, and PNA staining in cone bipolar cells (77). At the ganglion cell level, the *Lrit3^nob6* mutation abolishes the ON ganglion cell response and confers a delayed OFF ganglion cell response. However, their data show only 2-3 *Lrit3^nob6* OFF ganglion cells with a response latency of greater than 0.5 seconds. These studies determined the importance for LRIT3 in the retina.

A third LRR protein extracellular leucine rich repeat and fibronectin type III domain containing 1 (ELFN1) was identified as a novel mGluR6 interactor in a proteomics screen. ELFN1 was shown to be necessary for synaptic assembly of rod to rod ON bipolar cells (94). mGluR6 and ELFN1 were singly transfected but co-cultured in HEK293T cells and formed a *trans* complex, suggesting a direct interaction (94). The ELFN1 knockout mouse ERGs showed preserved scotopic and photopic a-waves and photopic b-wave while ablating the scotopic b-wave. This suggests that ELFN1 contributes to rod-selective synaptic signaling (94). Electron microscopy revealed a distinct absence of rod ON bipolar cell dendrites at rod synapses and disruption of horizontal cell contacts with rods in the ELFN1 knockout mice. These data suggest that rather than ELFN1 affecting synaptic signaling, ELFN1 affects rod to rod ON bipolar cell synaptic assembly, which when disrupted would lead to measurable signaling deficits (94).

Together these previous studies establish the functional importance for the LRR proteins in the retina: NYX and LRIT3 in photoreceptor to ON bipolar cell synaptic signaling and ELFN1 in rod to rod ON bipolar cell synaptic assembly.

The Leucine-Rich Repeat Domain

The LRR domain with concave and convex faces consists of anywhere from 2-45 tandem LRR motifs. Each motif contains a 20-30 amino acid stretch with a highly conserved N-terminal LxxLxLxxN/CxL sequence first identified in the human α2-glycoprotein (92). In these motifs leucine and asparagine residues can be replaced with hydrophobic residues. Further, the N-terminus forms the β strand and looping region where each motif contributes one β strand to the LRR domain's parallel β sheet region on the concave, or inner, face (92). The concave face of LRR domains has been shown to provide a large

inner binding surface for ligands, which was demonstrated and confirmed in crystallographic studies (95-97).

In comparison with the LRR motif's N-terminus, the helical C-terminus of each motif is more highly varied in its secondary structure. The C-termini of each LRR form the convex, or outer face, of the domain. Because of the alternating β strands with helical regions, LRR domains form a non-globular classic arc or horseshoe-shaped structure also known as a solenoid structure (Fig. 14). The length and number of LRR motifs within the LRR domain dictate the length and angle of curvature of the specifically formed arc structure of any LRR protein. Variation in LRR length and curvature contributes to its ability to bind a variety of ligands in LRR protein/protein interactions.
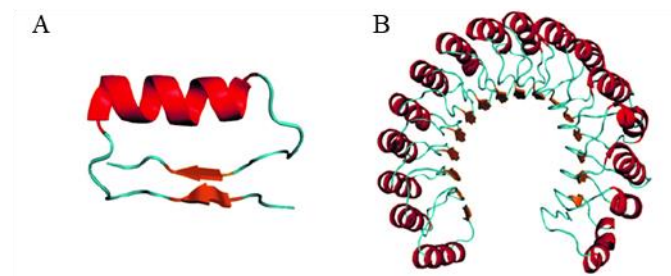
Fig. 14. LRR domain ribbon structure. A) Individual LRR motif from ribonuclease inhibitor. B) Ribbon structure of porcine ribonuclease inhibitor's LRR domain. A and B) A right-handed β strand (orange) is connected to the α-helical region (red) via a loop region (teal). α-helix enriched LRR domains have a more defined curvature. Adapted and modified from Joris de Wit *et al*. *Annu. Rev. Cell. Dev. Biol.* 2011;27:697-729.

Leucine-Rich Repeat Immunoglobulin-like Transmembrane Domain Protein 1 (LRIT1)

The LRR protein family in humans contains 375 members exhibiting diverse structures and functions in the development and differentiation of the mammalian nervous system (98-100). Ng *et al.* used a semiautomated method to cluster LRR proteins based on LRR classes using hidden Markov models combined with pattern-matching algorithms to predict secondary structures and irregular LRRs to yield a within-class LRR sequence similarity (99). They found 7 distinct classes: bacterial (S), ribonuclease inhibitor-like (RI), cysteine-containing (CC), SDS22, plant-specific (PS), typical (T), and Treponema pallidum (Tp). This model shows NYX, ELFN1, and LRIT3 all belong to the extracellular/transmembrane

cluster. LRIT3's closest relatives are LRIT1 and LRIT2 (Fig. 15). Murine LRIT1 is a 624 residue membrane-embedded protein containing an N-terminal LRR domain, 5 internal LRR domains, a C-terminal LRR domain, an immunoglobulin G-like domain, a fibronectin type III domain, and a transmembrane domain with an intracellular C-terminus. Murine *Lrit1* also encodes a signal sequence that yields a single pass type I transmembrane protein.

In the only published paper specifically addressing LRIT1, Gomi *et al.* showed increasing *Lrit1* expression via *in situ* hybridization in the developing rat retina and LRIT1 expression in the rat photoreceptor OS using immunofluorescence microscopy and immunogold particle-labeled electron microscopy (101). Importantly, *Lrit1* was not expressed in ten other assayed tissues, indicating it is retinal-specific. Gomi *et al.* did not attempt to characterize the function of LRIT1 in the retina (101). Taken together, these data suggest LRIT1 may play an important role in retinal function and/or structure.

The goal of my dissertation project is to characterize the impact of the loss of LRIT1 on mouse retinal structure and function. To achieve this, we created an *Lrit1*^{-/-} mouse model using the CRISPR/Cas9 system. I characterized the functional phenotypes using electroretinography and multi-electrode array experiments. The expression pattern of LRIT1 was assessed using RNA *in situ* hybridization and protein immunohistochemistry. The role of LRIT1 in retinal structure was examined using retinal morphology and morphometry.
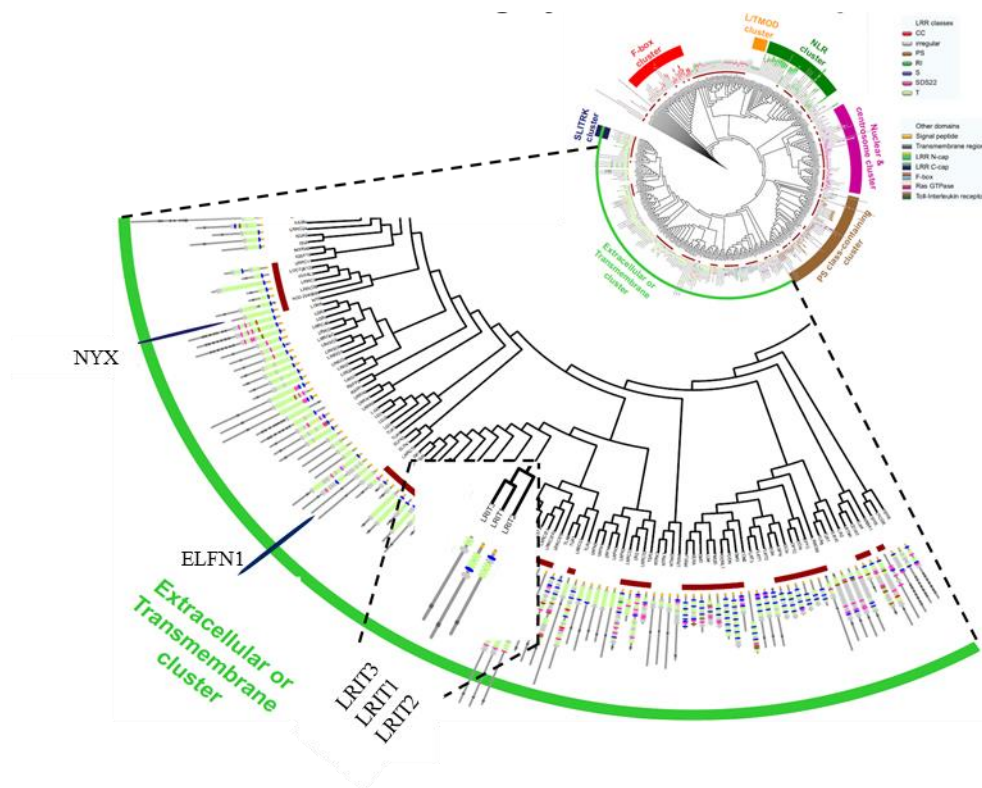
Fig. 15. LRR protein clustering by class composition. NYX, ELFN1, LRIT3, LRIT1, and LRIT2 all fit into the extracellular or transmembrane LRR cluster. Adapted and modified from Ng *et al. PNAS*. 2011;108:4631-8.

Using CRISPR/Cas9 to Generate Genetically Modified Mouse Models

CRISPR stands for clustered regularly interspaced short palindromic repeats. These arose first in Archae and later in bacteria for defense of viral infection or invasion. CRISPR comes from tandem repetitive sequences with short spacer sequences like memory devices for the sequences of past pathogens (102,103). To use CRISPR for gene editing, the system is assembled by first generating a fusion RNA: components of this are the protospacer element (also referred to as a single guide RNA or sgRNA), crRNA, linker loop, and tracrRNA. The protospacer element is a 20-nucleotide RNA complementary to one's target of interest; the crRNA is comprised of both the protospacer element and a downstream region complementary to the tracrRNA that allows for RNA secondary structure formation; the linker loop is the region between the crRNA and the tracrRNA that is not complementary to either; and the tracrRNA hybridizes to the crRNA with complementarity but also binds to the Cas9 nuclease resulting in nuclease

activation and introduction of double-strand breaks in the DNA at the sites targeted by the protospacer element (Fig. 16) (102,103). An additional requirement in the genomic DNA sequence for Cas9 binding is the protospacer adjacent motif (PAM) that must be present immediately downstream of the targeted site of interest.
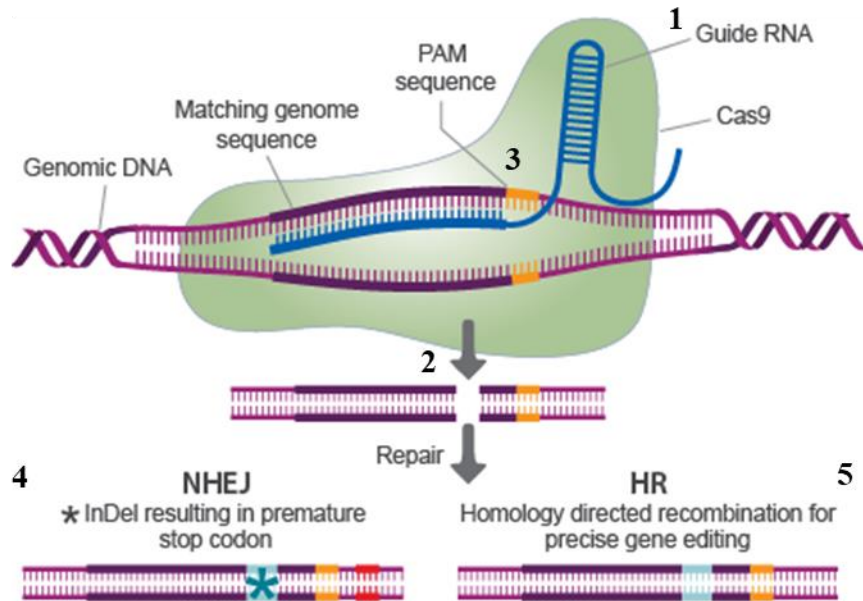
Fig. 16. Schematic of CRISPR/Cas9 gene editing system. 1) Mature CRISPR fusion RNA (blue) consisting of the protospacer element, crRNA, a linker region, and tracrRNA guides Cas9 to the target site in the gene of interest (purple). The protospacer element in the fusion RNA must be immediately followed by the PAM sequence (yellow) in the genomic DNA. 2) DNA matching the fusion RNA on one strand and its opposite strand are cut by Cas9 (gray arrows), creating a double-strand break. 3) CRISPR/Cas9-mediated DNA cleavage identifies specific targets through sequence matching of the fusion RNA and the PAM sequence located downstream of the target sequence. 4) Non-homologous end joining (NHEJ) repair results in insertions and/or deletions for knockout animal models. 5) Homology-directed repair (HR) results in recombination for knockin animal models. Adapted and modified from http://www.transomic.com/Products/CRISPR-Genome-Editing.aspx#1196d0f7-2c89-4fc0-9f4d-ed02072b5bb8,6689105.

Following induced double-strand breaks, the cell undergoes double-strand break repair, which can take one of two paths. These are homologous directed recombination (HR) and non-homologous end joining (NHEJ) (102,103). CRISPR/Cas9 induced DNA double-strand breaks undergoing HR can be used to yield knock-in models. However, when DNA double-strand breaks are repaired using NHEJ, CRISPR can induce a point mutation, insertion, or deletion, potentially resulting in a knockout model. Interestingly, NHEJ occurs at least an order of magnitude faster than HR as well as being active throughout the cell cycle with a higher capacity for DNA break repair. In NHEJ, the broken DNA ends are repaired without a homologous template, which is prone to generating mutations and critical for creating a knockout model.

The general steps in NHEJ are DNA end-binding, processing of the terminal end, and DNA ligation (104). The heterodimeric protein Ku70/80 recognizes broken DNA and binds to the ends. Ku70/80 is the scaffolding element for the DNA-dependent protein kinase and surrounds the DNA in a ring to add structural support to the broken DNA ends and prevent further degradation. This also protects other proteins from binding to the DNA before repair can be completed. Ku70/80 binding recruits the DNA-PKcs, which phosphorylates and binds to the Artemis protein. The DNA-PKcs/Artemis complex along with accessory proteins hold the DNA in a paired-end complex. Then the XRCC4/DNA ligase IV ligation complex can bind. DNA ligase IV ligates the DNA together in an XRCC4-dependent manner. XCCR4 is required to stabilize the DNA, enhance ligase activity, and direct ligase placement to the location of the DNA breaks during this process. Resulting mutations induced by the CRISPR/Cas9 system can be examined using DNA sequencing technologies combined with agarose gel electrophoresis if the mutation induces a resolvable insertion or deletion.

RNA *in situ* hybridization

RNAScope® *in situ* hybridization uses a complementary oligonucleotide target probe to bind a transcript of interest (105). The target probe is comprised of 20 double Z target probe pairs designed to specifically hybridize to one's gene of interest, but not to non-targeted molecules. The double Z target probes are synthesized such that two independent probes (from where the double Z arises) have to hybridize to the target sequence in tandem to result in signal amplification. Each target probe consists of 3 parts: a bottom 18-25 bp sequence complementary to the target mRNA, an oligonucleotide spacer region,

and a top 14 base tail sequence. When two of the Z probes hybridize in tandem, they form a 28bp sequence, all of which is required to bind the first preamplifier probe. Amplifiers then bind to different binding regions of the preamplifier probe. To achieve signal amplification specific to the mRNA target, it requires a minimum of 3 double Z probes and a maximum of all 20 pairs to bind. It is highly unlikely that two independent probes will hybridize to a non-specific target right next to each other, thus the selective amplification of target-specific signals can be ensured (105).

Electroretinography

Electroretinography (ERG) is a non-invasive assessment of the light-induced electrical response of the retina. ERGs provide an objective, quantitative measure of rod, cone, and ON bipolar cell function (106). To measure global retinal electrical activity, pupils of the examined eyes must be dilated to maximize the recorded responses and reduce the background noise to signal ratio. Further, the solution used to connect the corneal electrodes should contain methylcellulose to afford fluid viscosity and ensure better electrode connectivity in comparison to the less viscous and ion-rich saline solution. ERG recordings yield waveforms from which specific waveform components can be identified. The first, negative-going corneal a-wave corresponds to photoreceptor hyperpolarization, or closure of the OS CNG channels and minimization of the dark current, as discussed earlier in the introduction (Fig. 12). In animal models lacking an ERG b-wave, the a-wave is no longer pulled upward by the corneal positive b-wave leading the a-wave to become more negative with a deeper trough. Thus, comparisons of a-wave measurements in wild-type and nob mice can lead to the inaccurate conclusion that the a-wave is changed. Although the a-wave is often measured from baseline to the trough of the wave (106), it is more directly monitored by measuring it from baseline to the amplitude at a fixed time such as 15ms after the flash if the experimental models exhibit an ablated b-wave (107). The second, positive-going corneal b-wave corresponds to ON bipolar cell depolarization, or opening of the TRPM1 cation channels allowing cation influx into the cell. The b-wave is measured from the trough of the a-wave to the peak of the b-wave (106). Variation in these waves has been well established in specific strains of mice like the C57Bl/6J wherein the ERG b-wave mean responses ± standard deviations are $258 \pm 110\mu V$ (scotopic) and $95.7 \pm 35.8\mu V$ (photopic), respectively (108). Smaller reductions to the photoreceptor dark current measured as photoreceptor

hyperpolarization and reduced ON bipolar cell depolarization result in decreases to the ERG a- or b-waves, respectively. Several characteristic ERG phenotypes have been studied. The *nob* phenotype diagnostic of cCSNB exhibits an intact a-wave but no b-wave, indicating a lack of signal transmission through ON bipolar cells that converge on the TRPM1 cation channel (89). Retinitis Pigmentosa yields an ERG phenotype that has a decreased a-wave, indicating retinal degeneration (109). Because more than 40 visual diseases can be distinguished using the ERG alone or in conjunction with other tests, signs, and symptoms, the ERG is an invaluable, non-invasive tool by which retinal function can be examined (110,111).

Multi-electrode Arrays

Multi-electrode arrays (MEA) are a highly beneficial tool used in retinal neuroscience that affords researchers a way to perform one experiment to simultaneously capture information on the function of several ganglion cells. This information includes single cell spiking activity, spatio-temporal connectivity, and functional class type (112). The major drawback is that the sources of recorded spikes are not identified. One must sort all spikes in a principal component analysis to identify single cells. In contrast to the upstream photoreceptor and bipolar cell neurons that operate on graded potentials, ganglion cells respond via action potentials following the all-or-none principle: once the stimulus or input exceeds the cell's activating threshold, the cell will respond. A spike is the measured signal from the generated action potential commonly measured as voltage above threshold levels. In our experiments, retinal pieces are provided ten 5s light flash stimuli at each flash intensity to determine the mean ganglion cell response. Ganglion cells on an MEA may respond to either light on- or offset, which manifest as spiking and are referred to as ON or OFF responses, respectively. When a ganglion cell responds to both light on- and offset, it is called an ON/OFF cell whereas a ganglion cell that responds to neither is categorized as non-responsive. Additionally, ganglion cells may exhibit a specific absence of response phenotype characterized by a light-evoked absence of ganglion cell activity within the response time window compared to its spontaneous, or non-stimulus-evoked, activity. These ganglion cells are characterized as suppressed cells. The ganglion cell action potentials are transformed across the multi-electrode array components toward the recorded signal. The temporal aspect of ganglion cell responses is also relevant whereby normal, healthy ganglion cells respond within a short period of time if, in fact, those cells are

responsive to the applied stimulus. If ganglion cells do not respond within the time window threshold, those cells are considered to exhibit a delayed response. The choice of stimulus for an MEA experiment depends on the question being asked. One can test the spatial tuning of ganglion cells by presenting stimuli of varying spatial frequencies, which is like the visualization of sound waves of different frequencies but instead using black and white to correspond to the sound wave's peaks and troughs. One can also examine contrast tuning and center-surround receptive fields of ganglion cells by presenting stimuli of varying contrasts from white to gray to black and of various dot sizes where one can additionally vary the colors of the dots versus the colors of the surrounds.

Adeno-associated Viruses Drive Cell-Specific Retinal Gene Expression

Much of the research performed by retinal researchers requires *in vivo* approaches because of the three-dimensional complexity of the retina whereby *in vitro* models are difficult to use to recapitulate the structure and function of the retina. As a result, recently established molecular tools are revolutionizing the field of visual research like the work by Scalabrino *et al.* and Lu *et al.* infecting mouse retinas with ON bipolar cell-specific adeno-associated viruses (AAV) (76,113). Scalabrino *et al.* incorporated the novel human mini-promoter Ple155 to induce bipolar cell-specific transgene expression in mice (76). They show that intravitreal injection of their AAV2(quadY-F+T-V)-Ple155-YFP_*Nyx* into *nob* mice at P2 resulted in partial restoration of the ERG b-wave and at the cellular level, full restoration of light-evoked ON bipolar cell responses for cells successfully expressing the transgene (76). By incorporating the *Grm6* promoter with the 7m8 viral capsid variant containing a Y444F mutation in an AAV, Lu *et al.* maximized transfection efficiency while preserving the cell specificity of viral infection *in vivo*. They observed decreased transduction in off-target cell types in the retina compared to the previously used SV40 promoter. Taken together, the use of AAV-mediated genetic engineering will increase our overall understanding of normal retinal physiology and its dysfunction in vision diseases and disorders.

CHAPTER II

MATERIALS AND METHODS

Mice

All protocols involving animals were approved by the University of Louisville Institutional

Animal Use and Care (IACUC) committee. CD-1 mice were from Envigo (Indianapolis, IN). FVB mice

were from Jackson labs (Sacramento, CA). Swiss Webster mice were from Charles River (Wilmington,

MA). *Lrit1$^{-/-}$* mice were created in house as described below. *Lrit2, Lrit3, Nyx, Grm6,* and *Trpm1* mice were

maintained in the University of Louisville mouse colony. Animals of both sexes were used in all

experiments.

CRISPR/Cas9 Generation of LRIT1 Knockout Mice

We employed the CRISPR/Cas9 gene editing system to create our novel *Lrit1$^{-/-}$* mouse lines. For

this, we designed 2 sgRNAs, one targeted to exon 2 (5'- UAGAGAGAACCGCCAUUCGC) and the other

to exon 4 (5' – GUGACGGCUCAAGUUGGACU) of the *Lrit1* mouse gene. We injected both sgRNAs

(200ng/µL each), the Cas9 nuclease mRNA (500ng/µL), and injection buffer (cat. MR-095-F, Millipore,

Burlington, MA) into mouse embryos derived from female CD-1 and male FVB mice and then implanted

them into pseudopregnant Swiss Webster mice. Tail biopsies were obtained from the resulting G0

generation and DNA isolated for genotyping. Crude DNA was prepared using DirectPCR (cat. 102-T,

Viagen, Los Angeles, CA) and proteinase K (1µg/mL). The sgRNA target regions were PCR amplified and

the resulting PCR product sequenced. Primer sequences for exon 2 (Lrit1-7, Lrit1-02) and exon 4 (Lrit1-03,

Lrit1-4) are given in Table 1. PCR conditions are described below. We identified 3 founder animals with

heterozygous mutations and named these lines *Lrit1* A, B, and C (Fig. 1). We crossed all founder mice to

C57Bl/6J mice. Offspring were genotyped as described above. These mice are the N1 generation. We

crossed N1 heterozygous littermates to yield the N1F1 mice, and identified those homozygous for each of the mutant alleles by DNA sequencing (Fig. 17).

To efficiently genotype *Lrit1* A offspring, we performed allele-specific PCRs using either one of two forward primers LRIT1-15 (wild-type [WT] allele) or LRIT1-20 (mutant allele) with reverse primer LRIT1-19, or multiplexing of all three primers (Table 1). Together, these PCRs show one 122bp band for WT mice, 122 and 115bp for *Lrit1*$^{+/-}$ mice, and one 115bp band for *Lrit1*$^{-/-}$ mice. If low intensity bands showed up in either PCR compared to higher intensity positive control and sample bands, we used additional PCRs with alternate forward primers LRIT1-16 and LRIT1-17 in lieu of LRIT1-15 and LRIT1-20, respectively, or sequencing to clarify the ambiguous results (Table 1). To efficiently genotype *Lrit1* B and C offspring, we used PCR primers Lrit1-03 and Lrit1-4 (Table 1). We restriction enzyme-digested PCR products using *Tsp*45I (New England BioLabs, Ipswich, MA) that differentially cleaves WT and mutant *Lrit1* alleles. WT, *Lrit1*$^{+/-}$, and *Lrit1*$^{-/-}$ mice yield 3, 4, and 2 bands, respectively, of distinguishable size. This prevented the need to sequence all offspring for genotyping. We additionally screened all *Lrit1* mice for the *rd1* mutation, which causes early onset severe retinal degeneration, with primers Rd-f and Rd-r followed by restriction enzyme digest with *Dde*I (Promega, Madison, WI) to yield a 300bp WT or 150bp mutant allele DNA fragment (Table 1). In all later experiments we characterized *Lrit1* B mice using WT littermate controls.

Table 1. PCR and sequencing primers (continued on the next page).

Primer	Sequence (5'→3')*	Application
LRIT1InfFw2	<u>CGACCTCTAGTCCGC</u>ATGTGGGTGGCCCTG	PCR
LRIT1InfRv	<u>GCGTCGGTCCGCTCC</u>GCGCAGAAGTACTCATTGATGC	PCR
LRIT1SeqEx2R(364-384)[LRIT1-AAV R2]	TCACTGAGAGCATTGTAAGGT	Sequencing
LRIT1SeqEx2F(557-577)[LRIT1-AAV F3]	GAGAACCTTACTTTCCTGGAC	Sequencing
LRIT1SeqEx2R(662-681)[LRIT1-AAV R3]	AAGATTAGCCTGGCATGATG	Sequencing
LRIT1SeqEx4F(1011-1027)[LRIT1-AAV F4]	GTGACGGCTCAAGTTGG	Sequencing
LRIT1SeqEx4R(1130-1149)[LRIT1-AAV R4]	GAAGTCTGTGGCTCAGTGAC	Sequencing
LRIT1SeqEx4F(1509-1528)[LRIT1-AAV F5]	TGAGAAGGATGACTGTGGAG	Sequencing
LRIT1SeqEx4R(1640-1659)[LRIT1-AAV R5]	ACTGATGAGGTAGTGGATGC	Sequencing
Lrit1-7	CTTGACTCTGCCTCCAGCTT	PCR, Sequencing
Lrit1-02	AGCATGAGGGCACTAAGCTC	PCR, Sequencing
Lrit1-03	GGCCTAGGAAGAGAGCCTGT	PCR, Sequencing
Lrit1-4	GCTTGTTGTTGTAGGCAGCA	PCR, Sequencing
LRIT1-15	CGCTTAGAGAGAACCGCCATT	PCR
LRIT1-16	CGCTTAGAGAGAACCGCAG	PCR
LRIT1-17	CGCTTAGAGAGAACCGCAGG	PCR
LRIT1-19	CCCTGAGCATGAGGGCACTAA	PCR
LRIT1-20	CGCTTAGAGAGAACCGCAGGGT	PCR
Rd-f	CATCCCACCTGAGCTCACAGAAAG	PCR
Rd-r	GCCTACAACAGAGGAGCTTCTAGC	PCR

*Underlining indicates regions complementary to plasmid overhangs.

Table 1 continued. PCR and sequencing primers.

Primer	Sequence (5'→3')*	Application
Gnat2snp2F	TGCTACTAACTGGCCCCAAG	PCR
Gnat2snp2R	CTGGATTTGTGATGGCCTTT	PCR, Sequencing
Lrit1-RhoR1	GGATCCAAGCTTTATTAGCAGAAGTACTCATTGATGCG	PCR
Nyc-Lrit1F1	ATGACGACGATAAGGATGCATTCTGTCCTTCTGAATGC	PCR
Rho-NycF1	ATATCCATCACACTGGCGGCCGCATGCTGATCCTGCTT	PCR
Rho-NycR1	ATCCTTATCGTCGTCATCCTT	PCR
LRIT1-AAV Rho F1	GGCTGTGTGACGAGATGAGA	PCR
LRIT1-AAV Rho R1	ATCAGCATCTGGGAGATTGG	PCR
LRIT1-AAV F1	CAGATATCCATCACACTG	Sequencing
LRIT1-AAV R1	TTGCTGCCAGATCCTCTTCT	Sequencing
LRIT1-AAV F2	TGACTTGACTCTGCCTCCAG	Sequencing
LRIT1-AAV F6	TTGGAAAGACTGGGCCATAG	Sequencing
LRIT1-AAV R6	AGCGTATCCACATAGCGTA	Sequencing

*Underlining indicates regions complementary to plasmid overhangs.
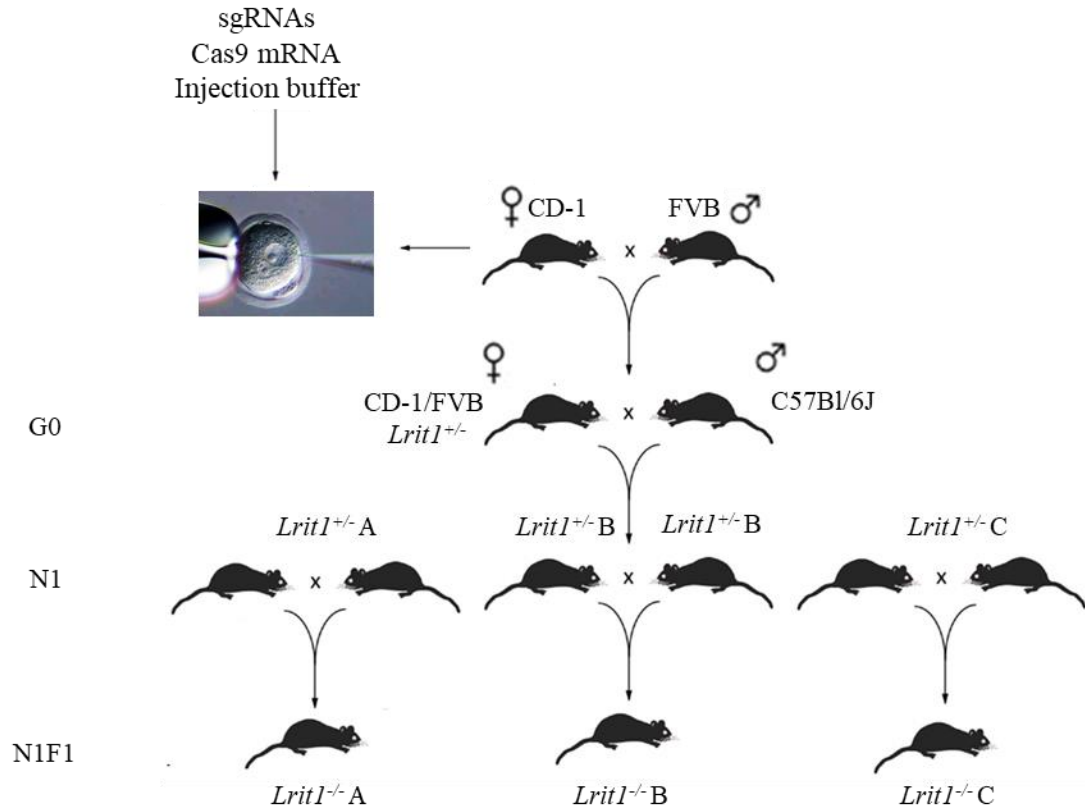
Fig. 17. Breeding scheme for generating *Lrit1* mutant mice. sgRNAs, Cas9 mRNA, and injection buffer were injected into female CD-1/male FVB mouse embryos and implanted into pseudopregnant Swiss Webster female mice. We identified 3 founder heterozygous mutations in the G0 generation named *Lrit1* A, B, and C. G0 founder mice were crossed to C57Bl/6J males to yield the N1 generation of heterozygotes. N1 heterozygous littermates were crossed to generate the N1F1 generation where homozygous mutants were identified for *Lrit1* A, B, and C lines.

Polymerase Chain Reaction (PCR)

We set up 20µL PCR reactions with the following: 4µLbuffer (either 5X Phire II buffer for tail PCRs [cat. F-524, Thermo Fisher Scientific, Waltham, MA] or 5X Phusion HF buffer [cat. F518, Thermo Fisher Scientific] for PCRs whose fragments were used for cloning), 0.4µL of 10 mM deoxynucleotide triphosphates (dNTPs, cat. U151B, Promega), 0.5µL of 20µM primers of forward and reverse primers, 0.4µL of DNA polymerase (Phire Taq [cat. F122L, Thermo Fisher Scientific] or Phusion DNA Polymerase [cat. F-549L, Thermo Fisher Scientific]), template DNA, and nuclease-free water. Added volumes of template DNA and water varied for each reaction. We performed all PCRs using the following thermal cycling protocol: (1) 98°C, 30s; (2) 98°C, 5s; (3) variable temperatures, 5s; (4) 72°C, 5s; (5) repeat steps 2-4 32 times; (6) 72°C, 300s; (7) 10°C, infinite hold. Annealing temperatures (step 3) were optimized for each primer pair.

Agarose Gel Electrophoresis

We made agarose solutions in TBE (10.8g/L Tris base, 5.5g/L boric acid, 0.75g/L ethylenediaminetetraacetic acid [EDTA], in water) and then microwaved the solution in 30 second increments until dissolved. Ethidium bromide (0.5µg/mL) was added to allow DNA visualization under UV light. Gels were cast and allowed to solidify for at least 45 minutes. We ran all gels at 160V for varied times as indicated in figure legends. We loaded 5µL each for all samples, controls, and blanks with 6X loading dye (cat. 50655, Lonza, Walkersville, MD) and added 7µL DNA ladder in a separate lane (cat. BN2050, BioNexus, Inc., Oakland, CA). After the appropriate time DNA was visualized and photographed under UV light.

***Lrit1* Cloning and Antibody Generation**

We inserted a full-length cDNA PCR fragment from *Lrit1* into the *Sac*II (Promega) restriction enzyme site of a phosphoglycerate kinase promoter (PGK)-myc-entry plasmid using InFusion cloning (Fig. 2). The PGK-myc-entry plasmid was made in our lab. Two PCR primers LRIT1InfFw2 and LRIT1InfRv with 15bp extensions matching the plasmid cloning site with 5' complementarity (Fig. 18; Table 1) were used to amplify the full–length *Lrit1* cDNA fragment using cDNA derived from total mouse retinal RNA.

This yielded a PCR product containing the murine *Lrit1* coding sequence (NCBI database, Accession #BC032270.1) but excluded the last three nucleotides encoding the stop codon. We cloned the PCR product into the linearized PGK-myc-entry plasmid using InFusion cloning (In-Fusion HD EcoDry™ Cloning Kit, ClonTech, Mountain View, CA) and transformed the reaction mix into Stellar competent cells (ClonTech). Transformed cells were plated on CircleGro agar plates containing ampicillin (100μg/mL) and incubated overnight at 37°C. Isolated clones were inoculated using toothpicks into 3mL of CircleGro media containing ampicillin (100μg/mL), and grown overnight at 37°C with shaking. Plasmid DNA was isolated from the overnight growths using a Wizard® Plus SV Miniprep DNA Purification System (Promega). We restriction enzyme-digested all mini-prep DNA with *Xba*I (Promega), which cuts the *Lrit1* plasmid twice, once in the *Lrit1* cDNA and once in the vector. This digest indicated if the plasmid contained the *Lrit1* cDNA. For all positive clones, we sequenced mini-prep DNA to confirm the mouse *Lrit1* reference sequence using the following sequencing primers: LRIT1InfFw2, LRIT1InfRv, and all LRIT1SeqEx2F, LRIT1SeqEx2R, LRIT1SeqEx4F, and LRIT1SeqEx4R primers (Table 1).

We used the validated sequence to select a peptide for production of a rabbit polyclonal anti-LRIT1 antibody. The peptide sequence used was from LRIT1's C-terminal residues 607-624 (NCBI database, Accession #AAH32270.2): DSQVLGVRGGRRINEYFC. The antibody was produced and affinity purified by Pierce Custom Antibodies, ThermoScientific (Waltham, MA).
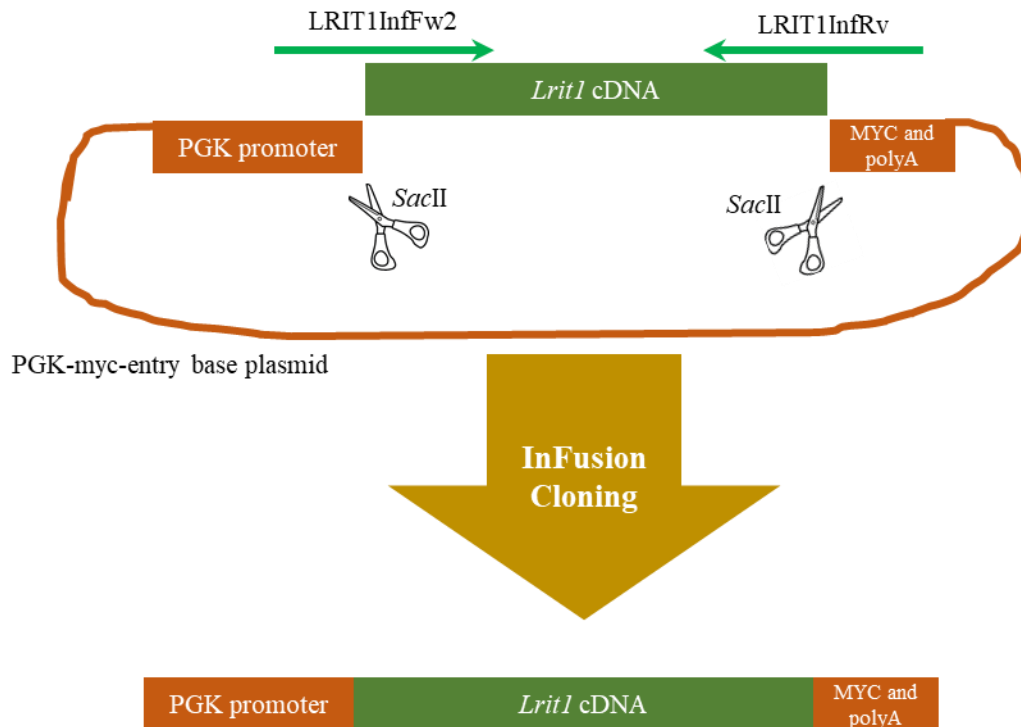
Fig. 18. Schematics for cloning *Lrit1* into a plasmid to confirm its reference sequence. The PGK-myc-entry base plasmid was digested (scissors) with *Sac*II into which the *Lrit1* cDNA was cloned. B) Schematic showing the final InFusion cloning PGK-*Lrit1* plasmid.

Adeno-associated Viral Vector Generation

We constructed a vector to express a tagged *Lrit1* cDNA. From AAV2/9-RHO-GFP and clones containing the desired regions in the lab, the plasmid was constructed to contain a rhodopsin (RHO) promoter, the nyctalopin (Nyc) signal sequence, N-terminal MYC and FLAG tags, and the *Lrit1* coding sequence without its N-terminal signal sequence or C-terminal stop codon (Fig. 19) (114). We used a Gibson assembly approach to insert the Nyc signal sequence, MYC and FLAG tags, and *Lrit1* cDNA into a AAV2/9-RHO-GFP vector (114), replacing eGFP with our insert. Briefly, the AAV2/9-RHO-GFP plasmid was digested with *Hind*III and *Not*I (Promega) in separate reactions because their optimal buffers were incompatible. We digested first with *Hind*III because it required the lower salt concentration (100mM NaCl), then added 1uL of 1M NaCl (nuclease-free water) to generate a 150mM NaCl reaction buffer and *Not*I. We used the *Bam*HI (Promega)-digested AAV-*Lrit3* plasmid that contains the Nyc signal sequence and MYC/FLAG with primers Rho-NycF1 and Rho-NycR1 (Table 1). We amplified the coding region of *Lrit1* from our PGK-*Lrit1* plasmid containing the *Lrit1* coding region using primers Nyc-Lrit1F1 and Lrit1-RhoR1 (Fig. 19; Table 1). The two PCR fragments were purified using a QIAquick PCR purification kit (cat. 28104, Qiagen, Germantown, MD), and the resulting DNA concentrations determined using a NanoDrop ND-1000 (NanoDrop Technologies, Wilmington, DE). The PCR products were cloned into *Hind*III/*Not*I digested AAV2/9-RHO-GFP plasmid using the In-Fusion HD EcoDry™ Cloning Kit (ClonTech). Two infusion reactions were set up with the (1) digested vector and fragments containing (2) the Nyc signal sequence with MYC/FLAG and (3) *Lrit1* in ratios of 150:57:27.2ng of DNA and 150:114.1:27.2ng of DNA, respectively, in a final volume of 10μL. After the infusion reaction was complete as per the manufacturer, Stellar competent cells (ClonTech) were transformed and plated on CircleGro agar containing ampicillin (100μg/mL). After overnight incubation at 37°C, toothpicks were used to transfer single colonies to 3mL of CircleGro media containing ampicillin (100μg/mL). Bacteria were incubated at 37°C overnight with shaking, and plasmid DNA from each colony was isolated using DNA Wizard® Plus SV Minipreps DNA Purification System (Promega). The presence of the correct inserts was assessed by restriction enzyme double-digest of DNA with *Sph*I and *Spe*I (Promega), and analyses of fragment size on agarose gels. Confirmation of the correct clone was done by sequencing the entire coding region using primers LRIT1-AAV F1-6 and LRIT1-AAV R1-6 (Table 1) and the RHO

promoter with LRIT1-AAV Rho F1 and LRIT1-AAV Rho R1 (Table 1). Sequencing identified 3

differences, two deletions (4bp and 1bp) and a 1bp insertion in the RHO promoter when compared to the

reference sequence sent to us from Dr. J. G. Flannery's lab (Helen Wills Neuroscience Institute, Berkeley,

CA). The RHO promoter in the AAV2/9-RHO-GFP plasmid has been used by us and others, and shows

strong and specific expression in photoreceptors (unpublished data and (114)). Therefore, the identified

mutations did not impact the desired function. To obtain sufficient plasmid for viral production, mini-prep

DNA was used to transform cells, new clones isolated, and 3ml cultures grown and used to inoculate

350mL of Circlegro media. Plasmid DNA was isolated using endo-free maxi prep kits (cat. 12362, Qiagen).

The sequence was confirmed as described above and the DNA used for virus production.
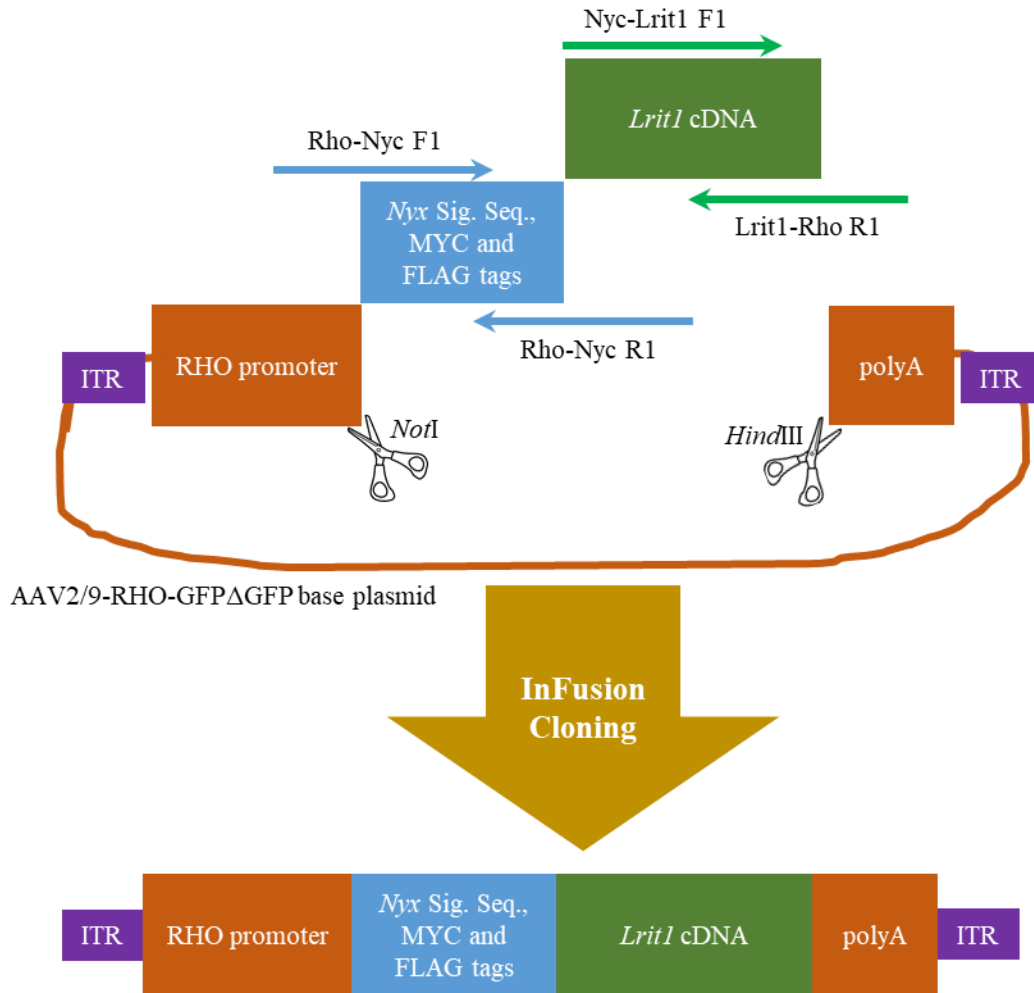
Fig. 19. Schematics for cloning *Lrit1* into a plasmid to be packaged into an adeno-associated virus. The AAV2/9-RHO-GFP base plasmid was digested (scissors) with *Hind*III and *Not*I into which the *nyctalopin* signal sequence with MYC and FLAG tags and *Lrit1* cDNA were cloned. B) Schematic showing the final InFusion cloning AAV-*Lrit1* plasmid.

Retinal dissections

We euthanized animals by CO_2 exposure followed by cervical dislocation as per AVMA guidelines. The eyes were enucleated and placed in ice-cold 1X PBS (3mM KCl, 2mM KH_2PO_4, 137mM NaCl, 8mM Na_2HPO_4). I punctured eyes directly posterior to the ora serrata with a 30g needle, cut along the vertical axis to separate the anterior and posterior parts of the eye, and removed the anterior portion of the eye leaving the lens intact and attached to the eyecup. I removed the lens and the vitreous humor, gently separated the retinal pigment epithelium (RPE) from the retina using forceps, and clipped the RPE at the optic nerve that exits from the center of the retina. The dissected retinas were washed in fresh, cold 1X PBS and fixed in 4% paraformaldehyde in PB (0.1M phosphate buffer, pH 7.2) for 24h for *in situ* experiments and 15m for immunohistochemistry. Immediately following fixation, the retinas were washed 4 times for 10 minutes each in 1X PBS at room temperature, incubated retinas serially for 1 hour each in 5%, 10%, and 15% sucrose in PB at room temperature followed by an overnight incubation in 20% sucrose in PB at 4°C, and finally incubated in 20% sucrose/OCT (1:2) for 1 hour at room temperature. The retinas were embedded in 20% sucrose/OCT (1:2) by freezing slowly on a 2-methylbutane bath cooled in liquid nitrogen. The embedded retinas were stored at -80°C. Prior to cryo-sectioning, tissue blocks were incubated in the cryostat (Leica CM 1850, Leica Biosystems, Richmond, IL) for 1 hour. 18μm transverse retinal sections were cut and transferred onto Superfrost Plus glass slides (Thermo Fisher Scientific) and stored at -80°C. Retinal integrity was validated via light microscopy.

Immunohistochemistry

Slides were removed from the -80°C freezer and warmed for 1 hour at 37°C. The embedding media was removed by washing in 1X PBS for 5 minutes, followed by washing in 1X PBS containing 0.5% Triton-X 100 (PBX) for 5 minutes. The retinal sections were circled with an Immedge oil pen (Vector Laboratories, Burlingame, CA) and incubated in blocking media [5% normal donkey serum (NDS) in PBX] at room temperature for 1 hour. Blocking media was replaced with primary antibodies at the appropriate dilution (Table 2) in blocking media, and incubated overnight at room temperature. The following morning, the sections were washed 3 times for 5 minutes each in PBX followed by one wash in 1X PBS for 5 minutes, all done at room temperature. Secondary antibodies were diluted in blocking media, added to the

slides, and the slides incubated at room temperature for 1 hour. Sections were washed 3 times for 5 minutes each in PBX followed by one wash in 1X PBS for 5 minutes all done at room temperature, coverslipped using VectaShield mounting media plus DAPI (Vector Laboratories), and sealed with clear nail polish to prevent tissue dehydration. Tissue sections were imaged using confocal microscopy at the appropriate wavelengths on an Olympus FV1000 microscope (Olympus, Center Valley, PA). Sequential scanning was employed to prevent bleed-through when multiple secondary antibodies are used. Objectives used were a 40x water (numerical aperture [NA]=1.15), 60x oil (NA=1.42) and 100x oil (NA=1.45) as appropriate.

Table 2. Primary antibodies for immunohistochemistry.

Antigen	Species	Dilution	Source	Retina Expression
α1F	Rabbit	1:1000	Dr. Amy Lee	Rod synaptic ribbons
PNA	Dye	1:1000	Life Technologies (PNA 568 - L32458; PNA 647 – L32460)	Cone inner and outer segments, cone pedicles
mCAR	Rabbit	1:1000	Dr. Sheryl Craft	Cones
Pikachurin	Rabbit	1:2000	Wako (011-22631)	Photoreceptor ribbon synapses: isolated puncta (rods) and clustered puncta (cones)
PSD95	Mouse	1:1000	Chemicon (MAB1596)	Photoreceptor axonal terminals
RIBEYE	Mouse	1:1000	BD Transduction Labs (612044 or 612045)	Photoreceptor synaptic ribbons
LRIT1	Rabbit	1:500 1:1000 1:2000	Thermo Fisher Scientific (custom antibody)	OPL
PKCα	Rabbit	1:1000	Sigma (4334)	ON bipolar cells
GPR179	Sheep	1:2000	Biosynthesis (n/a)	ON bipolar cell dendritic tips
TRPM1	Rabbit	1:2000	Biosynthesis (n/a)	ON bipolar cell dendritic tips
LRIT3	Guinea pig	1:1000	Biosynthesis (n/a)	ON bipolar cell dendritic tips
RGS11	Sheep	1:4000	Dr. Kirill Martemyanov	ON bipolar cell dendritic tips
mGluR6	Sheep	1:4000	Dr. Kirill Martemyanov	ON bipolar cell dendritic tips
HCN4	Mouse	1:500	Dr. Bart Borghuis	Cone OFF bipolar cells type 3a
PKAIIβ	Guinea pig	1:1500	Dr. Bart Borghuis	Cone OFF bipolar cells type 3b
Calsenilin	Mouse	1:1000	Dr. Bart Borghuis	Cone OFF bipolar cells type 4
Calbindin	Rabbit	1:1000	Swant (CB-38)	Horizontal cells
SNAP-25	Goat	1:250-1:1000	Millipore (AB5871)	Horizontal cells
GluR2/3	Rabbit	TBD	Milliporee (07-598)	Horizontal Cells

Western Blotting

Retinas were homogenized in a solution containing NP-40 (50mM Tris, 150mM NaCl, 2mM EDTA, and 1% Nonidet P40, pH 8.0) and 1X protease inhibitor cocktail (Sigma-Aldrich, St. Louis, MO) by pipetting several times and rotating for 1 hour at 4°C. Cell debris was removed by centrifugation at 17,000×g for 20 minutes at 4°C. The supernatant was collected and protein quantified using the Bradford reagent (Bio-Rad, Hercules, CA). Either 16 or 31µg total protein lysate was loaded per lane onto 4–12% NuPAGE gels (Invitrogen, Thermo Fisher Scientific) and electrophoresed at 190V for 1 hour. Proteins were transferred to polyvinylidene difluoride (PVDF) membranes using a BioRad electroblotter. The membranes were incubated in Odyssey Blocking Buffer (LI-COR, Lincoln, NE) for 2 hours, followed by incubation in primary antibodies diluted in Odyssey Blocking buffer. Antibody dilutions were rabbit anti-LRIT1, 1:100 and 1:1000; mouse anti-β-actin, 1:50,000. Membranes were washed four times with TBS (50mM Tris-Cl, pH 7.6; 150mM NaCl) containing 0.1% Tween-20 (TBS-T). The membranes were incubated with IRDye800 CW and IRDye680 CW-conjugated secondary antibodies (1:25,000) diluted in Odyssey Blocking Buffer for 45 minutes, then washed three times in TBS-T and once in TBS. Protein bands were visualized by scanning the membranes in the Odyssey Infrared Imaging System (LI-COR) using both 700 and 800nm channels.

RNA *in situ* hybridization

RNAScope® (ACDBio, Newark, CA) *in situ* hybridization was used to visualize target transcripts in fixed retinal sections. The standard protocol was used with slight modification (105). Slides were baked overnight at 60°C to ensure tissue remained attached, and slides were incubated in pre-treatment buffer 2 for 4 minutes at the temperature range of 90-105°C. The solution could not be actively boiling during this incubation as the tissue would detach from the slides. Pre-treatment buffer 3 was applied for 12 minutes. I added 50µL per slide for the FastRed incubation step. The positive and negative control probes are *Polr2a* (RNA polymerase II subunit A) and *DapB* (a bacterial gene). Target probes were synthesized (ACDBio) for transcripts encoded by the following genes: *Lrit1* (NCBI NM_146245.2, 488-1365bp), *Lrit2* (NCBI NM_173418.3, 675-1592bp), *Lrit3* (NCBI NM_001287224.1, 212-1111bp), and *Grm6* (NCBI NM_173372.2, 1001-2020bp). Slides were coverslipped, mounted, and sealed as described above for

immunohistochemistry. Tissue sections were imaged at the necessary wavelengths on an Olympus FV1000 microscope (Olympus).

Electroretinography

Electroretinography (ERG) is used to assess the light-induced electrical response of the retina through direct attachment of corneal electrodes to mouse eyes *in vivo*. 8-12 week old adult mice of either sex were used. ERG recordings were done in a dark room. Mice were dark-adapted overnight prior to beginning recordings. All manipulations were done under in dim red light. Mice were anesthetized with 80mg/kg ketamine/16mg/kg xylazine (AKORN Animal Health, Lake Forest, IL) in saline and their pupils were dilated (1% tropicamide in saline). After trimming nasal whiskers to prevent electrode disruption, mice are placed on a heating pad to maintain a normal body temperature. The heating pad rests on a stage that pushes into the LKC UTAS light box (LKC Technologies, Gaithersburg, MD) during assessment. Subcutaneous needles functioned as ground (tail) and reference (nasal bridge) electrodes. Corneal electrodes were connected using GONAK (2.5% hypromellose) to ensure good electrode connectivity. Upon a stable baseline, mice were inserted into the LKC UTAS light box for a 5-minute dark adaptation after which scotopic ERGs were performed. These were followed by a 5-minute light adaptation after which photopic ERGs were performed. Photopic ERGs were performed with a constant rod-saturating background (1.48 log cd sec/m^2). Electrical responses were recorded using 5ms full-field stimuli produced by a Ganzfeld (Phoenix Research Labs, Pleasanton, CA) at the following intensities in log cd sec/m^2: scotopic, -3.6, -3, -2.4, -1.8, -1.2, -0.6, 0.0, 0.6, 1.4, and 2.1; photopic, -0.8, -0.4, 0.0, 0.4, 0.9, 1.4, and 1.9. The average responses at each flash intensity were determined. ERG recordings are reported for individual animals as an average of the response from both eyes. The a-wave was measured from baseline to the trough, and the b-wave from the trough of the a-wave to the peak of the b-wave using a custom MATLAB program (MathWorks, Framingham, MA).

Morphometric Analysis of the Retina

Eyes were enucleated and prepared for morphological analysis by immediate immersion in fixative (2% paraformaldehyde/2% glutaraldehyde in 0.1M PB pH 7.2). Plastic sections were prepared as

previously described (115). Briefly, eyes were bisected from the cornea through the optic nerve such that each hemisphere contained retinal tissue from the ora serrata to the optic nerve. Hemispheres were dehydrated in ascending ethanol concentrations (50, 75, 80, 90, 95, 100%), infiltrated, and embedded in JB-4 Plus resin (Ted Pella, Redding, CA). Sections 4µm thick were cut on a Leica EMUC6 Ultramicrotome (Leica Microsystems, Buffalo Grove, IL), mounted on slides, dried, and stained with 1% cresyl violet (Sigma-Aldrich). Sections were examined at 40 or 100X using a NIKON EFD-3 Episcopic-Fluorescence microscope (Nikon Inc., Melville, NY). Photomicrographs were taken on a Moticam 2500 high-resolution camera (Motic) and digitally processed using Adobe Photoshop (Adobe Systems) to adjust brightness and contrast. Overall retina thickness and retinal lamina thickness were measured 200µm from the ora serrata and 200µm from the peripheral margin of the optic disc. A vertical line was drawn across the entire retinal section and then across each stratum for individual thickness measurements using Moticam Image Plus 2.0 (Motic China Group Co., Ltd., Xiamen, China) in 5 sections per location/eye and the mean was calculated for each location. A trained masked observer (Dr. Patrick Scott, Department of Ophthalmology and Visual Sciences, Louisville, KY) performed the retinal morphometry without knowledge of the genotype.

Multi-electrode Arrays

Multi-electrode array (MEA) recordings were obtained from *ex vivo* isolated flat mounted retinas. Mice were euthanized using an intraperitoneal injection of ketamine (60mg/mL) and xylazine (8mg/mL) followed by cervical dislocation. Eyes were enucleated, and retinas dissected from the eye cup under dim red light at room temperature in a solution of Ringer's (110mM NaCl, 2.5mM KCl, 1mM $CaCl_2$, 1.6mM $MgCl_2$, 10mM D-glucose, and 22mM $NaHCO_3$ [pH 7.4]) with collagenase (241 units/mL) and hyaluronidase (34.5nM) oxygenated with 95% O_2 and 5% CO_2 for 10 minutes. Dissected retinas were transferred to a solution containing only Ringer's that is oxygenated with 95% O_2 and 5% CO_2 for the duration of the recordings. Under dark conditions, ten 5s full-field light flashes were presented per light intensity to each piece of mouse retina at each of the following light intensities: scotopic -2.3, -1.5, and 0.2; and photopic 0.5, 1.2, and 2.5 in log cd sec/m^2. Light stimuli were presented using a custom MATLAB program where stimulus intensity, duration, and number of repetitions are entered. A light adapting background of -0.3 log cd sec/m^2 was presented between 0.2 and 0.5 log cd sec/m^2 to demarcate dark-

adapted scotopic and light-adapted photopic flashes. Signals were band-pass filtered (80-3,000 Hz) and digitized at 25kHz (MCRack software; Multi Channel Systems). Any signals less than -40μV are not collected. Spiking activity of retinal ganglion cells was recorded using a 60-channel MEA recording system (MultiChannel Systems, Reutlingen, Germany). All recordings were done by Dr. Gobinda Pangeni (Department of Ophthalmology and Visual Sciences, Louisville, KY). Spikes were recorded on individual electrodes, and if spikes reflected responses from more than one retinal ganglion cell, they were sorted into individual cells using principal component analysis (Offline Sorter; Plexon, Dallas, TX). Sorted units were exported for analysis of their spontaneous and visually evoked responses with NeuroExplorer software (Nex Technologies, Madison, AL). Average post-stimulus time histograms (PSTHs) were calculated for all retinal ganglion cells to 10 presentations for each of the 6 full-field luminance levels. The WT data set has been previously published (116). Excitatory responses were defined by responses to light onset or offset when the response exceeded 10 times the spontaneous activity standard error of the mean over 80% of trials. From the average PSTH, we calculated the time to peak response defined as the time from stimulus onset or offset to the retinal ganglion cell peak response amplitude. We classified the response of each retinal ganglion cell at each light intensity as ON (excitation at light onset), OFF (excitation at light offset), or ON/OFF (excitation at stimulus onset and offset). Time to peak thresholds were set from 0.1-0.5 seconds. Any response satisfying the spontaneous activity threshold and occurred after 0.5s for the light increment or decrement was classified as delayed. The percent responsive cells were characterized by calculating the sum of cells that responded in any functional class (ON, dON, OFF, dOFF, dON/OFF, ON/dOFF, and dON/dOFF) to the total number of cells including non-responsive (NR) cells and expressed as a percentage. The spontaneous activity, distribution of retinal ganglion cell functional classes, peak firing rate, and time to peak were all examined. Rhythmicity was analyzed using a power spectral density analysis (NeuroExplorer) with the following parameters: 20Hz maximum frequency, 4096 frequency values, raw PSD normalization, displayed frequencies of 0-5Hz, and smoothed with a Gaussian filter of 20 bins.

Statistical Analysis

A repeated measures ANOVA with the Bonferroni's post-hoc correction for multiple comparisons was used to analyze ERGs. A two-way ANOVA with factors for genotype and retinal layer was used to analyze retinal morphometry data. MEA time to peak and peak amplitude responses were analyzed with a Kruskal-Wallis test using a Dunn's post-hoc correction for multiple comparisons. The Kruskal-Wallis test is a non-parametric test that does not assume normality or equal variance among groups. All statistical analyses were performed using GraphPad Prism software (La Jolla, CA).

Lrit1 is Expressed in Mouse Photoreceptors

At the transcript level, *Lrit1* is expressed in the mouse retina. More detailed analyses of this RNA-Seq data set (117) in collaboration with Dr. TA Ray (Department of Neurobiology, Duke University, Durham, NC) illustrated high expression of *Lrit1* in rods and cones peaking at and after day 10 (Fig. 20). Importantly, the increase in *Lrit1* expression follows the timeline for photoreceptor development and the initiation of vision in mice.
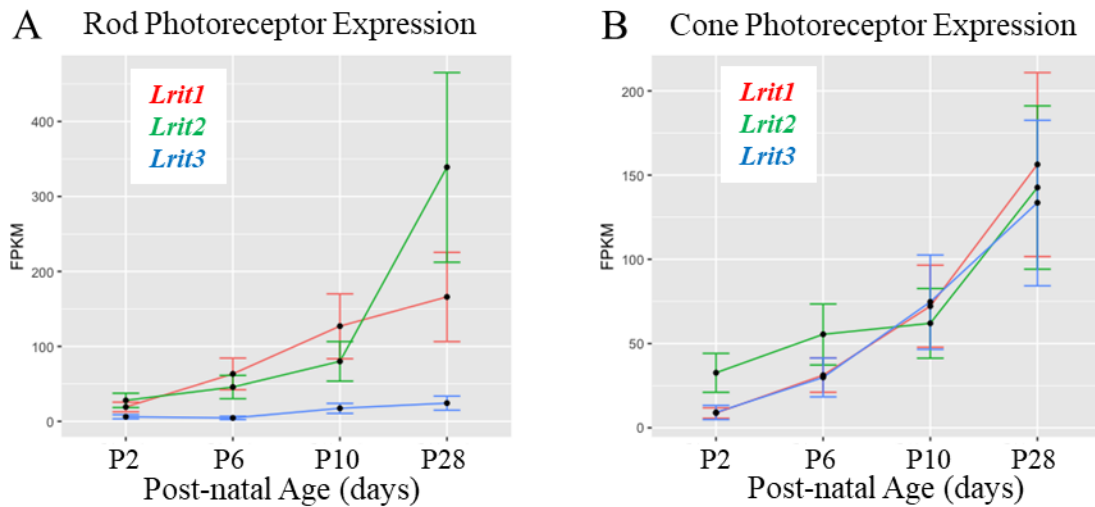
Fig. 20. Expression profile for *Lrit* genes in mouse rods and cones during development. *Lrit* gene expression in rods (A) and cones (B) from post-natal day 2 to post-natal day 28. *Lrit1* (red lines), *Lrit2* (green lines), *Lrit3* (blue lines). Data are from previously published RNA-Seq data (MJ Brooks *et al*. *Mol Vis*. 2011;17:3034-3054).

Generating the *Lrit1*^{-/-} Mouse Model

To investigate the function of LRIT1 in the mouse retina, we generated genetically modified mice in which its expression was deleted. We anticipated that this mouse would be viable based on the previous studies in rat tissue indicating *Lrit1* expression is limited to the retina (101). We designed two sgRNAs, one targeted to exon 2 and to exon 4 of *Lrit1*. The sgRNAs were combined with mRNA for CRISPR/Cas9 and injected into 160 one-cell mouse embryos, of which 78 survived. A total of 26 embryos were implanted into each of 3 pseudopregnant mice. Thirty-one offspring were produced. We refer to these founders as the G0 generation. The sgRNA target region for each G0 mouse was sequenced, and 3 mice were identified with *Lrit1* mutations. These mutations were a 7bp deletion in exon 2 (line A), a 1bp insertion in exon 4 (line B), and a 3bp deletion in exon 4 (line C) (Fig. 21A-B). These heterozygous G0 mice were crossed to wild-type (WT) C57Bl/6J mice. The resulting N1 heterozygous littermates were intercrossed to generate the N1F1 generation, and *Lrit1*^{-/-} mice for study. Sequencing confirmed homozygosity in *Lrit1*^{mut/mut} mice (Fig.21C). Line A was not characterized further. The official names of the other lines are Line B: *Lrit1*^{em1Rgg}; and Line C: *Lrit1*^{em2Rgg}.

Fig. 21. Creation of *Lrit1* mutant mouse lines. A) Schematic for *Lrit1* indicating the sgRNA sequences targeting exons 2 and 4 and the mutations created. *Lrit1* lines A and C have deletions (red circles) and *Lrit1* line B has an insertion (red text). Exon 2 mutations are determined using an allele-specific PCR (black arrows) with forward primers Lrit1-15 (WT allele) and Lrit1-20 (mutant allele) with reverse primer Lrit1-19. Exon 4 mutations are determined using PCR primers (black arrows) Lrit1-03 and Lrit1-4 followed by *Tsp*45I digest (see D). B) Corresponding WT and mutant LRIT1 protein sequences indicate amino acid changes in lines A-C with residue numbers indicated above with first mutated residues (red text). C) Sequencing reads of fragments showing WT , *Lrit1*+/-, and *Lrit1*-/- sequence at the identified exon 4 1bp insertion in *Lrit1* B mice. Overlapping peaks in *Lrit1*+/- mice demonstrate heterozygosity. Sequencing was from right to left (green arrow). Di) *Lrit1* B Lrit1-03/4 PCR products after *Tsp*45I restriction digest. Samples and DNA ladder (MM) were run on a 3% gel at 160V for 20 minutes. Three WT fragments, 82, 100, and 119bp; two *Lrit1*-/- fragments, 100 and 202bp; and heterozygotes exhibited all four fragments, 82, 100, 119, and 202bp. Dii) Lrit1-03/4 301bp PCR product (black) with *Tsp*45I restriction sites for WT and *Lrit1*-/- alleles (blue).

Allele-Specific Reactions for Genotyping *Lrit1*^{-/-} Mice

For genotyping of *Lrit1* litters, we designed custom assays (Fig. 22). For line B we used restriction fragment length polymorphism (RFLP) analyses. To genotype offspring from *Lrit1*^{-/-}, a fragment encompassing the mutation in exon 4 was amplified (primers Lrit1-03 and Lrit1-4 [Table 3]). We restriction enzyme-digested the PCR products using *Tsp*45I, which cuts the WT allele but not the mutant allele and cuts once outside of the mutation of interest. This yields more fragments from the WT alleles than from the mutant allele (Fig. 21D). G0 mice were a hybrid between CD-1 and FVB, the latter of which carries the *Rd1* allele. We screened all offspring for the *Rd1* mutation, which causes early onset severe retinal degeneration and would interfere with our studies (Fig. 23).
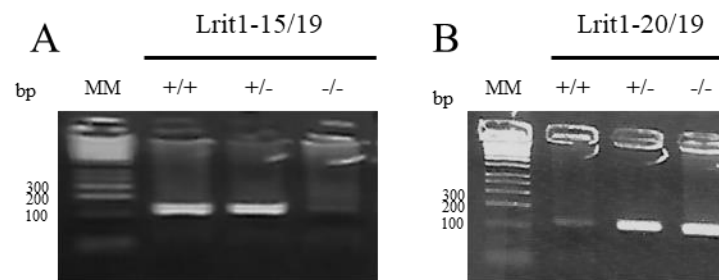
Fig. 22. PCRs of *Lrit1* A mice show allele-specific amplification. A) Lrit1-15/19 PCR primers amplify the WT allele at 122bp only. B) Lrit1-20/19 PCR primers amplify the mutant allele at 115bp only. Heterozygous animals display products in both PCRs. PCR products and DNA ladder (MM) were run on a 3% gel at 160V for 15-20 minutes. WT fragment, 122bp; fragments for heterozygous mice, 122bp and 115bp; homozygous fragments, 115bp.

Table 3. PCR Primer Pair Amplicons.

Primer	Amplicon Size (bp)
LRIT1InfFw2/LRIT1InfRv	1904
Lrit1-7/Lrit1-02	162
Lrit1-03/Lrit1-4	301
LRIT1-15/19	122
LRIT1-16/19	122
LRIT1-17/19	115
LRIT1-20/19	115
Rd-f/Rd-r	300
Gnat2snp2F/Gnat2snp2R	499
Nyc-Lrit1F1/Lrit1-RhoR1	1846
Rho-NycF1/Rho-NycR1	176
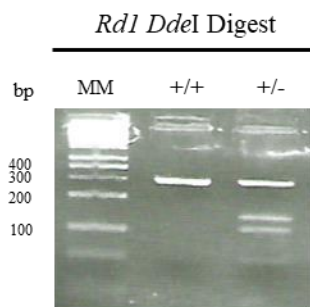
Fig. 23. Genotyping the *Rd1* allele by *Dde*I restriction enzyme digest. PCR fragments encompassing the *rd-1* mutation were generated (PCR primers Rd-f and Rd-r) and digested with *Dde*I. Samples and DNA ladder (MM) were run on a 3% gel at 160V for 22 minutes. WT fragment, 300bp; fragments for heterozygous mice, 300bp and 150bp; *rd-1* fragments, 150bp.

The *Lrit1^{-/-}* Mutation is Predicted to be Deleterious

With respect to line B, the 1bp insertion causes a frameshift and premature stop codon in exon 4. Transcripts with premature stop codons have been shown to activate nonsense-mediated decay of the transcript, causing no expression of the protein product (118) (Fig. 24A). Even if the *Lrit1* B exon 4 frameshift mutation did not lead to nonsense-mediated decay of the *Lrit1* B transcript, the translated LRIT1 protein would contain a truncated immunoglobulin-like domain and lack the fibronectin type III domain, the sixth LRR, and transmembrane domains (Fig. 24B). Without a transmembrane domain, LRIT1 would not properly localize to the membrane.
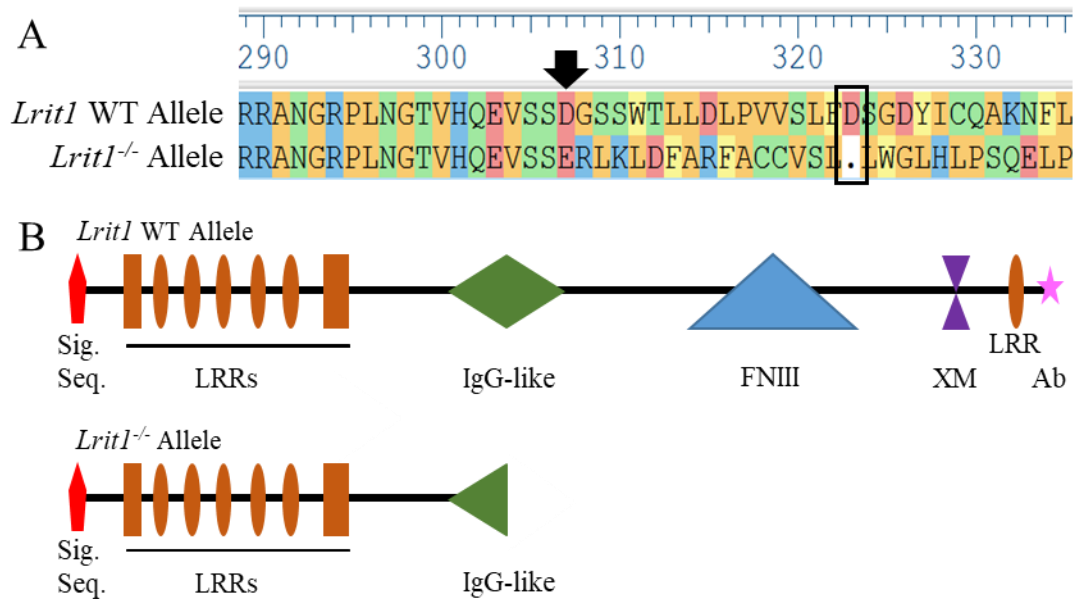
Fig. 24. The *Lrit1* B line contains a 1bp insertion that causes a frameshift mutation leading to a premature stop codon. A) Alignment of WT and *Lrit1^{-/-}* allele demonstrates the frameshift mutation at residue 307 (black arrow) and the premature stop codon (black box). B) LRIT1 structure for *Lrit1* WT (top) and *Lrit1^{-/-}* (bottom) alleles. Features shown are signal sequence (sig. seq.), leucine-rich repeats (LRR), immunoglobulin-like (IgG-like), fibronectin type III (FNIII), C-terminal transmembrane domain (XM), and antibody-binding domain (Ab). If the *Lrit1^{-/-}* allele results in truncated LRIT1 being produced, it would lack the C-terminal half of the IgG-like, the entire FNIII, XM, and the final LRR domains.

To assess the phenotypic impact of the mutations on LRIT1 protein function, we analyzed each predicted protein using the Protein Variation Effect Analyzer (Provean, http://provean.jcvi.org/index.php). The analyses predicted that all 3 mutations would be deleterious (Table 4). In all our studies we used Line B and hereafter refer to it as *Lrit1*$^{-/-}$. We then performed electroretinograms (ERGs) on *Lrit1*$^{-/-}$ mice to determine the functional impact of the loss of LRIT1 in the mouse retina.

Table 4. Provean prediction scores for *Lrit1* Lines A, B, and C.				
Lrit1 Line	DNA Mutation	Protein Mutation	Provean Score	Provean Prediction
A	c.204_210del	p.R69AfxX7	-12.587	deleterious
B	c.919_920insA	p.D307EfxX17	-4.350	deleterious
C	c.917_919del	p.S306del	-8.984	deleterious

Abnormal Electroretinograms (ERGs) in N1F1 *Lrit1*$^{-/-}$ mice

To examine retinal function of *Lrit1*$^{-/-}$ mice, we performed an ERG analysis. The ERGs record a gross electrical potential generated from the light-induced electrical response of the retina's photoreceptors and ON bipolar cells. Initially, we screened three *Lrit1* mice. ERGs revealed an abnormal no-cone photopic ERG in one *Lrit1*$^{+/+}$ mouse and one *Lrit1*$^{-/-}$ mouse (Fig. 25). The third *Lrit1*$^{+/+}$ mouse demonstrated a normal ERG (Fig. 25). Because these findings were discordant with our *Lrit1* genotyping, we hypothesized the presence of an additional mutation. One known cause of a no-cone photopic ERG is a diagnosis of achromatopsia (119,120). Mutations in genes known to cause a no-cone ERG are *Cnga3, Cngb3, Gnat2, Pde6c,* and *Pde6h.* We performed PCRs for *Gnat2* and found a known homozygous mutation in *Gnat2* referred to as *Gnat2*^{cpfl3} (119) in *Lrit1*$^{+/+}$ *and Lrit1*$^{-/-}$ mice with the no-cone ERG phenotype. *Gnat2*^{cpfl3}

causes deficits in cone-dependent a-wave ERG responses as early as 3 weeks of age and is completely

absent by 9 weeks of age, leading to a diagnosis of achromatopsia 4 (119). *Gnat2^cpfl3* is a single-base

substitution c.598G>A in exon 6, which causes a missense p.D200N mutation in α–cone transducin that

was first described in the ALS/LtJ mouse strain (119). We acquired additional CD-1 mice from Envigo and

demonstrated the presence of the *Gnat2^cpfl3* mutation in this strain. Mice homozygous for the

*Gnat2^cpfl3c*exhibited a no-cone ERG as predicted. Therefore, investigators using this strain for retina or

vision studies should genotype all mice before conclusions are made.
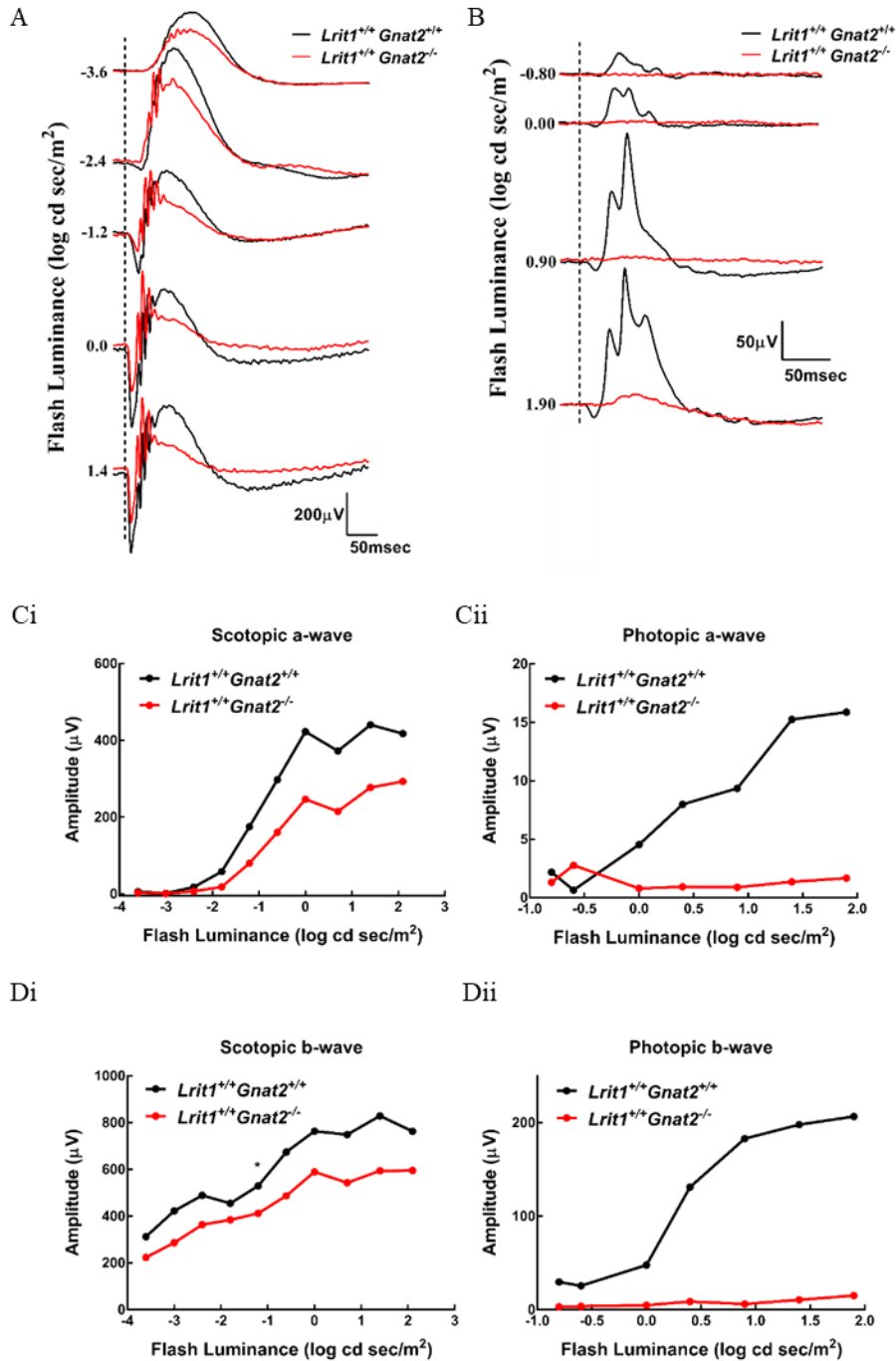
Fig. 25. ERGs of *Lrit1* B mice reveal a *Gnat2* mutation in the CD-1 background. Dark-adapted (A) and light-adapted (B) ERGs. Quantification of the dark-adapted (Ci, Di) and light-adapted (Cii, Dii) a- and b-wave amplitudes as a function of light intensity. The photopic cone b-wave is absent in the *Gnat2*$^{-/-}$ mouse. A-D) Plotted data are from *Lrit1*$^{+/+}$ *Gnat2*$^{+/+}$ (n=1; black) and *Lrit1*$^{+/+}$ *Gnat2*$^{-/-}$ (n=1; red) mice. These data indicate an interfering mutation is present in the *Lrit1* B mouse line.

62

LRIT1 Loss Causes Reduced ERG a- and b-waves

The *Gnat2cpfl3* mutation directly interfered with our studies. Thus, we screened all *Lrit1* mice for the *Gnat2cpfl3* mutation and eliminated it from our *Lrit1* breeding colony. We performed an ERG analysis on young adult *Lrit1$^{+/+}$*, *Lrit1$^{+/-}$*, and *Lrit1$^{-/-}$* littermates (n = 5-7 per group, 10-14 retinas per group) to determine if loss of LRIT1 affects retinal function (Fig. 26). On the leading edge of the scotopic ERG b-wave are a series of rhythmic, low amplitude superimposed oscillatory potentials (OPs) (63). OPs are hypothesized to reflect inner retinal function involving some combination of bipolar, amacrine, and ganglion cells, although from which cell types OPs specifically arise is unknown (63,121,122). We observed what appears to be abnormal OPs from *Lrit1$^{+/-}$* and *Lrit1$^{-/-}$* mice compared to OPs from *Lrit1$^{+/+}$* mice (Fig. 26A). This suggests that loss of LRIT1 may interfere with inner retinal function.

Analysis of the scotopic a- and b-waves showed both were decreased in *Lrit1$^{-/-}$* mice compared to *Lrit1$^{+/+}$* and *Lrit1$^{+/-}$* mice (Fig. 26Ci, Di). *Lrit1$^{-/-}$* mice also show reduced photopic a- and b-waves compared to *Lrit1$^{+/+}$* and *Lrit1$^{+/-}$* mice (Fig. 26Cii, Dii) (Table 5). For data analyses, I performed a repeated measures ANOVA with a Bonferroni's post-hoc correction for multiple comparisons. These data suggest LRIT1 affects photoreceptor hyperpolarization (decreased a-waves), which is transduced to and affects ON bipolar cell depolarization (decreased b-waves). Overall, the ERG data suggest two possible roles for LRIT1: 1) abnormal OPs in heterozygous and homozygous *Lrit1* mutants suggest altered inner retinal function and 2) homozygous loss of LRIT1 significantly alters rod and cone hyperpolarization and downstream ON bipolar cell depolarization.
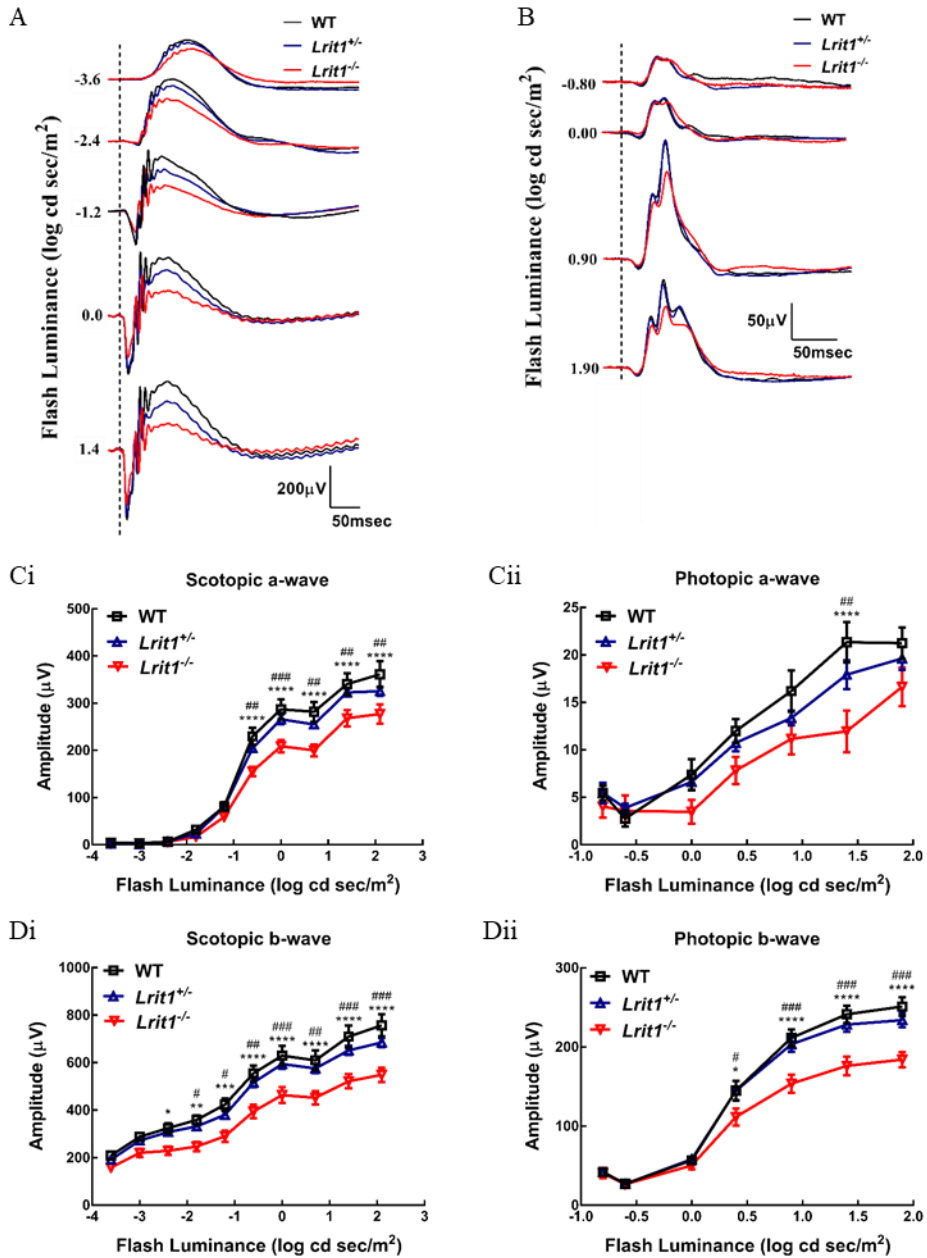
Fig. 26. ERGs of *Lrit1*^{-/-} mice show reduced dark- and light-adapted a- and b-waves. Dark-adapted (A) and light-adapted (B) ERGs. Quantification of the mean dark-adapted (Ci, Di) and light-adapted (Cii, Dii) a- and b-wave amplitudes as a function of light intensity with SEM (error bars). These data show reduced a- and b-waves in *Lrit1*^{-/-} mice. Data represent WT n=5,10; *Lrit1*^{+/-} n=7,14; and *Lrit1*^{-/-} n=5,10 where n= # mice, # retinas. Both eyes from all mice were subjected to ERGs. *,# $p<0.05$; **,## $p<0.01$; ***,### $p<0.001$; ****,#### $p<0.0001$. Asterisks, WT v *Lrit1*^{-/-}. Pound signs, *Lrit1*^{+/-} v *Lrit1*^{-/-}. WT v *Lrit1*^{+/-} were n.s. Repeated measures ANOVA with post-hoc Bonferroni's correction for multiple comparisons (a- and b-wave responses).

Table 5. ERG repeated measures ANOVA results*

Flash Intensity	a-wave			b-wave		
Scotopic (log cd sec/m²)	WT v $Lrit1^{+/-}$	WT v $Lrit1^{-/-}$	$Lrit1^{+/-}$ v $Lrit1^{-/-}$	WT v $Lrit1^{+/-}$	WT v $Lrit1^{-/-}$	$Lrit1^{+/-}$ v $Lrit1^{-/-}$
-3.6	>0.99	>0.99	>0.99	>0.99	0.4885	0.9765
-3.0	>0.99	>0.99	>0.99	>0.99	0.1951	0.3728
-2.4	>0.99	>0.99	>0.99	>0.99	0.0282	0.0585
-1.8	>0.99	>0.99	>0.99	>0.99	0.007	0.0375
-1.2	>0.99	0.5504	0.5245	0.596	0.001	0.0236
-0.6	0.3126	<0.0001	0.0051	0.7457	<0.0001	0.0011
0.0	0.5026	<0.0001	0.0009	0.8682	<0.0001	0.0005
0.7	0.2524	<0.0001	0.0015	0.9198	<0.0001	0.001
1.4	0.7559	<0.0001	0.0016	0.2637	<0.0001	0.0005
2.1	0.0639	<0.0001	0.0062	0.0984	<0.0001	0.0003
Photopic (log cd sec/m²)	WT v $Lrit1^{+/-}$	WT v $Lrit1^{-/-}$	$Lrit1^{+/-}$ v $Lrit1^{-/-}$	WT v $Lrit1^{+/-}$	WT v $Lrit1^{-/-}$	$Lrit1^{+/-}$ v $Lrit1^{-/-}$
-0.8	>0.99	>0.99	>0.99	>0.99	>0.99	>0.99
-0.6	>0.99	>0.99	>0.99	>0.99	>0.99	>0.99
0.0	>0.99	0.1828	0.3089	>0.99	>0.99	>0.99
0.4	>0.99	0.1406	0.3945	>0.99	0.0365	0.0223
0.9	0.4278	0.0506	0.7611	>0.99	<0.0001	0.0002
1.4	0.2355	<0.0001	0.0072	0.8471	<0.0001	0.0001
1.9	>0.99	0.0855	0.3631	0.4708	<0.0001	0.0002

WT (n=5,10), $Lrit1^{+/-}$ (n=7,14), and $Lrit1^{-/-}$ (n=5,10) mice where n= # mice, # retinas. Both eyes from all mice were subjected to ERGs.
*Post-hoc Bonferroni's correction for multiple comparisons adjusted p-values.
Blue shading indicates statistical significance for $\alpha = 0.05$.

Loss of LRIT1 Does Not Affect Retinal Morphology

Changes in retinal function can arise from alterations in retinal structure like the disrupted synapse assembly seen in ELFN1 knockout retinas (94) or decreased a- and b-waves in mice with retinal degeneration (123). To determine if *Lrit1* impacts retinal structure, we performed a double-blinded experiment to examine retinal morphology and morphometry. Retinal morphology can be altered in specific retinal regions, so we analyzed morphology in both central and peripheral retinal regions (124). *Lrit1*⁺/⁻ and *Lrit1*⁻/⁻ retinas (n=5 mice, 5 retinas per group) were embedded in plastic, stained with cresyl violet, and sectioned. Our images demonstrate no gross morphological changes in the central or peripheral

retinal regions of *Lrit1*^{-/-} retinas compared to *Lrit1*^{+/-} mice (Fig. 27). These sections also were used to

determine the thickness of each retinal layer (Table 6). A trained masked observer measured all individual

retinal layers (OS, IS, ONL, OPL, INL, IPL, and GCL) and the total retinal thickness from the OS to the

GCL. Welch's unpaired t-test was used to compare total retinal thickness between genotypes (*Lrit1*^{+/-} and

Lrit1^{-/-}) and found no statistical differences (Table 6). I also tested whether the thickness of the retinal

layers was different between genotypes using a two-way ANOVA with factors for genotype and retinal

layer. These results demonstrate there was no significant difference (p = 0.2858) in retinal layer thickness

between *Lrit1*^{+/-} and *Lrit1*^{-/-} mice (Table 6). These data suggest that the *Lrit1*^{-/-} retinas are morphologically

normal.
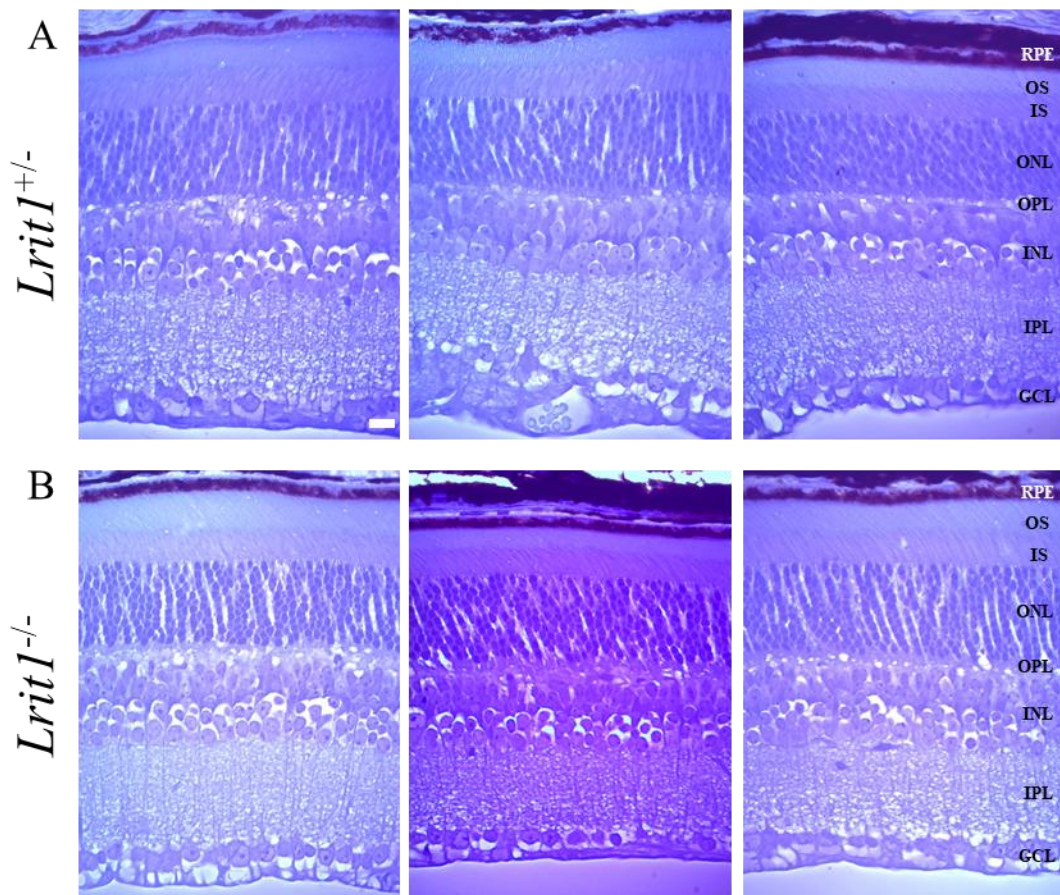
Fig. 27. Photomicrographs show normal retinal morphology and no retinal degeneration in *Lrit1*^{-/-} mice. A) *Lrit1*^{+/-} and B) *Lrit1*^{-/-} transverse retinal sections stained with 1% cresyl violet. Each image represents an independent animal. Right) Retinal pigment epithelium (RPE), outer segments (OS), inner segments (IS), outer nuclear layer (ONL), outer plexiform layer (OPL), inner nuclear layer (INL), inner plexiform layer (IPL), and the retinal ganglion cell layer (GCL). Scale bar, 20μm.

Table 6. Retinal morphometry is comparable for *Lrit1*$^{+/-}$ and *Lrit1*$^{-/-}$ retinas.

	Lrit1$^{+/-}$ ($n = 5$)	*Lrit1*$^{-/-}$ ($n = 5$)
Layer*	Mean ± SEM (µm)	Mean ± SEM (µm)
OS Central	17.36 ± 0.83	16.27 ± 0.39
OS Peripheral	12.44 ± 0.66	12.64 ± 0.71
IS Central	17.83 ± 0.80	16.84 ± 0.94
IS Peripheral	13.92 ± 0.98	12.85 ± 0.69
ONL Central	48.14 ± 0.96	47.17 ± 1.33
ONL Peripheral	38.20 ± 1.26	36.52 ± 1.02
OPL Central	9.87 ± 0.78	9.47 ± 1.41
OPL Peripheral	9.48 ± 1.26	9.46 ± 1.05
INL Central	40.72 ± 0.67	43.77 ± 1.02
INL Peripheral	30.47 ± 1.49	33.53 ± 2.26
IPL Central	51.26 ± 1.24	52.79 ± 4.07
IPL Peripheral	44.97 ± 1.67	41.30 ± 2.32
GCL Central	25.63 ± 2.04	22.55 ± 1.01
GCL Peripheral	15.46 ± 2.46	12.18 ± 0.40
Measured Central@	210.9 ± 0.89	209.1 ± 2.17
Measured Peripheral@	164.6 ± 1.48	158.2 ± 1.91
Calculated Central**@	210.8 ± 1.10	208.9 ± 2.17
Calculated Peripheral**@	164.9 ± 1.11	158.5 ± 1.92

The following retinal layers were measured at either the optic nerve (central) or retinal periphery (peripheral): photoreceptor outer segments (OS), photoreceptor inner segments (IS), outer nuclear layer (ONL), outer plexiform layer (OPL), inner nuclear layer (INL), inner plexiform layer (IPL), and retinal ganglion cell layer (GCL).
*Two-way ANOVA between genotypes is n.s. ($p = 0.2858$).
**Calculated values are the sums of all individual layers.
@Welch's unpaired t-tests for all measured versus calculated thicknesses are n.s.

RNA *in situ* hybridization localizes *Lrit1* mRNA to the ONL and INL

A previous *in situ* hybridization study showed *Lrit1* expression in the rat retina, specifically the photoreceptor cell bodies in the ONL (101). However, our ERG results suggesting a possible role for *Lrit1* in the inner retina led us to hypothesize that *Lrit1* may also be expressed in additional retinal cell types in the mouse. To localize *Lrit1* expression in the mouse retina, I performed RNA *in situ* hybridization on transverse retinal sections. RNA *in situ* hybridization utilizes a complementary oligonucleotide probe to bind its target RNA and visualize the transcript of interest. The positive control probe *Polr2a* encodes the RNA Polymerase II subunit A. *Polr2a* exhibited ubiquitous expression in all retinal nuclear layers (ONL, INL, GCL) (Fig. 28A). The negative control probe *DapB* encodes an *E. coli* enzyme, *DapB*, and was not expressed in any nuclear layers in the mouse retina (Fig. 28B).
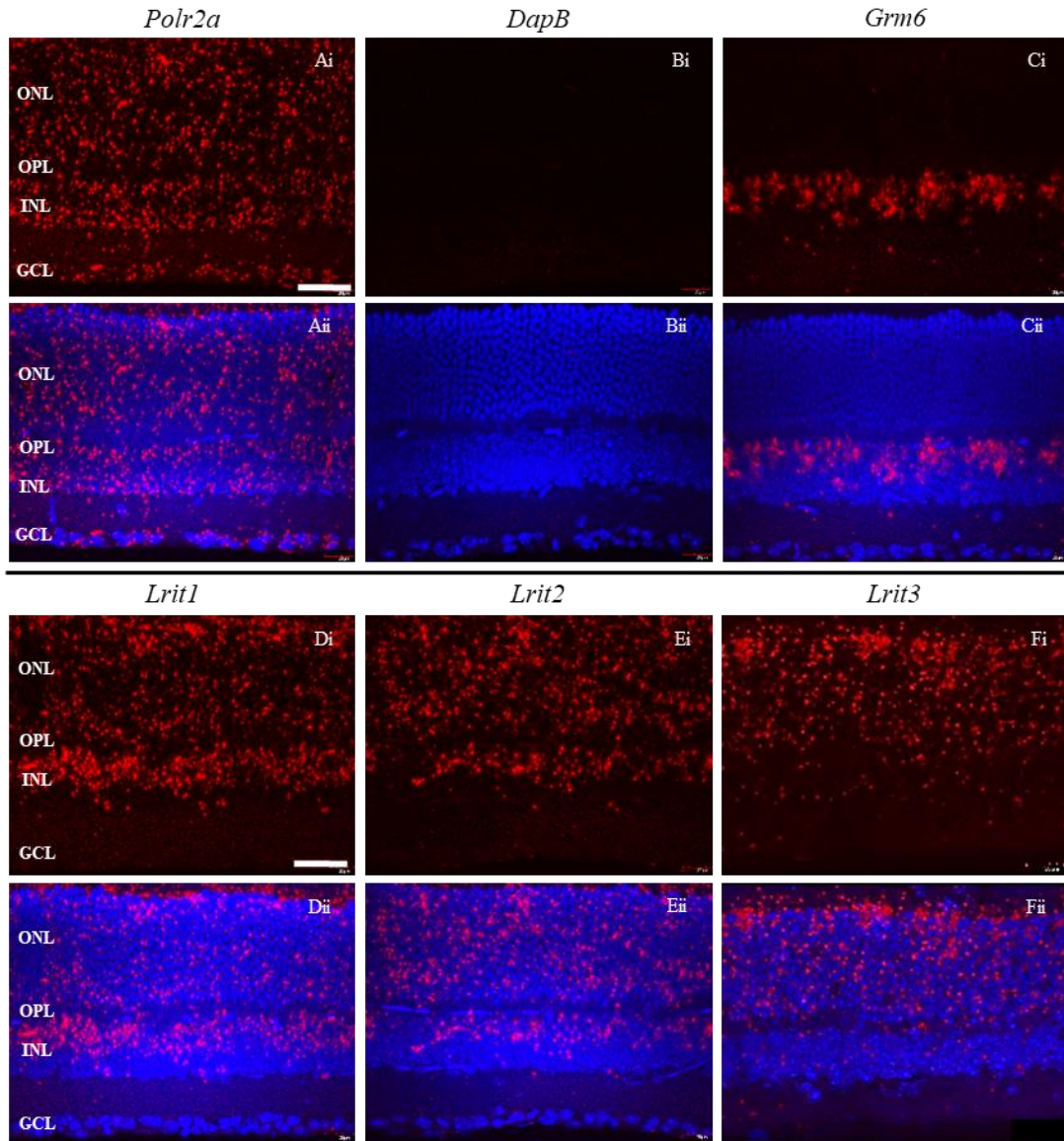
Fig. 28. *Lrit1* is expressed in the ONL and INL in the mouse retina. Ai, Aii) *Polr2a* hybridizes to ONL, INL, and GCL. Bi, Bii) *DapB* does not hybridize in the mouse retina. Ci, Cii) *Grm6* ON bipolar cell probe hybridizes to the upper INL. Di, Dii) *Lrit1* probe hybridizes to the ONL and upper INL. Ei, Eii) *Lrit2* probe hybridizes to the ONL and upper INL. Fi, Fii) *Lrit3* probe hybridizes to the ONL and middle INL. *Lrit1* expression is similar to but distinct from *Grm6* and *Lrit3* expression. These data indicate *Lrit1* is expressed in photoreceptors and one or more INL cell types. Images are from WT transverse retinal sections and representative of 6 experiments using independent mice. Outer nuclear layer (ONL), outer plexiform layer (OPL), inner nuclear layer (INL), and ganglion cell layer (GCL). DAPI stain nuclei (blue) and probes (red). Scale bar, 10μm.

We investigated the gene expression patterns for four mRNA targets: *Lrit1, Lrit2, Lrit3*, and *Grm6*. Our positive control for ON bipolar cells was *Grm6* (Fig. 28Ci, Cii). Previous RNA-Seq data suggested that *Lrit1, Lrit2,* and *Lrit3* are expressed in the mouse retina (Fig. 1) (117). Our data showed *Lrit1* was expressed in the ONL and INL (Fig. 28Di, Dii). *Lrit1* expression in the INL was similar to but distinct from *Grm6,* suggesting *Lrit1* may be expressed in ON bipolar cells but may also be expressed in horizontal, amacrine, or cone OFF bipolar cells. These data confirm our hypothesis that *Lrit1* expression is not limited to the OS as shown in the rat retina and may therefore contribute to inner retinal function (101). Transcriptional expression at any isolated time point is a balance of transcript synthesis and degradation. It is possible that although the transcript may be produced in *Lrit1$^{-/-}$* mice, the transcript is also degraded before translation occurs. To examine this, I did i*n situ* hybridization experiments using *Lrit1$^{+/+}$, Lrit1$^{+/-}$,* and *Lrit1$^{-/-}$* mice (Fig. 29). These data showed *Lrit1* is expressed in the ONL and INL in all *Lrit1$^{-/-}$* mice.

LRIT2 is a close relative of LRIT1 and LRIT3 (99). Our results showed *Lrit2* is expressed in the ONL and INL (Fig. 28Ei-Eii). The function for LRIT2 has not yet been elucidated.

Because LRIT3 has previously been shown to co-localize with ON bipolar cells and the *Lrit3^{nob6}* mouse had a no b-wave ERG, we speculated that LRIT3 is expressed in ON bipolar cells. Our results showed the *Lrit3* expression pattern in the INL is distinct from *Grm6* (Fig. 28Fi-Fii). Much to our surprise, our data also demonstrated *Lrit3* is expressed in the ONL. This suggests photoreceptors express *Lrit3* and is supported by our analysis of previous RNA-Seq data (Fig. 20).
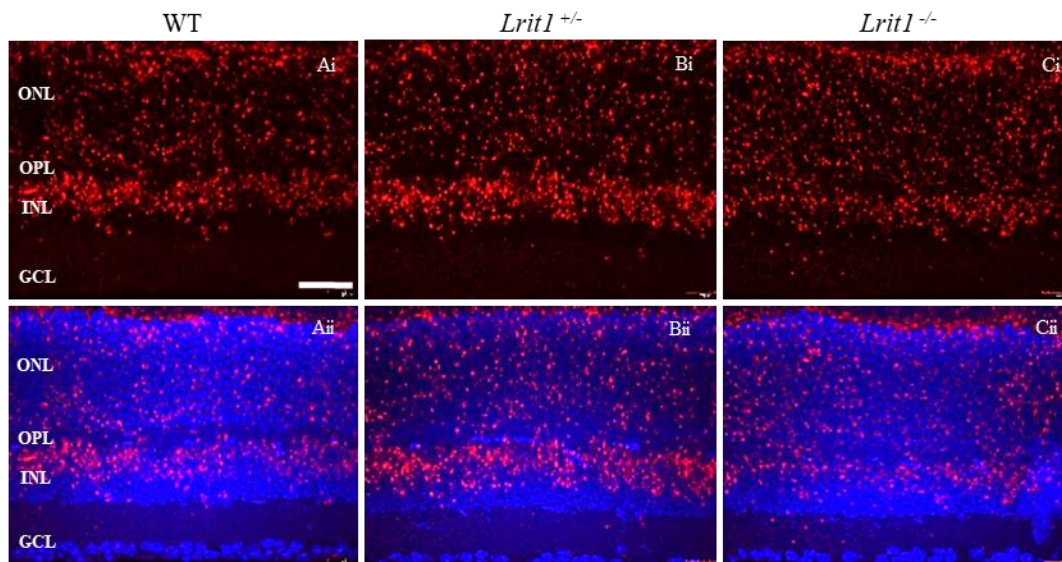
Fig. 29. *Lrit1* is expressed in WT (Ai, Aii), *Lrit1*$^{+/-}$ (Bi, Bii), and *Lrit1*$^{-/-}$ (Ci, Cii) mouse retinas. *Lrit1* target probe hybridizes to the ONL and upper INL. Images are representative of 3 experiments using independent mice. Outer nuclear layer (ONL), outer plexiform layer (OPL), inner nuclear layer (INL), and ganglion cell layer (GCL). DAPI stain nuclei (blue) and *Lrit1* probes (red). Scale bar, 10μm.

LRIT1 is Expressed at the OPL

To examine the expression pattern of the LRIT1 protein, we needed to generate an anti-LRIT1 antibody. I cloned full-length murine *Lrit1* cDNA into a PGK-myc-entry plasmid and confirmed the *Lrit1* sequence. This cDNA sequence matched that in the NCBI database, Accession #BC032270.1. We generated a rabbit anti-LRIT1 polyclonal antibody (Pierce Custom Antibody Service, Thermo Fisher Scientific) to a peptide on the C-terminal end of LRIT1. We used immunohistochemistry (IHC) to examine LRIT1 protein expression in transverse retinal sections. These data show that LRIT1 is expressed in a punctate pattern in the OPL of *Lrit1*$^{+/+}$ retinas and is absent in *Lrit1*$^{-/-}$ retinas, validating our antibody's specificity. The LRIT1 expression pattern shows both isolated and clustered puncta suggestive of rod and cone synapses, respectively (Fig. 30). Surprisingly, there was no staining in the photoreceptor OS as had been reported for rat (101).
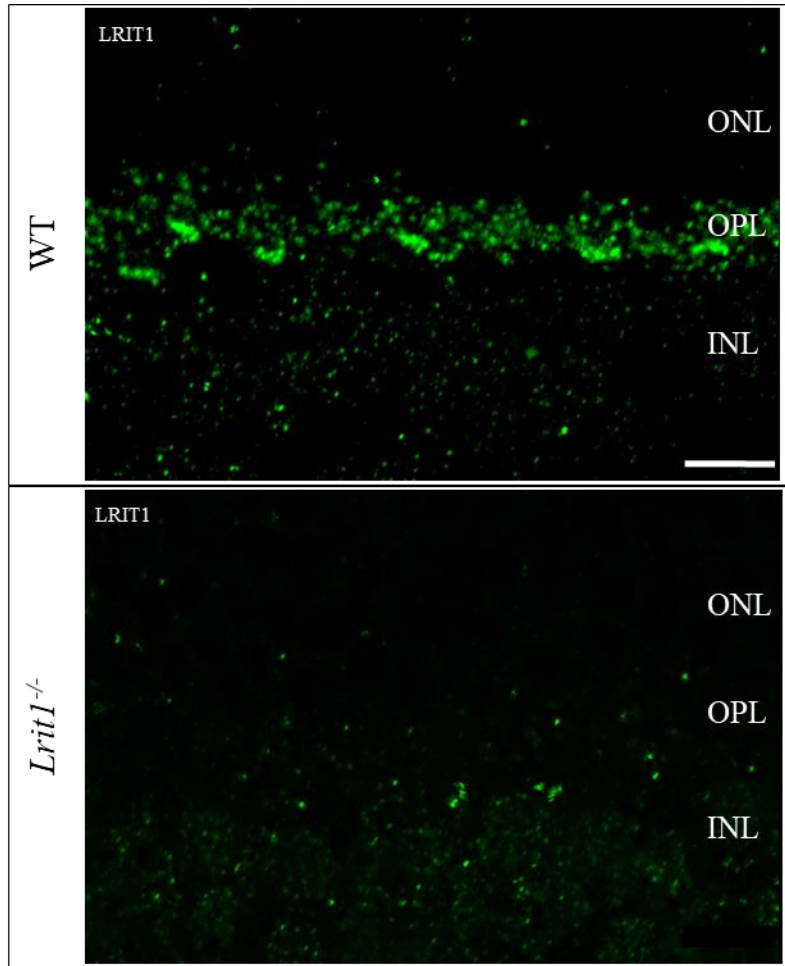
Fig. 30. LRIT1 is expressed in the OPL in mouse retina. LRIT1 labeling (green) in transverse retinal sections from WT (top) and *Lrit1*^{-/-} (bottom) mouse retinas. These data show a punctate staining pattern at the OPL that is absent in *Lrit1*^{-/-} mouse retinas. Note the non-specific staining in the ONL and INL in the *Lrit1*^{-/-} section. Data are representative for 17 WT and 10 *Lrit1*^{-/-} mouse retinas, respectively. Scale bar, 10μm.

Our attempts to visualize LRIT1 via western blot were unsuccessful. The antibody did yield bands, but we deemed this as non-specific expression because they were present in the *Lrit1⁻ᐟ⁻* retina lysates (Fig. 31).
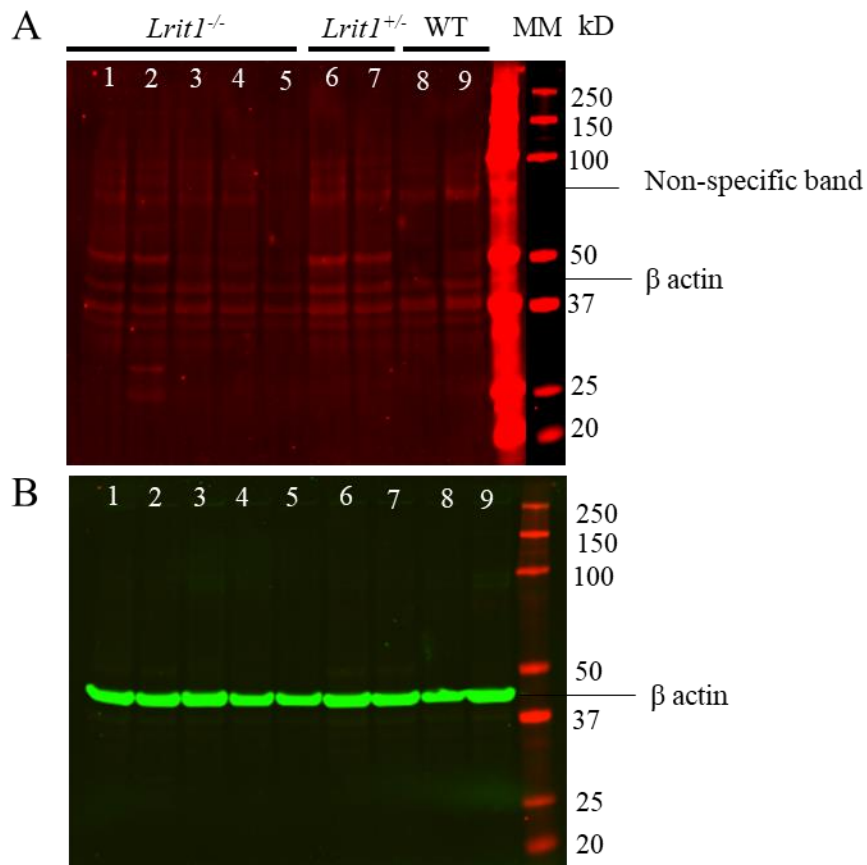
Fig. 31. The LRIT1 antibody does not detect LRIT1 on a Western blot. Anti-β actin (1:50,000; green) was used as a loading control with anti-LRIT1 (1:1000; red). A) The LRIT1 antibody fails to detect protein at the predicted size. Representative of 2 independent experiments (LRIT1; 1:100 and 1:1000) show a non-specific LRIT1 band (red). A, B) 31μg total protein loaded per lane. Each lane represents the retinal lysate from one independent animal. Broad range protein weight marker (MM; red) and β-actin bands (green).

Known Retinal Markers Localize Correctly in *Lrit1$^{-/-}$* Mouse Retinas

Because of the reduced dark- and light-adapted ERG a- and b-waves in *Lrit1$^{-/-}$* mice and its

punctate localization in the OPL, we next hypothesized that LRIT1 may affect the expression of proteins

previously shown to be critical for retinal function and with a similar expression pattern. We used IHC to

examine the expression pattern of photoreceptor (pikachurin, PNA, RIBEYE, PSD95), ON bipolar cell

(mGluR6, GPR179, LRIT3, RGS11, TRPM1, PKCα), and horizontal cell (calbindin) proteins in *Lrit1$^{+/+}$*

and *Lrit1$^{-/-}$* mice. Staining showed that all tested markers localized normally in *Lrit1$^{-/-}$* mice (Fig. 32-34).

These data suggest that loss of LRIT1 does not affect localization of known photoreceptor, bipolar, or

horizontal cell markers.
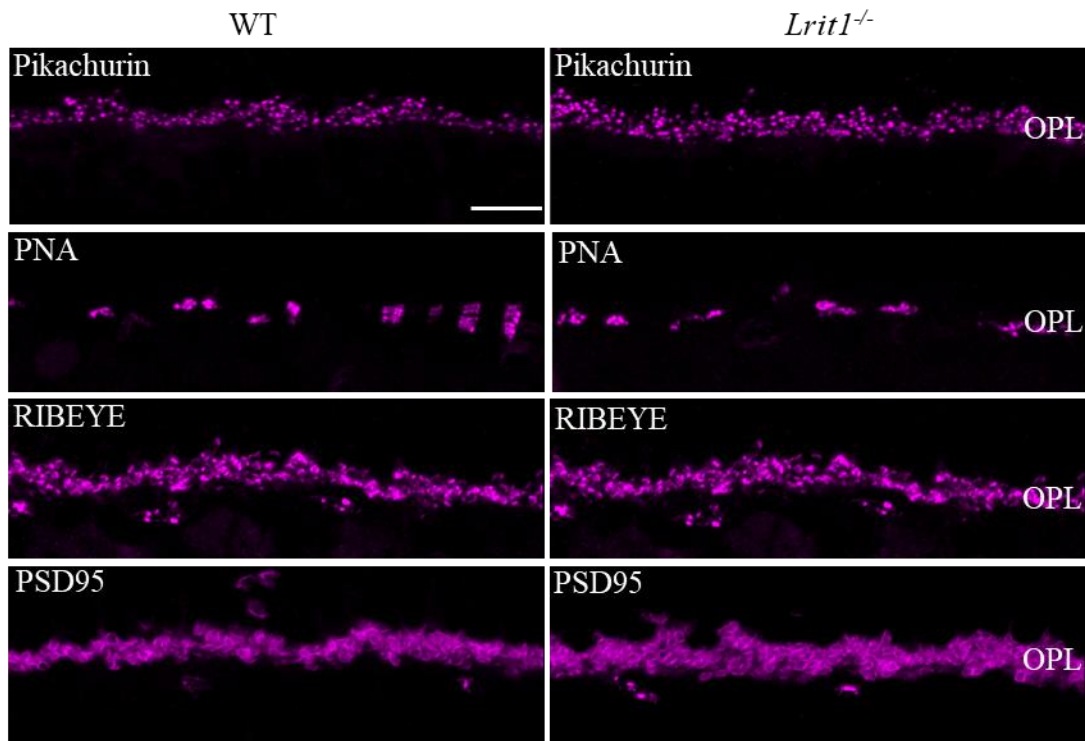
Fig. 32. Photoreceptor markers pikachurin, PNA, RIBEYE, and PSD95 localize normally at the OPL in *Lrit1$^{-/-}$* mice. Immunolabeling in transverse retinal sections for pikachurin, PNA, RIBEYE, and PSD95 in WT (left panel) and *Lrit1$^{-/-}$* (right panel) mouse retinas. Both genotypes exhibit punctate staining for pikachurin, large clusters for PNA, and staining of photoreceptor axon terminals for PSD95. Data are representative of 6 independent experiments. Scale bar, 10μm.
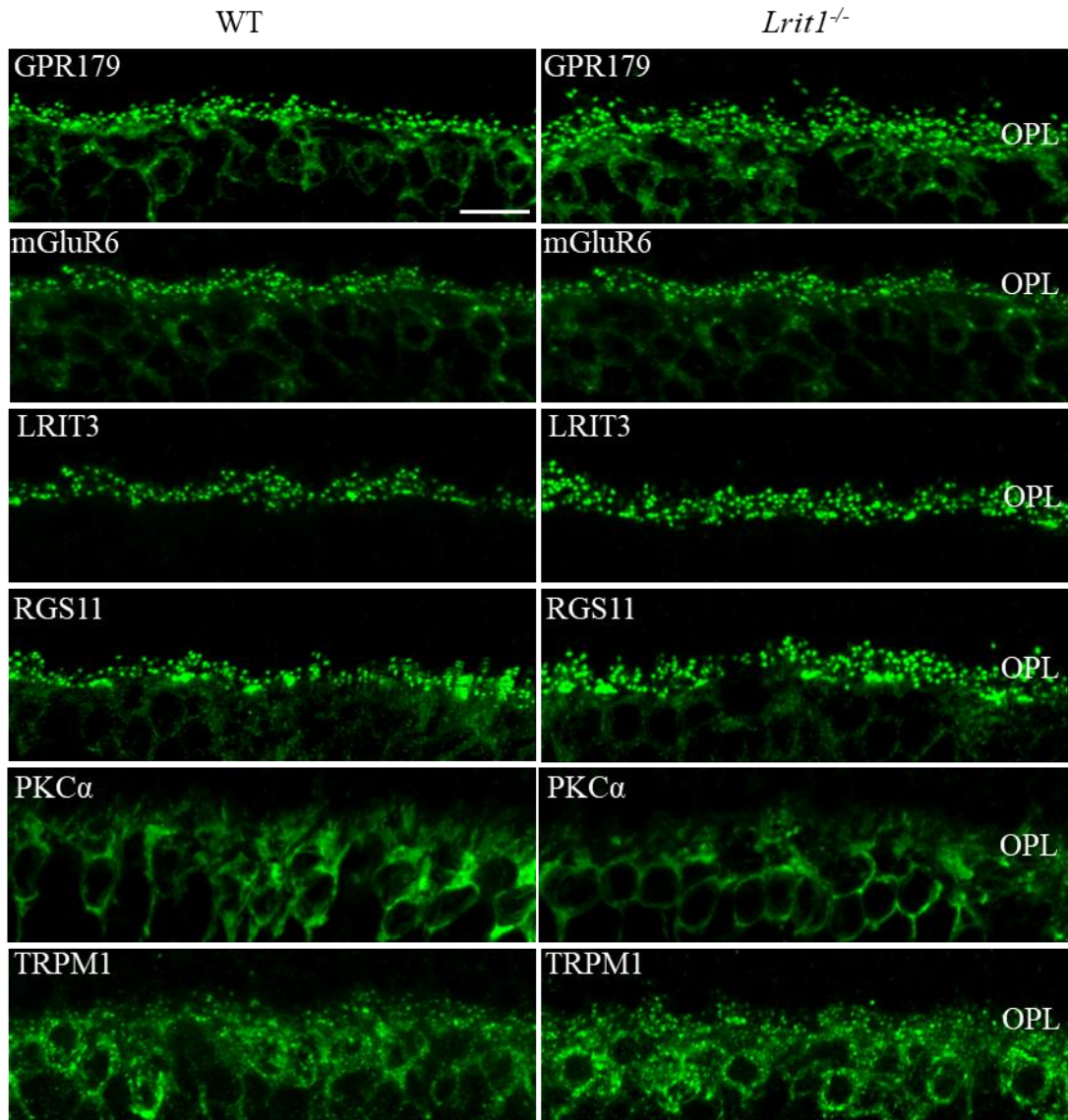
Fig. 33. ON bipolar cell markers GPR179, mGluR6, LRIT3, RGS11, PKCα, and TRPM1 localize normally at the OPL in *Lrit1⁻/⁻* mice. Immunolabeling in transverse retinal sections for GPR179, mGluR6, RGS11, TRPM1, LRIT3, and PKCα in WT (left panel) and *Lrit1⁻/⁻* (right panel) mouse retinas. All panels exhibit punctate staining patterns of the respective proteins and ON bipolar cell body staining for PKCα. Data are representative of 6 independent experiments. Scale bar, 10μm.
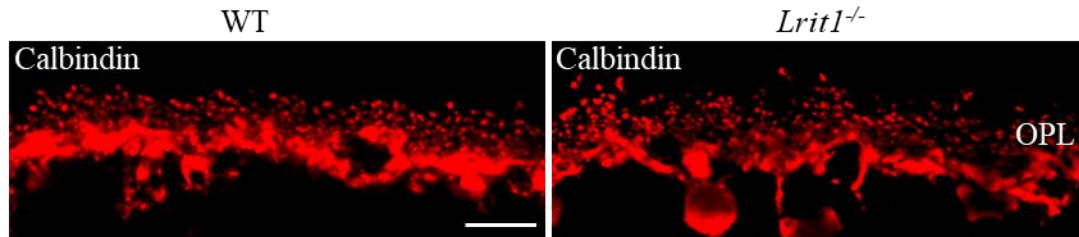
Fig. 34. The horizontal cell marker calbindin localizes normally at the OPL in *Lrit1*-/- mice. Immunolabeling in transverse retinal sections for calbindin in WT (left panel) and *Lrit1*-/- (right panel) mouse retinas. Both genotypes exhibit staining typical of horizontal cells. Data are representative of 3 independent experiments. Scale bar, 10μm.

LRIT1 Expression is Unchanged in *nob* Mouse Models

To determine if LRIT1 protein expression was dependent on nyctalopin, mGluR6, or TRPM1, I examined is localization in *Nyx*^nob, *Grm6*-/-, and *Trpm1*-/- mouse models (Fig. 35). These data show that LRIT1 expression pattern is not different in these mutants than in retinas from WT mice. This shows that the absence of these critical ON bipolar cell proteins does not affect LRIT1 expression.
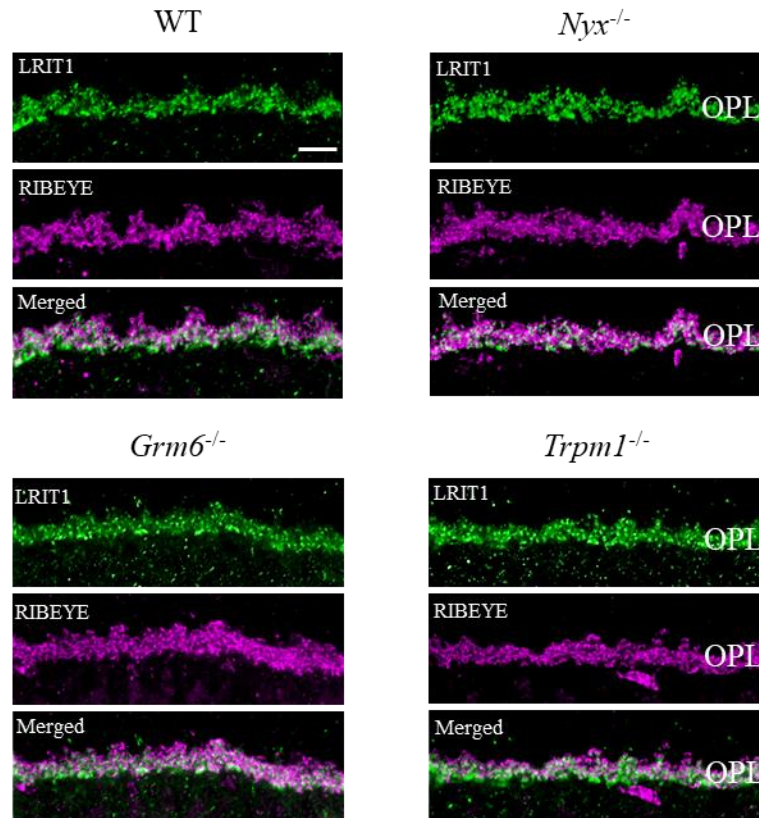
Fig. 35. LRIT1 localizes normally at the OPL in *nob* mouse models. Immunolabeling in transverse retinal sections for LRIT1 (green) and RIBEYE (magenta) in WT (top left), $Nyx^{-/-}$ (top right), $Grm6^{-/-}$ (bottom left), and $Trpm1^{-/-}$ (bottom right) mouse retinas. All genotypes exhibit LRIT1 punctate staining at the OPL. Data are representative of 3 independent experiments. Scale bar, 10μm.

LRIT1 Expression Localizes to OPL Synapses

Because LRIT1 staining localized to the OPL as puncta similar to mGluR6 and other ON Bipolar cell markers, I determined if it colocalized with these other synaptic proteins. I examined the colocalization of LRIT1 and PNA, a cone synaptic marker that binds to an as yet unidentified glycosylated protein (Fig. 36). These data show that LRIT1 localizes distal to PNA in the middle of the OPL. We next examined the colocalization of LRIT1 and RIBEYE, which marks the photoreceptor synaptic ribbons. LRIT1 does not localize with RIBEYE but resides within its arcs (Fig. 37). These data suggest that LRIT1 is present at horizontal cells, bipolar cell dendrites, or photoreceptor terminals.
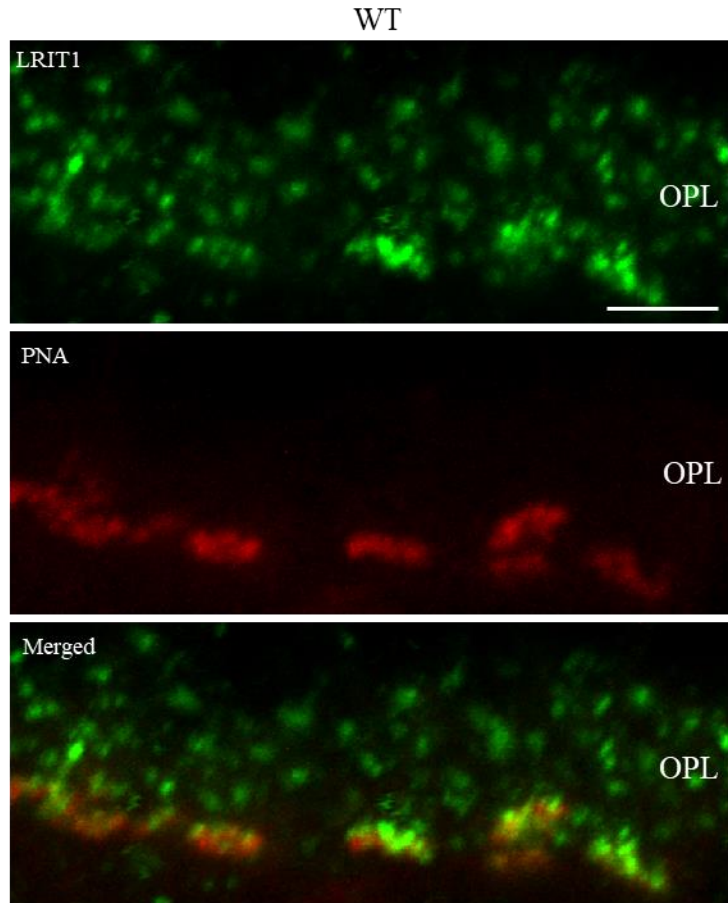
Fig. 36. LRIT1 localizes distal to PNA at cone terminals in WT mice. Immunolabeling in transverse retinal sections for LRIT1 (green) and PNA (red) in WT mouse retinas. Data are representative of 6 independent experiments. Scale bar, 10μm.
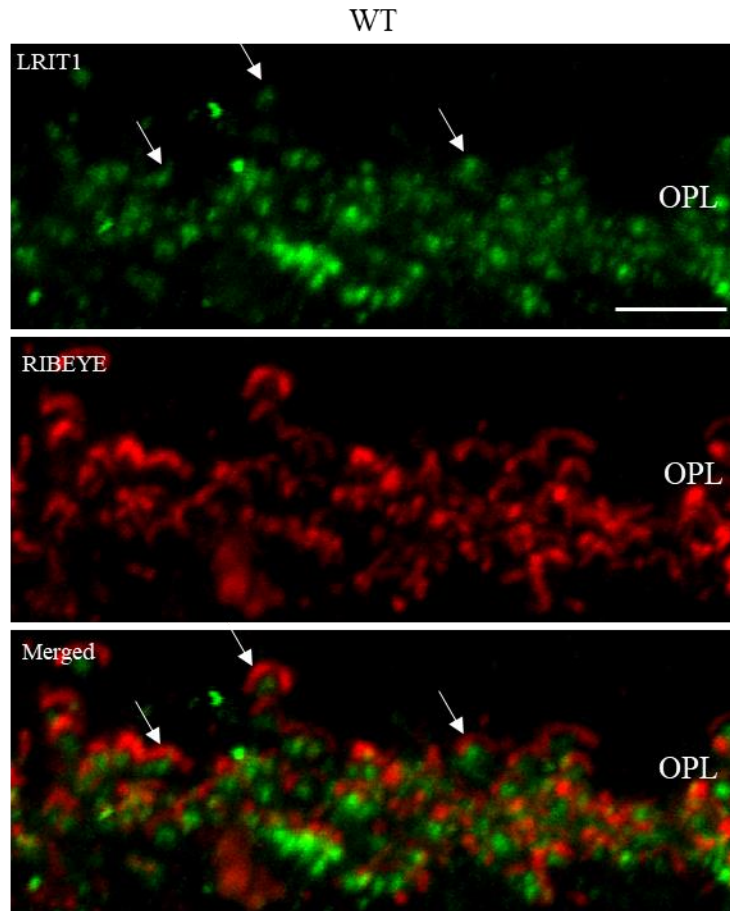
Fig. 37. LRIT1 localizes inside RIBEYE at photoreceptor ribbons in WT mice. Immunolabeling in transverse retinal sections for LRIT1 (green) and RIBEYE (red) in WT mouse retinas. WT mice exhibit LRIT1 punctate staining at the OPL inside RIBEYE crescents (arrows). Data are representative of 6 independent experiments. Scale bar, 10μm.

To determine if LRIT1 was localized to ON bipolar cells, I co-labelled for mGluR6 (Fig. 38-39). These data show that the two do not colocalize. Rather LRIT1 is localized in doublets distal to mGluR6 doublets, the latter of which mark the tips of the two rod ON bipolar cells that invaginate each rod spherule. This would suggest that the LRIT1 staining may be on horizontal cell axon terminals. We also co-labelled for LRIT1 and the ON bipolar cell protein GPR179 (Figs. 40-41). These data show that the two do not colocalize at rod spherules. Rather LRIT1 is localized distal to GPR179 puncta that mark the tips of the two rod ON bipolar cells that invaginate each rod spherule. LRIT1 does not colocalize with mGluR6 or GPR179 at cone pedicles. We observed mGluR6 colocalizes with PNA consistent with previous studies

(78) (Fig. 38). At cone pedicles LRIT1 localizes distally to PNA, mGluR6, and GPR179. These data

suggest that LRIT1 is expressed in horizontal cells.
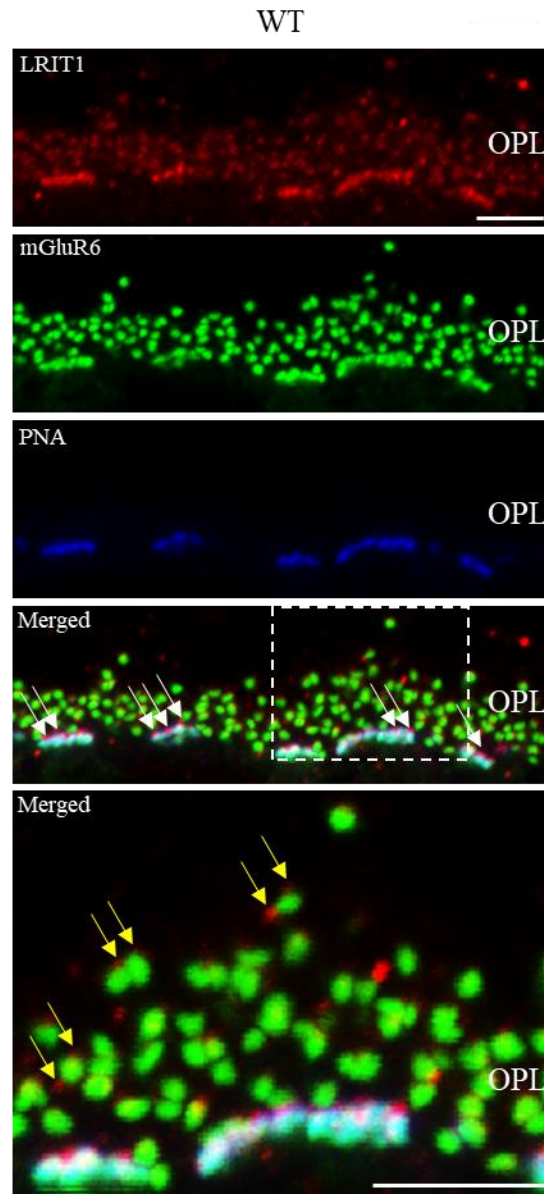
Fig. 38. LRIT1 localizes distal to mGluR6 and PNA at the OPL in WT mice. Immunolabeling in transverse retinal sections for LRIT1 (red), mGluR6 (green), and PNA (blue) in WT mouse retinas. WT mice exhibit LRIT1 punctate staining at the OPL distal to PNA (white arrows) and mGluR6 puncta (yellow arrows). Data are representative of 6 independent experiments. Scale bar, 10μm.
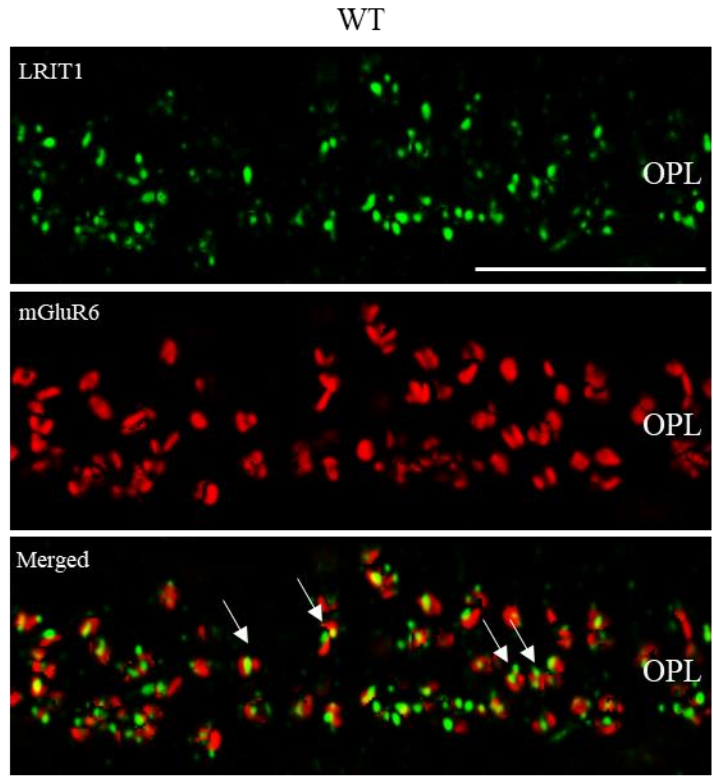
Fig. 39. LRIT1 localizes distal to mGluR6 in WT mice. Immunolabeling in transverse retinal sections for LRIT1 (green) and mGluR6 (red) in WT mouse retinas. WT mice exhibit LRIT1 punctate staining at the OPL distal to mGluR6 puncta (yellow arrows). Images were taken at 100X and deconvolved with 5 iterations. Data are representative of 2 independent experiments. Scale bar, 5μm.
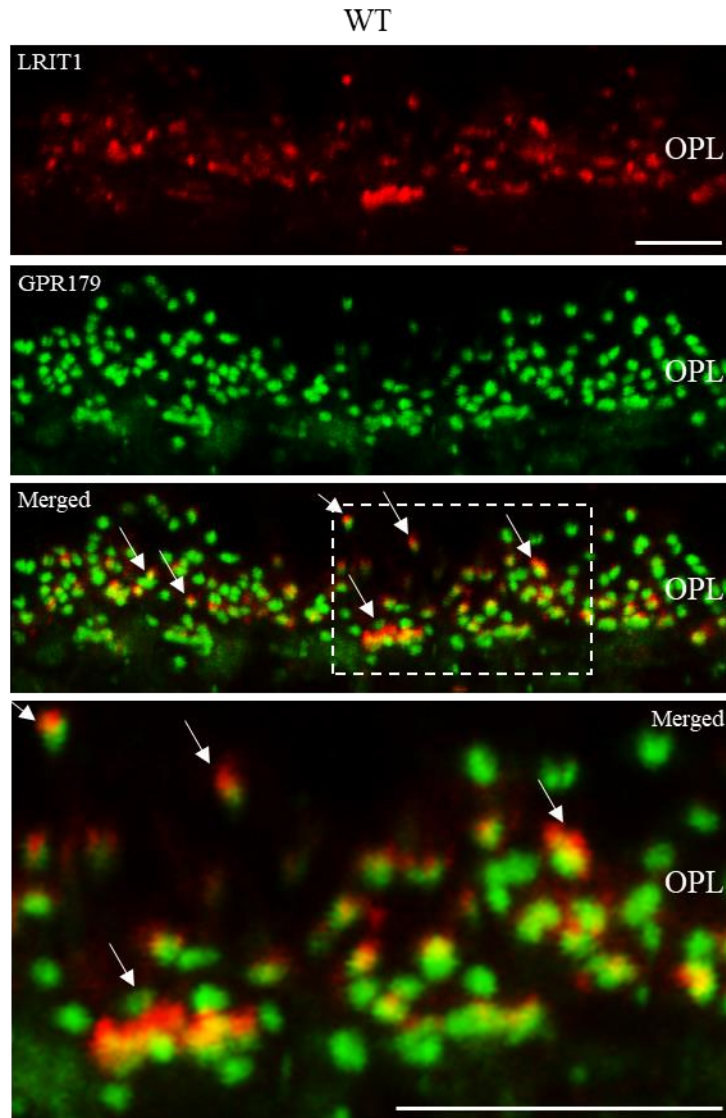
Fig. 40. LRIT1 localizes distal to GPR179 at the OPL in WT mice. Immunolabeling in transverse retinal sections for LRIT1 (red) and GPR179 (green) in WT mouse retinas. WT mice exhibit LRIT1 punctate staining at the OPL distal to GPR179 puncta (white arrows). Data are representative of 6 independent experiments. Scale bars, 10μm.
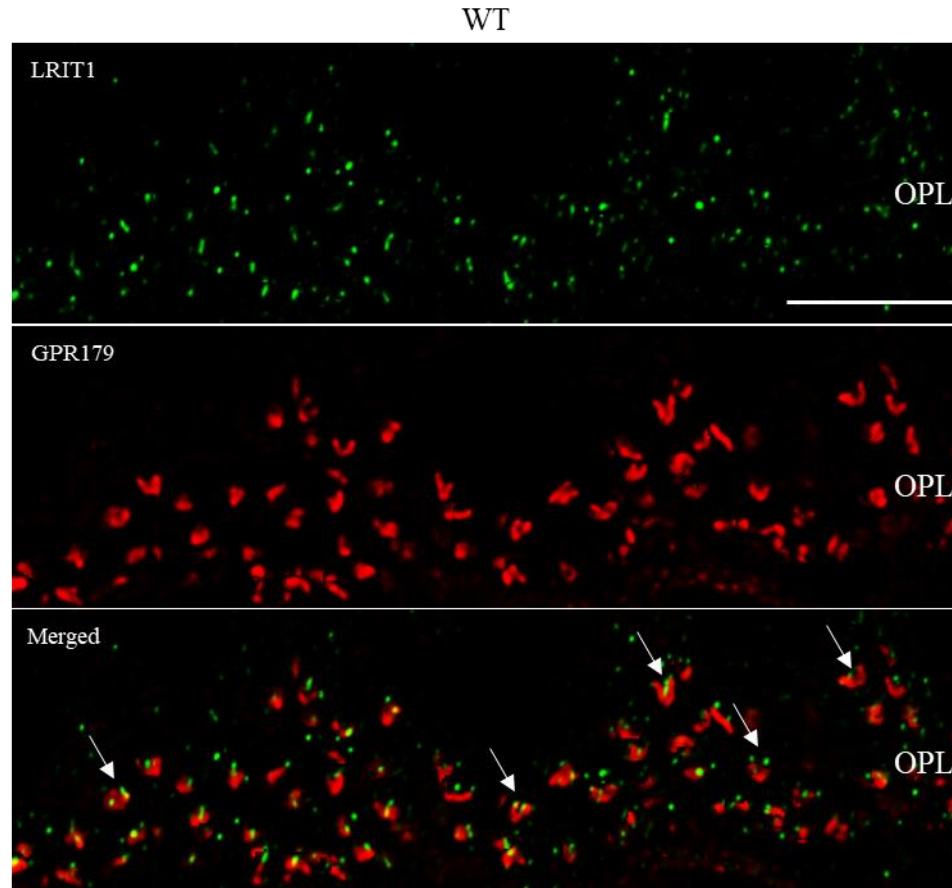
Fig. 41. LRIT1 localizes distal to GPR179 in WT mice. Immunolabeling in transverse retinal sections for LRIT1 (green) and GPR179 (red) in WT mouse retinas. WT mice exhibit LRIT1 punctate staining at the OPL distal to GPR179 puncta (yellow arrows). Images were taken at 100X and deconvolved with 5 iterations. Data are representative of 2 independent experiments. Scale bar, 5μm.

We examined the colocalization of LRIT1 with cone OFF bipolar cell type specific proteins HCN4 (type 3a) and PKAIIβ (type 3b). LRIT1 does not colocalize with either (Fig. 42). These data support our hypothesis that LRIT1 is not expressed in cone OFF bipolar cells.

Together, these data support the hypothesis that LRIT1 is expressed in horizontal cells, but not in ON or cone OFF bipolar cells.

WT
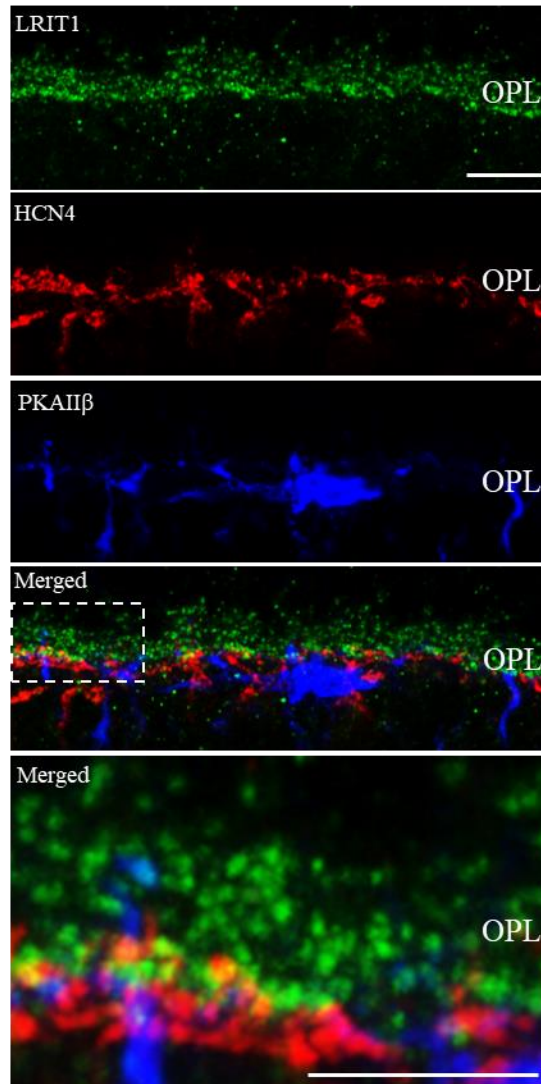
Fig. 42. LRIT1 does not co-localize with HCN4 or PKAIIβ in WT mice. Immunolabeling in transverse retinal sections for LRIT1 (green), HCN4 (red), and PKAIIβ (blue) in WT mouse retinas. WT mice exhibit LRIT1 punctate staining at the OPL that does not colocalize with OFF bipolar cell types 3a and 3b markers HCN4 and PKAIIβ, respectively. Data are representative of 2 independent experiments. Scale bars, 10μm.

LRIT1 Loss Does Not Affect Overall Ganglion Cell Responsiveness

After observing the reduced a- and b- wave ERGs in *Lrit1*^{-/-} mice and apparent abnormal OPs in *Lrit1*^{+/-} and *Lrit1*^{-/-} mice, we wanted to examine if and how the loss of LRIT1 affects retinal ganglion cell (RGC) function. We used multi-electrode arrays to record light-evoked electrical responses from *Lrit1*^{+/-} and *Lrit1*^{-/-} ganglion cells and compared them to a database of WT recordings (116). We tested light-evoked electrical responses at 3 dark-adapted and 3 light-adapted levels to assess responses from rods and cones, respectively. In WT mice there are three general functional classes of responsive retinal ganglion cells, ON, OFF, and ON/OFF. The ON cells respond at light onset, OFF cells respond at light offset, and ON/OFF cells respond at light on- and offset (Fig. 43A). There are a large number of non-responsive cells at the lowest stimulus intensity, -2.3 log cd sec/m^2 (Fig. 43E). There also are a small number of non-responsive cells at all other tested stimulus intensities (-1.5, 0.2, 0.5, 1.2, and 2.5 log cd sec/m^2) (Fig. 44). The proportions of responsive and non-responsive cells in WT, *Lrit1*^{+/-}, *Lrit1*^{-/-} are similar at all stimulus intensities (Fig. 43B-C).
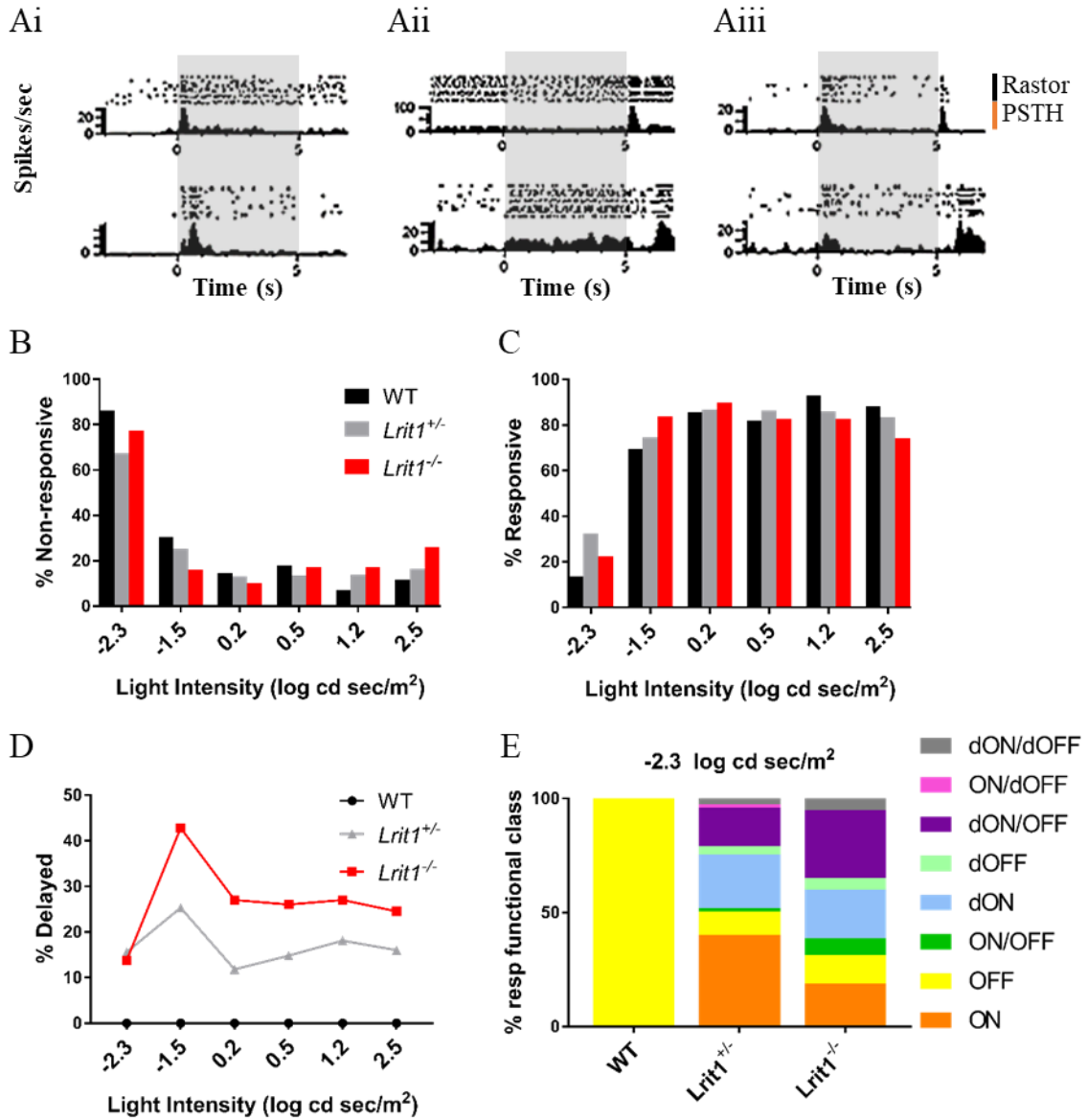
Fig. 43. Proportion of responsive *Lrit1⁻/⁻* retinal ganglion cells does not differ from WT cells. A) Normal (top) and delayed (bottom) responses over time for ON (Ai), OFF (Aii), and ON/OFF (Aiii) *Lrit1⁻/⁻* retinal ganglion cells. Light onset (superimposed gray boxes). Each response displays 10 raster plots for cell responses over 10 trials (top) and the post-stimulus time histogram (PSTH) response amplitude averaging all 10 raster plots in spikes/sec (bottom). Proportion of non-responsive (B) and responsive (C) WT (black), *Lrit1⁺/⁻* (gray), and *Lrit1⁻/⁻* (red) retinal ganglion cells by increasing light intensity (x-axis). D) Proportion of delayed WT , *Lrit1⁺/⁻* , and *Lrit1⁻/⁻* retinal ganglion cells as a function of light intensity. These data indicate *Lrit1⁻/⁻* cells have delayed responses. E) A stacked bar plot showing proportions of responsive WT, *Lrit1⁺/⁻*, and *Lrit1⁻/⁻* retinal ganglion cells by functional class at the lowest light intensity. d signifies delayed response functional classes. These data indicate a greater number of *Lrit1⁻/⁻* cells respond at the lowest light intensity. Light intensities at each level are scotopic -2.3, -1.5, 0.2; and photopic 0.5, 1.2, and 2.5 in log cd sec/m². WT n=2 mice, 2 retinas, 174 cells; *Lrit1⁺/⁻* n=2 mice, 4 retinas, 237 cells; and *Lrit1⁻/⁻* n=3 mice, 6 retinas, 355 cells.

LRIT1 Loss Leads to Prolonged Ganglion Cell Response Latencies

Although there were no observed differences in the proportions of responsive cells, the nature of the responses was different. For each cell two key parameters are measured, response latency to reach the peak response and peak response amplitude measured as spikes/second. All WT cells have response latencies <0.5 seconds. In contrast, we observed prolonged response latencies of >0.5 seconds in large numbers of *Lrit1*$^{+/-}$ and *Lrit1*$^{-/-}$ cells at all tested stimulus intensities. The responses in *Lrit1*$^{+/-}$ and *Lrit1*$^{-/-}$ cells yielded nine different functionally distinct classes: four normal (NR, ON, OFF, ON/OFF) and five abnormal with prolonged latency (dON, dOFF, dON/OFF, ON/dOFF, and dON/dOFF) (Fig. 44). This response delay is most pronounced at the lowest stimulus intensities, -2.3 and -1.5 log cd sec/m^2 (Fig. 43D, 44A-B). Further, *Lrit1*$^{-/-}$ ganglion cells have even greater numbers of delayed cells compared to *Lrit1*$^{+/-}$ cells. Frequency distributions plotting the time to peak (bin = 0.1s) are shown for *Lrit1*$^{+/-}$ (gray) and *Lrit1*$^{-/-}$ (red). For these two genotypes the distribution is right skewed much more than WT (black) (Fig. 45-48; Tables 7-10). These distributions are summarized as box and whiskers plots (Fig. 49-50) and show the skewed distributions for *Lrit1*$^{+/-}$ (gray) and *Lrit1*$^{-/-}$ (red) compared to WT (black). The observed delays were consistent among trials, suggesting the delay did not arise from abnormal adaptation to successive light flashes (see raster plots in Fig. 43A) (59).
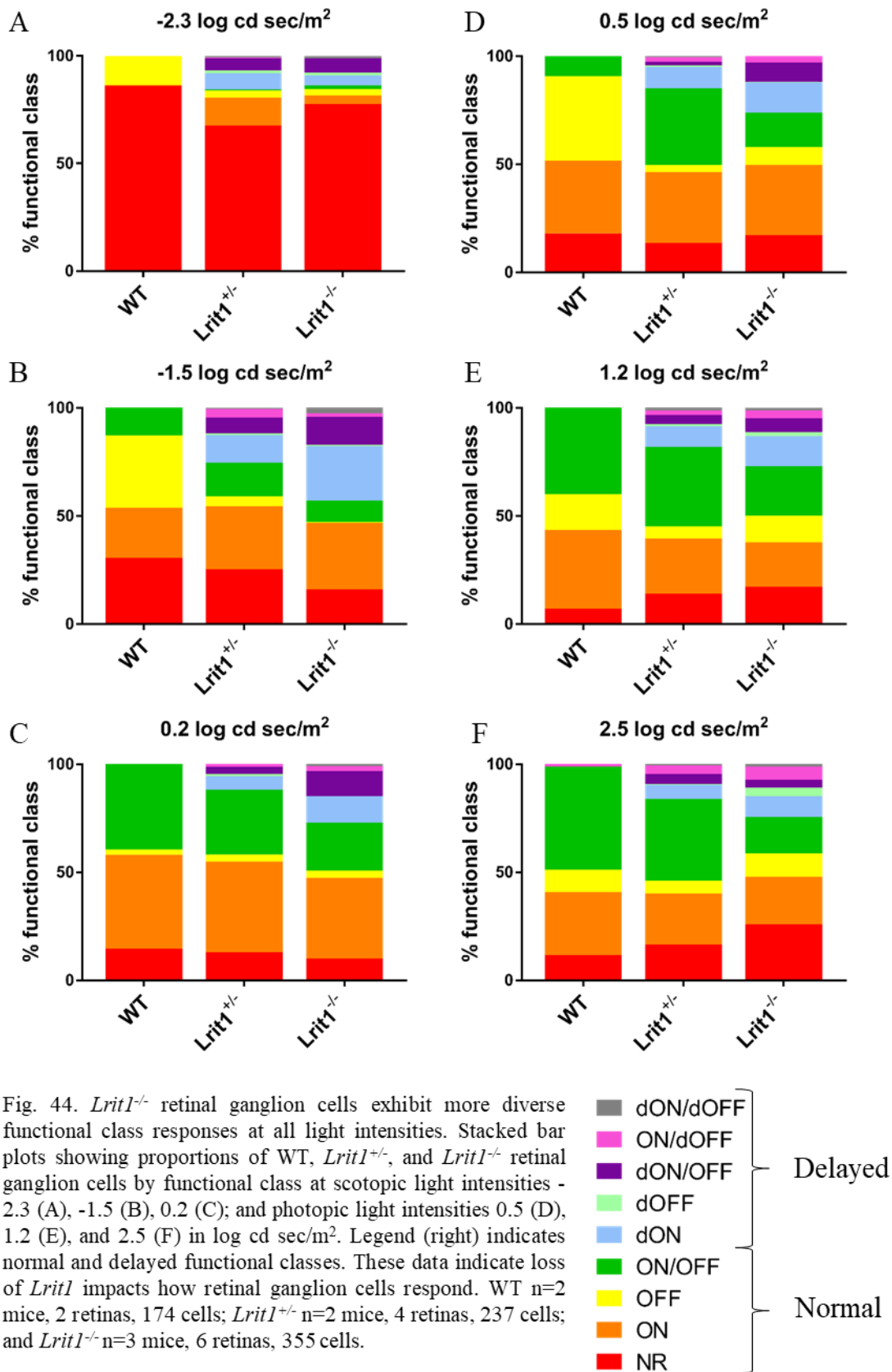
Fig. 44. *Lrit1*^{-/-} retinal ganglion cells exhibit more diverse functional class responses at all light intensities. Stacked bar plots showing proportions of WT, *Lrit1*^{+/-}, and *Lrit1*^{-/-} retinal ganglion cells by functional class at scotopic light intensities -2.3 (A), -1.5 (B), 0.2 (C); and photopic light intensities 0.5 (D), 1.2 (E), and 2.5 (F) in log cd sec/m^2. Legend (right) indicates normal and delayed functional classes. These data indicate loss of *Lrit1* impacts how retinal ganglion cells respond. WT n=2 mice, 2 retinas, 174 cells; *Lrit1*^{+/-} n=2 mice, 4 retinas, 237 cells; and *Lrit1*^{-/-} n=3 mice, 6 retinas, 355 cells.

Fig. 45. ON responses of *Lrit1*^{-/-} retinal ganglion cells exhibit prolonged response latencies under scotopic conditions. Frequency distributions plotting time to peak (response latency) in seconds for the proportion of ON (left panel) and the ON component of the ON/OFF (right panel) WT (black bars), *Lrit1*^{+/-} (gray bars), and *Lrit1*^{-/-} (red bars) retinal ganglion cells at scotopic light intensities -2.3 (A), -1.5 (B), 0.2 (C) in log cd sec/m². There were no ON or ON/OFF WT cells at the lowest light intensity. Histograms are binned (0.1s) as indicated on the x-axis. Data bins are 0.0-0.1s, 0.1-0.2s, 0.2-0.3s, etc. The x-axis displays either the end (odd x-axis values) or beginning (even x-axis values) value for every other consecutive bin. For example, x-axis odd value bin = 0.1 refers to bin 0-0.1s whereas even value bin = 0.2 refers to bin 0.2-0.3 s. WT n=2 mice, 2 retinas, 174 cells; *Lrit1*^{+/-} n=2 mice, 4 retinas, 237 cells; and *Lrit1*^{-/-} n=3 mice, 6 retinas, 355 cells.

Fig. 46. ON responses of *Lrit1-/-* retinal ganglion cells exhibit prolonged response latencies under photopic conditions. Frequency distributions plotting time to peak (response latency) in seconds for the proportion of ON (left panel) and the ON component of the ON/OFF (right panel) WT (black bars), *Lrit1+/-* (gray bars), and *Lrit1-/-* (red bars) retinal ganglion cells at photopic light intensities 0.5 (A), 1.2 (B), 2.5 (C) in log cd sec/m². Histograms are binned (0.1s) as indicated on the x-axis. Data bins are 0.0-0.1s, 0.1-0.2s, 0.2-0.3s, etc. The x-axis displays either the end (odd x-axis values) or beginning (even x-axis values) value for every other consecutive bin. For example, x-axis odd value bin = 0.1 refers to bin 0-0.1s whereas even value bin = 0.2 refers to bin 0.2-0.3 s. WT n=2 mice, 2 retinas, 174 cells; *Lrit1+/-* n=2 mice, 4 retinas, 237 cells; and *Lrit1-/-* n=3 mice, 6 retinas, 355 cells.

Fig. 47. OFF responses of *Lrit1⁻/⁻* retinal ganglion cells exhibit prolonged response latencies under scotopic conditions. Frequency distributions plotting time to peak (response latency) in seconds for the proportion of OFF (left panel) and the OFF component of the ON/OFF (right panel) WT (black bars), *Lrit1⁺/⁻* (gray bars), and *Lrit1⁻/⁻* (red bars) retinal ganglion cells at scotopic light intensities -2.3 (A), -1.5 (B), 0.2 (C) in log cd sec/m². There were no ON/OFF WT cells at the lowest light intensity. Histograms are binned (0.1s) as indicated on the x-axis. Data bins are 0.0-0.1s, 0.1-0.2s, 0.2-0.3s, etc. The x-axis displays either the end (odd x-axis values) or beginning (even x-axis values) value for every other consecutive bin. For example, x-axis odd value bin = 0.1 refers to bin 0-0.1s whereas even value bin = 0.2 refers to bin 0.2-0.3 s. WT n=2 mice, 2 retinas, 174 cells; *Lrit1⁺/⁻* n=2 mice, 4 retinas, 237 cells; and *Lrit1⁻/⁻* n=3 mice, 6 retinas, 355 cells.

Fig. 48. OFF responses of *Lrit1*^{-/-} retinal ganglion cells exhibit prolonged response latencies under photopic conditions. Frequency distributions plotting time to peak (response latency) in seconds for the proportion of OFF (left panel) and the OFF component of the ON/OFF (right panel) WT (black bars), *Lrit1*^{+/-} (gray bars), and *Lrit1*^{-/-} (red bars) retinal ganglion cells at photopic light intensities 0.5 (A), 1.2 (B), 2.5 (C) in log cd sec/m². Histograms are binned (0.1s) as indicated on the x-axis. Data bins are 0.0-0.1s, 0.1-0.2s, 0.2-0.3s, etc. The x-axis displays either the end (odd x-axis values) or beginning (even x-axis values) value for every other consecutive bin. For example, x-axis odd value bin = 0.1 refers to bin 0-0.1s whereas even value bin = 0.2 refers to bin 0.2-0.3 s. WT n=2 mice, 2 retinas, 174 cells; *Lrit1*^{+/-} n=2 mice, 4 retinas, 237 cells; and *Lrit1*^{-/-} n=3 mice, 6 retinas, 355 cells.

Table 7. Adjusted p-values Kruskal-Wallis test with Dunn's post-hoc correction for multiple comparisons for ON time to peak in retinal ganglion cells.

Genotype	Scotopic (log cd sec/m²)			Photopic (log cd sec/m²)		
	-2.3	-1.5	0.2	0.5	1.2	2.5
WT v Lrit1⁺/⁻	n/a	0.1606	0.0121	0.0359	0.0295	0.0032
WT v Lrit1⁻/⁻	n/a	0.0001	<0.0001	<0.0001	<0.0001	<0.0001
Lrit1⁺/⁻ v Lrit1⁻/⁻	>0.99	>0.99	0.0169	>0.99	0.2495	>0.99

Blue shading indicates statistically significant results at α = 0.05.

Table 8. Adjusted p-values Kruskal-Wallis test with Dunn's post-hoc correction for multiple comparisons for OFF time to peak in retinal ganglion cells.

Genotype	Scotopic (log cd sec/m²)			Photopic (log cd sec/m²)		
	-2.3	-1.5	0.2	0.5	1.2	2.5
WT v Lrit1⁺/⁻	>0.99	>0.99	>0.99	>0.99	0.1325	0.2273
WT v Lrit1⁻/⁻	>0.99	>0.99	>0.99	>0.99	0.0003	<0.0001
Lrit1⁺/⁻ v Lrit1⁻/⁻	>0.99	>0.99	>0.99	>0.99	>0.99	>0.99

Blue shading indicates statistically significant results at α = 0.05.

Table 9. Adjusted p-values Kruskal-Wallis test with Dunn's post-hoc correction for multiple comparisons for ON of ON/OFF time to peak in retinal ganglion cells.

Genotype	Scotopic (log cd sec/m^2)			Photopic (log cd sec/m^2)		
	-2.3	-1.5	0.2	0.5	1.2	2.5
WT v Lrit1$^{+/-}$	n/a	<0.0001	0.0216	0.8219	>0.99	>0.99
WT v Lrit1$^{-/-}$	n/a	<0.0001	<0.0001	0.001	<0.0001	<0.0001
Lrit1$^{+/-}$ v Lrit1$^{-/-}$	>0.99	>0.99	>0.99	0.1456	0.0436	0.1235

Blue shading indicates statistically significant results at α = 0.05.

Table 10. Adjusted p-values Kruskal-Wallis test with Dunn's post-hoc correction for multiple comparisons for OFF of ON/OFF time to peak in retinal ganglion cells.

Genotype	Scotopic (log cd sec/m^2)			Photopic (log cd sec/m^2)		
	-2.3	-1.5	0.2	0.5	1.2	2.5
WT v Lrit1$^{+/-}$	n/a	>0.99	>0.99	>0.99	0.7505	<0.0001
WT v Lrit1$^{-/-}$	n/a	>0.99	0.9198	>0.99	0.4262	<0.0001
Lrit1$^{+/-}$ v Lrit1$^{-/-}$	>0.99	>0.99	>0.99	>0.99	>0.99	>0.99

Blue shading indicates statistically significant results at α = 0.05.

Fig. 49. ON and OFF responses of *Lrit1*^{-/-} retinal ganglion cells exhibit prolonged response latencies under scotopic conditions. Box and whiskers plots for time to peak (response latency) in seconds for ON (left panel) and OFF (right panel) responses for WT (black), *Lrit1*^{+/-} (gray), and *Lrit1*^{-/-} (red) retinal ganglion cells at scotopic light intensities -2.3 (A), -1.5 (B), 0.2 (C) in log cd sec/m^2. Bars indicate means, and whiskers represent 5th to 95th percentile. Individual points indicate measures that fall outside of the 5th-95th percentile range. There were no WT ON or ON/OFF cells at the lowest light intensity. WT n=2 mice, 2 retinas, 174 cells; *Lrit1*^{+/-} n=2 mice, 4 retinas, 237 cells; and *Lrit1*^{-/-} n=3 mice, 6 retinas, 355 cells.

Fig. 50. ON and OFF responses of *Lrit1*^{-/-} retinal ganglion cells exhibit prolonged response latencies under photopic conditions. Box and whiskers plots for time to peak (response latency) in seconds for ON (left panel) and OFF (right panel) responses for WT (black), *Lrit1*^{+/-} (gray), and *Lrit1*^{-/-} (red) retinal ganglion cells at photopic light intensities 0.5 (A), 1.2 (B), 2.5 (C) in log cd sec/m^2. Bars indicate means, and whiskers represent 5th to 95th percentile. Individual points indicate measures that fall outside of the 5th-95th percentile range. WT n=2 mice, 2 retinas, 174 cells; *Lrit1*^{+/-} n=2 mice, 4 retinas, 237 cells; and *Lrit1*^{-/-} n=3 mice, 6 retinas, 355 cells.

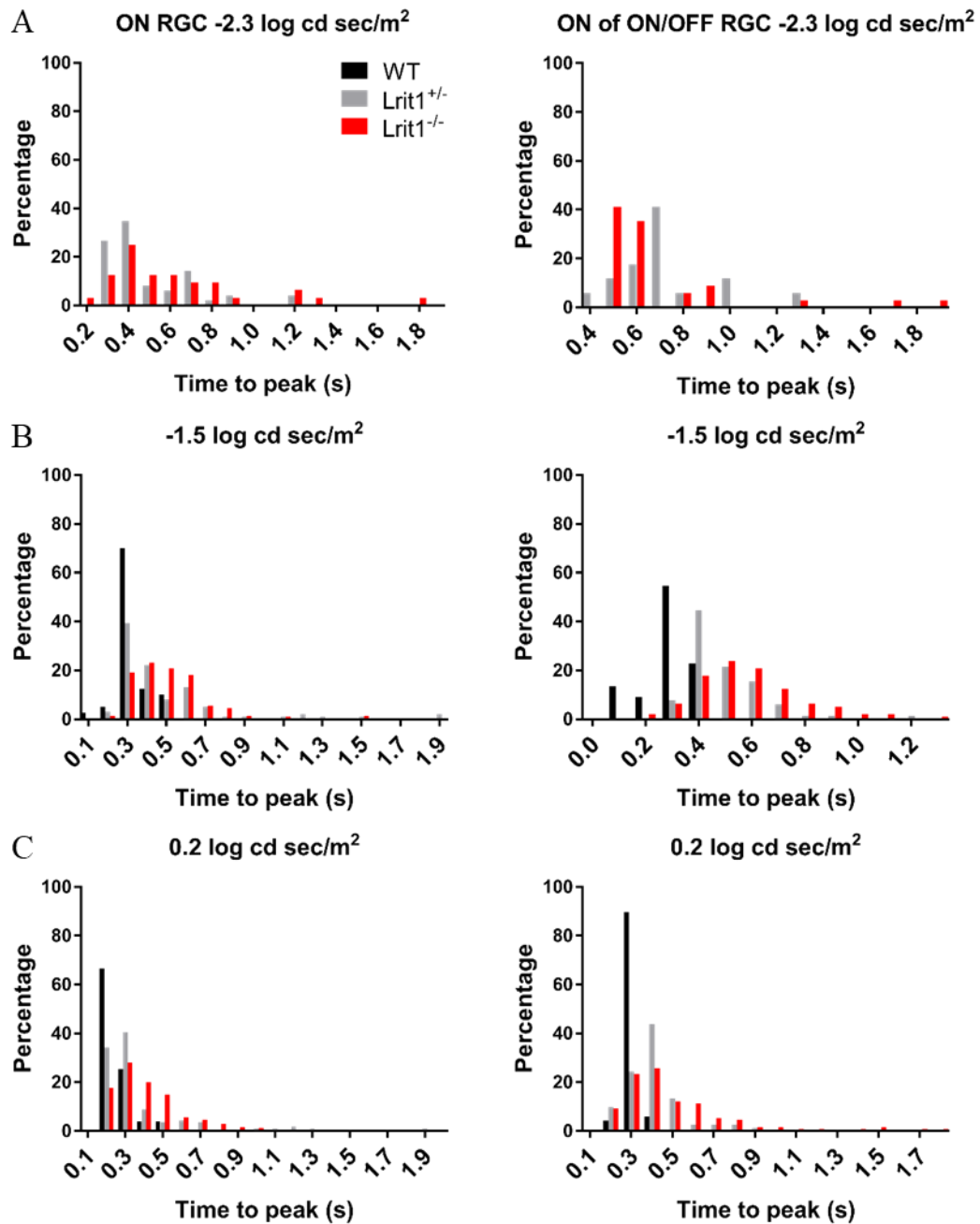**LRIT1 Loss Leads to Increased Light-Evoked responses**

We next examined how the loss of LRIT1 affects the peak amplitude of the ganglion cell response. Pre-synaptic input above the ganglion cell threshold causes an individual ganglion cell to generate an action potential. Each action potential is called a spike. The peak amplitude reflects the cell's spiking rate over time. Frequency distributions plotting the peak amplitude (bin = 10 spikes/sec) are shown for $Lrit1^{+/-}$ (gray) and $Lrit1^{-/-}$ (red). For these two genotypes the distribution is right skewed compared to WT (black) (Fig. 51-54; Tables 11-14). These distributions are summarized as box and whiskers plots (Fig. 55-56) and show the skewed distributions for $Lrit1^{+/-}$ (gray) and $Lrit1^{-/-}$ (red) compared to WT (black).

Fig. 51. ON responses of *Lrit1⁻/⁻* retinal ganglion cells exhibit increased peak amplitudes under scotopic conditions. Frequency distributions plotting peak amplitude in spikes/second for the proportion of ON (left panel) and the ON component of the ON/OFF (right panel) WT (black bars), *Lrit1⁺/⁻* (gray bars), and *Lrit1⁻/⁻* (red bars) retinal ganglion cells at scotopic light intensities -2.3 (A), -1.5 (B), 0.2 (C) in log cd sec/m². There were no ON or ON/OFF WT cells at the lowest light intensity. Histograms are binned (10 spikes/second) as indicated on the x-axis. Data bins in spikes/second are 0-10, 10-20, 21-30, etc. The x-axis displays the beginning value for every other consecutive bin. For example, x-axis bin = 0 refers to bin 0-10 spikes/second. WT n=2 mice, 2 retinas, 174 cells; *Lrit1⁺/⁻* n=2 mice, 4 retinas, 237 cells; and *Lrit1⁻/⁻* n=3 mice, 6 retinas, 355 cells.
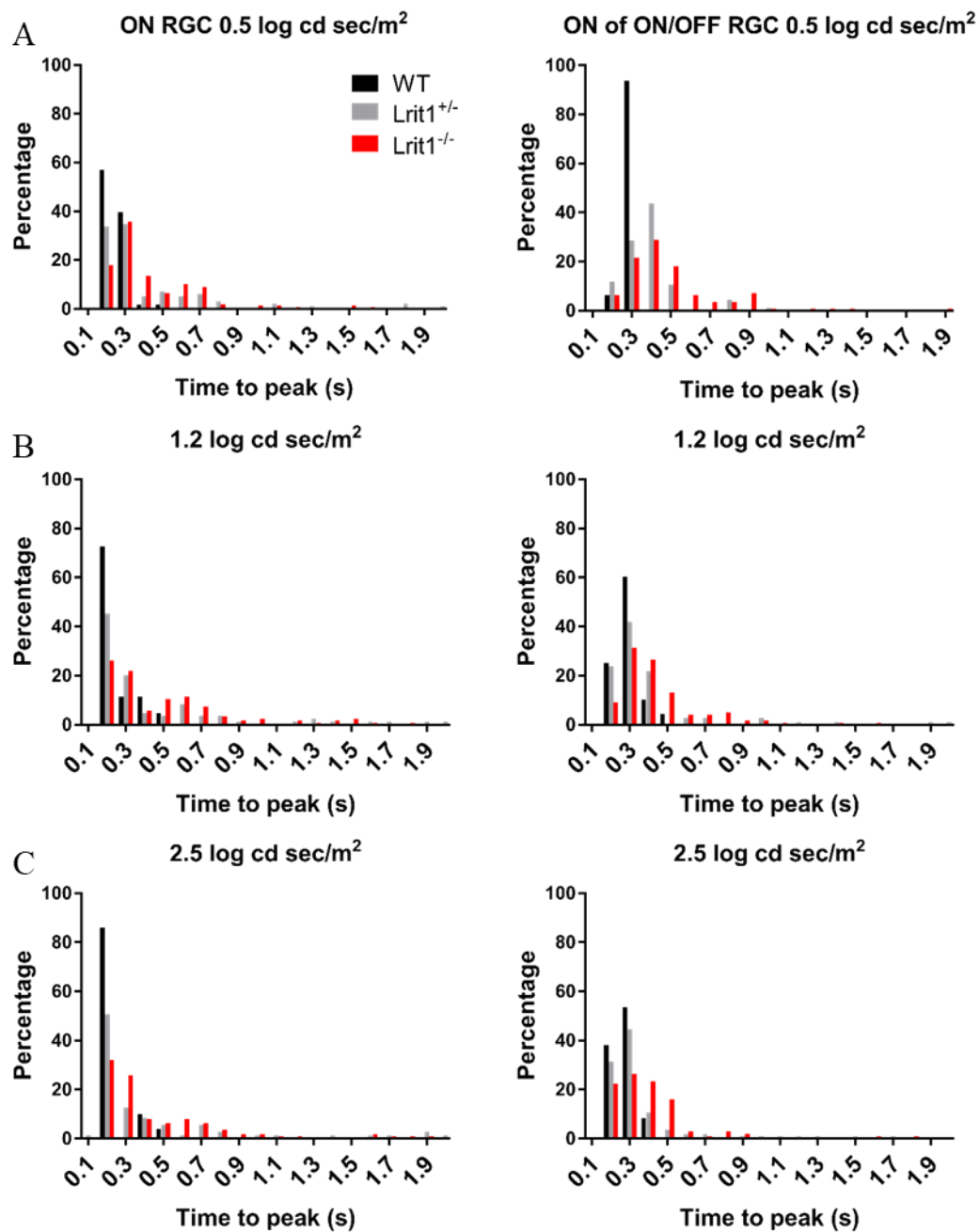
Fig. 52. ON responses of *Lrit1*$^{-/-}$ retinal ganglion cells exhibit increased peak amplitudes under photopic conditions. Frequency distributions plotting peak amplitudes in spikes/second for the proportion of ON (left panel) and the ON component of the ON/OFF (right panel) WT (black bars), *Lrit1*$^{+/-}$ (gray bars), and *Lrit1*$^{-/-}$ (red bars) retinal ganglion cells at photopic light intensities 0.5 (A), 1.2 (B), 2.5 (C) in log cd sec/m^2. Histograms are binned (10 spikes/second) as indicated on the x-axis. Data bins in spikes/second are 0-10, 10-20, 21-30, etc. The x-axis displays the beginning value for every other consecutive bin. For example, x-axis bin = 0 refers to bin 0-10 spikes/second. WT n=2 mice, 2 retinas, 174 cells; *Lrit1*$^{+/-}$ n=2 mice, 4 retinas, 237 cells; and *Lrit1*$^{-/-}$ n=3 mice, 6 retinas, 355 cells.
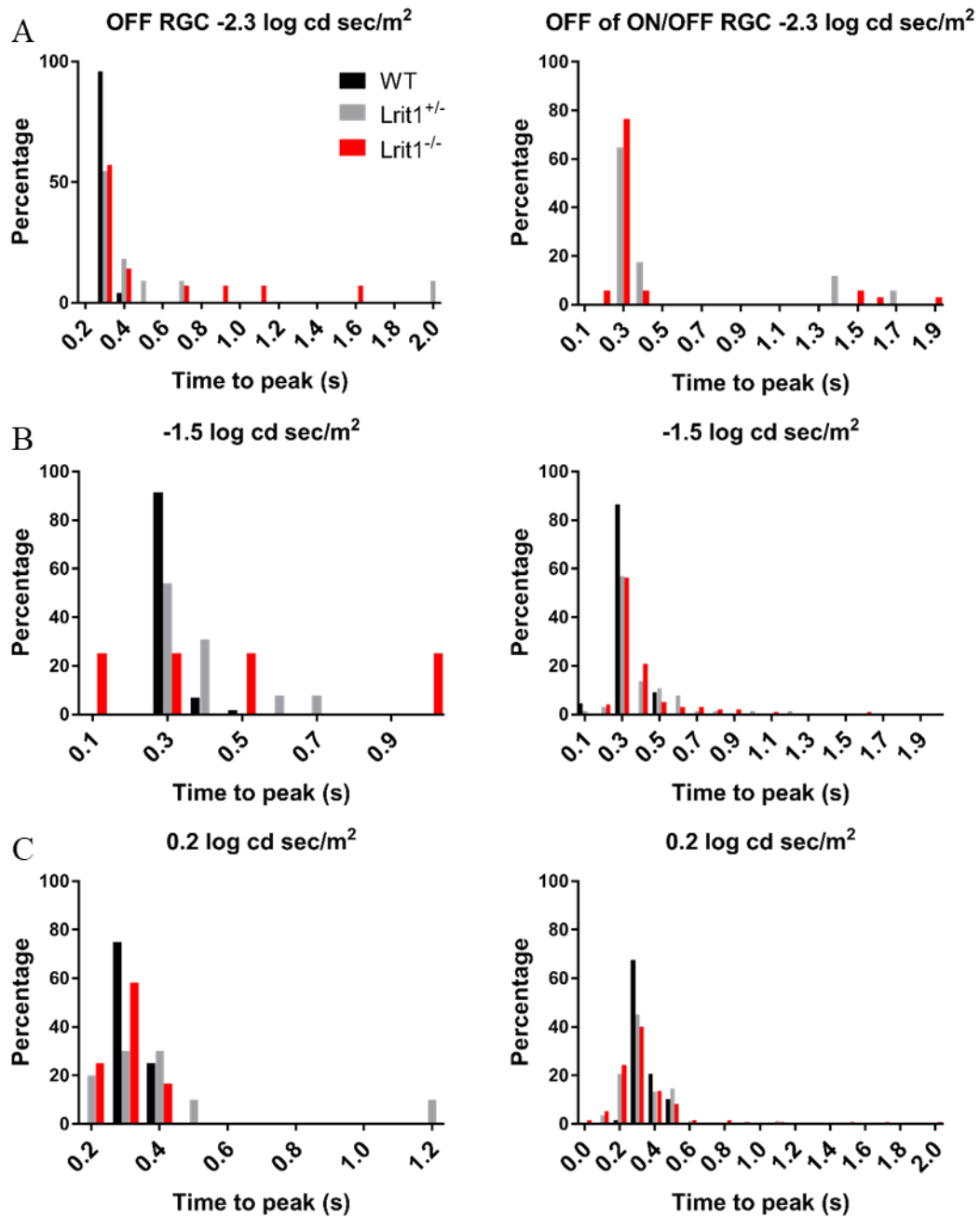
Fig. 53. OFF responses for *Lrit1*^{-/-} retinal ganglion cells exhibit increased peak amplitudes under scotopic conditions. Frequency distributions plotting peak amplitude in spikes/second for the proportion of OFF (left panel) and the OFF component of the ON/OFF (right panel) WT (black bars), *Lrit1*^{+/-} (gray bars), and *Lrit1*^{-/-} (red bars) retinal ganglion cells at scotopic light intensities -2.3 (A), -1.5 (B), 0.2 (C) in log cd sec/m². There were no ON/OFF WT cells at the lowest light intensity. Histograms are binned (10 spikes/second) as indicated on the x-axis. Data bins in spikes/second are 0-10, 10-20, 21-30, etc. The x-axis displays the beginning value for every other consecutive bin. For example, x-axis bin = 0 refers to bin 0-10 spikes/second. WT n=2 mice, 2 retinas, 174 cells; *Lrit1*^{+/-} n=2 mice, 4 retinas, 237 cells; and *Lrit1*^{-/-} n=3 mice, 6 retinas, 355 cells.

Fig. 54. OFF responses of *Lrit1*^{-/-} retinal ganglion cells exhibit increased peak amplitudes under photopic conditions. Frequency distributions plotting peak amplitudes in spikes/second for the proportion of OFF (left panel) and the OFF component of the ON/OFF (right panel) WT (black bars), *Lrit1*^{+/-} (gray bars), and *Lrit1*^{-/-} (red bars) retinal ganglion cells at photopic light intensities 0.5 (A), 1.2 (B), 2.5 (C) in log cd sec/m². Histograms are binned (10 spikes/second) as indicated on the x-axis. Data bins in spikes/second are 0-10, 10-20, 21-30, etc. The x-axis displays the beginning value for every other consecutive bin. For example, x-axis bin = 0 refers to bin 0-10 spikes/second. WT n=2 mice, 2 retinas, 174 cells; *Lrit1*^{+/-} n=2 mice, 4 retinas, 237 cells; and *Lrit1*^{-/-} n=3 mice, 6 retinas, 355 cells.
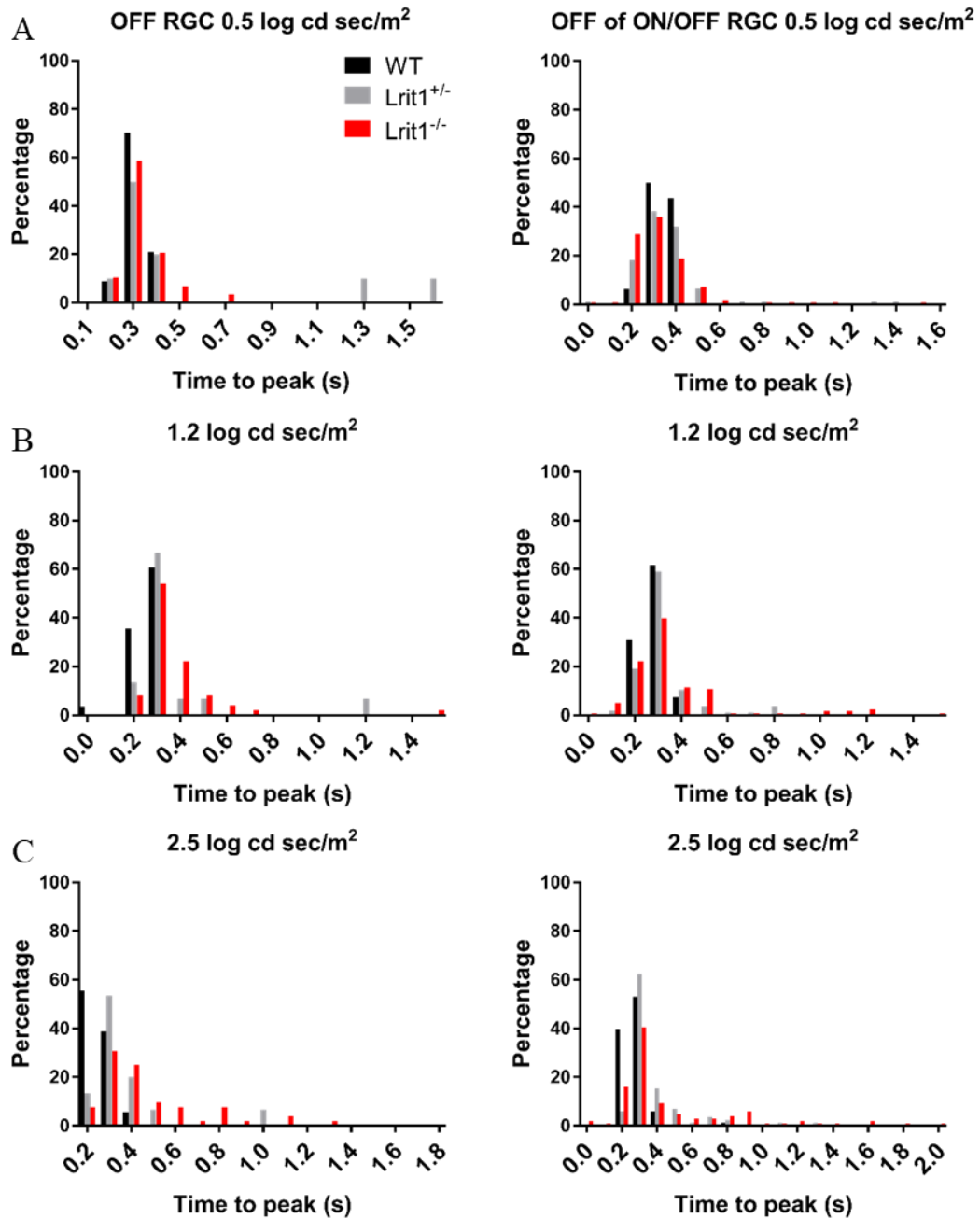
Table 11. Adjusted p-values for Kruskal-Wallis test with Dunn's post-hoc correction for multiple comparisons for ON peak amplitude in retinal ganglion cells.

Genotype	Scotopic (log cd sec/m^2)			Photopic (log cd sec/m^2)		
	-2.3	-1.5	0.2	0.5	1.2	2.5
WT v $Lrit1^{+/-}$	n/a	<0.0001	0.0503	<0.0001	0.0002	0.0444
WT v $Lrit1^{-/-}$	n/a	<0.0001	0.5211	<0.0001	0.0005	>0.99
$Lrit1^{+/-}$ v $Lrit1^{-/-}$	>0.99	>0.99	>0.99	>0.99	>0.99	>0.99

Blue shading indicates statistically significant results at $\alpha = 0.05$.

Table 12. Adjusted p-values Kruskal-Wallis test with Dunn's post-hoc correction for multiple comparisons for OFF peak amplitude in retinal ganglion cells.

Genotype	Scotopic (log cd sec/m^2)			Photopic (log cd sec/m^2)		
	-2.3	-1.5	0.2	0.5	1.2	2.5
WT v $Lrit1^{+/-}$	>0.99	>0.99	>0.99	>0.99	>0.99	>0.99
WT v $Lrit1^{-/-}$	>0.99	>0.99	>0.99	>0.99	>0.99	>0.99
$Lrit1^{+/-}$ v $Lrit1^{-/-}$	>0.99	>0.99	>0.99	>0.99	>0.99	>0.99

Blue shading indicates statistically significant results at $\alpha = 0.05$.

Table 13. Adjusted p-values Kruskal-Wallis test with Dunn's post-hoc correction for multiple comparisons for ON of ON/OFF peak amplitude in retinal ganglion cells.

Genotype	Scotopic (log cd sec/m^2)			Photopic (log cd sec/m^2)		
	-2.3	-1.5	0.2	0.5	1.2	2.5
WT v Lrit1$^{+/-}$	n/a	<0.0001	<0.0001	<0.0001	<0.0001	>0.99
WT v Lrit1$^{-/-}$	n/a	<0.0001	0.0008	0.0298	>0.99	>0.99
Lrit1$^{+/-}$ v Lrit1$^{-/-}$	>0.99	>0.99	>0.99	>0.99	0.0270	0.3284

Blue shading indicates statistically significant results at $\alpha = 0.05$.

Table 14. Adjusted p-values Kruskal-Wallis test with Dunn's post-hoc correction for multiple comparisons for OFF of ON/OFF peak amplitude in retinal ganglion cells.

Genotype	Scotopic (log cd sec/m^2)			Photopic (log cd sec/m^2)		
	-2.3	-1.5	0.2	0.5	1.2	2.5
WT v Lrit1$^{+/-}$	n/a	>0.99	<0.0001	0.3467	>0.99	>0.99
WT v Lrit1$^{-/-}$	n/a	>0.99	<0.0001	0.6317	>0.99	>0.99
Lrit1$^{+/-}$ v Lrit1$^{-/-}$	>0.99	>0.99	>0.99	>0.99	0.3577	0.2436

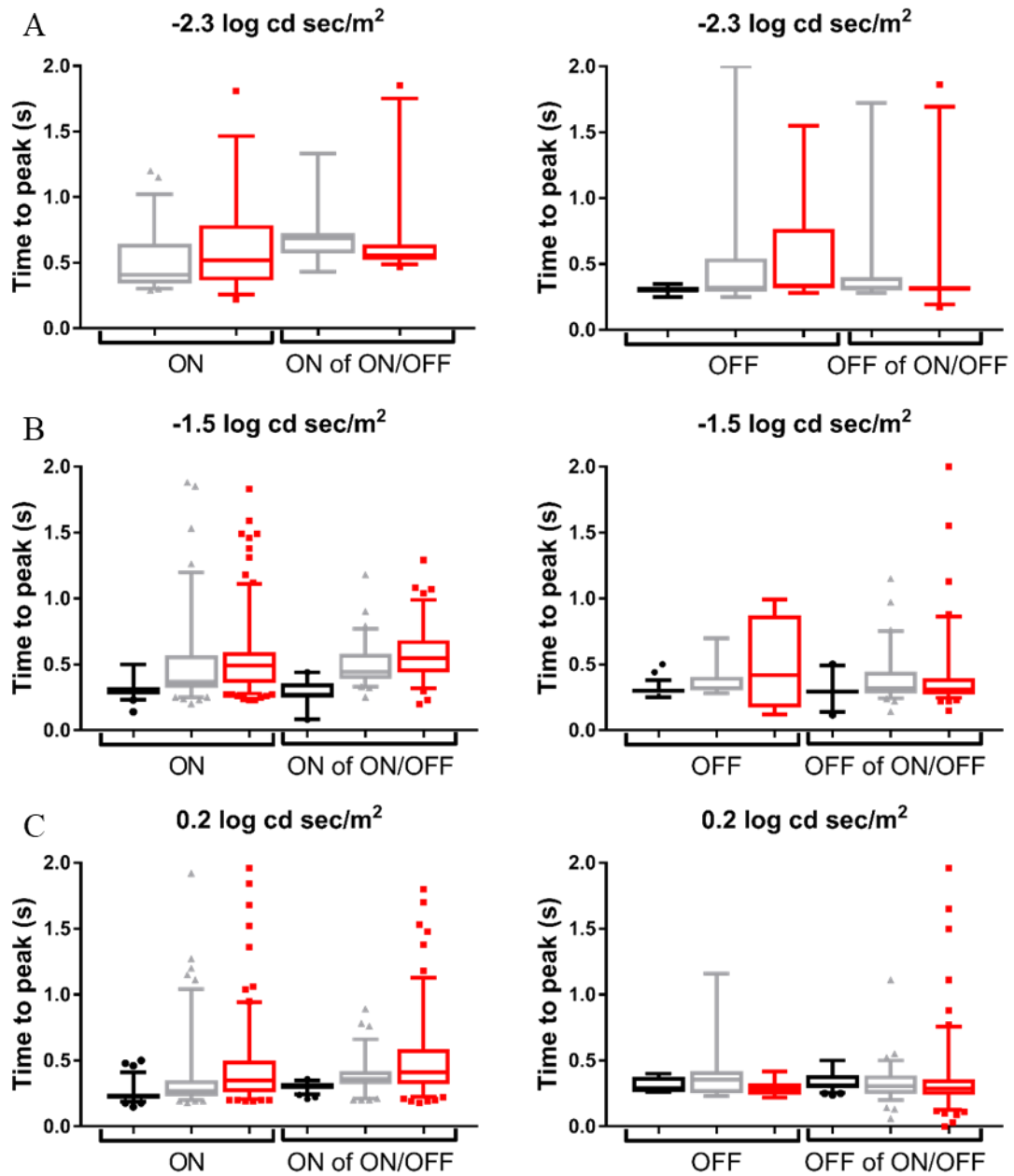Blue shading indicates statistically significant results at $\alpha = 0.05$.

Fig. 55. ON and OFF responses of *Lrit1*$^{-/-}$ retinal ganglion cells exhibit increased peak amplitudes under scotopic conditions. Box and whisker plots for peak amplitude in spikes/second for ON (left panel) and OFF (right panel) responses for WT (black), *Lrit1*$^{+/-}$ (gray), and *Lrit1*$^{-/-}$ (red) retinal ganglion cells at scotopic light intensities -2.3 (A), -1.5 (B), 0.2 (C) in log cd sec/m^2. Bars indicate means, and whiskers represent 5th to 95th percentile. Individual points indicate measures that fall outside of the 5th-95th percentile range. There were no WT ON or ON/OFF cells at the lowest light intensity. WT n=2 mice, 2 retinas, 174 cells; *Lrit1*$^{+/-}$ n=2 mice, 4 retinas, 237 cells; and *Lrit1*$^{-/-}$ n=3 mice, 6 retinas, 355 cells.
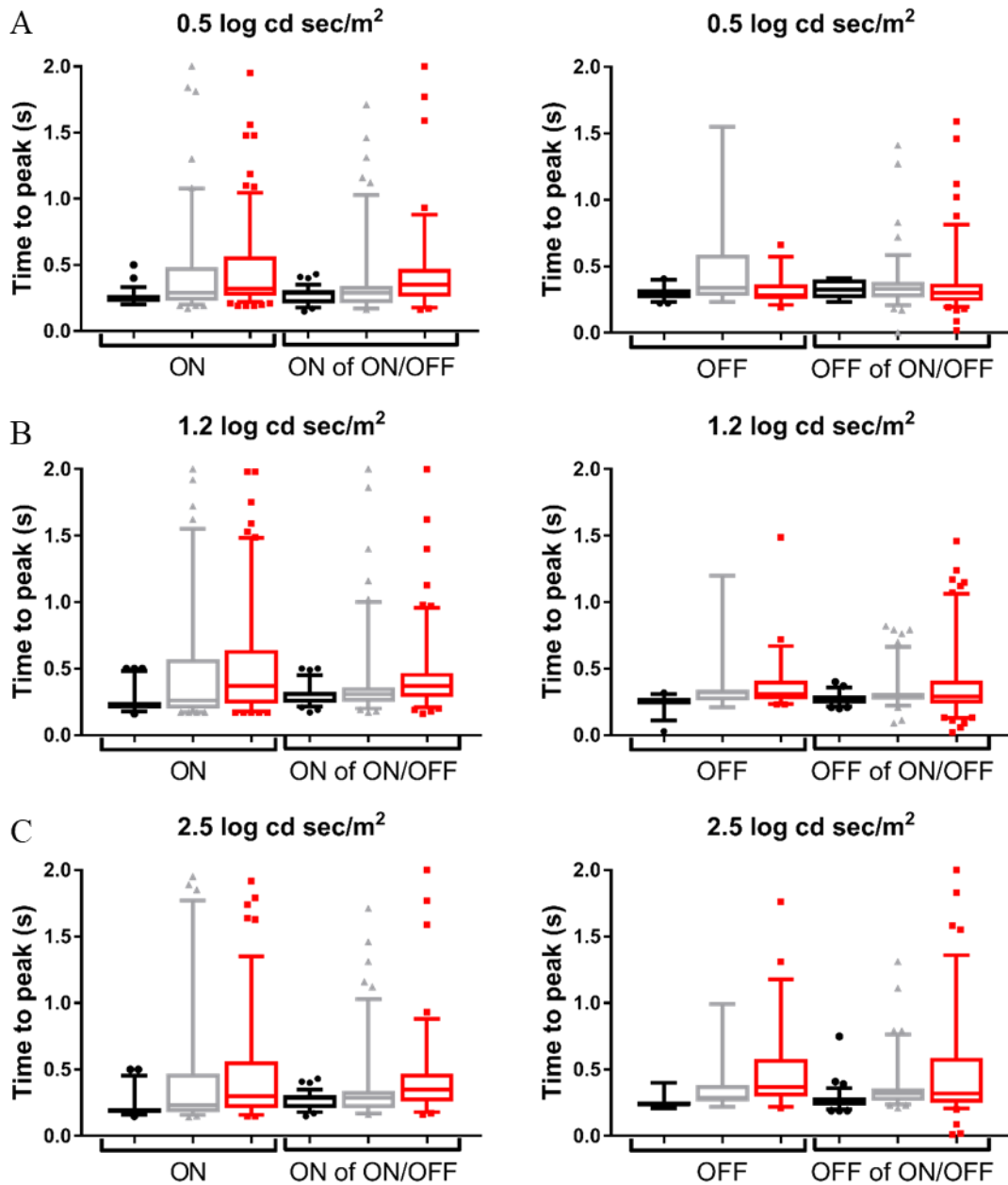
Fig. 56. ON and OFF responses of *Lrit1*^{-/-} retinal ganglion cells exhibit increased peak amplitudes under photopic conditions. Box and whisker plots for peak amplitude in spikes/second for ON (left panel) and OFF (right panel) responses for WT (black), *Lrit1*^{+/-} (gray), and *Lrit1*^{-/-} (red) retinal ganglion cells at photopic light intensities 0.5 (A), 1.2 (B), 2.5 (C) in log cd sec/m^2. Bars indicate means, and whiskers represent 5th to 95th percentile. Individual points indicate measures that fall outside of the 5th-95th percentile range. WT n=2 mice, 2 retinas, 174 cells; *Lrit1*^{+/-} n=2 mice, 4 retinas, 237 cells; and *Lrit1*^{-/-} n=3 mice, 6 retinas, 355 cells.

LRIT1 Loss Leads to Increased Ganglion Cell Spontaneous Activity and Sensitivity

We compared the spontaneous activities of *Lrit1$^{+/-}$*, *Lrit1$^{-/-}$*, and WT ganglion cells. These data demonstrated increased spontaneous activity in *Lrit1$^{+/-}$* and *Lrit1$^{-/-}$* ganglion cells (Fig. 57). These data show that *Lrit1$^{+/-}$* and *Lrit1$^{-/-}$* ganglion cells have higher spontaneous activity than WT cells.

We observed a noticeable change in the functional class composition of *Lrit1$^{+/-}$* and *Lrit1$^{-/-}$* ganglion cells at the lowest flash intensity -2.3 log cd sec/m^2 compared to WT cells: all normal and delayed retinal ganglion cell functional classes are represented in the *Lrit1$^{+/-}$* and *Lrit1$^{-/-}$* ganglion cells, but only two functional classes (NR and OFF) are present in WT retinas (Fig. 43E, 44A). Responses belonging to all normal functional classes do not arise until higher scotopic flash intensities, -1.5 and 0.2 log cd sec/m^2, in WT cells (Fig. 44B-C). This suggests that loss of LRIT1 increases ganglion cell sensitivity or the sensitivity of pre-synaptic cells that provide input to ganglion cells.
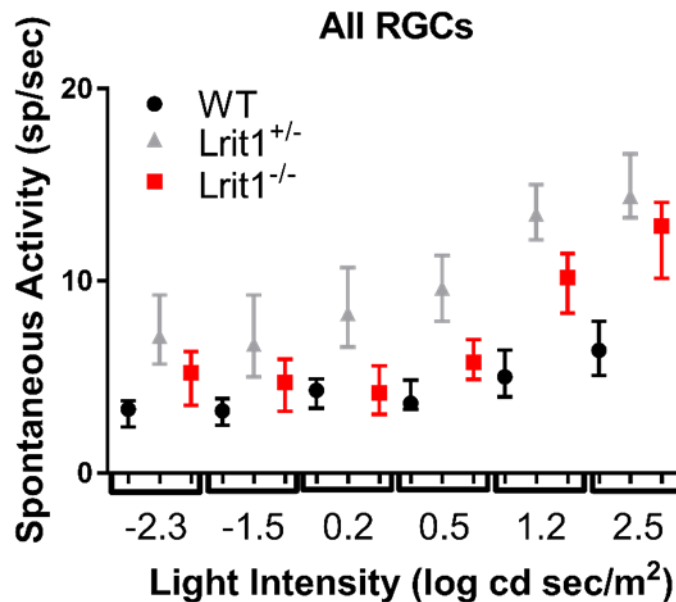
Fig. 57. *Lrit1$^{+/-}$* and *Lrit1$^{-/-}$* retinal ganglion cells have increased spontaneous activity. Plot for spontaneous activities in spikes per second for all non-responsive and responsive WT (black), *Lrit1$^{+/-}$* (gray), and *Lrit1$^{-/-}$* (red) retinal ganglion cells (RGCs) at scotopic light intensities -2.3, -1.5, and 0.2; and photopic light intensities 0.5, 1.2, and 2.5 in log cd sec/m^2. Shapes indicate medians, and error bars represent 95% confidence intervals. WT n=2 mice, 2 retinas, 174 cells; *Lrit1$^{+/-}$* n=2 mice, 4 retinas, 237 cells; and *Lrit1$^{-/-}$* n=3 mice, 6 retinas, 355 cells.
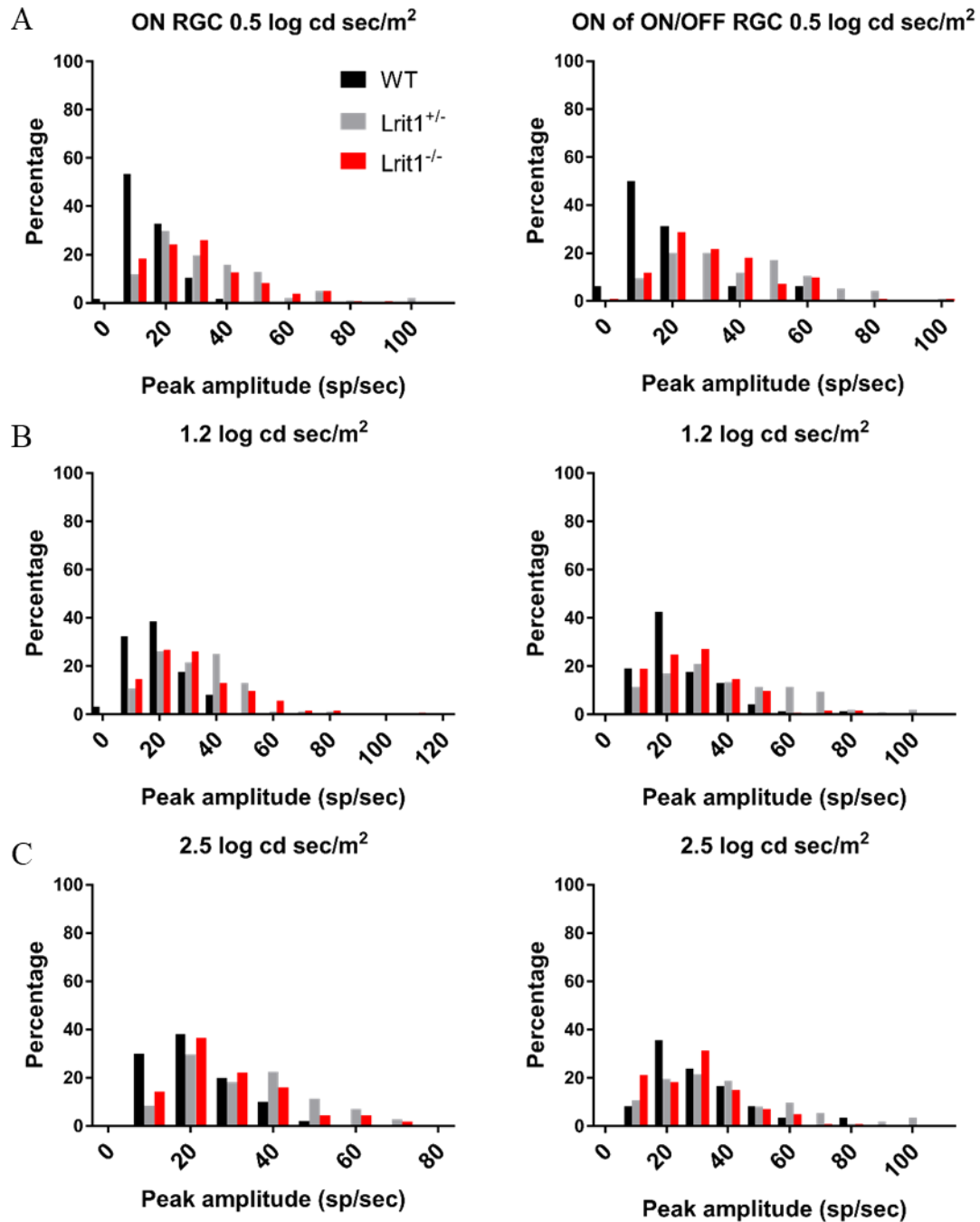
LRIT1 Loss Leads to Rhythmic Oscillations in Ganglion Cell Responses

Previous reports have demonstrated spontaneous rhythmic oscillations of up to 10Hz in *rd1* mice, which exhibit early onset severe retinal degeneration (125). Retinal oscillations also occur in the *Nyx^nob* mouse retinas (63,126). To examine this, we used fast Fourier transform (FFT) in a power spectral density to determine if there was rhythmicity to the spontaneous activity. WT retinas lack oscillating ganglion cells. This analysis reveals two distinct subgroups of cells in *Lrit1^+/-* and *Lrit1^-/-* retinas: those that display rhythmic bursting at ~1 or ~5 Hz (Fig. 58). Approximately 19% of retinal ganglion cells in both of the *Lrit1^+/-* and *Lrit1^-/-* retinas exhibited rhythmic spontaneous activity (Fig. 58B). The raster plots and PSTHs are shown for four examples (Fig 58A). These cells are indicated with arrows on Fig. 58B. These data support the hypothesis that the loss of LRIT1 induces abnormal rhythmicity as a component of their spontaneous activity.
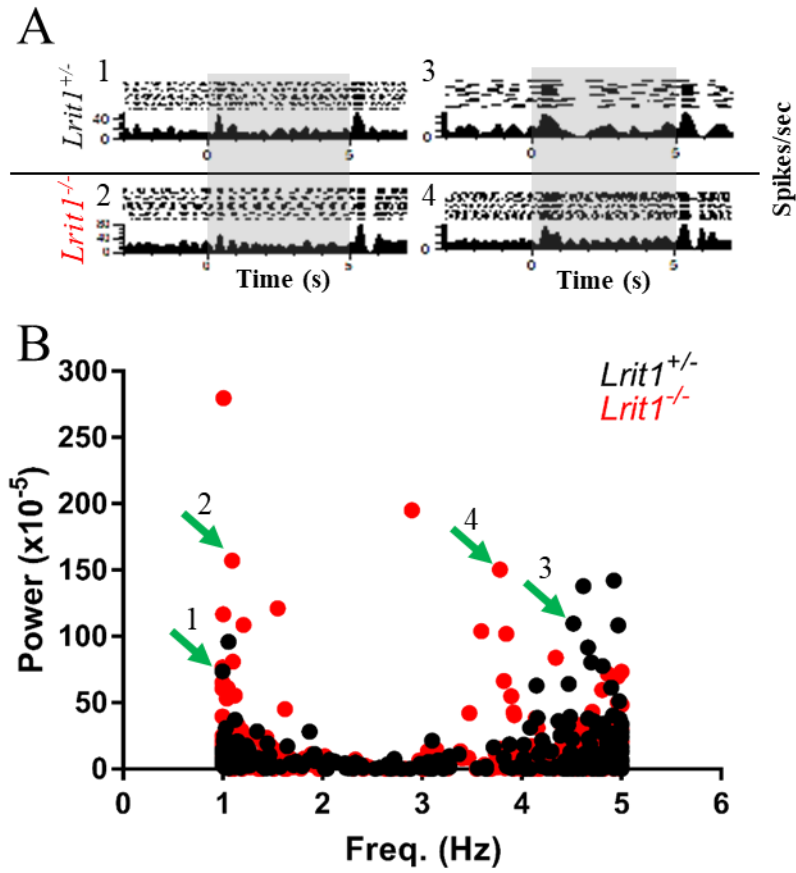
Fig. 58. Many *Lrit1^-/-* retinal ganglion cells exhibit rhythmic oscillations. A) Representative responses display 10 raster plots for cell response over 10 trials (top) and the post-stimulus time histogram (PSTH) response amplitude averaging all 10 raster plots in spikes/sec (bottom). PSTHs of individual *Lrit1^+/-* (top: 1, 3) and *Lrit1^-/-* (bottom: 2, 4) cells with a rhythmic oscillations are shown. These demonstrate spikes occur at specific frequencies across time within trials to indicate rhythmicity. B) Power spectral density analysis showing rhythmic oscillations. Numbered arrows correspond to PSTHs shown in (A).

CHAPTER IV

DISCUSSION

To determine the function of LRIT1 we created a mouse model that resulted in *Lrit1* deletion. We utilized the CRISPR/Cas9 system to generate 3 lines and fully characterized one that was predicted to have a frameshift, and likely null allele. We confirmed loss of the LRIT1 protein with immunohistochemistry (IHC).

Retinal morphometry of *Lrit1*$^{+/-}$ and *Lrit1*$^{-/-}$ mouse retinas revealed no gross morphological abnormalities in *Lrit1*$^{-/-}$ mice, or alterations in the thickness of retinal lamina (OS, IS, ONL, OPL, INL, IPL, and GCL). These data suggest LRIT1 is not required for development and formation of normal retinal structure in the mouse, similar to the close family member LRIT3 (77,78,127).

Immunohistochemical analyses localizes LRIT1 to the OPL, in a punctate pattern similar to that seen for many ON bipolar cell proteins (mGluR6, GPR179, TRPM1) (25,73,78,128). Surprisingly, we did not observe LRIT1 immunohistochemical staining in the OS as reported previously for the rat (101). This incongruity may be due to a bona fide lack of LRIT1 expression in the OS. Another explanation is that LRIT1 expression at the OPL is much greater than its OS expression. Due to the quality of our LRIT1 antibody, we may not be able to detect diffuse low-intensity signals at the OS. We observed isolated LRIT1 puncta marking the rod to rod ON bipolar and horizontal cell synapses and clustered LRIT1 puncta marking cone terminals of the cone to cone bipolar and horizontal cell synapses. These puncta are absent in the *Lrit1*$^{-/-}$ mouse. IHC also shows that photoreceptor (pikachurin, PNA, RIBEYE, PSD95), ON bipolar cell (mGluR6, GPR179, LRIT3, RGS11, TRPM1, PKCα), and horizontal cell (calbindin) proteins localized normally in the absence of LRIT1.

We next wanted to examine if LRIT1 expression depends on the retinal proteins NYX, mGluR6, and TRPM1 in *Nyx*^{nob}, *Grm6*$^{-/-}$, and *Trpm1*$^{-/-}$ mouse models, respectively. IHC data showed LRIT1 localizes normally in the absence of NYX, mGluR6, and TRPM1, which have all been shown to be critical for ON

bipolar cell function (28,63,71,73,81,128,129). Together these data suggest that LRIT1 expression localizes normally in the examined *nob* mouse models.

To determine the synaptic location of LRIT1, we double-labeled with several well characterized synaptic proteins. LRIT1 does not colocalize with the photoreceptor synaptic ribbon marker RIBEYE, but LRIT1 does reside within RIBEYE's crescents that mark rod terminals. Prior work has shown that the ON bipolar cell markers LRIT3 (78), NYX (63,73), mGluR6 (130), and TRPM1 (131) show a similar localization. Previous studies also showed that the horizontal cell markers calbindin and syntaxin-4 localize adjacent to piccolino or RIBEYE crescents, respectively (132,133). Piccolino is another synaptic ribbon marker shown to colocalize with RIBEYE (134,135). This suggests LRIT1 may be expressed on ON bipolar cell dendritic tips, horizontal cell axons and dendrites, photoreceptor terminals, or some combination of these.

Additional IHC colocalization experiments with ON bipolar cell markers mGluR6 and GPR179 showed LRIT1 did not colocalize with either protein. This provides further evidence that LRIT1 is not expressed in ON bipolar cells. LRIT1 puncta lie distal to mGluR6 and GPR179 at rod synapses.

At cone terminals LRIT1 localizes distal to PNA, GPR179, and mGluR6. The exact synaptic location of PNA is unknown, but it is thought to be on the base of the cone terminal. Our observation that mGluR6 and PNA colocalize is consistent with previous studies (130). Prior studies have shown that GPR179 also colocalizes with PNA (25). Because LRIT1 did not colocalize with GPR179, mGluR6, or PNA, this suggests that LRIT1 is not expressed in ON bipolar cell dendrites. To rule out the possibility that LRIT1 is expressed in cone OFF bipolar cells at cone terminals, IHC data showed LRIT1 does not colocalize with proteins marking cone OFF bipolar cell type 3a (HCN4) and type3b (PKAIIβ). These data suggest LRIT1 is likely not expressed in cone OFF bipolar cells. Previous work has shown that the horizontal cell markers calbindin, syntaxin-4, and GluA2 all localize distal to PNA, which is similar to our data for LRIT1 and PNA (133,136), suggesting LRIT1 may be localized on the horizontal cell invaginating contacts at cone terminals. Our observed LRIT1 staining pattern with mGluR6 and GPR179 is consistent with previously shown staining patterns for the horizontal cell marker calbindin with LRIT3 (78), NYX (63), or TRPM1 (unpublished data). mGluR6, GPR179, LRIT3, NYX, and TRPM1 have all been shown to

colocalize in the OPL (25,63,73,78,83). Together, these data are consistent with our hypothesis that LRIT1 is expressed in horizontal cells.

Analysis of a previously published RNA-Seq dataset demonstrated *Lrit1* expression in the mouse retina, specifically in rods and cones (Fig. 20). To examine if *Lrit1* may also be expressed in horizontal cells, I performed RNA *in situ* hybridization experiments and showed that *Lrit1* is expressed in the ONL and INL. *Lrit1* ONL expression was robust, suggesting its expression in rods because rods comprise up to 97% of mouse retinal photoreceptors in the ONL. Our *in situ* data cannot discount that *Lrit1* may also be expressed in cones. Gomi *et al*. showed that *Lrit1* was expressed only in the rat ONL (101). However, they neglect to show a positive control for their *in situ* experiment, and the only negative control is the lack of *Lrit1*-positive signals in the immature rat retina at P1 (101). *Lrit1* INL expression was exclusively limited to the upper INL sublamina and is similar to but distinct from the ON bipolar cell marker *Grm6* and *Lrit3* expression. It is possible *Lrit1* is expressed in ON bipolar cells from the *in situ* results alone, but in conjunction with our IHC data, LRIT1 at the OPL is unlikely to originate from ON bipolar cell expression. Because amacrine and cone OFF bipolar cell nuclei typically reside in the lower INL sublamina of the INL, this suggests *Lrit1* may also be expressed in horizontal cells. Overall, our *in situ* results suggest that *Lrit1* is expressed in rods, possibly cones, and is consistent with our hypothesis that *Lrit1* is additionally expressed in horizontal cells.

LRIT1 and Retinal Function

To assess the impact of the loss of LRIT1 on retinal function, we performed ERGs. These data found *Lrit1*$^{-/-}$ mice have reduced dark- and light-adapted ERG a-waves. The reduction in the a-wave is transduced to ON bipolar cells, which displayed proportionally reduced dark- and light-adapted ERG b-waves. *Lrit1*$^{+/-}$ mice were comparable to wild-type (WT) littermates. These data suggest a recessive loss of function. To our knowledge, no other mouse model demonstrates a similar ERG phenotype that is not also accompanied by associated retinal degeneration or abnormal retinal morphology.

Our ERG data support our *in situ* findings that demonstrate *Lrit1* is expressed in the ONL. However, these data are inconsistent with IHC data showing LRIT1 expression limited to the OPL. This led us to question the source of our observed reduction in the ERG dark- and light-adapted a-waves.

Photoreceptor hyperpolarization is responsible for the negative corneal a-wave and is generated by closure of the dark current. The reduced a-waves in *Lrit1*$^{-/-}$ mice suggest a phototransduction deficit that may occur upstream to or at the closure of the circulating dark current in either the OS or IS. Thus, LRIT1 is necessary but not sufficient for the normal closure or regulation of the circulating dark current.

We hypothesized that LRIT1 through its LRR may directly interact with an LRR in a Na$^+$ channel in the OS or Na$^+$ pump in the IS known to be involved in the dark current in the mouse retina. The OS Na$^+$ channels include the cyclic nucleotide-gated (CNG) channels comprised of CNGA1 and CNGB1 in rods and CNGA3 and CNGB3 in cones. The Na$^+$/K$^+$ pump proteins in the IS are currently unknown, and there is likely to be more than one. For the loss of LRIT1 to affect dark- and light-adapted a-waves, LRIT1 would need to affect at least one CNG subunit in rods and cones or IS Na$^+$/K$^+$ pump protein. To determine if any of the CNG channel proteins contains an LRR, I entered their amino acid sequences into an LRR finder database (http://smart.embl-heidelberg.de/smart/set_mode.cgi?NORMAL=1#). None contained LRRs. Because the IS pumps have not been identified, I could not search their amino acid sequences. It is still possible that LRIT1 interacts with one or more of the aforementioned proteins through an LRR domain that was not predicted, through another LRIT1 domain, or through an indirect interaction involving a protein complex. Because we saw only reduced rather than ablated dark and light-adapted ERG a-waves, it is likely that LRIT1 directly or indirectly interacts with one or more but not all of the OS CNG or IS pump proteins. OS and IS proteins are synthesized and processed in the cell nucleus and IS where they must traffic appropriately to their destinations of function. So it may also be true that LRIT1 is important for the localization of one or more of these proteins. This is an unlikely mechanism because most known proteins involved in phototransduction when mutated do not reach their destinations and cause retinal degeneration (123,137-147), which does not occur with loss of LRIT1.

Dark- and light-adapted ERGs also demonstrated possibly abnormal OPs of *Lrit1*$^{+/-}$ and *Lrit1*$^{-/-}$ mice. OPs are hypothesized to reflect inner retinal potential possibly involving some combination of bipolar, amacrine, and ganglion cells, although the exact cellular source(s) is unknown (63,121,122). In contrast to the reduced a- and b-waves seen specifically in *Lrit1*$^{-/-}$ mice, abnormal OPs are present in both *Lrit1*$^{+/-}$ and *Lrit1*$^{-/-}$ mutants. These data suggest that the *Lrit1*$^{-/-}$ mutation has a dominant negative loss of

function where loss of a single WT copy disrupts inner retinal function without affecting outer retinal function.

Our observed effects on outer and inner retinal function upon the loss of LRIT1 led us to ask if retinal ganglion cells in these mice respond normally. Further, if they respond abnormally, in what way(s) are they abnormal? Sonntag *et al.* generated the first mouse model selectively removing horizontal cells from the adult retina using diphtheria toxin and its receptor to create *Cx57$^+$/DTR* mice (148). They illustrated significantly reduced ERG a- and b-waves in scotopic conditions and a significantly reduced b-wave in photopic conditions. They provided no quantification of the photopic a-wave. Additionally, they demonstrated delayed responses in ON and the ON component of ON/OFF *Cx57$^+$/DTR* ganglion cells that was not seen in OFF or the OFF component of ON/OFF *Cx57$^+$/DTR* ganglion cells. They attributed the reduced ERG b-waves and altered ganglion cell function to the lack of horizontal cell inhibition. However, they also demonstrated that rod number was significantly decreased and most remaining rods had retracted their terminals. This showed horizontal cells were critical for rod synapse formation. Even though cone number is unchanged in *Cx57$^+$/DTR* mice, cones were unevenly distributed throughout mutant retinas compared to WT control retinas. Retinas in *Cx57$^+$/DTR* mice exhibited rod degeneration and synaptic disruption. Thus, they cannot claim any role for horizontal cell regulation of retinal function because of the many structural defects in this model.

A recent study by Ströh *et al.* describes a second horizontal cell mouse model where the glutamate receptors GluA2 and -4 are selectively deleted in horizontal cells (35). Horizontal cell-specific GluA2/4 deletion yields development and formation of normal synaptic triads. They use these mice to examine the ganglion cell effects of ablating glutamatergic horizontal cell input. Their GluA2/4-deficient mice received no photoreceptor input and thus could not provide any lateral feedback to visual circuits. They examined the effects on only one type of ganglion cell, the transient OFF α ganglion cells (tαOFFs). They found a decreased dynamic range in their tαOFFs with marked changes in temporal and contrast tuning responses but no change in spatial tuning responses when horizontal cell glutamatergic input is absent. Overall, their work demonstrates that changes in horizontal cell signaling can extensively alter inner retina ganglion cell function without measurably impacting retinal structure at the OPL. If our hypothesis that LRIT1 is

expressed and functional in photoreceptors and horizontal cells is correct, we would expect to see marked changes in the ganglion cell responses of $Lrit1^{+/-}$ and $Lrit1^{-/-}$ mice.

We performed multi-electrode arrays to assess light-evoked ganglion cell response. Our results first establish there is no loss of responsive cells. Similar proportions of non-responsive and responsive cells indicate that LRIT1 likely does not contribute to whether or not ganglion cells respond. We observed the early appearance of all functional classes in $Lrit1^{+/-}$ and $Lrit1^{-/-}$ cells compared to WT cells. WT cells at the lowest intensity flash are limited to being non-responsive with some cells in the OFF functional class. WT ganglion cells do not exhibit responses belonging to all functional classes until the -1.5 log cd sec/m^2 intensity flash. In contrast, we observed $Lrit1^{+/-}$ and $Lrit1^{-/-}$ ganglion cells belonging to all functional classes at the lowest intensity flash. This suggests LRIT1 is involved in shaping how a ganglion cell responds and that the loss of LRIT1 provides increased ganglion cell sensitivity. Results also demonstrated increased spontaneous activity of $Lrit1^{+/-}$ and $Lrit1^{-/-}$ ganglion cells. This suggests that loss of LRIT1 increases spontaneous ganglion cell activity. Our results additionally showed increased peak amplitudes in $Lrit1^{+/-}$ and $Lrit1^{-/-}$ ganglion cells compared to WT cells. This suggests that the loss of LRIT1 results in a more robust ganglion cell response.

The absence of horizontal cell hyperpolarization cannot feedback inhibit photoreceptors by shifting photoreceptor calcium current activation curves, leading to increased photoreceptor hyperpolarization and ON bipolar cell depolarization (149). This amplifies both ON bipolar cell glutamate release and connected ganglion cell responses. Thus, we hypothesize that the loss of LRIT1 reduces horizontal cell-mediated lateral inhibition. This decreases light-evoked horizontal cell hyperpolarization and increases ON bipolar cell depolarization and OFF bipolar cell hyperpolarization. This leads to increased pre-synaptic input to $Lrit1^{+/-}$ and $Lrit1^{-/-}$ ganglion cells. Thus, $Lrit1$ mutant ganglion cells generate action potentials at lower intensity flashes. They also exhibit stronger ganglion cell responses at all stimulus intensities.

Increased ganglion cell input can arise from several sources: either increased excitatory input, decreased inhibitory input, or a combination of both. Excitatory and inhibitory ganglion cell input arise from pre-synaptic bipolar and amacrine cells, respectively. But it is not that simple. Horizontal cells feedback and inhibit photoreceptor input to bipolar cells. Horizontal cells also feedforward and inhibit

bipolar cell output. Amacrine cells receive this horizontal cell-modulated output from bipolar cells. Amacrine cells then directly provide two forms of inhibition. First, amacrine cells feedback and inhibit bipolar cells, which indirectly modulates the excitatory input to post-synaptic ganglion cells. Second, amacrine cells feedforward and inhibit ganglion cells, which directly modulates ganglion cell ability to reach and surpass the threshold for action potential generation. From our experimental results, we cannot therefore completely discount an amacrine cell contribution. This is because amacrine cell function is shaped by horizontal cell-mediated bipolar cell input. We propose that the loss of LRIT1 decreases horizontal cell lateral inhibition, leads to increased ON bipolar cell depolarization, OFF bipolar cell hyperpolarization, increased excitatory input to post-synaptic ganglion cells, and ultimately causes more sensitive and robust ganglion cell activity.

We also demonstrated increased response latencies in $Lrit1^{+/-}$ and $Lrit1^{-/-}$ ON, OFF, and ON/OFF cells. Further, $Lrit1^{-/-}$ ganglion cells appear to have double the proportion of delayed cells compared to $Lrit1^{+/-}$ cells. This suggests the loss of LRIT1 causes inner retinal signaling pathway crossover. When retinal signals cannot proceed through their normal paths, they still cross over and influence alternate signaling paths, which may explain the delayed retinal ganglion cell responses (150). This is further evidenced because the peak amplitude of retinal ganglion cell responses in the absence of LRIT1 are maintained and even increased, suggesting responses are delayed but not lessened.

We observed rhythmic ganglion cell firing in $Lrit1^{-/-}$ mice. The fast Fourier transforms demonstrate two distinct frequency clusters at ~1 Hz and ~4-5 Hz. The pre-synaptic input source that causes ganglion cell rhythmic firing is unknown (151). However, rhythmicity is commonly seen in abnormally functioning or degenerating retinas but typically absent in healthy retinas (152-154). Menzler *et al.* induced rhythmicity (~4 Hz) in healthy mouse retinas with partial photoreceptor photobleaching (152). Their blind *rd-10* retinas exhibited an equivalent oscillatory frequency. These findings suggest that pre-synaptic neurons in the outer retina can induce ganglion cell rhythmicity. Thus, the loss of LRIT1 in photoreceptors and/or horizontal cells may be responsible for our observed oscillations.

Our data showed *Lrit1* is expressed in the ONL and INL. We also showed LRIT1 is expressed in the OPL in a pattern consistent with horizontal cells. $Lrit1^{-/-}$ mice displayed no gross morphological abnormalities. This suggests LRIT1 is not important for development and formation of normal retinal

structure. *Lrit1*$^{-/-}$ mice exhibited reduced dark- and light-adapted ERG a- and b-waves. *Lrit1*$^{+/-}$ and *Lrit1*$^{-/-}$ mice exhibited abnormal dark- and light-adapted OPs and abnormal spontaneous and light-evoked retinal ganglion cell responses. These data suggest LRIT1 contributes to synaptic signaling. These results align with NYX and LRIT3 mutants having structurally intact retinas but exhibiting retinal dysfunction, supporting their roles in synaptic transmission (73,78). ELFN1 mutants exhibited disrupted synaptic assembly causing major retinal structure changes accompanied by retinal dysfunction (94). We hypothesize that like NYX and LRIT3 but unlike ELFN1, LRIT1 is expressed in photoreceptors and horizontal cells where it is important for normal retinal function in the mouse (Fig. 59). LRIT1 specifically was shown to play a role in the photoreceptor dark current. LRIT1 also possibly influences horizontal cell lateral inhibition. We interpret our results to implicate LRIT1 in previously unknown roles in photoreceptor and horizontal cell synaptic function with no likely contribution to synaptic assembly. In conclusion, our data characterized the effects of the loss of LRIT1 on retinal structure and function in our novel *Lrit1*$^{-/-}$ mouse. We support its use as a novel mouse model for future studies of photoreceptor and horizontal cell signaling.

Note Added in Proof

      Two publications reporting similar results appeared (155,156). Both publications showed IHC data similarly localizing LRIT1 to the OPL in the mouse retina. In addition, a conditional knockout mouse model (CKO) for ON bipolar cell-specific LRIT1 showed LRIT1 staining was lost in the IPL but retained in the OPL, suggesting OPL LRIT1 is not expressed in ON bipolar cells (156). They also tested the ON bipolar cell LRIT1 CKO model using ERGs and saw no difference between genotypes, suggesting IPL LRIT1 does not affect photoreceptor hyperpolarization or ON bipolar cell depolarization.
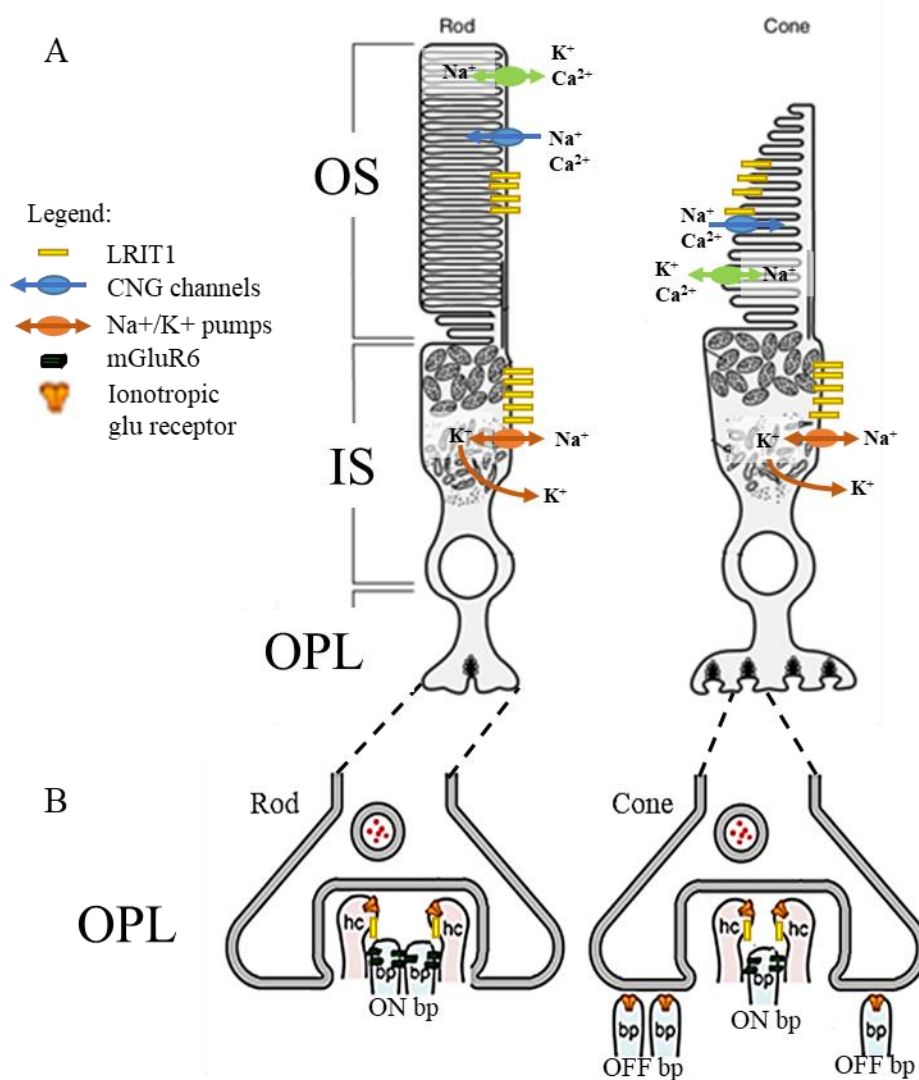
Fig. 59. Model of LRIT1 localization in the mouse retina. A) Proposed model for LRIT1 localization at photoreceptor outer segments (OS) near the CNG channels or inner segments (IS) near the Na$^+$/K$^+$ pumps. B) Proposed model for LRIT1 localization in the outer plexiform layer (OPL) at horizontal cell (hc) axons and dendrites at rod and cone ribbon synapses, respectively, distal to ON bipolar cell (ON bp) protein mGluR6. OFF bipolar cells (OFF bp) make flat contacts at cone pedicles. Adapted and modified from Michael J. Berridge. *Cell Signalling Biology*. 2014; 6csb0001010; doi: 10.1042/csb0001010.

CHAPTER V

FUTURE DIRECTIONS

At present, there are several unanswered questions about the functional and structural impact of the loss of LRIT1 in the mouse retina. First, why did we observe a reduced ERG a-wave even though we only observed LRIT1 staining in the OPL arising from what we hypothesize is LRIT1 expression in horizontal cells? Our *in situ* data suggest robust *Lrit1* expression in photoreceptors, even though we saw no photoreceptor OS or IS staining for LRIT1 protein by immunohistochemistry. One explanation is diffuse *Lrit1* expression in photoreceptors that affects the dark current seen as a reduction in the scotopic and photopic ERG a-waves. We will examine how rod-specific re-expression of *Lrit1* will impact the scotopic ERG a- and b-waves. To perform this study, I have already cloned *Lrit1* cDNA into a plasmid containing the rhodopsin promoter and N-terminal MYC and FLAG tags. The rhodopsin promoter will drive rod-specific *Lrit1* expression. The plasmid was packaged into an AAV for intravitreal injection into *Lrit1*$^{-/-}$ mice. The intravitreal AAV approach has previously been successful in our lab to express either GFP infection control or another protein (unpublished data). We will test infected mice, infected GFP control, and uninfected *Lrit1*$^{-/-}$ mice using ERGs to determine if rod-specific re-expression of LRIT1 is necessary and sufficient to restore the scotopic ERG a-wave. We expect that expression of wild-type (WT) *Lrit1* in rods of *Lrit1*$^{-/-}$ mice will restore the scotopic a-wave.

ERGs on rod AAV-*Lrit1* mice will additionally show if restoration of the a-wave concurrently restores the scotopic b-wave. It is possible that re-expression of WT LRIT1 in rods will only restore the a-wave. If the a-wave is restored but the b-wave is still reduced or otherwise abnormal, this will suggest WT LRIT1 in rods rescues the rod dark current but will not be sufficient to restore normal retinal function. This would suggest that LRIT1 is expressed in another cell type. Because we have evidence suggesting that LRIT1 is expressed in horizontal cells, we will generate an AAV with the *Lrit1* cDNA and MYC and FLAG tags using the connexin57 promoter to drive horizontal cell-specific expression (157). If

the horizontal cell AAV-*Lrit1* does affect the b-wave, we will need to co-infect rod- and horizontal AAV-*Lrit1* to see complete restoration of the ERG a- and b-waves.

If the a-wave is restored following rod AAV-*Lrit1* infection, this model will serve as an independent measure of LRIT1 expression in rods. We will visualize rod LRIT1 expression using anti-MYC and –FLAG antibodies. Similarly, if the ERG a- and b-waves are restored following co-infection, we will visualize rod and horizontal cell LRIT1 expression simultaneously. We expect that horizontal cell LRIT1 expression will recapitulate the LRIT1 staining we observed at the OPL in *Lrit1*^{+/+} mice, though it is possible that rod LRIT1 may also localize to the OPL. We will alternatively localize LRIT1 expression at a higher resolution using our LRIT1 antibody in ultrastructural localization studies using electron microscopy. These proposed studies are similar to what has been done for GPR179 in mouse (83) or using immunogold particles with our LRIT1 antibody as previously shown in the rat (101). This experiment may additionally serve to demonstrate LRIT1 is expressed in mouse OS or IS, photoreceptor terminals, and horizontal cells.

We were unable to visualize LRIT1 via Western blotting. MYC and FLAG tags on the AAV expression constructs will allow us to probe for LRIT1 expression via Western blot. While this will not show quantifiable endogenous LRIT1 expression, we can derive important information from these blots. For example, by running native and SDS PAGE gels, we will gain information regarding the oligomerization state of LRIT1. It has previously been shown that several LRR proteins form oligomers (158-160) while others like NYX, for example, do not at least in yeast (92). Glycosylation is a post-translational modification added to proteins in the secretory pathway during processing in the endoplasmic reticulum and Golgi apparatus. We presume mature LRIT1 will be glycosylated because it follows the secretory pathway to reach the plasma membrane due to the presence of its N-terminal signal sequence and C-terminal transmembrane domain. We will be able to detect LRIT1 glycosylation on future Western blots as it will cause a shift in the predicted molecular weight.

Both rod and horizontal cell AAV-*Lrit1* MYC and FLAG-tagged proteins expressed *in vivo* will be used to immunoprecipitate LRIT1in an attempt to identify interacting partners. Proteins in the immunoprecipitate would be identified by mass spectrometry. This will identify candidate LRIT1-binding proteins that may explain its mechanism of function(s) in rods and horizontal cells.

The multi-electrode array data revealed that loss of LRIT1 leads to abnormal retinal ganglion cell responses. We propose that one explanation for this is that loss of LRIT1 disrupts horizontal cell-mediated feedback and/or horizontal cell-mediated center surround organization. Assuming this is true, either of these would cause changes to retinal ganglion cell responses. We will investigate this by crossing $Lrit1^{-/-}$ mice with a horizontal cell-specific Cre mouse and infecting offspring with a floxed stop AAV for $Lrit1$ (161). This will enable us to express LRIT1 only in horizontal cells to yield Cx57-$Lrit1^{+/+}$ and Cx57-$Lrit1^{-/-}$ mice.

Electrical cell-paired recordings in horizontal and bipolar or retinal ganglion cells in mammalian and non-mammalian models showed that horizontal cell hyperpolarization caused ON bipolar cell and ON ganglion cell hyperpolarization but caused OFF bipolar cell and OFF ganglion cell depolarization (149). The converse was also shown to be true for horizontal cell depolarization (149). These prior studies demonstrated that horizontal cells laterally inhibit bipolar cells, which provide direct input to ganglion cells and indirect input via amacrine cells to ganglion cells. Previous studies in the rabbit and goldfish showed that horizontal cell gap junctions are increasingly uncoupled as light intensity increases (162,163). This suggests the horizontal cell receptive field decreases as a function of light intensity. These changes are analogous to the decreased ganglion cell receptive field surround size as light intensity increases shown in the cat retina (164-166). These studies therefore suggest that horizontal cells play a role in shaping the receptive field surrounds of bipolar and ganglion cells. This is consistent with our hypothesis that the loss of LRIT1 changing horizontal cell lateral inhibition would also alter the ganglion cell receptive field center surround organization (167). To determine if horizontal cell LRIT1 is disrupting retinal ganglion cell responses in $Lrit1^{+/-}$ and $Lrit1^{-/-}$ mice, we will record from Cx57-$Lrit1^{+/+}$ and Cx57-$Lrit1^{-/-}$ retinal ganglion cells using stimuli with increasing spot sizes over a range of light intensities and also fix the spot size while varying light intensity. This study will test the hypothesis that horizontal cell LRIT1 alters bipolar and thus ganglion cell center surround organization.

Assuming horizontal cell LRIT1 expression causes our observed abnormal retinal ganglion cell responses, we will elucidate the mechanism by separating the two sources of ganglion cell input. We observed increased ganglion cell activity, which results from increased ganglion cell input that can arise from two sources: either increased excitatory input, decreased inhibitory input, or a combination of both.

Excitatory and inhibitory pathways can be isolated in patch-clamping experiments with *Lrit1* ganglion cells. We would hold the membrane potential stable and present spots of light decrements on a grey background for 2s to ganglion cells. This would be repeated several times by clamping at increasing membrane potentials in 10-20 mV steps similar to experiments done in mouse (35). The excitatory and inhibitory synaptic conductances can be calculated from these data. This will separate excitatory and inhibitory inputs and determine the contributions from each in *Lrit1*$^{+/-}$ and *Lrit1*$^{-/-}$ mice. These experiments would additionally determine if amacrine cells are also contributing to our observed abnormal retinal ganglion cell responses. We would expect that one or both of these inputs would be changed compared to WT littermates.

REFERENCES

1.   Imamoto, Y., and Shichida, Y. (2014) Cone visual pigments. *Biochimica et biophysica acta* **1837**, 664-673

2.   Institute, N. E. (2016) Facts About the Cornea and Corneal Disease. National Institutes of Health, Bethesda, MD

3.   Blind, N. F. o. t. (2017) Statistical Facts about Blindness in the United States. National Federation of the Blind, Baltimore, MD

4.   National Data. in *Vision Health Initiative* Center for Disease Control and Prevention

5.   Eye Diseases in *Genetic and Rare Diseases Information Center*, National Institute of Health

6.   Lamb, T. D., Collin, S. P., and Pugh, E. N., Jr. (2007) Evolution of the vertebrate eye: opsins, photoreceptors, retina and eye cup. *Nature reviews. Neuroscience* **8**, 960-976

7.   Mustafi, D., Engel, A. H., and Palczewski, K. (2009) Structure of cone photoreceptors. *Progress in retinal and eye research* **28**, 289-302

8.   Fain, G. L., Hardie, R., and Laughlin, S. B. (2010) Phototransduction and the evolution of photoreceptors. *Current biology : CB* **20**, R114-124

9.   Diamond, J. S. (2017) Inhibitory Interneurons in the Retina: Types, Circuitry, and Function. *Annual review of vision science* **3**, 1-24

10.   Ortin-Martinez, A., Nadal-Nicolas, F. M., Jimenez-Lopez, M., Alburquerque-Bejar, J. J., Nieto-Lopez, L., Garcia-Ayuso, D., Villegas-Perez, M. P., Vidal-Sanz, M., and Agudo-Barriuso, M. (2014) Number and distribution of mouse retinal cone photoreceptors: differences between an albino (Swiss) and a pigmented (C57/BL6) strain. *PloS one* **9**, e102392

11.   Kefalov, V., Fu, Y., Marsh-Armstrong, N., and Yau, K. W. (2003) Role of visual pigment properties in rod and cone phototransduction. *Nature* **425**, 526-531

12.   Lamb, T. D. (2016) Why rods and cones? *Eye (London, England)* **30**, 179-185

13.   Mercer, A. J., and Thoreson, W. B. (2011) The dynamic architecture of photoreceptor ribbon synapses: cytoskeletal, extracellular matrix, and intramembrane proteins. *Visual neuroscience* **28**, 453-471

14.   Sugita, Y., Araki, F., Chaya, T., Kawano, K., Furukawa, T., and Miura, K. (2015) Role of the mouse retinal photoreceptor ribbon synapse in visual motion processing for optokinetic responses. *PloS one* **10**, e0124132

15.   Smith, R. L., Sivaprasad, S., and Chong, V. (2016) Retinal Biochemistry, Physiology and Cell Biology. *Developments in ophthalmology* **55**, 18-27

16. Grossniklaus, H. E., Geisert, E. E., and Nickerson, J. M. (2015) Introduction to the Retina. *Progress in molecular biology and translational science* **134**, 383-396

17. Euler, T., Haverkamp, S., Schubert, T., and Baden, T. (2014) Retinal bipolar cells: elementary building blocks of vision. *Nature reviews. Neuroscience* **15**, 507-51

18. Arshavsky, V. Y., and Wensel, T. G. (2013) Timing is everything: GTPase regulation in phototransduction. *Investigative ophthalmology & visual science* **54**, 7725-7733

19. Shim, H., Wang, C. T., Chen, Y. L., Chau, V. Q., Fu, K. G., Yang, J., McQuiston, A. R., Fisher, R. A., and Chen, C. K. (2012) Defective retinal depolarizing bipolar cells in regulators of G protein signaling (RGS) 7 and 11 double null mice. *The Journal of biological chemistry* **287**, 14873-14879

20. Cao, Y., Pahlberg, J., Sarria, I., Kamasawa, N., Sampath, A. P., and Martemyanov, K. A. (2012) Regulators of G protein signaling RGS7 and RGS11 determine the onset of the light response in ON bipolar neurons. *Proceedings of the National Academy of Sciences of the United States of America* **109**, 7905-7910

21. Sarria, I., Orlandi, C., McCall, M. A., Gregg, R. G., and Martemyanov, K. A. (2016) Intermolecular Interaction between Anchoring Subunits Specify Subcellular Targeting and Function of RGS Proteins in Retina ON-Bipolar Neurons. *The Journal of neuroscience : the official journal of the Society for Neuroscience* **36**, 2915-2925

22. Rao, A., Dallman, R., Henderson, S., and Chen, C. K. (2007) Gbeta5 is required for normal light responses and morphology of retinal ON-bipolar cells. *The Journal of neuroscience : the official journal of the Society for Neuroscience* **27**, 14199-14204

23. Martemyanov, K. A., Yoo, P. J., Skiba, N. P., and Arshavsky, V. Y. (2005) R7BP, a novel neuronal protein interacting with RGS proteins of the R7 family. *The Journal of biological chemistry* **280**, 5133-5136

24. Orlandi, C., Posokhova, E., Masuho, I., Ray, T. A., Hasan, N., Gregg, R. G., and Martemyanov, K. A. (2012) GPR158/179 regulate G protein signaling by controlling localization and activity of the RGS7 complexes. *The Journal of cell biology* **197**, 711-719

25. Ray, T. A., Heath, K. M., Hasan, N., Noel, J. M., Samuels, I. S., Martemyanov, K. A., Peachey, N. S., McCall, M. A., and Gregg, R. G. (2014) GPR179 is required for high sensitivity of the mGluR6 signaling cascade in depolarizing bipolar cells. *The Journal of neuroscience : the official journal of the Society for Neuroscience* **34**, 6334-6343

26. Koike, C., Nishida, A., Ueno, S., Saito, H., Sanuki, R., Sato, S., Furukawa, A., Aizawa, S., Matsuo, I., Suzuki, N., Kondo, M., and Furukawa, T. (2007) Functional roles of Otx2 transcription factor in postnatal mouse retinal development. *Molecular and cellular biology* **27**, 8318-8329

27. Shen, Y., Heimel, J. A., Kamermans, M., Peachey, N. S., Gregg, R. G., and Nawy, S. (2009) A transient receptor potential-like channel mediates synaptic transmission in rod bipolar cells. *The Journal of neuroscience : the official journal of the Society for Neuroscience* **29**, 6088-6093

28. Morgans, C. W., Zhang, J., Jeffrey, B. G., Nelson, S. M., Burke, N. S., Duvoisin, R. M., and Brown, R. L. (2009) TRPM1 is required for the depolarizing light response in retinal ON-bipolar cells. *Proceedings of the National Academy of Sciences of the United States of America* **106**, 19174-19178

29. Irie, S., and Furukawa, T. (2014) TRPM1. *Handbook of experimental pharmacology* **222**, 387-402

30. Li, Z., Sergouniotis, P. I., Michaelides, M., Mackay, D. S., Wright, G. A., Devery, S., Moore, A. T., Holder, G. E., Robson, A. G., and Webster, A. R. (2009) Recessive mutations of the gene TRPM1 abrogate ON bipolar cell function and cause complete congenital stationary night blindness in humans. *American journal of human genetics* **85**, 711-719

31. Audo, I., Kohl, S., Leroy, B. P., Munier, F. L., Guillonneau, X., Mohand-Said, S., Bujakowska, K., Nandrot, E. F., Lorenz, B., Preising, M., Kellner, U., Renner, A. B., Bernd, A., Antonio, A., Moskova-Doumanova, V., Lancelot, M. E., Poloschek, C. M., Drumare, I., Defoort-Dhellemmes, S., Wissinger, B., Leveillard, T., Hamel, C. P., Schorderet, D. F., De Baere, E., Berger, W., Jacobson, S. G., Zrenner, E., Sahel, J. A., Bhattacharya, S. S., and Zeitz, C. (2009) TRPM1 is mutated in patients with autosomal-recessive complete congenital stationary night blindness. *American journal of human genetics* **85**, 720-729

32. van Genderen, M. M., Bijveld, M. M., Claassen, Y. B., Florijn, R. J., Pearring, J. N., Meire, F. M., McCall, M. A., Riemslag, F. C., Gregg, R. G., Bergen, A. A., and Kamermans, M. (2009) Mutations in TRPM1 are a common cause of complete congenital stationary night blindness. *American journal of human genetics* **85**, 730-736

33. Nakamura, M., Sanuki, R., Yasuma, T. R., Onishi, A., Nishiguchi, K. M., Koike, C., Kadowaki, M., Kondo, M., Miyake, Y., and Furukawa, T. (2010) TRPM1 mutations are associated with the complete form of congenital stationary night blindness. *Molecular vision* **16**, 425-437

34. Cenedese, V., de Graaff, W., Csikos, T., Poovayya, M., Zoidl, G., and Kamermans, M. (2017) Pannexin 1 Is Critically Involved in Feedback from Horizontal Cells to Cones. *Frontiers in molecular neuroscience* **10**, 403

35. Stroh, S., Puller, C., Swirski, S., Holzel, M. B., van der Linde, L. I. S., Segelken, J., Schultz, K., Block, C., Monyer, H., Willecke, K., Weiler, R., Greschner, M., Janssen-Bienhold, U., and Dedek, K. (2018) Eliminating Glutamatergic Input onto Horizontal Cells Changes the Dynamic Range and Receptive Field Organization of Mouse Retinal Ganglion Cells. *The Journal of neuroscience : the official journal of the Society for Neuroscience*

36. Byzov, A. L., and Cervetto, L. (1977) Effects of applied currents on turtle cones in darkness and during the photoresponse. *The Journal of physiology* **265**, 85-102

37. Hirasawa, H., and Kaneko, A. (2003) pH changes in the invaginating synaptic cleft mediate feedback from horizontal cells to cone photoreceptors by modulating Ca2+ channels. *The Journal of general physiology* **122**, 657-671

38. Thoreson, W. B., Babai, N., and Bartoletti, T. M. (2008) Feedback from horizontal cells to rod photoreceptors in vertebrate retina. *The Journal of neuroscience : the official journal of the Society for Neuroscience* **28**, 5691-5695

39. Verweij, J., Kamermans, M., and Spekreijse, H. (1996) Horizontal cells feed back to cones by shifting the cone calcium-current activation range. *Vision research* **36**, 3943-3953

40. Prochnow, N., Hoffmann, S., Vroman, R., Klooster, J., Bunse, S., Kamermans, M., Dermietzel, R., and Zoidl, G. (2009) Pannexin1 in the outer retina of the zebrafish, Danio rerio. *Neuroscience* **162**, 1039-1054

41. Klaassen, L. J., Sun, Z., Steijaert, M. N., Bolte, P., Fahrenfort, I., Sjoerdsma, T., Klooster, J., Claassen, Y., Shields, C. R., Ten Eikelder, H. M., Janssen-Bienhold, U., Zoidl, G., McMahon, D. G., and Kamermans, M. (2011) Synaptic transmission from horizontal cells to cones is impaired by loss of connexin hemichannels. *PLoS biology* **9**, e1001107

42.   Kranz, K., Dorgau, B., Pottek, M., Herrling, R., Schultz, K., Bolte, P., Monyer, H., Penuela, S., Laird, D. W., Dedek, K., Weiler, R., and Janssen-Bienhold, U. (2013) Expression of Pannexin1 in the outer plexiform layer of the mouse retina and physiological impact of its knockout. *The Journal of comparative neurology* **521**, 1119-1135

43.   Country, M. (2017) Advancing the pH hypothesis of negative feedback to photoreceptors: sources of protons and a role for bicarbonate in feedback. *The Journal of physiology* **595**, 1023-1024

44.   Chapot, C. A., Euler, T., and Schubert, T. (2017) How do horizontal cells 'talk' to cone photoreceptors? Different levels of complexity at the cone-horizontal cell synapse. *The Journal of physiology* **595**, 5495-5506

45.   Endeman, D., Fahrenfort, I., Sjoerdsma, T., Steijaert, M., Ten Eikelder, H., and Kamermans, M. (2012) Chloride currents in cones modify feedback from horizontal cells to cones in goldfish retina. *The Journal of physiology* **590**, 5581-5595

46.   Kemmler, R., Schultz, K., Dedek, K., Euler, T., and Schubert, T. (2014) Differential regulation of cone calcium signals by different horizontal cell feedback mechanisms in the mouse retina. *The Journal of neuroscience : the official journal of the Society for Neuroscience* **34**, 11826-11843

47.   Cadetti, L., and Thoreson, W. B. (2006) Feedback effects of horizontal cell membrane potential on cone calcium currents studied with simultaneous recordings. *Journal of neurophysiology* **95**, 1992-1995

48.   Verweij, J., Hornstein, E. P., and Schnapf, J. L. (2003) Surround antagonism in macaque cone photoreceptors. *The Journal of neuroscience : the official journal of the Society for Neuroscience* **23**, 10249-10257

49.   Hare, W. A., and Owen, W. G. (1996) Receptive field of the retinal bipolar cell: a pharmacological study in the tiger salamander. *Journal of neurophysiology* **76**, 2005-2019

50.   Herrmann, R., Heflin, S. J., Hammond, T., Lee, B., Wang, J., Gainetdinov, R. R., Caron, M. G., Eggers, E. D., Frishman, L. J., McCall, M. A., and Arshavsky, V. Y. (2011) Rod vision is controlled by dopamine-dependent sensitization of rod bipolar cells by GABA. *Neuron* **72**, 101-110

51.   Marchiafava, P. L. (1978) Horizontal cells influence membrane potential of bipolar cells in the retina of the turtle. *Nature* **275**, 141-142

52.   (2013) *Retina*, 5th ed., Elsevier, New York

53.   Sanes, J. R., and Masland, R. H. (2015) The types of retinal ganglion cells: current status and implications for neuronal classification. *Annual review of neuroscience* **38**, 221-246

54.   Helmstaedter, M., Briggman, K. L., Turaga, S. C., Jain, V., Seung, H. S., and Denk, W. (2013) Connectomic reconstruction of the inner plexiform layer in the mouse retina. *Nature* **500**, 168-174

55.   Hokfelt, T. (1991) Neuropeptides in perspective: the last ten years. *Neuron* **7**, 867-879

56.   O'Malley, D. M., and Masland, R. H. (1989) Co-release of acetylcholine and gamma-aminobutyric acid by a retinal neuron. *Proceedings of the National Academy of Sciences of the United States of America* **86**, 3414-3418

57.   Baden, T., Berens, P., Franke, K., Roman Roson, M., Bethge, M., and Euler, T. (2016) The functional diversity of retinal ganglion cells in the mouse. *Nature* **529**, 345-350

58.   Farrow, K., and Masland, R. H. (2011) Physiological clustering of visual channels in the mouse retina. *Journal of neurophysiology* **105**, 1516-1530

59.   Mani, A., and Schwartz, G. W. (2017) Circuit Mechanisms of a Retinal Ganglion Cell with Stimulus-Dependent Response Latency and Activation Beyond Its Dendrites. *Current biology : CB* **27**, 471-482

60.   Demb, J. B., and Pugh, E. N. (2002) Connexin36 forms synapses essential for night vision. *Neuron* **36**, 551-553

61.   Kolb, H. (2018) Glial Cells of the Retina. in *Webvision the organization of the retina and visual system*

62.   Cobb, C. A., and Cole, M. P. (2015) Oxidative and nitrative stress in neurodegeneration. *Neurobiology of disease* **84**, 4-21

63.   Gregg, R. G., Kamermans, M., Klooster, J., Lukasiewicz, P. D., Peachey, N. S., Vessey, K. A., and McCall, M. A. (2007) Nyctalopin expression in retinal bipolar cells restores visual function in a mouse model of complete X-linked congenital stationary night blindness. *Journal of neurophysiology* **98**, 3023-3033

64.   Zeitz, C., Robson, A. G., and Audo, I. (2015) Congenital stationary night blindness: an analysis and update of genotype-phenotype correlations and pathogenic mechanisms. *Progress in retinal and eye research* **45**, 58-110

65.   Naeem, M. A., Chavali, V. R., Ali, S., Iqbal, M., Riazuddin, S., Khan, S. N., Husnain, T., Sieving, P. A., Ayyagari, R., Riazuddin, S., Hejtmancik, J. F., and Riazuddin, S. A. (2012) GNAT1 associated with autosomal recessive congenital stationary night blindness. *Investigative ophthalmology & visual science* **53**, 1353-1361

66.   Carrigan, M., Duignan, E., Humphries, P., Palfi, A., Kenna, P. F., and Farrar, G. J. (2016) A novel homozygous truncating GNAT1 mutation implicated in retinal degeneration. *The British journal of ophthalmology* **100**, 495-500

67.   Neuille, M., Malaichamy, S., Vadala, M., Michiels, C., Condroyer, C., Sachidanandam, R., Srilekha, S., Arokiasamy, T., Letexier, M., Demontant, V., Sahel, J. A., Sen, P., Audo, I., Soumittra, N., and Zeitz, C. (2016) Next-generation sequencing confirms the implication of SLC24A1 in autosomal-recessive congenital stationary night blindness. *Clinical genetics* **89**, 690-699

68.   Zeitz, C., Kloeckener-Gruissem, B., Forster, U., Kohl, S., Magyar, I., Wissinger, B., Matyas, G., Borruat, F. X., Schorderet, D. F., Zrenner, E., Munier, F. L., and Berger, W. (2006) Mutations in CABP4, the gene encoding the Ca2+-binding protein 4, cause autosomal recessive night blindness. *American journal of human genetics* **79**, 657-667

69.   Wycisk, K. A., Zeitz, C., Feil, S., Wittmer, M., Forster, U., Neidhardt, J., Wissinger, B., Zrenner, E., Wilke, R., Kohl, S., and Berger, W. (2006) Mutation in the auxiliary calcium-channel subunit CACNA2D4 causes autosomal recessive cone dystrophy. *American journal of human genetics* **79**, 973-977

70.   Dryja, T. P., McGee, T. L., Berson, E. L., Fishman, G. A., Sandberg, M. A., Alexander, K. R., Derlacki, D. J., and Rajagopalan, A. S. (2005) Night blindness and abnormal cone electroretinogram ON responses in patients with mutations in the GRM6 gene encoding mGluR6. *Proceedings of the National Academy of Sciences of the United States of America* **102**, 4884-4889

71. Bech-Hansen, N. T., Naylor, M. J., Maybaum, T. A., Sparkes, R. L., Koop, B., Birch, D. G., Bergen, A. A., Prinsen, C. F., Polomeno, R. C., Gal, A., Drack, A. V., Musarella, M. A., Jacobson, S. G., Young, R. S., and Weleber, R. G. (2000) Mutations in NYX, encoding the leucine-rich proteoglycan nyctalopin, cause X-linked complete congenital stationary night blindness. *Nature genetics* **26**, 319-323

72. Gregg, R. G., Mukhopadhyay, S., Candille, S. I., Ball, S. L., Pardue, M. T., McCall, M. A., and Peachey, N. S. (2003) Identification of the gene and the mutation responsible for the mouse nob phenotype. *Investigative ophthalmology & visual science* **44**, 378-384

73. Pearring, J. N., Bojang, P., Jr., Shen, Y., Koike, C., Furukawa, T., Nawy, S., and Gregg, R. G. (2011) A role for nyctalopin, a small leucine-rich repeat protein, in localizing the TRP melastatin 1 channel to retinal depolarizing bipolar cell dendrites. *The Journal of neuroscience : the official journal of the Society for Neuroscience* **31**, 10060-10066

74. Pesch, K., Zeitz, C., Fries, J. E., Munscher, S., Pusch, C. M., Kohler, K., Berger, W., and Wissinger, B. (2003) Isolation of the mouse nyctalopin gene nyx and expression studies in mouse and rat retina. *Investigative ophthalmology & visual science* **44**, 2260-2266

75. Pusch, C. M., Zeitz, C., Brandau, O., Pesch, K., Achatz, H., Feil, S., Scharfe, C., Maurer, J., Jacobi, F. K., Pinckers, A., Andreasson, S., Hardcastle, A., Wissinger, B., Berger, W., and Meindl, A. (2000) The complete form of X-linked congenital stationary night blindness is caused by mutations in a gene encoding a leucine-rich repeat protein. *Nature genetics* **26**, 324-327

76. Scalabrino, M. L., Boye, S. L., Fransen, K. M., Noel, J. M., Dyka, F. M., Min, S. H., Ruan, Q., De Leeuw, C. N., Simpson, E. M., Gregg, R. G., McCall, M. A., Peachey, N. S., and Boye, S. E. (2015) Intravitreal delivery of a novel AAV vector targets ON bipolar cells and restores visual function in a mouse model of complete congenital stationary night blindness. *Human molecular genetics* **24**, 6229-6239

77. Neuille, M., El Shamieh, S., Orhan, E., Michiels, C., Antonio, A., Lancelot, M. E., Condroyer, C., Bujakowska, K., Poch, O., Sahel, J. A., Audo, I., and Zeitz, C. (2014) Lrit3 deficient mouse (nob6): a novel model of complete congenital stationary night blindness (cCSNB). *PloS one* **9**, e90342

78. Neuille, M., Morgans, C. W., Cao, Y., Orhan, E., Michiels, C., Sahel, J. A., Audo, I., Duvoisin, R. M., Martemyanov, K. A., and Zeitz, C. (2015) LRIT3 is essential to localize TRPM1 to the dendritic tips of depolarizing bipolar cells and may play a role in cone synapse formation. *The European journal of neuroscience* **42**, 1966-1975

79. Zeitz, C., Jacobson, S. G., Hamel, C. P., Bujakowska, K., Neuille, M., Orhan, E., Zanlonghi, X., Lancelot, M. E., Michiels, C., Schwartz, S. B., Bocquet, B., Antonio, A., Audier, C., Letexier, M., Saraiva, J. P., Luu, T. D., Sennlaub, F., Nguyen, H., Poch, O., Dollfus, H., Lecompte, O., Kohl, S., Sahel, J. A., Bhattacharya, S. S., and Audo, I. (2013) Whole-exome sequencing identifies LRIT3 mutations as a cause of autosomal-recessive complete congenital stationary night blindness. *American journal of human genetics* **92**, 67-75

80. Bellone, R. R., Forsyth, G., Leeb, T., Archer, S., Sigurdsson, S., Imsland, F., Mauceli, E., Engensteiner, M., Bailey, E., Sandmeyer, L., Grahn, B., Lindblad-Toh, K., and Wade, C. M. (2010) Fine-mapping and mutation analysis of TRPM1: a candidate gene for leopard complex (LP) spotting and congenital stationary night blindness in horses. *Briefings in functional genomics* **9**, 193-207

81. Peachey, N. S., Pearring, J. N., Bojang, P., Jr., Hirschtritt, M. E., Sturgill-Short, G., Ray, T. A., Furukawa, T., Koike, C., Goldberg, A. F., Shen, Y., McCall, M. A., Nawy, S., Nishina, P. M., and

Gregg, R. G. (2012) Depolarizing bipolar cell dysfunction due to a Trpm1 point mutation. *Journal of neurophysiology* **108**, 2442-2451

82.   Audo, I., Bujakowska, K., Orhan, E., Poloschek, C. M., Defoort-Dhellemmes, S., Drumare, I., Kohl, S., Luu, T. D., Lecompte, O., Zrenner, E., Lancelot, M. E., Antonio, A., Germain, A., Michiels, C., Audier, C., Letexier, M., Saraiva, J. P., Leroy, B. P., Munier, F. L., Mohand-Said, S., Lorenz, B., Friedburg, C., Preising, M., Kellner, U., Renner, A. B., Moskova-Doumanova, V., Berger, W., Wissinger, B., Hamel, C. P., Schorderet, D. F., De Baere, E., Sharon, D., Banin, E., Jacobson, S. G., Bonneau, D., Zanlonghi, X., Le Meur, G., Casteels, I., Koenekoop, R., Long, V. W., Meire, F., Prescott, K., de Ravel, T., Simmons, I., Nguyen, H., Dollfus, H., Poch, O., Leveillard, T., Nguyen-Ba-Charvet, K., Sahel, J. A., Bhattacharya, S. S., and Zeitz, C. (2012) Whole-exome sequencing identifies mutations in GPR179 leading to autosomal-recessive complete congenital stationary night blindness. *American journal of human genetics* **90**, 321-330

83.   Klooster, J., van Genderen, M. M., Yu, M., Florijn, R. J., Riemslag, F. C., Bergen, A. A., Gregg, R. G., Peachey, N. S., and Kamermans, M. (2013) Ultrastructural localization of GPR179 and the impact of mutant forms on retinal function in CSNB1 patients and a mouse model. *Investigative ophthalmology & visual science* **54**, 6973-6981

84.   Balmer, J., Ji, R., Ray, T. A., Selber, F., Gassmann, M., Peachey, N. S., Gregg, R. G., and Enzmann, V. (2013) Presence of the Gpr179(nob5) allele in a C3H-derived transgenic mouse. *Molecular vision* **19**, 2615-2625

85.   Peachey, N. S., Ray, T. A., Florijn, R., Rowe, L. B., Sjoerdsma, T., Contreras-Alcantara, S., Baba, K., Tosini, G., Pozdeyev, N., Iuvone, P. M., Bojang, P., Jr., Pearring, J. N., Simonsz, H. J., van Genderen, M., Birch, D. G., Traboulsi, E. I., Dorfman, A., Lopez, I., Ren, H., Goldberg, A. F., Nishina, P. M., Lachapelle, P., McCall, M. A., Koenekoop, R. K., Bergen, A. A., Kamermans, M., and Gregg, R. G. (2012) GPR179 is required for depolarizing bipolar cell function and is mutated in autosomal-recessive complete congenital stationary night blindness. *American journal of human genetics* **90**, 331-339

86.   O'Connor, E., Allen, L. E., Bradshaw, K., Boylan, J., Moore, A. T., and Trump, D. (2006) Congenital stationary night blindness associated with mutations in GRM6 encoding glutamate receptor MGluR6. *The British journal of ophthalmology* **90**, 653-654

87.   Tummala, S. R., Neinstein, A., Fina, M. E., Dhingra, A., and Vardi, N. (2014) Localization of Cacna1s to ON bipolar dendritic tips requires mGluR6-related cascade elements. *Investigative ophthalmology & visual science* **55**, 1483-1492

88.   Candille, S. I., Pardue, M. T., McCall, M. A., Peachey, N. S., and Gregg, R. G. (1999) Localization of the mouse nob (no b-wave) gene to the centromeric region of the X chromosome. *Investigative ophthalmology & visual science* **40**, 2748-2751

89.   Pardue, M. T., McCall, M. A., LaVail, M. M., Gregg, R. G., and Peachey, N. S. (1998) A naturally occurring mouse model of X-linked congenital stationary night blindness. *Investigative ophthalmology & visual science* **39**, 2443-2449

90.   Ball, S. L., Pardue, M. T., McCall, M. A., Gregg, R. G., and Peachey, N. S. (2003) Immunohistochemical analysis of the outer plexiform layer in the nob mouse shows no abnormalities. *Visual neuroscience* **20**, 267-272

91.   Koike, C., Obara, T., Uriu, Y., Numata, T., Sanuki, R., Miyata, K., Koyasu, T., Ueno, S., Funabiki, K., Tani, A., Ueda, H., Kondo, M., Mori, Y., Tachibana, M., and Furukawa, T. (2010) TRPM1 is a component of the retinal ON bipolar cell transduction channel in the mGluR6

cascade. *Proceedings of the National Academy of Sciences of the United States of America* **107**, 332-337

92.   Bojang, P., Jr., and Gregg, R. G. (2012) Topological analysis of small leucine-rich repeat proteoglycan nyctalopin. *PloS one* **7**, e33137

93.   O'Connor, E., Eisenhaber, B., Dalley, J., Wang, T., Missen, C., Bulleid, N., Bishop, P. N., and Trump, D. (2005) Species specific membrane anchoring of nyctalopin, a small leucine-rich repeat protein. *Human molecular genetics* **14**, 1877-1887

94.   Cao, Y., Sarria, I., Fehlhaber, K. E., Kamasawa, N., Orlandi, C., James, K. N., Hazen, J. L., Gardner, M. R., Farzan, M., Lee, A., Baker, S., Baldwin, K., Sampath, A. P., and Martemyanov, K. A. (2015) Mechanism for Selective Synaptic Wiring of Rod Photoreceptors into the Retinal Circuitry and Its Role in Vision. *Neuron* **87**, 1248-1260

95.   Kobe, B., and Deisenhofer, J. (1995) A structural basis of the interactions between leucine-rich repeats and protein ligands. *Nature* **374**, 183-186

96.   Papageorgiou, A. C., Shapiro, R., and Acharya, K. R. (1997) Molecular recognition of human angiogenin by placental ribonuclease inhibitor--an X-ray crystallographic study at 2.0 A resolution. *The EMBO journal* **16**, 5162-5177

97.   Kobe, B., and Kajava, A. V. (2001) The leucine-rich repeat as a protein recognition motif. *Current opinion in structural biology* **11**, 725-732

98.   Ko, J. (2012) The leucine-rich repeat superfamily of synaptic adhesion molecules: LRRTMs and Slitrks. *Molecules and cells* **34**, 335-340

99.   Ng, A. C., Eisenberg, J. M., Heath, R. J., Huett, A., Robinson, C. M., Nau, G. J., and Xavier, R. J. (2011) Human leucine-rich repeat proteins: a genome-wide bioinformatic categorization and functional analysis in innate immunity. *Proceedings of the National Academy of Sciences of the United States of America* **108 Suppl 1**, 4631-4638

100.   de Wit, J., Hong, W., Luo, L., and Ghosh, A. (2011) Role of leucine-rich repeat proteins in the development and function of neural circuits. *Annual review of cell and developmental biology* **27**, 697-729

101.   Gomi, F., Imaizumi, K., Yoneda, T., Taniguchi, M., Mori, Y., Miyoshi, K., Hitomi, J., Fujikado, T., Tano, Y., and Tohyama, M. (2000) Molecular cloning of a novel membrane glycoprotein, pal, specifically expressed in photoreceptor cells of the retina and containing leucine-rich repeat. *The Journal of neuroscience : the official journal of the Society for Neuroscience* **20**, 3206-3213

102.   Zhang, F., Wen, Y., and Guo, X. (2014) CRISPR/Cas9 for genome editing: progress, implications and challenges. *Human molecular genetics* **23**, R40-46

103.   Ma, Y., Zhang, L., and Huang, X. (2014) Genome modification by CRISPR/Cas9. *The FEBS journal* **281**, 5186-5193

104.   Ranjha, L., Howard, S. M., and Cejka, P. (2018) Main steps in DNA double-strand break repair: an introduction to homologous recombination and related processes. *Chromosoma*

105.   Wang, F., Flanagan, J., Su, N., Wang, L. C., Bui, S., Nielson, A., Wu, X., Vo, H. T., Ma, X. J., and Luo, Y. (2012) RNAscope: a novel in situ RNA analysis platform for formalin-fixed, paraffin-embedded tissues. *The Journal of molecular diagnostics : JMD* **14**, 22-29

106. Kumar, U., Ramkumar, H., Epley, K., Tripathy, K., Karth, P., and Shah, V. (2015) Electroretinogram. (Karth, P. ed.

107. Shirato, S., Maeda, H., Miura, G., and Frishman, L. J. (2008) Postreceptoral contributions to the light-adapted ERG of mice lacking b-waves. *Experimental eye research* **86**, 914-928

108. Bogue, M. A., Grubb, S. C., Walton, D. O., Philip, V. M., Kolishovski, G., Stearns, T., Dunn, M. H., Skelly, D. A., Kadakkuzha, B., TeHennepe, G., Kunde-Ramamoorthy, G., and Chesler, E. J. (2018) Mouse Phenome Database: an integrative database and analysis suite for curated empirical phenotype data from laboratory mice. *Nucleic Acids Research* **46**, D843-D850

109. Lim, J., Chow, C., Genead, M., Akkara, J., Epley, K., and Shah, V. (2016) Retinitis Pigmentosa. (Lim, J. ed.

110. Pardue, M. T., and Peachey, N. S. (2014) Mouse b-wave mutants. *Documenta ophthalmologica. Advances in ophthalmology* **128**, 77-89

111. Peachey, N. S., and Ball, S. L. (2003) Electrophysiological analysis of visual function in mutant mice. *Documenta ophthalmologica. Advances in ophthalmology* **107**, 13-36

112. Obien, M. E., Deligkaris, K., Bullmann, T., Bakkum, D. J., and Frey, U. (2014) Revealing neuronal function through microelectrode array recordings. *Frontiers in neuroscience* **8**, 423

113. Lu, Q., Ganjawala, T. H., Ivanova, E., Cheng, J. G., Troilo, D., and Pan, Z. H. (2016) AAV-mediated transduction and targeting of retinal bipolar cells with improved mGluR6 promoters in rodents and primates. *Gene therapy*

114. Pellissier, L. P., Quinn, P. M., Alves, C. H., Vos, R. M., Klooster, J., Flannery, J. G., Heimel, J. A., and Wijnholds, J. (2015) Gene therapy into photoreceptors and Muller glial cells restores retinal structure and function in CRB1 retinitis pigmentosa mouse models. *Human molecular genetics* **24**, 3104-3118

115. Scott, P. A., Fernandez de Castro, J. P., Kaplan, H. J., and McCall, M. A. (2014) A Pro23His mutation alters prenatal rod photoreceptor morphology in a transgenic swine model of retinitis pigmentosa. *Investigative ophthalmology & visual science* **55**, 2452-2459

116. Peachey, N. S., Hasan, N., FitzMaurice, B., Burrill, S., Pangeni, G., Karst, S. Y., Reinholdt, L., Berry, M. L., Strobel, M., Gregg, R. G., McCall, M. A., and Chang, B. (2017) A missense mutation in Grm6 reduces but does not eliminate mGluR6 expression or rod depolarizing bipolar cell function. *Journal of neurophysiology* **118**, 845-854

117. Brooks, M. J., Rajasimha, H. K., Roger, J. E., and Swaroop, A. (2011) Next-generation sequencing facilitates quantitative analysis of wild-type and Nrl(-/-) retinal transcriptomes. *Molecular vision* **17**, 3034-3054

118. He, F., and Jacobson, A. (2015) Nonsense-Mediated mRNA Decay: Degradation of Defective Transcripts Is Only Part of the Story. *Annual review of genetics* **49**, 339-366

119. Chang, B., Dacey, M. S., Hawes, N. L., Hitchcock, P. F., Milam, A. H., Atmaca-Sonmez, P., Nusinowitz, S., and Heckenlively, J. R. (2006) Cone photoreceptor function loss-3, a novel mouse model of achromatopsia due to a mutation in Gnat2. *Investigative ophthalmology & visual science* **47**, 5017-5021

120. Aboshiha, J., Dubis, A. M., Carroll, J., Hardcastle, A. J., and Michaelides, M. (2016) The cone dysfunction syndromes. *The British journal of ophthalmology* **100**, 115-121

121. Akula, J. D., Mocko, J. A., Moskowitz, A., Hansen, R. M., and Fulton, A. B. (2007) The oscillatory potentials of the dark-adapted electroretinogram in retinopathy of prematurity. *Investigative ophthalmology & visual science* **48**, 5788-5797

122. Gauvin, M., Dorfman, A. L., Trang, N., Gauthier, M., Little, J. M., Lina, J. M., and Lachapelle, P. (2016) Assessing the Contribution of the Oscillatory Potentials to the Genesis of the Photopic ERG with the Discrete Wavelet Transform. *BioMed research international* **2016**, 2790194

123. Humphries, M. M., Rancourt, D., Farrar, G. J., Kenna, P., Hazel, M., Bush, R. A., Sieving, P. A., Sheils, D. M., McNally, N., Creighton, P., Erven, A., Boros, A., Gulya, K., Capecchi, M. R., and Humphries, P. (1997) Retinopathy induced in mice by targeted disruption of the rhodopsin gene. *Nature genetics* **15**, 216-219

124. Chang, B., Hawes, N. L., Hurd, R. E., Davisson, M. T., Nusinowitz, S., and Heckenlively, J. R. (2002) Retinal degeneration mutants in the mouse. *Vision research* **42**, 517-525

125. Goo, Y. S., Park, D. J., Ahn, J. R., and Senok, S. S. (2015) Spontaneous Oscillatory Rhythms in the Degenerating Mouse Retina Modulate Retinal Ganglion Cell Responses to Electrical Stimulation. *Frontiers in cellular neuroscience* **9**, 512

126. Demas, J., Sagdullaev, B. T., Green, E., Jaubert-Miazza, L., McCall, M. A., Gregg, R. G., Wong, R. O., and Guido, W. (2006) Failure to maintain eye-specific segregation in nob, a mutant with abnormally patterned retinal activity. *Neuron* **50**, 247-259

127. Neuille, M., Cao, Y., Caplette, R., Guerrero-Given, D., Thomas, C., Kamasawa, N., Sahel, J. A., Hamel, C. P., Audo, I., Picaud, S., Martemyanov, K. A., and Zeitz, C. (2017) LRIT3 Differentially Affects Connectivity and Synaptic Transmission of Cones to ON- and OFF-Bipolar Cells. *Investigative ophthalmology & visual science* **58**, 1768-1778

128. Qian, H., Ji, R., Gregg, R. G., and Peachey, N. S. (2015) Identification of a new mutant allele, Grm6(nob7), for complete congenital stationary night blindness. *Visual neuroscience* **32**, E004

129. Zeitz, C., van Genderen, M., Neidhardt, J., Luhmann, U. F., Hoeben, F., Forster, U., Wycisk, K., Matyas, G., Hoyng, C. B., Riemslag, F., Meire, F., Cremers, F. P., and Berger, W. (2005) Mutations in GRM6 cause autosomal recessive congenital stationary night blindness with a distinctive scotopic 15-Hz flicker electroretinogram. *Investigative ophthalmology & visual science* **46**, 4328-4335

130. Chang, B., Heckenlively, J. R., Bayley, P. R., Brecha, N. C., Davisson, M. T., Hawes, N. L., Hirano, A. A., Hurd, R. E., Ikeda, A., Johnson, B. A., McCall, M. A., Morgans, C. W., Nusinowitz, S., Peachey, N. S., Rice, D. S., Vessey, K. A., and Gregg, R. G. (2006) The nob2 mouse, a null mutation in Cacna1f: anatomical and functional abnormalities in the outer retina and their consequences on ganglion cell visual responses. *Visual neuroscience* **23**, 11-24

131. Agosto, M. A., Anastassov, I. A., and Wensel, T. G. (2018) Differential epitope masking reveals synapse-specific complexes of TRPM1. *Visual neuroscience* **35**, E001

132. Fuchs, M., Brandstatter, J. H., and Regus-Leidig, H. (2014) Evidence for a Clathrin-independent mode of endocytosis at a continuously active sensory synapse. *Frontiers in cellular neuroscience* **8**, 60

133. Hirano, A. A., Brandstatter, J. H., Vila, A., and Brecha, N. C. (2007) Robust syntaxin-4 immunoreactivity in mammalian horizontal cell processes. *Visual neuroscience* **24**, 489-502

134. Regus-Leidig, H., Ott, C., Lohner, M., Atorf, J., Fuchs, M., Sedmak, T., Kremers, J., Fejtova, A., Gundelfinger, E. D., and Brandstatter, J. H. (2013) Identification and immunocytochemical characterization of Piccolino, a novel Piccolo splice variant selectively expressed at sensory ribbon synapses of the eye and ear. *PloS one* **8**, e70373

135. Regus-Leidig, H., Specht, D., Tom Dieck, S., and Brandstatter, J. H. (2010) Stability of active zone components at the photoreceptor ribbon complex. *Molecular vision* **16**, 2690-2700

136. Babai, N., Sendelbeck, A., Regus-Leidig, H., Fuchs, M., Mertins, J., Reim, K., Brose, N., Feigenspan, A., and Brandstatter, J. H. (2016) Functional Roles of Complexin 3 and Complexin 4 at Mouse Photoreceptor Ribbon Synapses. *The Journal of neuroscience : the official journal of the Society for Neuroscience* **36**, 6651-6667

137. Lem, J., Krasnoperova, N. V., Calvert, P. D., Kosaras, B., Cameron, D. A., Nicolo, M., Makino, C. L., and Sidman, R. L. (1999) Morphological, physiological, and biochemical changes in rhodopsin knockout mice. *Proceedings of the National Academy of Sciences of the United States of America* **96**, 736-741

138. Calvert, P. D., Krasnoperova, N. V., Lyubarsky, A. L., Isayama, T., Nicolo, M., Kosaras, B., Wong, G., Gannon, K. S., Margolskee, R. F., Sidman, R. L., Pugh, E. N., Jr., Makino, C. L., and Lem, J. (2000) Phototransduction in transgenic mice after targeted deletion of the rod transducin alpha -subunit. *Proceedings of the National Academy of Sciences of the United States of America* **97**, 13913-13918

139. Tsang, S. H., Gouras, P., Yamashita, C. K., Kjeldbye, H., Fisher, J., Farber, D. B., and Goff, S. P. (1996) Retinal degeneration in mice lacking the gamma subunit of the rod cGMP phosphodiesterase. *Science (New York, N.Y.)* **272**, 1026-1029

140. LaVail, M. M., and Sidman, R. L. (1974) C57BL-6J mice with inherited retinal degeneration. *Archives of ophthalmology (Chicago, Ill. : 1960)* **91**, 394-400

141. Carter-Dawson, L. D., LaVail, M. M., and Sidman, R. L. (1978) Differential effect of the rd mutation on rods and cones in the mouse retina. *Investigative ophthalmology & visual science* **17**, 489-498

142. Bowes, C., Li, T., Danciger, M., Baxter, L. C., Applebury, M. L., and Farber, D. B. (1990) Retinal degeneration in the rd mouse is caused by a defect in the beta subunit of rod cGMP-phosphodiesterase. *Nature* **347**, 677-680

143. Farber, D. B., and Lolley, R. N. (1974) Cyclic guanosine monophosphate: elevation in degenerating photoreceptor cells of the C3H mouse retina. *Science (New York, N.Y.)* **186**, 449-451

144. Farber, D. B., and Lolley, R. N. (1976) Enzymic basis for cyclic GMP accumulation in degenerative photoreceptor cells of mouse retina. *Journal of cyclic nucleotide research* **2**, 139-148

145. Huttl, S., Michalakis, S., Seeliger, M., Luo, D. G., Acar, N., Geiger, H., Hudl, K., Mader, R., Haverkamp, S., Moser, M., Pfeifer, A., Gerstner, A., Yau, K. W., and Biel, M. (2005) Impaired channel targeting and retinal degeneration in mice lacking the cyclic nucleotide-gated channel subunit CNGB1. *The Journal of neuroscience : the official journal of the Society for Neuroscience* **25**, 130-138

146. Chen, C. K., Burns, M. E., Spencer, M., Niemi, G. A., Chen, J., Hurley, J. B., Baylor, D. A., and Simon, M. I. (1999) Abnormal photoresponses and light-induced apoptosis in rods lacking rhodopsin kinase. *Proceedings of the National Academy of Sciences of the United States of America* **96**, 3718-3722

147.   Yang, R. B., Robinson, S. W., Xiong, W. H., Yau, K. W., Birch, D. G., and Garbers, D. L. (1999) Disruption of a retinal guanylyl cyclase gene leads to cone-specific dystrophy and paradoxical rod behavior. *The Journal of neuroscience : the official journal of the Society for Neuroscience* **19**, 5889-5897

148.   Sonntag, S., Dedek, K., Dorgau, B., Schultz, K., Schmidt, K. F., Cimiotti, K., Weiler, R., Lowel, S., Willecke, K., and Janssen-Bienhold, U. (2012) Ablation of retinal horizontal cells from adult mice leads to rod degeneration and remodeling in the outer retina. *The Journal of neuroscience : the official journal of the Society for Neuroscience* **32**, 10713-10724

149.   Thoreson, W. B., and Mangel, S. C. (2012) Lateral interactions in the outer retina. *Progress in retinal and eye research* **31**, 407-441

150.   McCall, M. A., and Gregg, R. G. (2008) Comparisons of structural and functional abnormalities in mouse b-wave mutants. *The Journal of physiology* **586**, 4385-4392

151.   Margolis, D. J., and Detwiler, P. B. (2011) Cellular origin of spontaneous ganglion cell spike activity in animal models of retinitis pigmentosa. *Journal of ophthalmology* **2011**

152.   Menzler, J., Channappa, L., and Zeck, G. (2014) Rhythmic ganglion cell activity in bleached and blind adult mouse retinas. *PloS one* **9**, e106047

153.   Margolis, D. J., Newkirk, G., Euler, T., and Detwiler, P. B. (2008) Functional stability of retinal ganglion cells after degeneration-induced changes in synaptic input. *The Journal of neuroscience : the official journal of the Society for Neuroscience* **28**, 6526-6536

154.   Goo, Y. S., Ahn, K. N., Song, Y. J., Ahn, S. H., Han, S. K., Ryu, S. B., and Kim, K. H. (2011) Spontaneous Oscillatory Rhythm in Retinal Activities of Two Retinal Degeneration (rd1 and rd10) Mice. *The Korean journal of physiology & pharmacology : official journal of the Korean Physiological Society and the Korean Society of Pharmacology* **15**, 415-422

155.   Sarria, I., Cao, Y., Wang, Y., Ingram, N. T., Orlandi, C., Kamasawa, N., Kolesnikov, A. V., Pahlberg, J., Kefalov, V. J., Sampath, A. P., and Martemyanov, K. A. (2018) LRIT1 Modulates Adaptive Changes in Synaptic Communication of Cone Photoreceptors. *Cell reports* **22**, 3562-3573

156.   Ueno, A., Omori, Y., Sugita, Y., Watanabe, S., Chaya, T., Kozuka, T., Kon, T., Yoshida, S., Matsushita, K., Kuwahara, R., Kajimura, N., Okada, Y., and Furukawa, T. (2018) Lrit1, a Retinal Transmembrane Protein, Regulates Selective Synapse Formation in Cone Photoreceptor Cells and Visual Acuity. *Cell reports* **22**, 3548-3561

157.   Hombach, S., Janssen-Bienhold, U., Sohl, G., Schubert, T., Bussow, H., Ott, T., Weiler, R., and Willecke, K. (2004) Functional expression of connexin57 in horizontal cells of the mouse retina. *The European journal of neuroscience* **19**, 2633-2640

158.   Scott, P. G., Grossmann, J. G., Dodd, C. M., Sheehan, J. K., and Bishop, P. N. (2003) Light and X-ray scattering show decorin to be a dimer in solution. *The Journal of biological chemistry* **278**, 18353-18359

159.   Scott, P. G., Dodd, C. M., Bergmann, E. M., Sheehan, J. K., and Bishop, P. N. (2006) Crystal structure of the biglycan dimer and evidence that dimerization is essential for folding and stability of class I small leucine-rich repeat proteoglycans. *The Journal of biological chemistry* **281**, 13324-13332

160.   Le Goff, M. M., Hindson, V. J., Jowitt, T. A., Scott, P. G., and Bishop, P. N. (2003) Characterization of opticin and evidence of stable dimerization in solution. *The Journal of biological chemistry* **278**, 45280-45287

161.   Hirano, A. A., Liu, X., Brecha, N. C., and Barnes, S. (2018) Analysis of Feedback Signaling from Horizontal Cells to Photoreceptors in Mice. *Methods in molecular biology (Clifton, N.J.)* **1753**, 179-189

162.   Ribelayga, C., and Mangel, S. C. (2010) Identification of a circadian clock-controlled neural pathway in the rabbit retina. *PloS one* **5**, e11020

163.   Ribelayga, C., and Mangel, S. C. (2003) Absence of circadian clock regulation of horizontal cell gap junctional coupling reveals two dopamine systems in the goldfish retina. *The Journal of comparative neurology* **467**, 243-253

164.   Barlow, H. B., Fitzhugh, R., and Kuffler, S. W. (1957) Change of organization in the receptive fields of the cat's retina during dark adaptation. *The Journal of physiology* **137**, 338-354

165.   Troy, J. B., Bohnsack, D. L., and Diller, L. C. (1999) Spatial properties of the cat X-cell receptive field as a function of mean light level. *Visual neuroscience* **16**, 1089-1104

166.   Troy, J. B., Oh, J. K., and Enroth-Cugell, C. (1993) Effect of ambient illumination on the spatial properties of the center and surround of Y-cell receptive fields. *Visual neuroscience* **10**, 753-764

167.   Chaya, T., Matsumoto, A., Sugita, Y., Watanabe, S., Kuwahara, R., Tachibana, M., and Furukawa, T. (2017) Versatile functional roles of horizontal cells in the retinal circuit. *Scientific reports* **7**, 5540

APPENDIX I

SUPPLEMENTARY MATERIAL

Lrit3 Expression in Mouse Photoreceptors

Our observed *Grm6* ON bipolar cell-specific expression pattern is consistent with previous *in situ* hybridization data (1). Because LRIT3 has previously been shown to co-localize with ON bipolar cells and the *Lrit3^nob6* mouse had a no b-wave ERG (2,3), we speculated that LRIT3 is expressed in ON bipolar cells. The Lrit3 expression pattern in the INL is distinct from Grm6. Our finding that *Lrit3* is expressed in photoreceptors was unexpected. Our laboratory is currently examining this hypothesis using AAV-mediated rod-specific *Lrit3* intravitreal injections in the *Lrit3^nob6* mouse to express and characterize the role of LRIT3 in murine rods (unpublished data). Mutations in LRIT3 have been shown to affect rod and cone synapses differentially. In *Lrit3^nob6* retinas, rod synapses form appropriate synaptic contacts to horizontal and rod ON bipolar cells. However, cone synapses lack contacts to ON bipolar cells despite evidence of normal horizontal and OFF bipolar cell contacts, suggesting cone-specific LRIT3 effects (4). Additional experiments may be needed to determine the role of LRIT3 in cones independently of rods. Because *Lrit3^nob6* ERGs show no difference in scotopic and photopic a-waves, it is likely that *Lrit3*'s role in photoreceptors is not critical for its function in the mouse retina (2). While LRIT3 may not affect photoreceptor function assessed by ERG, it is possible that its expression in photoreceptors is necessary but not sufficient for its function in ON bipolar cell signal transmission.

AAV-*Lrit1* Plasmid Sequence

```
LOCUS       pAAV2.1\RHO\eGFP        5582 bp    DNA     circular UNA 12-
JUL-2016

DEFINITION  .

ACCESSION   urn.local...10-6cuqcun

VERSION     urn.local...10-6cuqcun

KEYWORDS    .

SOURCE

  ORGANISM

            .

FEATURES             Location/Qualifiers

    misc_feature    248..377

                    /note="ITR"

    misc_feature    458..1296

                    /note="Geneious type promoter eukaryotic  RHO

PROMOTOR"

    misc_feature    3287..3828

                    /note="WPRE"

    polyA_signal    3835..4049

                    /note="PolyA Signal"

    misc_feature    4091..4136

                    /note=""

    misc_feature    4137..4266

                    /note="ITR"

    source          1..6830

                    /dnas_title="171116_BaseClone_654

                        pAAV_RHO_eGFP_Minus-eGFP_PlusNycSS-cMyc-

                        FLAG_PlusLrit1NoSigSeq_WithPrimers_--"
```

```
    sig_peptide       1305..1361

                      /note="Nyx- signal seq"

    misc_feature      1371..1385

                      /note="Enterokinase sequence"

    misc_feature      1386..1415

                      /note="MYC tag"

    misc_feature      1431..1454

                      /note="DDK tag"

    misc_feature      1461..3269

                      /note="Lrit1 cDNA no SS"

    PCR_primer        complement(1437..1457)

                      /pair=""

                      /primer="ATCCTTATCGTCGTCATCCTT"

                      /current=0

                      /dnas_title="Reverse (1437..1457)"

    PCR_primer        1441..1478

                      /pair=""

                      /primer="ATGACGACGATAAGGATGCATTCTGTCCTTCTGAATGC"

                      /current=0

                      /dnas_title="Forward (1441..1478)"

    PCR_primer        complement(3249..3286)

                      /pair=""

                      /primer="GGATCCAAGCTTTATTAGCAGAAGTACTCATTGATGCG"

                      /current=0

                      /dnas_title="Reverse (3249..3286)"

    misc_feature      3276..3286

                      /note="After HindIII RE from Rho eGFP construct

overhang"

    misc_feature      1458..1460
```

136

/note="changed from %22atc%22 Iso to

                         %22gca%22 Ala to preserve 6bp region,

                         nonpolar residue, and introduce NsiI

                    RE site for future fusion gene expression"

     misc_feature   1297..1298

                    /note="End of Rho from where NotI cuts Rho eGFP "

     misc_feature   1299..1304

                    /note="Added to introduce Not1 RE site, keeps ORF

in

                    frame"

     misc_feature   3270..3275

                    /note="added stop codons"

     PCR_primer   1282..1319

                    /pair=""

                    /primer="ATATCCATCACACTGGCGGCCGCATGCTGATCCTGCTT"

                    /current=1

                    /dnas_title="Forward (1282..1319)"

ORIGIN

1   agcgcccaat acgcaaaccg cctctccccg cgcgttggcc gattcattaa tgcagctggc

61   acgacaggtt tcccgactgg aaagcgggca gtgagcgcaa cgcaattaat gtgagttagc

121   tcactcatta ggcaccccag gctttacact ttatgcttcc ggctcgtatg ttgtgtggaa

181   ttgtgagcgg ataacaattt cacacaggaa acagctatga ccatgattac gccagattta

241   attaaggctg cgcgctcgct cgctcactga ggccgcccgg gcaaagcccg ggcgtcgggc

301   gacctttggt cgcccggcct cagtgagcga gcgagcgcgc agagagggag tggccaactc

361   catcactagg ggttccttgt agttaatgat taacccgcca tgctacttat ctacgtagcc

421   atgctctagg aagatcggaa ttcgccctta agctagcaga tcttccccac ctagccacct

481   ggcaaactgc tccttctctc aaaggcccaa acatggcctc ccagactgca accccaggc

541   agtcaggccc tgtctccaca acctcacagc caccctggac ggaatctgct tcttcccaca

601   tttgagtcct cctcagcccc tgagctcctc tgggcagggc tgtttctttc catctttgta

                                137

```
661   ttcccagggg cctgcaaata aatgtttaat gaacgaacaa gagagtgaat tccaattcca

721    tgcaacaagg attgggctcc tgggccctag gctatgtgtc tggcaccaga aacggaagct

781    gcaggttgca gcccctgccc tcatggagct cctcctgtca gaggagtgtg gggactggat

841    gactccagag gtaacttgtg ggggaacgaa caggtaaggg gctgtgtgac gagatgagag

901    actgggagaa taaaccagaa agtctctagc tgtccagagg acatagcaca gaggcccatg

961    gtccctattt caaacccagg ccaccagact gagctgggac cttgggacag acaagtcatg

1021 cagaagttag gggaccttct cctccctttt cctggatgga tcctgagtac cttctcctcc

1081 ctgacctcag gcttcctcct agtgtcacct tggcccctct tagaagccaa ttaggccctc

1141 agtttctgca gcggggatta atatgattat gaacaccccc aatctcccag atgctgattc

1201 agccaggagc ttaggagggg gaggtcactt tataagggtc tggggggggtc agaacccaga

1261 gtcatcccct gaattctgca gatatccatc acactggcgg ccgcATGCTG ATCCTGCTTC

1321 TTCATGCGGT GGTCTTCAGT CTGCCCTACA CCAGGGCCAC CGGTGCAGGT GATGACGACG

1381 ACAAGGAGCA GAAACTCATC TCAGAAGAGG ATCTGGCAGC AAATGATCTG GATTACAAGG

1441 ATGACGACGA TAAGGATgca TTCTGTCCTT CTGAATGCAG CTGCAGTCTG CGCATCCTGA

1501 GTGACGGCAG CAAGGCCAGG ACAGTGGTGT GCAGCGACCC TGACTTGACT CTGCCTCCAG

1561 CTTCGATTCC TCCAGACACC TGCAAGCTGC GCTTAGAGAG AACCGCCATT CGCAGGGTGC

1621 CGGGAGAGAC CTTCAGGCCT CTCAGCCGCC TGGAGCAGCT GTGGCTACCT TACAATGCTC

1681 TCAGTGAGCT TAGTGCCCTC ATGCTCAGGG GCCTGAGACG CCTACGAGAG CTGCGGCTGC

1741 CTGGGAACCG CCTGGTCACG TTCCCCTGGG CTGCGCTGAG GGACACTCCG CAGCTGCAGC

1801 TGCTGGACCT GCAGGCCAAT CGCCTCTCGA CCTTGCCACC CGAGGCTGCA CACTTCCTGG

1861 AGAACCTTAC TTTCCTGGAC CTGTCCAATA ACCAGCTGAT GAGGCTTCCT GAGGAGCTAC

1921 TGGACGTGTG GGCTCACCTG AAGACCGGGC CCTTCCTTTC CGGCCATCAT GCCAGGCTAA

1981 TCTTAGGGCT TCAGGACAAC CCCTGGGTGT GTGACTGTCG GCTCTATGAC CTGGTTCATC

2041 TTCTAGATGG CTGGGTTTCT TCAAACCTGA TCTTCATCGA GGCTAGACTG AGATGTGCCA

2101 GTCCACGCAG CCTGGCTGGA GTGGCCTTCA GCCAGCTGGA GCTAAGAAAG TGTCAGAGCC

2161 CAGAGCTCCG TCCAGGGGTG ACCAGCATCA TATCCCCTTT GGGTAGCACA GTATTGCTAC

2221 GTTGTGGAGC AACTGGGATC CCAGGACCTG AGATGAGCTG GAGAAGGGCC AATGGACGAC

2281 CACTCAATGG CACAGTACAC CAGGAAGTCT CCAGTGACGG CTCAAGTTGG ACTTTGCTAG

2341 ATTTGCCTGT TGTGTCTCTC TTTGACTCTG GGGACTACAT CTGCCAAGCC AAGAACTTCC
```

138

2401 TGGGAGCTTC TGAAACCCTG ATCTCCTTGA TTGTCACTGA GCCACAGACT TCTACCGGAT

2461 ACAGTGGGAT TCCAGGTGTC CTGTGGGCAA GAACAGGGGA GGGGGCAGAA GCTGCTGCCT

2521 ACAACAACAA GCTGGTGGCC AGGCATGTTC CTCATATGCC CGAGCATGTA GCCCTGGCTA

2581 CCAAGCCCTC AATGCCCAGC ATAAAGGAGG AGCTGGCTCT CCAGAACTTT CAGATGGATG

2641 TCCCAGGAGA GTTCTCCAGA GAGCCATCAG AACACCAGGA GGCACAGATG GTCAGGTCTC

2701 TCAAGGTAGT AGGAGATACT TACCACAGTG TGTCTTTGGT GTGGAAGGCC CCTCAAGCTG

2761 GGAACACAAC CGCCTTTAGT GTCCTTTATG CAGTCTTTGG GCATCGAGAC ATGAGAAGGA

2821 TGACTGTGGA GCCTGGGAAG ACTAGTGTCA CTATCGAGGG ACTTGCTCCA AAGACCAAGT

2881 ATGTGGCATG TGTCTGTGTG CGGGGCTTGG TGCCTACGAA GGAGCAATGT GTCATCTTCT

2941 CTACTGATGA GGTAGTGGAT GCAGAGGGCA CCCAGCGACT CATCAACATG GTGGTGATCA

3001 GCGTGGCCGC CATCATCGCG CTGCCTCCCA CCCTGCTGGT TTGCTGTGGG GCTCTCCGAA

3061 GACGCTGCCA CAAGTGCCGC ACTGGGGGTT CTGCAGAGGC CTCTGGGGCC TATGTTAATT

3121 TGGAAAGACT GGGCCATAGT GAGGACAGCT CAGAAGTTCT GTCCAGGAGC AGCCTCAGTG

3181 AGGGAGATAG GCTTCTCTCA GCCCGTTCCA GCCTGGACTC CCAGGTCTTG GGTGTCAGGG

3241 GCGGCAGACG CATCAATGAG TACTTCTGCt aataaagctt ggatccaatc aacctctgga

3301 ttacaaaatt tgtgaaagat tgactggtat tcttaactat gttgctcctt ttacgctatg

3361 tggatacgct gctttaatgc ctttgtatca tgctattgct tcccgtatgg ctttcatttt

3421 ctcctccttg tataaatcct ggttgctgtc tctttatgag gagttgtggc ccgttgtcag

3481 gcaacgtggc gtggtgtgca ctgtgtttgc tgacgcaacc cccactggtt ggggcattgc

3541 caccacctgt cagctccttt ccgggacttt cgctttcccc ctccctattg ccacggcgga

3601 actcatcgcc gcctgccttg cccgctgctg gacaggggct cggctgttgg gcactgacaa

3661 ttccgtggtg ttgtcgggga agctgacgtc ctttccatgg ctgctcgcct gtgttgccac

3721 ctggattctg cgcgggacgt ccttctgcta cgtcccttcg gccctcaatc cagcggacct

3781 tccttcccgc ggcctgctgc cggctctgcg gcctcttccg cgtcttcgag atctgcctcg

3841 actgtgcctt ctagttgcca gccatctgtt gtttgcccct cccccgtgcc ttccttgacc

3901 ctggaaggtg ccactcccac tgtcctttcc taataaaatg aggaaattgc atcgcattgt

3961 ctgagtaggt gtcattctat tctgggggt ggggtggggc aggacagcaa gggggaggat

4021 tgggaagaca atagcaggca tgctggggac tcgagttaag ggcgaattcc cgattaggat

4081 cttcctagag catggctacg tagataagta gcatggcggg ttaatcatta actacaagga

```
4141 accccctagtg atggagttgg ccactccctc tctgcgcgct cgctcgctca ctgaggccgg

4201 gcgaccaaag gtcgcccgac gcccgggctt tgcccgggcg gcctcagtga gcgagcgagc

4261 gcgcagcctt aattaaccta attcactggc cgtcgtttta caacgtcgtg actgggaaaa

4321 ccctggcgtt acccaactta atcgccttgc agcacatccc cctttcgcca gctggcgtaa

4381 tagcgaagag gcccgcaccg atcgcccttc ccaacagttg cgcagcctga atggcgaatg

4441 ggacgcgccc tgtagcggcg cattaagcgc ggcgggtgtg gtggttacgc gcagcgtgac

4501 cgctacactt gccagcgccc tagcgcccgc tcctttcgct ttcttccctt cctttctcgc

4561 cacgttcgcc ggctttcccc gtcaagctct aaatcggggg ctccctttag ggttccgatt

4621 tagtgcttta cggcacctcg accccaaaaa acttgattag ggtgatggtt cacgtagtgg

4681 gccatcgccc cgatagacgg tttttcgccc tttgacgctg gagttcacgt tcctcaatag

4741 tggactcttg ttccaaactg gaacaacact caaccctatc tcggtctatt cttttgattt

4801 ataagggatt tttccgattt cggcctattg gttaaaaaat gagctgattt aacaaaaatt

4861 taacgcgaat tttaacaaaa tattaacgtt tataatttca ggtggcatct ttcggggaaa

4921 tgtgcgcgga acccctattt gtttattttt ctaaatacat tcaaatatgt atccgctcat

4981 gagacaataa ccctgataaa tgcttcaata atattgaaaa aggaagagta tgagtattca

5041 acatttccgt gtcgccctta ttcccttttt tgcggcattt tgccttcctg tttttgctca

5101 cccagaaacg ctggtgaaag taaaagatgc tgaagatcag ttgggtgcac gagtgggtta

5161 catcgaactg gatctcaata gtggtaagat ccttgagagt tttcgccccg aagaacgttt

5221 tccaatgatg agcacttttta aagttctgct atgtggcgcg gtattatccc gtattgacgc

5281 cgggcaagag caactcggtc gccgcataca ctattctcag aatgacttgg ttgagtactc

5341 accagtcaca gaaaagcatc ttacggatgg catgacagta agagaattat gcagtgctgc

5401 cataaccatg agtgataaca ctgcggccaa cttacttctg acaacgatcg gaggaccgaa

5461 ggagctaacc gcttttttgc acaacatggg ggatcatgta actcgccttg atcgttggga

5521 accggagctg aatgaagcca taccaaacga cgagcgtgac accacgatgc ctgtagtaat

5581 ggtaacaacg ttgcgcaaac tattaactgg cgaactactt actctagctt cccggcaaca

5641 attaatagac tggatggagg cggataaagt tgcaggacca cttctgcgct cggcccttcc

5701 ggctggctgg tttattgctg ataaatctgg agccggtgag cgtgggtctc gcggtatcat

5761 tgcagcactg gggccagatg gtaagccctc ccgtatcgta gttatctaca cgacggggag

5821 tcaggcaact atggatgaac gaaatagaca gatcgctgag ataggtgcct cactgattaa
```
140

```
5881 gcattggtaa ctgtcagacc aagtttactc atatatactt tagattgatt taaaacttca

5941 tttttaattt aaaaggatct aggtgaagat ccttttttgat aatctcatga ccaaaatccc

6001 ttaacgtgag ttttcgttcc actgagcgtc agaccccgta gaaaagatca aaggatcttc

6061 ttgagatcct tttttttctgc gcgtaatctg ctgcttgcaa acaaaaaaac caccgctacc

6121 agcggtggtt tgtttgccgg atcaagagct accaactctt tttccgaagg taactggctt

6181 cagcagagcg cagataccaa atactgtcct tctagtgtag ccgtagttag gccaccactt

6241 caagaactct gtagcaccgc ctacatacct cgctctgcta atcctgttac cagtggctgc

6301 tgccagtggc gataagtcgt gtcttaccgg gttggactca agacgatagt taccggataa

6361 ggcgcagcgg tcgggctgaa cggggggttc gtgcacacag cccagcttgg agcgaacgac

6421 ctacaccgaa ctgagatacc tacagcgtga gctatgagaa agcgccacgc ttcccgaagg

6481 gagaaaggcg gacaggtatc cggtaagcgg cagggtcgga acaggagagc gcacgaggga

6541 gcttccaggg ggaaacgcct ggtatcttta tagtcctgtc gggtttcgcc acctctgact

6601 tgagcgtcga tttttgtgat gctcgtcagg ggggcggagc ctatggaaaa acgccagcaa

6661 cgcggccttt ttacggttcc tggccttttg ctgcggtttt gctcacatgt tctttcctgc

6721 gttatcccct gattctgtgg ataaccgtat taccgccttt gagtgagctg ataccgctcg

6781 ccgcagccga acgaccgagc gcagcgagtc agtgagcgag gaagcggaag

//
```

141

APPENDIX II

ESTABLISHING BEST PRACTICES FOR ONLINE LEARNING MODULES: A SINGLE
INSTITUTION STUDY

Abstract

To reduce lecture hours, medical schools turned to online teaching modalities to re-engage students and reduce cognitive overload and burnout. Importantly, developing effective online learning modules expands the teaching product toolbox and enhances schedule flexibility. Various authorship tools are available, but there is a significant need for faculty development to successfully build these novel resources. We performed this study to establish best practices for creating effective online learning modules. Our mixed-methods survey generated data on student perceptions for overall effectiveness of 19 online learning modules employed in a single course of the first year medical curriculum. These surveys also obtained data on additional parameters to assess their impact on overall effectiveness. Our data revealed that transitioning content from a lecture format to an interactive online exercise can be challenging because online instructors no longer have a real-time presence to assess and redirect learning on an ad hoc basis. Thus, the manner in which an online module is organized, clarity of provided written information, and helpfulness of figures all correlated strongly with student perceptions of overall effectiveness of an online module. In contrast, formative feedback and brief audio/visual lecture capture clips, while viewed very positively by students, appeared more as independent variables correlating less well with overall effectiveness. These data will help guide faculty development as medical education transitions from traditional lectures to an increasing number of online learning resources.

Background

The Four Levels of Teaching and Learning

Learning theories provide the foundation for teachers to understand how their students learn to be effective teachers. This shifts the focus from teaching to learning. Learning theories inform and inspire growth of increasingly dynamic educators who contribute to the design, implementation, and evolution of individual learning modules, whole courses, and entire curricula in higher education. I will examine four different levels of teaching and learning theories that provide the framework for my research project.

In Paulo Freire's *Pedagogy of the Oppressed,* he describes the most fundamental level of teaching and learning (5), the theory of instructivism. He addresses instructivist educational "narration" using the novel phrase "banking concept of education" (6). Freire describes the students' roles in his banking framework: "records, memorizes, and repeats without perceiving" where "education thus becomes an act of depositing … instead of communicating," (6). The educator deposits knowledge into the student's knowledge account where it rests for an indefinite amount of time. Then a student performs a knowledge withdrawal whereby the educator accepts or rejects the regurgitated deposit in the form of a grade as proof for the depth of student learning. The student's knowledge account balance falls back to zero following withdrawal and payment to the educator. Instructivism is the default teaching approach in traditional learning. Instructivism is direct, teacher-centric instruction that delivers truth to students. Direct instruction may be appropriate and beneficial for sharply focused goals depending on the circumstances surrounding and expectations for learning. More often than not, however, learning requires much more than teacher telling and student listening. This makes teacher-centric instructivism a poor approach when it is the only one used.

In contrast, constructivism is the pedagogical antithesis to instructivism accomplishing goals beyond student listening. Learning involving higher-order cognitive processes such as analysis, evaluation, creation, logic, judgment, problem solving, and creative thinking needs student-centered instruction (7). Constructivism provides a creative, student-centric solution for successfully developing higher-order skills (8). Constructivism recognizes the student/material interaction through the lens of the student's personal experiences to build new knowledge (9). Constructivist learning relies on and enriches content connection, schema construction, and information integration. Constructivist teachers challenge students to create their

own content understanding by providing "tasks to be accomplished or problems to be solved, especially those that have personal relevance for learners" (5). Importantly, constructivism redefines the roles of educator and student such that the student assumes responsibility for his or her learning through which the educator is a guide (10). Constructivism requires that teacher and student understand their new responsibilities and how this may differ from past teaching and learning experiences.

The second level of teaching and learning concerns the manner in which a student learns. These are behaviorism and cognitivism (5), which parallel instructivism and constructivism, respectively. On one hand, behaviorist learning is cyclical: stimulus, response, feedback, reinforcement, repeat. This type is still passive because the feedback depends only on providing the correct or incorrect answer, not in understanding necessary logic to reach the correct answer and exclude incorrect ones. On the other hand, cognitive learning accentuates the learner's mental state, what they think, and what they know. Thus, cognitivism aligns with constructivist tenets. If behavioral learning is stimulus/response, then cognitive learning is appropriate stimulus/contextual application. Cognitive learning beseeches students to embed new information within a contextual framework to offer deeper understanding and authentic learning (11). By blending behaviorism and cognitivism, teachers can match learning objectives for learners to appropriately apply new knowledge based on the teacher's expectations. These expectations may be lower-level learning objectives when using behavioral learning and higher-level learning objectives when using cognitive learning.

The third level regards the teacher's role, which is subject to change within and among lessons. Teachers can be didactic or facilitative (5). Didactic instruction tells students "a" and "b" and concludes each concept is important. In contrast, facilitative teaching transpires when the teacher guides the students to conclusions. One example of facilitative teaching is by inquiry. Teachers use inquiry to determine students' baseline knowledge, bridge students' thinking so that students provide the answers that reveal new information to be taught, and provide students a situation or analogy for them to connect that information. Thus, facilitative teachers contextualize the principles on which the importance of "a" and "b" arise and anticipate how students might relate to or apply that knowledge (11,12).

The fourth level of teaching and learning is the source of student motivation. These are categorized as intrinsic or extrinsic (5). Examples of extrinsic motivation may include parental

expectations, financial reward for their career path, and course grades, the latter of which is typically required for semester or annual scholarship renewal. Extrinsic motivators are less likely to result in authentic learning because extrinsically motivated students lose their motivation when rewards or consequences for extrinsic motivators are removed. However, if a student has an innate passion for a field, a sense of accomplishment when they master it, or a sense that a career path is their true calling, they have intrinsic motivation to do well. These motivations are similar to what the authors in Freakonomics define as incentives:

> There are three basic flavors of incentive: economic, social, and moral. Very often a single incentive scheme will include all three varieties. Think about the anti-smoking campaign of recent years. The addition of a $3-per-pack 'sin tax' is a strong economic incentive against buying cigarettes. The banning of cigarettes in restaurants and bars is a powerful social incentive. And when the U.S. government asserts that terrorists raise money by selling black-market cigarettes, that acts as a rather jarring moral incentive. (13)

If teachers can convince students that learning specific content will be important for explicitly stated, intrinsically motivated reasons, students will be more interested in learning over a long-term scale and more likely to achieve those goals (14).

Modes for Delivering Instruction

Both instructivist and constructivist teachers can deliver material in several ways. These include traditional, blended, flipped, or fully online learning. First, traditional learning is in-class learning usually in the form of a teacher-directed live lecture with an audience of listening students. Traditional learning is geographically and time-dependent. Second, blended learning is any combination of in-class and online learning regardless of synchronicity. A blended classroom can utilize online activities, provide online resources and/or discussion boards, or deliver course content online while in-class time is reserved for other learning approaches (15). Third, flipped classrooms are a specific example of the blended classroom that use before-class preparation time for students to study lecture material independently (10,16). These online preparation modules are followed by in-class active learning activities with faculty-guided instruction to develop teamwork and collaborative skills and practice the application of the pre-learned content within

real-life situations. Flipped classrooms additionally allow students to view content through an online

medium without temporal or spatial constraints. Students can review the content as many times as needed

for mastery. Within the content may be embedded questions that provide feedback about the degree of

mastery to the student. Last, online learning is learning via the internet and can occur in several formats:

synchronous, asynchronous, or blended, the latter of which is a mixture of synchronous and asynchronous

formats (17). Synchronous online learning is geographically independent but time-dependent where all

learning takes place simultaneously like a live online classroom accessed from anywhere with internet

access (18,19). Asynchronous online learning is both geographically and time-independent where all

learning takes place at the student's discretion (18,19). An additional advantage to asynchronous online

learning is the student's unlimited review of material until they reach content mastery.

How Constructivism Encourages Active Learning

Active learning is defined as purposeful student engagement in an activity to encourage content

and skills building and can be incorporated in traditional, blended, flipped, or fully online learning

environments. Active learning has been shown to boost content comprehension, critical thinking, problem

solving, and information analysis compared to passive teaching models (10,20,21). Constructivist teaching

actively engages learners to participate in their outcome-guided learning process in a self-regulated way.

When teachers choose the right combination of activities for the expected learning levels of new content,

learners engage and participate in outcome-guided active constructivist learning (9,22). Cognitivism,

facilitative instruction, and intrinsic student motivation all provide additional theoretical support for

constructivist active learning. By using a constructivist teaching approach, learning becomes active and

student-centric with a focus on developing specific knowledge and skills.

Adult Learning Theory is Similar to Online Learning Principles

Adult learners comprise a subgroup of learners with characteristics distinct from younger students.

Adult learning theory, or andragogy, demonstrates that adult students in higher education are dynamically

engaged, decidedly motivated, and chiefly self-directed learners when given new content (7). This is

because students transform and improve how they approach learning as they progress into adulthood,

causing a shift from teacher- to self-directed learning. The adult craving for independence contributes to this shift and incites a desire for self-guided learning. Adult learners have more personal experience than younger learners on which they can construct their own knowledge. Teachers can use this expanded experience scaffold to create deep, authentic adult learning experiences.

Similar to adult learners, online learners must also have intrinsic motivation to "control, manage, and plan their learning actions" in "self-regulated learning" (7,17). Self-regulated online learners must champion their independence to achieve academic success. Online learners must take static information and construct their own knowledge and make meaning (10). Online learners remain engaged when they encounter examples or assessments that apply to their every-day lives, which leads to deep learning (17). Thus, the shared characteristics of adult and online learners must be applied to effectively design courses that meet their learning needs.

Replacing traditional learning with online learning is an attempt to provide students with a convenient, flexible, active learning experience guided by constructivism, cognitivism, facilitative teaching, and intrinsic motivation. In the past, online learning in higher education was aimed at non-traditional adult students (23) that at the time made up a minor proportion of enrollees. These non-traditional adult students took advantage of the benefits of online learning such as the autonomy, convenience, flexibility, accessibility, quality, increased access to additional resources, increased use of technology in education, and increased ability to teach to a variety of learning styles (22). They also directly benefitted from the overall increase in technological literacy of teachers and students due to marked improvements in technology and frequent technological use in our society (24). Traditional instruction is transforming to either incorporate online learning or completely replace traditional instruction with online learning. Statistics from 2014 show that 28.5% of students enrolled in degree-granting postsecondary public, non-profit private, and for-profit private institutions were enrolled in one or more online learning courses (25). This suggests that adult students are now aware of the advantages of online learning and capitalizing on them. Higher education is undergoing a paradigm shift to meet the projections that online courses will soon be half of all learning (26).

How Online Learning is Unique

Online learning differs from traditional learning wherein teachers are not present to immediately assess and redirect student learning on the spot. The first step in implementing an online learning classroom is determining which software teachers will use to create online learning modules. This software category is typically referred to as content authoring software for generating interactive, multimedia-based online learning modules delivered via the internet. Content authoring software is the solution to incorporating content from myriad media formats, increasing interactivity of online learning to create active learning environments independent of the teacher's presence, and tailoring lessons for individual learning styles where content can be presented in a multitude of ways with the added advantage of providing a sheet of additional resources as needed for students who may need extra help or different explanations. Some examples of these programs include Adobe Captivate, Articulate Storyline, Camtasia Studio, Lectora Inspire, and SoftChalk (27). The technological literacy of faculty, staff, and students varies. We must also consider the ease in implementing a new technology. Senior computer education and IT students (n=28) conducted a usability study on online learning tools (n=15) to assess their user-friendliness in three competency categories: technical, media, and assessment (27). Adobe Captivate was ranked first and SoftChalk ranked second of 15 evaluated tools for its overall competencies in usability (discrete score on a 1-5 scale [Table 4]: Captivate, 4.95; SoftChalk, 4.36) (27). These data suggest that not all content authoring software is created equal in its user-friendliness, which can directly impact faculty motivation and time spent to use and develop online learning modules if a specific software is required.

Second, online learning resources must be created with theory-based instructional design to anticipate the most common ways students will stray from main points or misunderstand concepts (28). This requires direct, clear, and coherent material chunked into small bites coupled with adequate assessment and feedback. To address material chunking, content should be designed and presented in such a way as to require a minimal amount of possible effort for the learner. This is based on the cognitive load theory, which is the total amount of mental effort required for learning new content dependent on the content presentation (29). All learning initially takes place in the working memory (11,30). Our working memories are finite and can handle limited amounts of processing or mental elements at any one time. Cognitive load theory has 3 distinct components that contribute to the working memory: intrinsic, germane, and extraneous loads (11,28). Intrinsic load refers to the inherent difficulty of the information and the

number of components students require in their working memory to process the information. Teachers should aim to manage intrinsic load using approaches based on theories like the sequencing and segmenting effects (11,28,30). The sequencing effect is organizing content in a stepwise manner from simple to complex or presenting complex material in isolated steps before combining them all together (30). The latter can also be referred to as the pre-training effect (30). The segmenting effect chunks small pieces of content into discrete "bite-sized" pieces for new learners (30). Blissett *et al.* proposed the claim that approaches used to create schema-based lessons rather than traditional lessons minimizes intrinsic load and directly increased first-year medical student diagnostic performance by 20% in the schema-based group (n=53 schema students versus n=48 traditional students) (11). Germane load is the mental effort to permanently store information also known as schema creation (11). Teachers should maximize germane load by choosing relevant mental work that will directly build the necessary skills and support understanding of the new information (28). This is where it is paramount to carefully choose activities based on what learning level a student should understand the content during an assessment. Extraneous load is the manner in which content is presented to the student. This type should be minimized using approaches based on phenomena such as the split-effect (11,28,30). The split effect requires the student to split their attention to integrate several pieces of information, which requires more mental effort overall (30). Thus, intrinsic, extraneous, and germane loads directly apply to the organization and specific articulation of provided material in online lessons (29). Thus, teachers should carefully choose included written text, graphics, audio/visual files, and additional resources to balance the overall cognitive load and ease learning for novice students.

Last, adequate assessment and feedback as defined by Sadler is "specially intended to generate feedback on performance to improve and accelerate learning" (31). The role of feedback is especially important for self-directed online learning modules. Oftentimes with online learning, students allow formative assessment to guide their learning when lessons lack explicit, specific learning objectives. Assessments should be designed to determine if the student understands the material at the expected level, *i.e.* lower- versus higher-order thinking and learning according to Bloom's taxonomy. Assessments that test memorization are unsuitable if students are expected to analyze a concept in a graded assignment or exam. Additionally, feedback should aim to include indicating the correct answer and all possible iterations of a

correct answer if necessary as in the case of fill-in-the-blank assessment questions for example. Feedback should also include reasoning for how and why provided incorrect answers are wrong. Feedback failing to address every incorrect answer frustrates students by not providing a comprehensive guide to the correct destination (answer) distinct from each proposed path (all given answer choices). Consistent assessments and feedback keep the student engaged and learning actively and acts as their self-reflective bridge from no understanding before the lesson to content mastery after the lesson.

Literature Search

Several studies have demonstrated advantages for online learning. McLaughlin's study assessed the effectiveness of the flipped classroom for pharmacy students (10). They concluded that flipped classrooms resulted in significant differences in final exam scores compared to the traditional classroom (independent *t*-test for traditional to blended exam scores: 160.06 ± 14.65 to 165.48 ± 13.34 out of 200 total points; p=0.001) (10). In an undergraduate nursing study on the effectiveness of case-based learning using SoftChalk, Cleveland *et al.* found a significant difference in the pre- and post-activity assessments (paired *t*-test p<0.001, n=315) (32). A study on dental students using SoftChalks for reviews at the beginning of a course instead of lectures found that review modules significantly increased post-test outcomes by 46% (n=114-115) (33). An examination of a SoftChalk module for screening Alzheimer's disease was performed by Coffman *et al.* where they surveyed n=43 physicians (34). They found that the post-test score was 24 points higher than the pre-test score (97.3% to 72.8%, respectively) (34).

However, several studies have shown no added benefits regarding online learning. A flipped classroom study for a pharmacokinetics course utilized written and audiovisual recordings followed by in-class activities (35). They found no significant difference in student outcomes compared to a traditional course (35). A second online learning effectiveness study in human anatomy courses for pharmacy students found no significant differences in student outcomes between traditional (n=110) and online students (n=55-60) (36). A comparison study for online and classroom instruction in undergraduate pharmacology courses showed no significant difference in mean exam scores (14). Munson's dissertation work using a detailed statistical analysis found no significant difference between a traditional or blended pharmaceutical calculations course (37). Her study included Camtasia online lectures and SoftChalk tutorials (37). Another

study analyzed third-year medical students (n=147) in traditional versus blended courses in evidence-based medicine concluding no significant difference in outcomes (38). A meta-analysis of blended learning studies in the health professions compared 1) blended learning to no intervention or 2) blended and non-blended learning (39). They found that blended learning has either no effect or a positive effect when compared to no intervention or non-blended learning. Half of the studies examined in their meta-analysis examined medical student performance (39).

Previous studies have demonstrated positive student perceptions of online learning that describe its myriad benefits. A study examining online learning (n=71 students) showed that respondents claim the "online format is convenient, flexible, and may be beneficial for learning (40)." The study by Limpach *et al.* showed a more positive student perception of the distance course compared to the traditional course (36). In the study by Buxton *et al.* on pharmacists' synchronous or asynchronous continuing education formats, pharmacist perception data revealed that the asynchronous cohort had greater satisfaction, *i.e.* physical comfort, external distractions, and audio and video quality of slides (41). In a combined study on 3 online graduate courses using SoftChalk modules, Carver *et al.* found that students (n=81) responded favorably to visual appearance, engagement, enhanced understanding, and interactive review chunking of information (42). Another SoftChalk-based online learning study by Newman *et al.* for medical students (n=13) in genetics found that 83% of respondents had better knowledge retention when completing self-directed learning modules (43). Survey data from Coffman *et al.* indicates online learning led to transformational learning experience in 75% of respondents that agreed the module would change how they practice medicine (34). This suggests that online learning positively impacts student perceptions on individual mindsets to and motivation for online learning and understanding online content.

However, online learning is not without its distinctive set of challenges. Online learning requires a re-education of adult students who, up to now, learned predominantly through traditional instruction through which they may or may not have developed the necessary skill set of a successful online learner, *i.e.* a self-regulated learner. Online learning is completed at the discretion of the student. Each student may learn new information at a different rate, so it may take some students much longer to complete assigned lessons than others. This can negatively impact their motivation to learn. Another challenge is the social aspect of online learning (5,12). Thus, there are significant challenges for both faculty and students to

design and achieve a successful online learning approach. When online learning does not include any collaborative or team activities, students can feel isolated, which affects their engagement, motivation, and outcomes (24). Hale *et al.* found that "students in the online course were less satisfied [than in classroom courses] with 8 criteria related to student satisfaction with instructor rapport, course excellence, peer interaction, and self-perceived knowledge gains," (14). In a descriptive study using SoftChalks in oncology palliative care for medical, nursing, social work, and chaplain students (n=228 total), they found that student feedback specified online learning modules were too long and had too much content (44). These findings suggest that online learning may limit social interaction and the student's ability to determine how much they learned (9). They also suggest that educators must design online learning with the student's time allocation in mind (45,46). This may require educators to know their audience's initial knowledge level to consider the difference between a novice and an expert learner because a novice learner will take more time to learn new material (45).

In addition to student outcomes, previous studies have also shared valuable information on student perceptions of online learning. The implementation of online learning is assumed to result in increased faculty and student productivity and flexibility, decreased cost, student-centric teaching, and comparable student achievement (47). In opposition to these assumptions, McLaughlin *et al.* found that one of the greatest barriers to implementing a successful flipped classroom was the estimate for faculty time and resources (10). Moreover, Dyrbye *et al.* showed students commented on "issues relate[d] to: clarity of communication, difficulties in negotiating team work and in building relationships, technical demands, learning style preferences, and time commitment," (40). These findings suggest that we may vastly underestimate time, social skills, and resources needed to transition from traditional to online learning (47).

Taken together, the literature on online learning some of which specifically investigate SoftChalks either demonstrated no difference (14,35-39) or a positive significant difference (10,32-34,39) on student outcomes and perceptions. These studies support that online approaches at the least do not harm student learning. These studies also suggest at the most a positive role for online education in the healthcare profession. The contribution of online education, however, still requires extensive further study to determine critical criteria to generate and implement teaching and learning innovations in the online world (15,17).

Online Learning in Medical Education

Recently, professors in medical education estimate that around 70% of medical students no longer attend lectures (48). Recently, the American governing body on medical education, the Liaison Committee on Medical Education, has expressed concerns for majority traditional instruction in medical education. Therefore, medical schools nationwide began integrating online learning into their curricula in a much higher proportion than ever before to reduce instructional lecture hours and student burn-out. However, there is increased accountability to meet the expected teaching standards in the newly widespread medium of online learning. The future of medical education to survive in the face of the transition to incorporate online learning depends on engaged, knowledgeable, collaborative, and self-regulated faculty educators. Simply using technology in the classroom does not ensure increased student motivation to learn (8). Only well-incorporated technology nurture intrinsic motivation and self-directed learning (24). The shift from traditional to online learning implores faculty to rethink their teaching strategies using instructional design approaches to deliver content specifically designed for the virtual arena (49,50). Teachers are constantly improving their teaching skills in the online classroom to more effectively guide student learning. This leads to an increased demand on teachers' time and expertise in modern-day medical education (51). As a result, educators need to buy into the benefits of online learning to be willing to put in the increased time required upfront to generate highly effective online learning modules. Our goal is to describe our experience in implementing online learning modules to establish best practices and inform other educators seeking to create and integrate online learning in their curricula.

Introduction

A recent provision by the Liaison Committee on Medical Education (LCME) challenges medical schools to reduce their traditional lecture hours to increase interactivity, collaboration, teamwork, and active learning. One approach to decreasing lecture hours is constructing online learning modules using cloud-based authoring tools. Such tools allow individual faculty to create interactive online learning modules for implementation in various instructional settings. As a substitute for traditional lectures, online learning modules accomplish myriad functions beyond meeting the LCME's challenge to reduce lecture

hours. Online learning modules provide standardized instructional content for multi-campus medical schools needing to document instructional comparability among sites. Online learning modules also afford considerable flexibility in curriculum design by reducing faculty scheduling constraints and allowing student access to instructional content tailored to their individual learning styles. Finally, online learning modules fulfill a critical role in delivering instructional content as part of a flipped classroom prior to in-class active learning experiences.

There are a number of cloud-based authoring tools available for faculty to create online learning modules. While we have predominantly used the SoftChalk Cloud® to generate e-learning content, we expect that the lessons learned in our study are generalizable to many different authoring platforms.

Several studies compare asynchronous online learning to synchronous online learning or traditional learning to investigate the effectiveness of online learning modules (10,14,32-39,41,43). Other studies discuss strengths and weaknesses for online learning and using content authoring software (27,40-42,44). Although tips for creating online learning modules have been published (18,40,52), no studies have analyzed the effectiveness of several online learning modules to establish best practices.

Adult learning theory states that adult students are actively engaged, highly motivated, and predominantly self-directed in their mastery of new content (53). Similar to adult learners, online learners must also have intrinsic motivation to "control, manage, and plan their learning actions" in what Broadbent refers to as "self-regulated learning" (17,26). Online learning offers autonomy to adult learners through convenience, flexibility, accessibility, quality, and increased ability to teach various learning styles; it also encourages students to seek resources and develop skills on their own, both of which are critical skills for developing and instilling lifelong learning in future medical doctors. By placing medical education learning experiences within the adult learning theoretical framework, faculty can create student-centered, self-directed online learning modules. This study examines our faculty-generated online learning modules.

At our institution the decision to use online learning platforms as an alternative to traditional lectures is made on a voluntary basis. At present, our medical curriculum lacks specific guidelines for developing online learning modules. This study was performed to guide best practices for online learning module design to ultimately shape future faculty development initiatives for online learning module improvement.

154

Methods

Course Structure

All procedures performed in studies involving human participants were in accordance with the ethical standards of the Institutional Review Board of the University of Louisville (IRB #16.0979) and with the ethical standards set by the 1964 Declaration of Helsinki and its later amendments or comparable ethical standards. All online learning modules in the study were created using an online authoring tool developed by the SoftChalk® Corporation. For those unfamiliar with SoftChalk online learning modules, see example SoftChalk components (Supplementary Fig. 1). The University provides site licenses enabling access to the cloud-based authoring software for individual faculty members. This access includes storage space within the SoftChalk Cloud and seamless integration with curriculum management software for dissemination of online learning modules within the existing course structure. All evaluated online learning modules were included as part of the Molecular Basis of Life, Defense, and Disease (MBLD&D) course. This is a multidisciplinary course integrating biochemistry, genetics, and immunology with foundational principles of pharmacology, physiology, pathology, and microbiology. The MBLD&D course spans 16 weeks in the spring semester of the first year medical curriculum during which enrollment for this study was 160 students. Student participation was voluntary and did not affect students' grades. Survey completion was considered implied consent. There were 19 online learning modules included in the study covering a range of topics: viruses and cancer, glycolipids, lipoproteins, fast-fed metabolism, eicosanoids, nucleotide metabolism, drug absorption and distribution, drug metabolism and elimination, anti-inflammatory drugs, vitamins, anti-neoplastics, pharmacodynamics, antibiotics, the pentose phosphate pathway, the citric acid cycle, oxidative phosphorylation, bacterial physiology and metabolism, genetics of bacterial pathogenesis, and sterilization and disinfection.

WATER SOLUBLE VITAMINS

F. Pyridoxine (B6)

Pyridoxine can be found in several states; pyridoxine (pyridoxol), pyridoxamine, and pyridoxal. The co-enzyme form is pyridoxal phosphate. Other forms must be converted to pyridoxal phosphate through the actions of pyridoxal kinase and pyridox(am)ine phosphate oxidase.
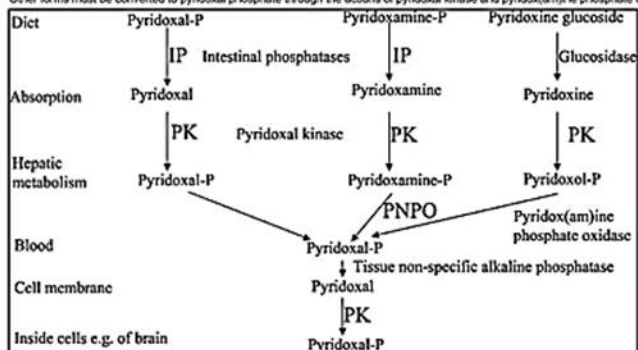
On this Page

F. Pyridoxine (B6)
1. Diet
2. Reactions
3. Deficiencies
4. Toxicity
5. Additional drug interactions
6. Miscellaneous

Clayton (2006) J Inhert Metab Dis 29:317-326

Value: 1

The 10-year-old girl in the previous question did not have dietary history suggestive of pellagra (she did not have corn as a staple of her diet) but she was somewhat undernourished. Labs revealed the child had a neutral aminoaciduria. The most likely factor contributing to the pellagratic symptoms in this child is a deficiency of

- a. phenylalanine.
- b. glutamic acid.
- c. tryptophan.
- d. alanine.
- e. arginine.

[Check Answer]

✖ Sorry, incorrect answer.

This girl has Hartnup's disease, which is caused by a defect in a neutral amino acid transporter involved in gut absorption and the kidney reuptake of neutral amino acids. Tryptophan is taken up by this transporter and since it is used as a source of niacin within the human body, Hartnup patients can present with symptoms of niacin deficiency.

B. Riboflavin (B2)

The coenzyme forms of riboflavin are flavin adenine dinucleotide (FAD) and flavin mononucleotide (FMN).

1. Diet

- Found in milk and other dairy products (major source in North American diet), meats, whole and enriched grains, and some vegetables. Flavin gets its name from Latin for yellow since solutions containing flavin are yellow when in the oxidized state.

2. Reactions

- Electron carrier - oxidation/reductions. Functions in energy metabolism as part of pyruvate and α-ketoglutarate dehydrogenases and as an electron carrier in the TCA cycle and electron transport chain. Also functions in fat catabolism.

3. Deficiencies

- Causes
  - Flavin deficiencies are often found in association with deficiencies of other B vitamins in North America (chronic alcoholism), but can be found on its own in other parts of the world where consumption of dairy and meat productions is low.
- Diseases/Symptoms
  - Ariboflavinosis - inflammation of eyes, skin (seborrheic dermatitis becoming red, scaly and greasy), lips (cheilosis), mouth, and tongue.
  - Flavin deficiency can influence iron absorption and mobilization and as a consequence can affect the production and function of red blood cells.

4. Miscellaneous

- Riboflavin participates in the metabolism of other vitamins: pyridoxine, folic acid, and niacin.
- Riboflavin is destroyed by light, explaining why milk is not stored in glass bottles or clear plastic.

Supplementary Figure 1. Examples of online learning module criteria assessed in the survey. A title page showing number of pages (top center), hierarchical pyridoxine text with a figure (left), an assessment question with a corresponding explanation (right), and overall organization using section headers and text formatting (bottom left) are shown.

Measures and Statistics

Upon completion of an online learning module, students were asked complete a 10-item Likert scale survey including the opportunity for open response (Supplementary Fig. 2). The survey addressed the following topics: teaching effectiveness, learner engagement, professor nuance and personality, access to resources and tools, organization, text, figures, audio/visual lecture capture clips using Tegrity® software,

formative assessment, and other learning activities such as drag-and-drop labelling, flash cards, matching

exercises, and others. In addition to student evaluations, online learning modules were evaluated for word

count, number of figures, number and length of audio/visual lecture capture clips, the number of formative

assessment questions with and without feedback, and the number of additional activities included in the

cloud-based authorship software such as drag-and-drop labelling, flash cards, matching exercises, and

others.

End of SoftChalk Survey

Please identify the SoftChalk you are evaluating:
List the approximate time it took you to complete the SoftChalk
30 minutes   60 minutes   90 minutes   120 minutes   > 120 minutes
Use the scale below to answer the following questions:
 Strongly agree (5), Agree (4), Neutral (3), Disagree (2), Strongly Disagree (1)
- I feel that overall this SoftChalk was **effective** in helping me learn the content presented
- I felt that I was **more engaged** when working on this SoftChalk than I typically am when listening to a lecture
- I had **more tools** to process information and assess my learning during this SoftChalk than I typically receive when listening to a lecture
- I felt that the author of this SoftChalk's **nuances and biases** towards objectives for my learning came across in a similar fashion to what I would expect during lecture

SoftChalks have many different components. Please use the scale below to evaluate how effective each of the following components was as a part of your learning experience with this SoftChalk:
 Very effective (5), Moderately effective (4), Neutral (3), moderately ineffective (2), Very ineffective (1)
- Overall organization, clarity of text, helpfulness of figures, Tegrity clips, formative assessment questions (multiple choice, true/false, short answer) including feedback, learning activities (flash cards, drag and drop, labeling, hot spot, others)

Open Response

Supplementary Figure 2. The composition of the End of SoftChalk survey administered immediately following completion of each individual SoftChalk module to first-year undergraduate medical students.

In the survey the Likert scale used values from 1-5 representing "strongly disagree," "disagree,"

"neutral," "agree," or "strongly agree" or "very ineffective," "moderately ineffective," "neutral,"

"moderately effective," or "very effective" depending on the nature of the survey item (Supplementary Fig.

2). For online learning modules missing one or more surveyed items, survey responses for those items were

excluded from analysis. Survey data were analyzed in aggregate to examine global trends in the studied

online learning modules and increase our study's statistical power. We performed a Spearman's rank nonparametric test to assess correlations between surveyed variables (overall organization, clarity of text, helpfulness of figures, audio/visual lecture capture clips, formative assessment, and learning activities) and the rated overall effectiveness of online learning modules. In addition, in an attempt to account for effects of lecturer, we also performed linear regression and ordinal logistic regression. In both linear and ordinal logistic regression models, the independent variables (overall organization, clarity of text, helpfulness of figures, audio/visual lecture capture clips, formative assessment, and learning activities) were each individually assessed for their contribution to variance observed in the dependent variable, overall effectiveness. In the case of linear models, both the dependent and independent variables were treated as continuous, with lecturer encoded as a factor variable. In contrast, for ordinal logistic regression, the dependent variable was treated as ordinal, whereas the independent variable was treated as continuous, again with lecturer encoded as a factor variable. All statistics were conducted in R (54) using the following packages/functions: "cor.test()" for Spearmans rank; "lm()" for linear regression; and "polr()" for ordinal logistic regression.

Open response data was thematically analyzed to determine the student perception of what criteria constitute an effective SoftChalk. We examined open responses by reading the data to code it using inductive thematic analysis. This was repeated iteratively until no new codes were found. All quoted open responses are representatives for the determined themes.

Results

Online Learning Module Review

Review of our online learning modules revealed extensive heterogeneity among the various faculty-generated online learning modules (Supplementary Fig. 3). Each online learning module varied broadly in all assessed parameters (data range): number of pages (5-23), the number of figures (5-27), the number of audio/visual lecture capture clips (0-10), the number of assessment questions (0-20), the number of assessment questions with accompanying feedback (0-19), and inclusion of other activities (0-10). Online learning modules contained means of 12 figures and 3,821 words. Notably, the more text-heavy online learning modules approached 7,500 words. Of interest, while online learning modules altogether

contained a total of 152 formative assessment questions, only 100 questions included any form of feedback

or explanation. These data illustrate the great degree of diversity in our online learning modules and

suggest a need for establishing best practices for individual faculty creating online learning modules.
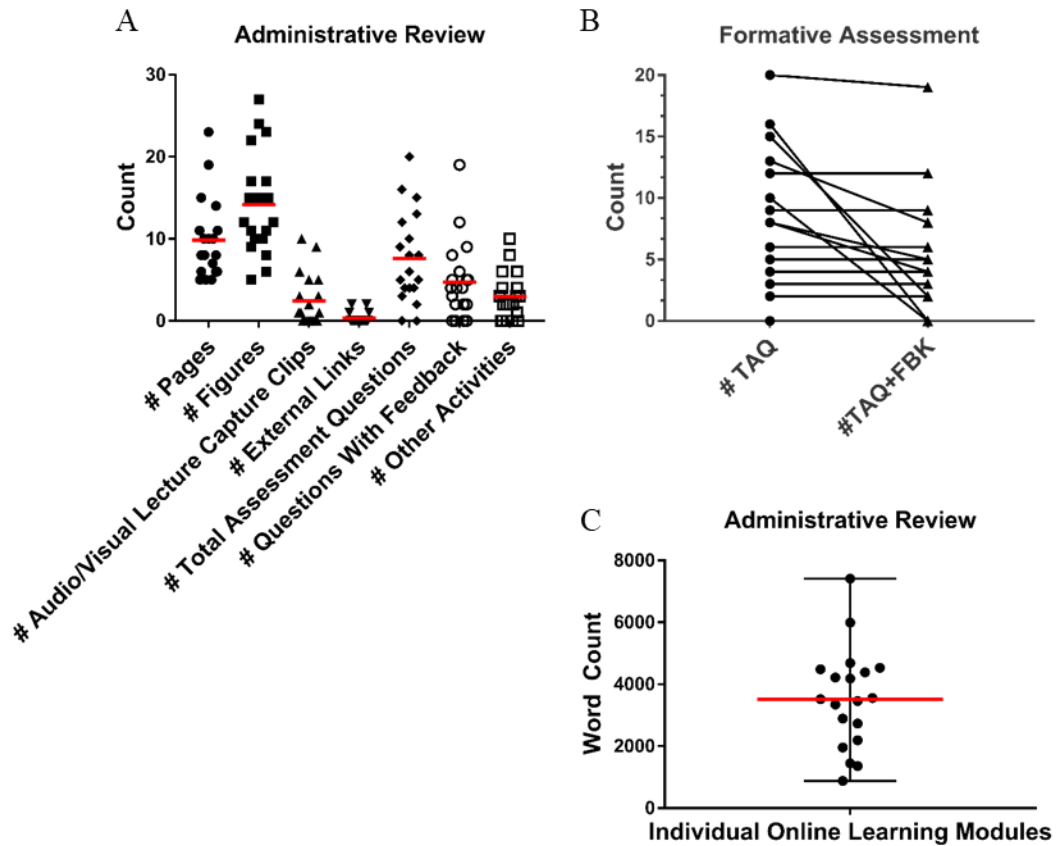
Supplementary Figure 3. Online learning module administrative review. All 19 surveyed online learning modules were reviewed for the indicated parameters. A) Plot shows the number of pages, figures, audio/visual lecture capture clips, external links, assessment questions, assessment questions with feedback, and other activities for individual online learning modules (points) and means (bars). B) Plot shows paired data for individual online learning modules indicating the total number of assessment questions (#TAQ) versus assessment questions with included feedback (#TAQ+FBK). C) Plot for word count excluding words in figures for individual online learning modules (points) and the mean (bar).

Online Learning Module Surveys

To fulfill the need to establish best practices for creating online learning modules, our voluntary surveys were administered to all students in the MLBD&D course following each online learning module to investigate teaching effectiveness, learner engagement, professor nuance and personality, access to resources and tools, organization, text, figures, audio/visual lecture capture clips, formative assessment, and other learning activities. Surveys yielded low to moderate response numbers where the lowest, highest, and mean response rates were 6, 77, and 30 responses, respectively, out of an eligible $n = 160$ participants for each survey (Supplementary Table 1). We determined student perceptions of our online learning modules by analyzing survey responses in aggregate to examine the global effectiveness of online learning modules rather than the effects a specific module, lecturer, or topic (Supplementary Fig. 4; Supplementary Table 2). Our initial results demonstrate that the majority of respondents (1) agreed (50%) or strongly agreed (29%) the online learning modules were effective and (2) rated overall organization and formative assessment extremely positively for an online learning module (Supplementary Fig. 2).

Supplementary Table 1. Individual Online Learning Module Survey Response Rate	
Individual Online Learning Module	n Survey Participants (% Response)
1	71 (44)
2	77 (48)
3	54 (34)
4	49 (31)
5	19 (12)
6	16 (10)
7	16 (10)
8	18 (11)
9	34 (21)
10	21 (13)
11	27 (17)
12	29 (18)
13	7 (4)
14	37 (23)
15	19 (12)
16	36 (23)
17	10 (6)
18	20 (13)
19	6 (4)
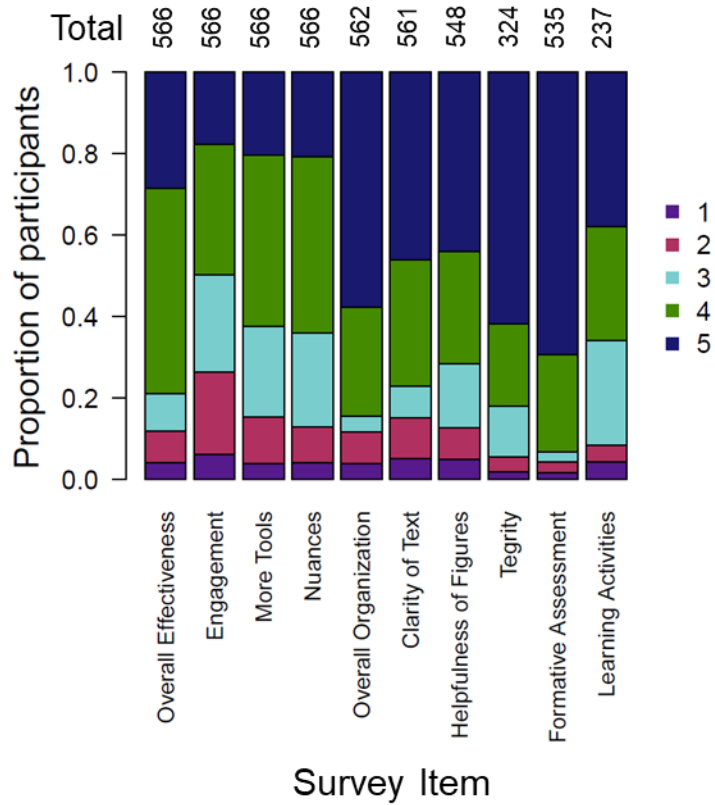
Supplementary Figure 4. Stacked bar plot for the proportion of aggregate Likert-scale survey responses (1-5) by survey item. See methods for scoring and supplementary table 2 for n responses per item per score.

Supplementary Table 2. Survey Responses by Survey Item (see methods for scoring)

Survey Item	n Response by Score (%)					Total n
	1	2	3	4	5	
I feel that overall this SoftChalk was effective in helping me learn the content presented.	23 (4)	44 (8)	52 (9)	285 (50)	162 (29)	566
I felt that I was more engaged when working on this SoftChalk than I typically am when listening to a lecture.	35 (6)	114 (20)	135 (24)	181 (32)	101 (18)	566
I had more tools to process information and assess my learning during this SoftChalk than I typically receive when listening to a lecture.	22 (4)	65 (11)	126 (22)	238 (42)	115 (20)	566
I felt that the author of this SoftChalk's nuances and biases towards objectives for my learning came across in a similar fashion to what I would expect during a lecture.	23 (4)	50 (9)	130 (23)	245 (43)	118 (21)	566
Effectiveness of overall organization	22 (4)	44 (8)	21 (4)	150 (27)	325 (58)	562
Effectiveness of clarity of text	29 (5)	56 (10)	43 (8)	174 (31)	259 (46)	561
Effectiveness of helpfulness of figures	27 (5)	42 (8)	86 (16)	151 (28)	242 (44)	548
Effectiveness of audio/visual lecture capture clips	6 (2)	12 (4)	40 (12)	66 (20)	200 (62)	324
Effectiveness of formative assessment	9 (2)	14 (3)	13 (2)	128 (24)	371 (69)	535
Effectiveness of learning activities	10 (4)	10 (4)	61 (26)	66 (28)	90 (38)	237

163

To assess the relationship between each of six aspects (overall organization, clarity of text, helpfulness of figures, audio/visual lecture capture clips, formative assessment, and learning activities) and overall effectiveness in greater detail, we performed a Spearman's rank test. We found that all six of these variables were positively correlated with overall effectiveness, with overall organization, clarity of text, and helpfulness of figures representing the strongest correlations (Supplementary Table 3). However, plotting our survey data on overall effectiveness versus lecturer for all six lecturers, the graph illustrates that effectiveness varies among lecturers but also that each lecturer's effectiveness varies with distinct patterns (Supplementary Fig. 5). Because correlation analysis cannot account for potential effects of variation observed among lecturers (Supplementary Fig. 5), we also performed linear and ordinal logistic regression (see Methods). Consistent with results from the Spearman's rank test, we observed statistically significant associations between each of the six aspects and overall effectiveness using both regression methods (Supplementary Table 4).

Supplementary Table 3. Spearman Rank Correlation Test Results	
Survey Item Compared to Overall Effectiveness Item	Spearman's ρ (p-value)
Effectiveness of overall organization	$0.65\ (1.52 \times 10^{-68})$
Effectiveness of clarity of text	$0.65\ (1.78 \times 10^{-67})$
Effectiveness of helpfulness of figures	$0.55\ (1.60 \times 10^{-45})$
Effectiveness of learning activities	$0.51\ (4.04 \times 10^{-17})$
Effectiveness of formative assessment	$0.46\ (1.13 \times 10^{-29})$
Effectiveness of audio/visual lecture capture clips	$0.39\ (2.561 \times 10^{-13})$
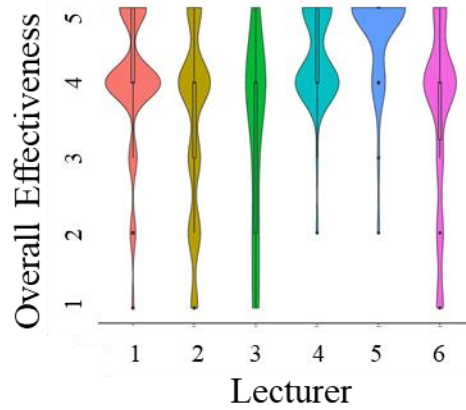
Supplementary Figure 5. Violin plot showing overall effectiveness varies as a function of lecturer.

Supplementary Table 4. Regression Analyses' Results		
Survey Item Compared to Overall Effectiveness Item	Linear Regression p value (β)	Ordinal Logistic Regression Value (p value)
Effectiveness of overall organization	7.60×10^{-75} (0.68)	1.80 (5.05×10^{-47})
Effectiveness of clarity of text	1.79×10^{-74} (0.58)	1.52 (1.10×10^{-47})
Effectiveness of helpfulness of figures	5.60×10^{-53} (0.51)	1.21 (2.21×10^{-38})
Effectiveness of formative assessment	5.02×10^{-30} (0.57)	1.24 (1.33×10^{-21})
Effectiveness of learning activities	1.10×10^{-18} (0.54)	1.03 (4.79×10^{-15})
Effectiveness of audio/visual lecture capture clips	1.56×10^{-17} (0.47)	0.95 (1.70×10^{-14})

When analyzing themes for the open response item for all surveyed online learning modules, the majority of participants commented on the most common themes of content presentation (*i.e.* aesthetic, length, organization, and coherence) and the incorporation of formative assessment question feedback. These specific themes are addressed in the representative student comments in Supplementary Table 5 and aided the formulation of the tips presented in the discussion section below.

Supplementary Table 5. Representative Themes From Open Response Comments

"A outline of what the student was going to learn …to focus in on the content"

"Goes into detail way beyond the learning objectives"

"Unsure of what is relevant"

"Poor organization makes it hard to review and get the key points"

"Organization did not flow…tegrities did not serve to clarify the content…questions lacked feedback…would have preferred a board review book"

"Info does not flow…extremely difficult to follow…attention was not brought to what we should really focus on"

"Cutting down unneeded info will be helpful"

"Appreciate the length limitation on each page"

"Breaking up the info rather than big blocks of text made it easier without getting burnt out"

"The more questions the better! Bolded words/phrases for importance perfect!"

"No text to help comprehend…the tegrity clips"

"More detail of how to reason the way to the correct answer"

"Like the explicit explanations for the graphs and charts"

"Tegrity clips to explain info that hits the high points" "

"Shorter and clearer paragraphs…less grammar mistakes…better references to figures in text…more tegrity clips…outline general concepts"

"This soft chalk was well organized, emphasized the key points and provided helpful information along the way"

Discussion

Necessity for Online Learning Modules

Our study builds our understanding for what motivates students to use online learning modules they perceive as effective. Online learning modules are sustainable, reusable educational products that provide an alternative to or supplement for traditional lectures. From a practical standpoint, online learning modules afford significant flexibility: curriculum planners can plan the best suited faculty for lessons if faculty have online learning modules. Instead of faculty preparing individual lectures requiring their attendance, energy, and personality, they can interchange lectures with their arsenal of online learning modules. Finally, students can access and complete the modules without the limitations for attending a traditional class session at a particular location within a specified time window. Moreover, there is an increasing need for medical schools and educational institutions to demonstrate comparable education among courses with multiple sections or one course across multiple campuses. Implementing online learning modules resolves this need as they are easily documented, reviewable, and revisable educational products. As a result of these benefits, it is crucial to establish best practices to generate effective online learning modules.

Student Perceptions of Online Learning Modules

Our results exhibited that overall organization and formative assessment were rated extremely positively. However, the Spearman's rank test results demonstrate that overall organization, clarity of text, and helpfulness of figures most strongly correlate with overall effectiveness. The discrepancy between the survey data and Spearman's rank correlation led us to visually examine this relationship further. When these data are represented in bubble density plots, the visualized trends suggest two distinct groups. Factors grouped in Fig. 6A such as overall organization exhibit a diagonal trend supporting the strong correlations to overall effectiveness whereas factors grouped in Fig. 6B such as formative assessment exhibit a distinct horizontal, right-shifted trend indicating that independent of overall effectiveness, respondents enjoyed the incorporation of these factors into the online learning modules and rated them highly (Fig. 6B, x-axis scores). This suggests that while overall organization and formative assessment were both rated positively in the surveys, these ratings were dependent and independent, respectively, of overall effectiveness.

167

Additionally, our results demonstrated only 29% of participants strongly agreed compared to 50% of participants that agreed the online learning modules were effective. Here we discuss practical improvements to online learning modules that may shift the 50% from agree to strongly agree that our online learning modules are effective overall.
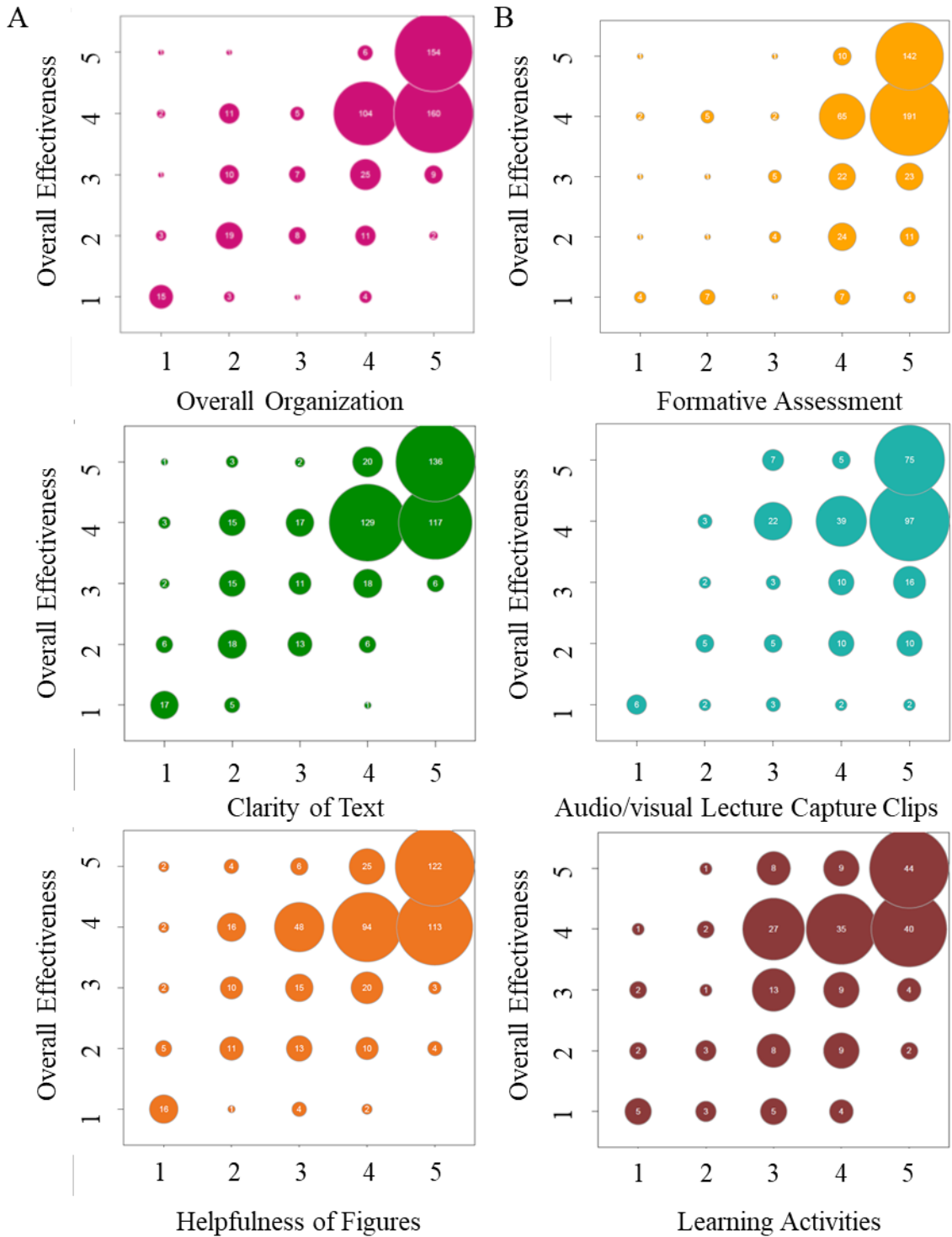
Supplementary Figure 6. Bubble density plots for independent variables (overall organization, clarity of text, helpfulness of figures, formative assessment, audio/visual lecture capture clips, and learning activities) to the dependent variable, overall effectiveness. Each plot represents the distribution of responses for survey items scored 1-5 in our data set across the range of two variables as indicated on x- and y-axes. Data are plotted for A) overall organization, clarity of text, helpfulness of figures; and B) formative assessment, audio/visual lecture capture clips, and learning activities.

Because our online learning modules are asynchronous lessons (17,40), the teacher is not present to redirect student learning such that teachers must make assumptions about the best way to organize and present content (18). Themes from our open response analysis specify student perceptions concerning overall organization like using bolded fonts to indicate important or high-yield information (Supplementary Table 5). Thus, consistent formatting and aesthetic of online learning modules reduces extraneous cognitive load and can indicate changes in importance or structure of new information (55). This can be accomplished with differential font sizes, indentation, colors, headings and subheadings, etc. The overall aesthetic should be clean, easy to navigate, and easy to follow for the novice learner. Use the interplay among text, embedded audio/video clips, additional activities, and assessments to reference and guide the students' introduction to and integration of new content (56). Explicit references for all embedded files, figures, and links in the text aids the lesson's coherence and students' understanding of the function(s) of activities and figures (9,57).

Additionally, it is hard for novice learners to initially determine important or fundamental points from supporting details when trying to learn new information (45) supporting our finding that an online learning module's clarity of text is important (Supplementary Table 5). This is not to say educators should tell students this is all you need to know but rather guide student learning in explicitly stating crucial points (12,32,44,47).

One of the challenges for self-led online learning according to previous studies and our open responses comments is receiving immediate feedback (31,46). The overwhelming response that 93% of participants found formative assessment either very effective or moderately effective for their learning suggests a dependence on formative assessment to monitor self-directed learning. Consistent feedback throughout the online learning module may keep the student engaged, guide the self-directed critical reflection of their content comprehension, and help them understand why their approach to assessment questions was adequate or inadequate (7,10,58). Effective feedback should consist of two major items: the correct answer with relevant reasoning and faculty anticipation of why a student may choose each incorrect answer with logic as to why these answers are incorrect (44). Appropriate formative assessments should supplement a well-designed online learning module, not rescue a poorly designed one.

Last, one of the chief complaints received in the open response comments was that the online learning modules were essentially too heavy: contained too much information overall or trivial and/or repetitive information and took novice learners longer to complete than the time allotted. Simplifying an online learning module by cutting down the amount of and carefully choosing text, accompanying figures, and assessment questions reduces cognitive load and reading time to ease learning while requiring less time (18,45,59).

The following tips on designing an effective online learning module arising from our survey findings and open response themes during our study provide a starting point for integrating student perceptions, faculty challenges, and learning theories into online learning (Supplementary Table 6).

Supplementary Table 6. Best Practice Tips for Creating Effective Online Learning Modules

---

Tip 1 – Format online learning modules consistently, i.e. section headings, fonts, colors, etc.

Tip 2 – Purposefully choose included figures, audio/visual lecture clips, and activities and embed with explicit in-text references

Tip 3 – Summarize critically important points to provide take-home messages

Tip 4 – Organize each online learning module to form a coherent lesson including all desired learning objectives

Tip 5 – Supplement with feedback-based formative assessments

Tip 6 – Simplify length and content of text, figures, audio/visual lecture clips, and activities

---

Limitations

Online learning modules are asynchronous and lack the immediate feedback of a live class. This suggests that online learning modules must be designed well and with great foresight. Not all faculty have equivalent technological literacy to generate online learning modules; this may require additional IT support, a teaching assistant, and faculty development to ease the faculty transition from traditional instruction to online learning.

Our survey study is further limited by a low response number, no link to student outcomes, and no evaluation of faculty perceptions of online learning modules. Analysis of our survey response rate as a function of time, online learning module effectiveness, or lecturer or analysis of word count length of paired open responses to overall effectiveness ratings yielded no significant correlations (data not shown). Our aggregate analysis of survey data combined with anonymity of participants requires us to consider the same subgroup of students responded to each survey resulting in a biased dataset. Our study is skewed toward improved, more effective online learning modules generated from six different faculty members, taught at different points in a semester-long course, and covered topics of various difficulty. A limitation to our survey is some online learning modules did not incorporate surveyed items (Supplementary Fig. 3, y-axis scores of 0) for which we could have included a "non-applicable" choice. All of these limit the impact of our findings.

Acknowledgements

Future Directions

Considerations for Future Faculty Development Initiatives

Flexner recommended to integrate medical schools within universities to encourage a partnership between basic science and medicine (51). Flexner's goal in doing so was delivering the underlying principles that explain the "why" of most medical questions to medical students (51). Students' understanding of the "why" is paramount for their ability to critically reason through applying certain knowledge to one circumstance but not another. The partnership between basic science and medicine thus began the purpose of not only preparing physicians with the base knowledge they need in a clinical setting but how to adapt and transform that knowledge amidst changing circumstances. The first two years of medical education provides an intense, detailed, often clinically integrated basic sciences curriculum as the foundation for developing clinical knowledge and expertise in the later years.

Although most basic science and clinician educators are experts in their fields of study, they are oftentimes deprived of formal educational training from their scholarly programs. In an article for Inside Higher Ed, Grasgreen writes:

> Some certificate programs began in the late 1980s and 1990s, von Hoene says, but the majority were created over the past decade' to answer the call for 'faculty who can not only conduct research at top-tier universities, but also be effective in the classroom. (60)

While some educators actively seek voluntary teaching certificates during or after completing field-specific training, most are expected to passively absorb nuances of effective teaching under this working model of instructivism: "'We don't learn how to teach...our stereotype is that a teacher gets up there and hands you a lot of knowledge. You're the empty glass, they're the pitcher of water [sic] and they pour their knowledge into you,'" (60). This quote echoes Paulo Freire's "banking concept of education" (6). The Faculty Survey of Student Engagement revealed:

> Faculty members teaching courses in Biological Sciences, Engineering, and Physical Sciences allocated more than half of their class time to lecturing whereas faculty members in Education committed less than one quarter, indicating variation across disciplines in the use of innovative teaching techniques versus traditional lecturing and low-tech teaching strategies. (61)

No teacher can be expected to develop expert teaching skills without first learning those skills or being provided the time and resources for learning them in a self-directed manner, even if that teacher is a subject matter expert. This is why appropriate faculty development initiatives are vital. Teaching effectiveness, therefore, is not exclusively the fault of the educator. Educational institutions must properly design and provide adequate faculty development in teaching and learning and establish communities of practice for educators to encourage and support skills improvement together (19).

Online learning modules provide increased flexibility to curriculum planners to assign teaching hours to best-fit faculty. Importantly, faculty have added flexibility to fulfill simultaneous teaching responsibilities without lengthening their absolute hours spent teaching. However, for these benefits to be applicable, faculty must generate effective online learning modules. This requires that institutions offer faculty development initiatives for online learning module improvement for which faculty should attend.

A recent systematic review of the faculty development literature in higher education shows faculty development studies (n=39) explicitly incorporate and provide the following information for their training either all of the time or a lot: principles of good practice (92%), research on online learning (62%), and theories of learning (44%) (62). Less than half of the reviewed studies provided underlying theories upon which teaching is implemented. The majority of these studies only provided training on the "principles of good practice" (62). While there are great how-to handbooks for faculty development in the traditional classroom, none such comprehensive manuals exist for online teaching (62). Thus, most faculty development supplies principles of best practice with no connections for why these are the established principles of good practice. Without understanding the underlying theories of learning from which best practices arise, faculty are deprived of honing their ability to discern in which circumstances certain practices should be preserved or changed to maintain an effective, active, deep, authentic student learning experience (9). Previous work by Carter, Solberg, and Solberg shows that one of the critical obstacles for faculty in generating an online learning module or platform was "the challenge of transitioning our faculty from a traditional face-to-face learning environment" to online learning (63). Providing appropriate faculty development interventions will ease the transition to online learning, support faculty during the transition, and provide them with the necessary tools to succeed as teachers in a new online learning environment.

Teachers must understand how their students learn to be effective teachers, shifting the focus from teaching to learning. No teacher can be expected to attain expert teaching skills without the time, support, and resources to learn, apply, and critically reflect on those skills. This same logic applies to faculty developers who train teachers: faculty developers must understand how their teachers learn to effectively transfer any theories or skills in a meaningful way. Theories of learning lay the foundation for this understanding to advise and shape our educators. By comparing online learning modules, we now know what online learning module components on which we should offer faculty development interventions to improve our online learning modules. Further, by plotting our online learning module survey data for overall effectiveness as a function of lecturer, it is obvious that effectiveness varies among lecturers but also that each lecturer's effectiveness varies differently. By using our survey data, we can even propose personalized faculty development plans to improve our online learning modules. Thus, faculty can attend and participate in applicable development initiatives incorporating theory, best practices, and practical applications to improve their online learning modules.

APPENDICES I & II REFERENCES

1.   Kim, D. S., Matsuda, T., and Cepko, C. L. (2008) A core paired-type and POU homeodomain-containing transcription factor program drives retinal bipolar cell gene expression. *The Journal of neuroscience : the official journal of the Society for Neuroscience* **28**, 7748-7764

2.   Neuille, M., El Shamieh, S., Orhan, E., Michiels, C., Antonio, A., Lancelot, M. E., Condroyer, C., Bujakowska, K., Poch, O., Sahel, J. A., Audo, I., and Zeitz, C. (2014) Lrit3 deficient mouse (nob6): a novel model of complete congenital stationary night blindness (cCSNB). *PloS one* **9**, e90342

3.   Neuille, M., Morgans, C. W., Cao, Y., Orhan, E., Michiels, C., Sahel, J. A., Audo, I., Duvoisin, R. M., Martemyanov, K. A., and Zeitz, C. (2015) LRIT3 is essential to localize TRPM1 to the dendritic tips of depolarizing bipolar cells and may play a role in cone synapse formation. *The European journal of neuroscience* **42**, 1966-1975

4.   Neuille, M., Cao, Y., Caplette, R., Guerrero-Given, D., Thomas, C., Kamasawa, N., Sahel, J. A., Hamel, C. P., Audo, I., Picaud, S., Martemyanov, K. A., and Zeitz, C. (2017) LRIT3 Differentially Affects Connectivity and Synaptic Transmission of Cones to ON- and OFF-Bipolar Cells. *Investigative ophthalmology & visual science* **58**, 1768-1778

5.   Reeves, P. M., and Reeves, T. C. (2008) Design considerations for online learning in health and social work education. *Learning in Health and Social Care* **7**, 46-58

6.   Freire, P. (2000) *Pedagogy of the Oppressed*, Continuum, New York

7.   Decelle, G. (2016) Andragogy: A Fundamental Principle of Online Education for Nursing. *Journal of Best Practices in Health Professions Diversity* **9**, 1263-1273

8.   Roe, D., Carley, S., and Sherratt, C. (2010) Potential and limitations of e-learning in emergency medicine. *Emerg Med J* **27**, 100-104

9.   Dunlap, J. C., Sobel, D., and Sands, D. I. (2007) Supporting students' cognitive processing in online courses: Designing for Deep and Meaningful Student-to-Content Interactions. *TechTrends* **51**, 20-31

10.   McLaughlin, J. E., Roth, M. T., Glatt, D. M., Gharkholonarehe, N., Davidson, C. A., Griffin, L. M., Esserman, D. A., and Mumper, R. J. (2014) The flipped classroom: a course redesign to foster learning and engagement in a health professions school. *Acad Med* **89**, 236-243

11.   Blissett, S., Goldszmidt, M., and Sibbald, M. (2015) Do research findings on schema-based instruction translate to the classroom? *Perspectives on medical education* **4**, 334-338

12.   Laksov, K. B., McGrath, C., and Josephson, A. (2014) Let's talk about integration: a study of students' understandings of integration. *Adv in Health Sci Educ* **19**, 709-720

13.   Levitt, S. D., and Dubner, S. J. (2006) *Freakonomics: A Rogue Economist Explores the Hidden Side of Everything (Revised and Expanded)*, Harper Collins

14.   Hale, L. S., Mirakian, E. A., and Day, D. B. (2009) Online vs classroom instruction: student satisfaction and learning outcomes in an undergraduate Allied Health pharmacology course. *J Allied Health* **38**, e36-42

15.   McPherson, M. S., and Bacow, L. S. (2015) Online Higher Education: Beyond the Hype Cycle. *Journal of Economic Perspectives* **29**, 135-154

16. Hurtubise, L., Hall, E., Sheridan, L., and Han, H. (2015) The Flipped Classroom in Medical Education: Engaging Students to Build Competency. *Journal of Medical Education and Curricular Development* **2**, 35-43

17. Broadbent, J., and Poon, W. L. (2015) Self-regulated learning strategies & academic achievement in online higher education learning environments: A systematic review. *The Internet and Higher Education* **27**, 1-13

18. Zoumenou, V., Sigman-Grant, M., Coleman, G., Malekian, F., Zee, J. M. K., Fountain, B. J., and Marsh, A. (2015) Identifying Best Practices for an Interactive Webinar. *Journal of Family and Consumer Sciences* **107**, 62-69

19. King, F. B., Smith, B. C., and Mathews, M. B. (2006) Health Professions' Education and Practice: A Commentary on Transformation Through the Internet. *Journal of Allied Health* **35**, 174-178(175)

20. Freeman, S., Eddy, S. L., McDonough, M., Smith, M. K., Okoroafor, N., Jordt, H., and Wenderoth, M. P. (2014) Active learning increases student performance in science, engineering, and mathematics. *Proceedings of the National Academy of Sciences of the United States of America* **111**, 8410-8415

21. McCoy, L., Pettit, R. K., Lewis, J. H., Bennett, T., Carrasco, N., Brysacz, S., Makin, I. R., Hutman, R., and Schwartz, F. N. (2015) Developing technology-enhanced active learning for medical education: challenges, solutions, and future directions. *The Journal of the American Osteopathic Association* **115**, 202-211

22. Romanelli, F., Bird, E., and Ryan, M. (2009) Learning styles: a review of theory, application, and best practices. *American journal of pharmaceutical education* **73**, 9

23. Cuellar, N. (2002) The transition from classroom to online learning. *Nursing Forum* **37**, 5-13

24. Hay, A., Peltier, J. W., and Drago, W. A. (2004) Reflective learning and on-line management education: a comparison of traditional and on-line MBA students. *Strategic Change* **13**, 169-182

25. Fast Facts. National Center for Education Statistics

26. Bennett, L. A. (2008) The Potential and Uniqueness of Virtual Environments for Education. *New Horizons in Adult Education and Human Resource Development* **22**, 53-59

27. Celik, S. (2012) Development of Usability Criteria for E-Learning Content Development Software. *Turkish Online Journal of Distance Education* **13**, 336-345

28. Naismith, L. M., Haji, F. A., Sibbald, M., Cheung, J. J., Tavares, W., and Cavalcanti, R. B. (2015) Practising what we preach: using cognitive load theory for workshop design and evaluation. *Perspectives on medical education* **4**, 344-348

29. Young, J. Q., Van Merrienboer, J., Durning, S., and Ten Cate, O. (2014) Cognitive Load Theory: implications for medical education: AMEE Guide No. 86. *Medical teacher* **36**, 371-384

30. Fraser, K. L., Ayres, P., and Sweller, J. (2015) Cognitive Load Theory for the Design of Medical Simulations. *Simulation of Healthcare* **10**, 295-307

31. Sadler, D. R. (1998) Formative Assessment: revisiting the territory. *Assessment in Education: Principles, Policy & Practice* **5**, 77-84

32.   Cleveland, L. M., Carmona, E. V., Paper, B., Solis, L., and Taylor, B. (2015) Baby Boy Jones Interactive Case-Based Learning Activity: A Web-Delivered Teaching Strategy. *Nurse educator* **40**, 179-182

33.   Miller, C. J., Aiken, S. A., and Metz, M. J. (2015) Perceptions of D.M.D. student readiness for basic science courses in the United States: Can online review modules help? *European Journal of Dental Education* **19**, 1-7

34.   Coffman, A. G., Grant; Jordan, Matthew; Marden, Erica; Pan, Xiaofan; Willis, Cornelia; Xue, Emily; Richardson, Martha; and Pendlebury, William. (2014) *Creating an Online CME Module: Early Detection and Diagnosis of Dementia and Alzheimer's Disease*,

35.   Schneider, J., Munro, I., and Krishnan, S. (2014) Flipping the Classroom for Pharmacokinetics. *American Journal of Educational Research* **2**, 1225-1229

36.   Limpach, A. L., Bazrafshan, P., Turner, P. D., and Monaghan, M. S. (2008) Effectiveness of human anatomy education for pharmacy students via the Internet. *American journal of pharmaceutical education* **72**, 145

37.   Munson, C. E. (2010) *Assessment of the Efficacy of Blended Learning in an Introductory Pharmacy Class.* Ph.D. Dissertation, University of Kansas

38.   Ilic, D., Nordin, R. B., Glasziou, P., Tilson, J. K., and Villanueva, E. (2015) A randomised controlled trial of a blended learning education intervention for teaching evidence-based medicine. *BMC Med Educ* **15**, 39

39.   Liu, Q., Peng, W., Zhang, F., Hu, R., Li, Y., and Yan, W. (2016) The Effectiveness of Blended Learning in Health Professions: Systematic Review and Meta-Analysis. *Journal of medical Internet research* **18**, e2

40.   Dyrbye, L., Cumyn, A., Day, H., and Heflin, M. (2009) A qualitative study of physicians' experiences with online learning in a masters degree program: benefits, challenges, and proposed solutions. *Medical teacher* **31**, e40-46

41.   Buxton, E. C. (2014) Pharmacists' perception of synchronous versus asynchronous distance learning for continuing education programs. *American journal of pharmaceutical education* **78**, 8

42.   Carver, L., and Todd, C. (2013) Student Perception of Content Master and Engagement in Using an e-Authoring Tool. *High. Learn. Res. Commun.* **3**, 64-73

43.   Newman, A., and Gillis, J. (2013) *Strategies in undergraduate medical education: Web-based self-directed learning in genetics*,

44.   Head, B. A., Schapmire, T., Hermann, C., Earnshaw, L., Faul, A., Jones, C., Kayser, K., Martin, A., Shaw, M. A., Woggon, F., and Pfeifer, M. (2014) The Interdisciplinary Curriculum for Oncology Palliative Care Education (iCOPE): meeting the challenge of interprofessional education. *Journal of palliative medicine* **17**, 1107-1114

45.   Klatt, E. C., and Klatt, C. A. (2011) How much is too much reading for medical students? Assigned reading and reading rates at one medical school. *Acad Med* **86**, 1079-1083

46.   Phillips, J. A., Schumacher, C., and Arif, S. (2016) Time Spent, Workload, and Student and Faculty Perceptions in a Blended Learning Environment. *American journal of pharmaceutical education* **80**, 102

47.   McDonald, P. L., Lyons, L. B., Straker, H. O., Barnett, J. S., Schlumpf, K. S., Cotton, L., and Corcoran, M. A. (2014) Educational Mixology: A Pedagogical Approach to Promoting Adoption of Technology to Support New Learning Models in Health Science Disciplines. *Online Learning* **18**, 1-18

48.   Mackay, R. (2012) Online learning initiative reinventing medical school courses. Stanford Medicine

49.   McDonald, P. L. (2012) *Adult learners and blended learning: A phenomenographic study of variation in adult learners' experiences of blended learning in higher education* Doctoral dissertation

50.   Tabor, S. (2007) Narrowing the distance: Implementing a hybrid learning model for information security education. *The Quarterly Review of Distance Education* **8**, 47-57

51.   Norman, G. (2012) Medical education: past, present and future. *Perspectives on medical education* **1**, 6-14

52.   Pickering, J. D., Henningsohn, L., DeRuiter, M. C., de Jong, P. G. M., and Reinders, M. E. J. (2017) Twelve tips for developing and delivering a massive open online course in medical education. *Medical teacher* **39**, 691-696

53.   Abela, J. (2009) Adult learning theories and medical education: a review. *Malta Medical Journal* **21**, 11-18

54.   Team, R. C. (2016) R: A language and environment for stastistical computing., R Foundation for Statistical Computing, Vienna, Austria

55.   Kirschner, P., Sweller, J., and Clark, R. (2006) Why Minimal Guidance During Instruction Does Not Work: An Analysis of the Failure of Constructivist, Discovery, Problem-Based, Experiential, and Inquiry-Based Teaching. *Educational Psychologist* **41**, 75-86

56.   Mania, K., and Chalmers, A. (2001) The effects of levels of immersion on memory and presence in virtual environments: a reality centered approach. *Cyberpsychology & behavior : the impact of the Internet, multimedia and virtual reality on behavior and society* **4**, 247-264

57.   van Merrienboer, J. J., and Sweller, J. (2010) Cognitive load theory in health professional education: design principles and strategies. *Med Educ* **44**, 85-93

58.   Hunter, T. S., Deziel-Evans, L., and Marsh, W. A. (2003) Assuring Excellence in Distance Pharmaceutical Education. *American journal of pharmaceutical education* **67**, 519-544

59.   Spring, K. (2012) "Takin' It to the Web": Updating Operations Manuals for Today's Techno-Realities. *Journal of Interlibrary Loan, Document Delivery & Electronic Reserve* **22**, 33-46

60.   Grasgreen, A. (2010) Preparing professors to teach. Inside Higher Ed, Washington, D.C.

61.   Colleen Marzilli, J. D., Shelly Marmion, Rochell McWhorter, Paul Roberts, and T. Scott Marzilli. (2014) FACULTY ATTITUDES TOWARDS INTEGRATING TECHNOLOGY AND INNOVATION. *International Journal on Integrating Technology in Education* **3**, 20

62.   Meyer, K. A., and Murrell, V. S. (2014) A National Survey of Faculty Development Evaluation Outcome Measures and Procedures. *Online Learning* **18**, 1-18

63.   Carter, C. S., Solberg, L. B., and Solberg, L. M. (2017) Applying theories of adult learning in developing online programs in gerontology. *Journal of Adult and Continuing Education* **0**, 1-9

APPENDIX III

COPYRIGHT CLEARANCE

Appendix II contains the full text, figures, and tables for a manuscript submitted to *Medical Science Educator*. At the date the final version of this dissertation is submitted, the manuscript was not yet accepted or rejected. If accepted for publication in this journal, the manuscript components in Appendix II covered by the copyright clearance are the manuscript's title and abstract (pg. 142) and its introduction, methods, results, and discussion sections (pgs. 153-172). Below is the copyright clearance for the submitted manuscript from Peter de Jong, Editor in Chief, for *Medical Science Educator*:

Copyright Clearance

CA Cobb,Catherine Ann
Mon 3/19, 8:33 AM
journal@iamse.org ⌄   👍   ↩ Reply all | ⌄

Sent Items

To Whom It May Concern:

I am the first author on a manuscript submitted a week ago entitled "Establishing Best Practices for Effective Online Learning Modules: A Single Institution Study." We received an e-mail that the submission may take up to 10 weeks for review. I am in the process of completing my dissertation, the final copy of which must be submitted by April 27, 2018. I need to determine how I go about getting copyright clearance for the work we submitted but hasn't and may not yet be accepted by the time I submit my final dissertation just in case it is later accepted, or if I do not need clearance before it is accepted and can still reproduce the figures and text in my thesis. Thank you!

Sincerely,

Catherine Cobb

P P.G.M.de_Jong@lumc.nl
Sun 4/8, 9:49 AM
Cobb,Catherine Ann; journal@iamse.org ⌄   👍   ↩ Reply all | ⌄

Inbox

Dear Catherine,

Yes, you have permission to use the figures and text from your own article in your thesis.

Thanks,
Peter

181

CURRICULUM VITAE

Catherine Cobb

Health Sciences Center, Building A, #603

University of Louisville

Louisville, KY 40202

Education

2006-2011   B.S., Biology, Middle Tennessee State University, Murfreesboro, Tennessee

                  Focus: Physiology

2006-2011   B.S., Chemistry, Middle Tennessee State University, Murfreesboro, Tennessee

                  Minor: English

2013-2015   M.S., Dept. of Biochemistry and Molecular Genetics, University of Louisville,

                  Louisville, Kentucky

2015-   Ph.D. Candidate, Dept. of Biochemistry and Molecular Genetics, University of

                  Louisville, Louisville, Kentucky

Positions and Employment

2008   Summer Internship, Office of Dr. Roger Gibson, Germantown, Tennessee

2010   Research Assistant, Dept. of Chemistry, Middle Tennessee State University,

                  Murfreesboro, Tennessee

                  Project: Inhibition of topoisomerase II by gossypol treatment in cancer cell survival

2010-2011   Emergency Medical Technician, MedStat, Manchester, Tennessee

2011-2012   Environmental Chemist, Organic Dept., Empirical Laboratories, Nashville,

                  Tennessee

2012-2013	Learning Specialist, Student Athlete Enhancement Center, Middle Tennessee State University, Murfreesboro, Tennessee
2013-	Graduate Student, Dept. of Biochemistry and Molecular Genetics, Louisville, Kentucky

Project 1: Functional and Structural Impact of the Loss of the Leucine-Rich Repeat Protein LRIT1 in the Mouse Retina

Project 2: Establishing Best Practices for Online Learning Modules as an Alternative to Traditional Lectures

Teaching Experience

2009-2011	Teaching Assistant, Dept. of Chemistry, Middle Tennessee State University, Murfreesboro, Tennessee
2011	New Jersey Third Grade Writing Exam Evaluator, Measurement, Inc., Nashville, Tennessee
2011	Completion of Step One for Math and Science Educators, MTeach Program, Middle Tennessee State University, Murfreesboro, Tennessee
2014	Teaching Assistant (Advanced Methods in Biochemistry), Dept. of Biochemistry and Molecular Genetics, Louisville, Kentucky
2015	Mini STEM GTA Academy Certificate, School of Interdisciplinary and Graduate Studies, Louisville, Kentucky
2015-2016	Graduate Teaching Assistant (Dental Biochemistry), Dept. of Biochemistry and Molecular Genetics, Louisville, Kentucky
2015-2016	GEAR Up! Weekend, Event Chair, Science Policy and Outreach Group, Louisville, Kentucky

Professional Memberships

2014-	American Association of University Women, Graduate Student Member, Louisville, Kentucky

2014-2017	Science Policy and Outreach Group, Member, Louisville, Kentucky
2016-2017	Association for Research in Vision and Ophthalmology (ARVO), Graduate Student Member, Baltimore, MD
2017	Association of Biochemistry Educators (ABE), Graduate Student Member
2017	National Association of Science Writers, Graduate Student Member

Honors and Awards

2006	Dean's List
2006-2010	Academic Service Scholarship, Middle Tennessee State University, Murfreesboro, Tennessee
2006-2010	Tennessee HOPE Scholarship, Middle Tennessee State University, Murfreesboro, Tennessee
2007	General Education Writing Award Nominee, Middle Tennessee State University, Murfreesboro, Tennessee
2010	Dean's List
2010	General Education Writing Award Nominee, Middle Tennessee State University, Murfreesboro, Tennessee
2013-	Integrated Programs in Biomedical Sciences (IPIBS) Fellowship Ph.D. Program, Dept. of Biochemistry and Molecular Genetics, University of Louisville, Louisville, Kentucky
2014-2015	Inez Bailey Scholarship Recipient, PEO International
2015-2016	Dean's Reception attendee and awardee (Graduate Student Council, 2015; Mini STEM GTA Academy, 2016), Louisville, Kentucky
2017	Association for Research in Vision and Ophthalmology (ARVO) National Eye Institute Travel Grant Recipient, ARVO 2017, Baltimore, MD
2017	GSC Travel Funding Recipient, Association of Biochemistry Educators International Conference 2017, Clearwater, FL
2017	Dept. of Biochemistry and Molecular Genetics Biennial Selected Abstract for Oral Presentation, Kingfish Restaurant, Louisville, Kentucky

| 2017 | Dept. of Biochemistry and Molecular Genetics Biennial Retreat Poster Presentation 2nd Place Winner, Kingfish Restaurant, Louisville, Kentucky |
| 2018 | Doctoral Dissertation Completion Award Recipient, School of Interdisciplinary and Graduate Studies, University of Louisville, Louisville, Kentucky |

Professional Service

2008	Math and Science Olympiad Volunteer, Middle Tennessee State University, Murfreesboro, Tennessee
2010	AVID Mentoring Program Mentor, Glencliff High School, Nashville, Tennessee
2014	East Coffee Elementary School Career Day, Experimental Demonstrations by a Scientist for third through fifth grade, Manchester, Tennessee
2014-	Dept. of Biochemistry and Molecular Genetics Student Mentor, Louisville, Kentucky
2014-2016	Academic Grievance Committee Student Representative, Dept. of Biochemistry and Molecular Genetics, Louisville, Kentucky
2014-2016	Dept. of Biochemistry and Molecular Genetics Graduate Student Council Representative, Louisville, Kentucky
2015	Judge, DuPont Manual High School Science Fair, Louisville, Kentucky
2015	Health Sciences Campus Chair (Spring) and Co-Chair (Fall), Graduate Student Council, Louisville, Kentucky
2015-	Kentucky Academy of Science Member, Louisville, Kentucky
2015-2016	Dept. of Biochemistry and Molecular Genetics Student President, Louisville, Kentucky
2015-2016	Dept. of Biochemistry and Molecular Genetics Graduate Executive Committee Student Representative, Louisville, Kentucky
2016-2017	Dept. of Biochemistry and Molecular Genetics Student Vice President, Louisville, Kentucky

A. Publications, Presentations, and Posters

Peer-Reviewed Publications and Manuscripts Submitted

1. **Cobb, CA**. Cole, MP. Oxidative and Nitrative Stress in Neurodegeneration. Neurobiology of Disease. 2015; 84: 4-21. doi: 10.1016/j.nbd.2015.04.020.

2. **Cobb, CA**. Watson, CT. Ellis, SR. Establishing Best Practices for Effective Online Learning Modules: A Single Institution Study. Manuscript submitted. 2018.

Presentations

1. **Cobb, CA.** Ray, T. and Gregg, RG. Visualizing *Lrit1* and *Lrit3* in the Mouse Retina Using RNAScope® *In Situ* Hybridization. Presentation, ACDBio Seminar (August 2017), Louisville, KY.

2. **Cobb, CA.** Hasan, N. Ji, R. Hoffman, TA. and Gregg, RG. Identification of Mouse Mutant Lacking Cone Vision. Poster and presentation, Dept. of Biochemistry and Molecular Genetics Biennial Retreat (August 2017), Louisville, KY.

Posters

1. **Cobb, CA**, Piell, KM. Van Hoose, PM. and Cole, MP. 8-Isoprostane Generation Following Co-Treatment With Conjugated Linoleic Acid and Nitrite May Promote Myocardial Protection. Poster, Research!Louisville (Sept 2014), University of Louisville, Louisville, KY.

2. **Cobb, CA**, Piell, KM. Van Hoose, PM. and Cole, MP. 8-Isoprostane Generation Following Co-Treatment With Conjugated Linoleic Acid and Nitrite May Promote Myocardial Protection. Poster, Dept. of Biochemistry and Molecular Genetics Biennial Retreat (August 2015), Louisville, KY.

3. **Cobb, CA.** Hasan, N. Ji, R. Hoffman, TA. and Gregg, RG. Identification of Mouse Mutant Lacking Cone Vision. Poster, ARVO (May 2017), Baltimore, MD.

4. **Cobb, CA.** Ellis, SR. SoftChalk as an Interactive Learning Alternative to Traditional Lectures. Poster, ABE (May 2017), Clearwater, FL.

5. **Cobb, CA.** Hasan, N. Ji, R. Hoffman, TA. and Gregg, RG. Identification of Mouse Mutant Lacking Cone Vision. Poster and presentation, Dept. of Biochemistry and Molecular Genetics Biennial Retreat (August 2017), Louisville, KY.

B. Research Support

2013-2014   Integrated Programs in Biomedical Sciences (IPIBS) Fellowship Ph.D. Program, Dept. of

Biochemistry and Molecular Genetics, University of Louisville, Louisville, Kentucky

2018   Doctoral Dissertation Completion Award, School of Interdisciplinary and Graduate

Studies, University of Louisville, Louisville, Kentucky